

Design and Optimization of Hydrofoil-Assisted Catamarans.

Dissertation presented in partial fulfilment of
the requirements for the degree

**Doctor of Philosophy
in Engineering Science**
(Mechanical Engineering)



GÜNTHER MIGEOTTE

in the Faculty of Engineering
Department of Mechanical Engineering
University of Stellenbosch
Stellenbosch, South Africa

March, 2002

SUPERVISORS:

Prof. Dr.-Ing. K.G. Hoppe - University of Stellenbosch
Prof. G.D. Thiar - University of Stellenbosch

DECLARATION

I, the undersigned, hereby declare that the work contained in this dissertation is my own original work and that I have not previously in its entirety or in part submitted it at any university for a degree.

Signature:

Date:

Abstract

This work is concerned with the hydrodynamic design of hydrofoil-assisted catamarans. Focus is placed on the development of new and suitable design methods and application of these to identify the most important geometric parameters of catamaran hulls and hydrofoil configurations that influence efficiency and performance. These goals are pursued by firstly gaining a thorough understanding of the governing hydrodynamic principles involved in the design process. This knowledge is then applied to develop new and improved experimental techniques and theoretical methods needed for design. Both are improved to the extent where they can be applied as design tools covering the important semi-displacement and semi-planing speeds, which are the focus of this study.

The operational speed range of hydrofoil-assisted catamarans is shown to consist of three distinct hydrodynamic phases (displacement, transition and planing) and that different hydrodynamic principles govern vessel performance in each phase. The hydrodynamics are found to differ substantially from that of conventional high-speed craft, primarily due to the interaction between the hull and the hydrofoils, which is found to vary with speed and results in the need for more complex experimental procedures to be followed if accurate predictions of resistance are to be made.

Experimental predictions based on scaled model tests of relatively small hydrofoil-assisted catamaran models are found to be less accurate than that achievable for conventional ships because of the inability to correct for all scaling errors encountered during model testing. With larger models scaling errors are encountered to a lesser degree. The most important scale effect is found to be due to the lower Reynolds number of the flow over the scaled foils. The lower Reynolds number results in higher drag and lower lift coefficients for hydrofoils compared with those achieved at full scale. This effect can only be partially corrected for in the scaling procedure using the available theoretical scaling methods.

Presently available theoretical methods commonly used for the design of conventional ships were found to be ill adapted for modeling the complex hydrodynamics of hydrofoil-assisted catamarans and required further development. Vortex lattice theory was chosen to model the flow around hydrofoil-assisted catamarans as vortex theory models the flow around lifting surfaces in the most natural way. The commercial code AUTOWING is further developed and generalized to be able to model the complex hull-hydrofoil interactions that change with speed. The method is shown to make good predictions of all hydrodynamic quantities with accuracies at least as good as that achievable through model testing and therefore fulfills the requirements for a suitable theoretical design tool.

The developed theoretical and experimental design tools are used to investigate the design of hydrofoils for hydrofoil-assisted catamarans. It is found that the main parameter needing consideration in the hydrofoil design is selection of a suitable hydrofoil lift fraction. A foil lift fraction in the order of 20-30% of the displacement weight is needed if resistance improvements using hydrofoil assistance are to be obtained over the hull without foils. It is often more favorable to use higher foil lift fractions (50%+) as the resistance improvements are better, although careful attention should then be given to directional and pitch-heave instabilities. The Hysuwac hydrofoil system patented by the University of Stellenbosch is found to be hydrodynamically optimal for most hullforms.

The hullform and in particular the curvature of the aft buttock lines of the hull are found to have an important influence on the achievable resistance improvements and behaviour of the hydrofoil-assisted hull at speed. Hull curvature is detrimental to hydrodynamic performance as the suction pressures resulting from the flow over the curved hull counter the hydrofoil lift. The hullform best suited to hydrofoil assistance is found to be one with relatively straight lines and hard chine deep-V sections.

The main conclusion drawn from this study is that hydrofoil-assistance is indeed suitable for improving the performance and efficiency of catamarans. The design and optimization of such vessels nevertheless requires careful consideration of the various resistance components and hull-foil interactions and in particular, how these change with speed. The evaluation of resistance for design purposes requires some discipline between theoretical analysis and experimental measurements as the complexity of the hydrodynamics reduce the accuracies of both. Consideration of these factors allows hulls and hydrofoils to be designed that are efficient and also free of dynamic instabilities.

Opsomming

Hierdie studie is gerig op die hidrodinamiese ontwerp van hidrovleuel-gesteunde katamarans. Daar word gefokus op die ontwikkeling van nuwe en geskikte ontwerpmetodes, asook die toepassing van hierdie metodes om die belangrikste geometriese parameters van katamaranrompe en hidrovleuel-konfigurasies wat 'n invloed op doeltreffendheid en werkverrigting het, te identifiseer. As aanloop tot die studie is 'n deeglike begrip van die onderliggende hidrodinamiese beginsels bekom. Hierdie kennis is toegepas om nuwe en verbeterde eksperimentele en teoretiese tegnieke te ontwikkel wat nodig is vir die ontwerp van hidrovleuel-gesteunde katamarans in die belangrike deels-verplasing en deels-planering spoedbereike.

Daar word getoon dat die bedryfspoedbereik van 'n hidrovleuel-gesteunde katamaran uit drie onderskeibare hidrodinamiese fases bestaan, naamlik verplasing, oorgang en planering, en dat verskillende hidrodinamiese beginsels die vaartuig se werkverrigting in elke fase bepaal. Daar is ook gevind dat die hidrodinamika wesentlik verskil van dié van konvensionele hoëspoed-vaartuie, hoofsaaklik as gevolg van die interaksie tussen die romp en die hidrovleuels wat wissel na gelang van die spoed. Hierdie interaksies moet in ag geneem word gedurende die ontwerpproses en beide eksperimentele en teoretiese metodes is nuttig om die omvang daarvan te bepaal.

Daar is gevind dat die eksperimentele voorspellings gebaseer op toetse met relatief klein skaalmodelle van hidrovleuel-gesteunde katamarans minder akkuraat is as dié wat bereik kan word met konvensionele skepe. Dit is omdat al die skaalfoute wat tydens die toetsing met die model ontstaan, nie gekorrigeer kan word nie. Die belangrikste skaaleffek is as gevolg van die laer Reynoldsgetal van die vloei oor die afgeskaalde vleuels. Groter modelle Die laer Reynoldsgetal lei tot hoër sleur- en hefkoëffisiënte in vergelyking met dié vir die volskaal-hidrovleuels. Wanneer die beskikbare teoretiese metodes gebruik word, kan daar slegs gedeeltelik vir hierdie effek in die skaalprosedure gekorrigeer word. Daar is ook vasgestel dat die skaaleffekte op die Reynoldsgetal verminder word wanneer die hidrovleuels baie naby aan die vrye oppervlakte is. Dit lei daartoe dat eksperimentele voorspellings van werkverrigting meer akkuraat is vir die ontwerpe waar die hidrovleuels nie so diep onder die water is nie.

Daar is gevind dat die teoretiese metodes wat tans beskikbaar is en algemeen vir die ontwerp van konvensionele skepe gebruik word nie die komplekse hidrodinamika van hidrovleuel-gesteunde katamarans kan modelleer nie. Die werwelroosterteorie is gekies om die vloei om hidrovleuel-gesteunde katamarans te modelleer aangesien dié teorie die vloei om hefvlakke op die natuurlikste manier weergee. Die kommersiële kode AUTOWING is verder ontwikkel en veralgemeen om ook die komplekse spoed-

afhanklike interaksies van die romp en hidrovleuel te kan modelleer. Hierdie metode lewer goeie voorspellings van al die hidrodinamiese maatstawwe met akkuraathede wat ten minste so goed is soos di wat met modeltoetsing bereik word en voldoen daarom aan die vereistes vir 'n geskikte teoretiese ontwerpmetode.

Die teoretiese en eksperimentele ontwerpmetode wat ontwikkel is, word gebruik om die ontwerp van hidrovleuels vir hidrovleuel-gesteunde katamarans te ondersoek. Daar is gevind dat die belangrikste parameter wat in die hidrovleuel-ontwerp in ag geneem moet word, die keuse van 'n geskikte hidrovleuelhefverhouding is. Om in rompe met hidrovleuelsteun verbeterings in die weerstand te kry in vergelyking met rompe sonder vleuels, is 'n vleuel-hef-verhouding van 20-30 persent van die verplasingsgewig nodig. Dit is dikwels beter om hoër vleuel-hef-verhoudings (van 50 persent of meer) te gebruik omdat die verbetering in weerstand dan groter is. Daar moet dan egter gewaak word teen rigtings- en hef-hef-onstabieleite. Daar is gevind dat die Hysuwac-hidrovleuel-stelsel wat deur die Universiteit van Stellenbosch gepatenteer is, hidrodinamies optimaal is vir die meeste rompvorms.

Daar is gevind dat die vorm van die romp en veral die kromming van die lyne gevorm deur vertikale snitte deur die romp (Engels: "aft buttock lines") van die romp 'n belangrike invloed het op die bereikbare weerstandsverbeterings en die gedrag van die hidrovleuel-gesteunde romp wat op spoed is. Die kromming van die romp is nadelig vir die hidrodinamiese werksverrigting aangesien die suigdruk as gevolg van die vloei oor die gekromde romp die hefkrag van die hidrovleuels teenwerk. Die rompvorm wat die geskikste is vir hidrovleuel-ondersteuning is 'n romp met relatiewe reguit lyne en skerp hoekige diep-V seksies.

Die belangrikste gevolgtrekking waartoe tydens die studie gekom is, is dat hidrovleuel-ondersteuning wel geskik is vir die verbetering van die werkverrigting en die doeltreffendheid van katamarans. Die ontwerp en optimering van sodanige vaartuie verg nogtans die noukeurige oorweging van die verskeie weerstandskomponente en rompvleuel-interaksies en veral hoe hierdie interaksies verander met spoed. Die evaluering van die weerstand vir die doeleindes van ontwerp verg dissipline tussen die teoretiese analise en die eksperimentele metings aangesien die kompleksiteit van die hidrodinamika die akkuraatheid van die algemeen-gebruikte teoretiese en eksperimentele metodes vir die hidrodinamiese ontwerp verminder. As hierdie faktore in ag geneem word, kan rompe en hidrovleuels ontwerp word wat doeltreffend is en ook vry is van dinamiese onstabieleite.

Acknowledgements

A number of people deserve mention as having supported this study in different ways. Firstly *my parents* for supporting me down the long road of graduate study and providing the means for me to present my work and attend international conferences as well as giving me the opportunity to study in Germany and Russia under some very brilliant scientists.

Thank you to *Prof. K.G. Hoppe* whose teachings I have followed throughout my career as a graduate student. His assistance and guidance as well as countless hours spent in the towing tank solving hydrodynamic problems has given me the experience and understanding needed to complete this study and will undoubtedly stand me in good stead for the future. Furthermore Prof. Hoppe and Unistel provided the opportunity for me to gain experience working on a number of commercial design projects. This has added much value to my studies. Unistel is further thanked for partially supporting this study financially.

Special thanks to *Prof. Nikolai Kornev* of the State Marine Technical University of St. Petersburg. His assistance with the practical application of vortex methods for complex hydrodynamic problems such as those I have encountered in this study is greatly appreciated and has been of such value that it would not have been easily possible to pursue the development of these methods within the scope of this study without his assistance. His help, advice and substantial theoretical input has allowed me to present a complete numerical tool for modeling hydrofoil-assisted catamarans. It has been a great privilege and an honor to work together with Prof. Kornev during the course of this study.

The theoretical work is based largely on the teachings of *Prof. Gerri Thiart* who guided my initial probes in the development of a computational design tool and I benefited from his experience of numerical methods when I ran into difficulties.

Thank you to *Prof. Heinrich Söding* of the Institut für Schiffbau in Hamburg, Germany and also to the Schiffbau-Versuchsanstalt Potsdam for allowing me to make use of their KELVIN software during my studies in Hamburg. Prof. Söding's assistance in helping me understand the application of numerical methods to high-speed ships has been very helpful. I am indebted to him for spending his time to teach me.

Thank you to *Dr. Volker Bertram* of the HSVA who has helped me in all kinds of ways to solve problems ranging from hard to get literature to introducing me to people who could be of assistance to me in my study. Further, Dr. Bertram's assistance in creating

ACKNOWLEDGEMENTS

viii

opportunities for me to present my work internationally is greatly appreciated.

Last but not least, thank you to *my wife Iris*, who has had to put up with my long hours behind the computer preparing this script. She has had to motivate me through the difficult parts and has done her best to assist me so that I had the maximum amount of time to work on this thesis. This she did sometimes at the expense of her own studies. Thank you to the best wife.

I would like to dedicate this work to the two great pioneers of modern hydrofoil craft:

Baron *Hans Schertel von Burtenbach* Dessau-Rosslau, Germany, 1937

Rostislav Evgenievich Alekseyev, Krasnoye Sormovo Shipyards, Gorki (Nizhny Novgorod), USSR, 1943.

Günther Migeotte

Contents

1	Introduction	1
1.1	General	1
1.1.1	Fast Ferry Catamarans	2
1.1.2	Pleasure Craft	3
1.1.3	High-Speed Patrol Craft	4
1.2	Past, Present and Future Developments	5
1.3	Early Developments	6
1.3.1	Pioneering Soviet Research	6
1.3.2	The Hycat Development	7
1.3.3	The Hysucat Development	8
1.3.4	Chinese Channel Hydrofoil Boats	11
1.4	Recent Developments	12
1.4.1	The Hitachi Zosen Development	12
1.4.2	The Hyundai Development	13
1.4.3	The Daewoo Development	16
1.4.4	The Canard-Interceptor Hydrofoil-Assisted Catamaran	16
1.4.5	The Hysuwac Development	17
1.5	Current and Future Research	18
1.5.1	Speed, Range and Efficiency	20
1.5.2	Wake Wash	23
1.5.3	Sea-Keeping	23

CONTENTS

x

1.6	Design of Hydrofoil-Assisted Catamarans	25
1.6.1	Objectives	27
2	Hydrodynamics and Resistance	29
2.1	Introduction	29
2.2	The Displacement Phase	33
2.3	The Transition Phase	35
2.3.1	The Hull Shape	35
2.3.2	Foil-Hull Interactions	36
2.3.3	Transition to Planing	40
2.4	The Planing Phase	42
2.5	Resistance Components	43
2.6	Hull Resistance	44
2.6.1	Hull Viscous Resistance R_V	44
2.6.2	Hull Wave-Making Resistance R_W	47
2.6.3	Hull Interference Resistance R_{ICAT}	50
2.6.4	Foil Interference Resistance R_{IF}	52
2.7	Air and Wind Resistance R_{AA}	54
2.8	Hydrofoil Drag D_F	54
2.8.1	Wave Drag D_W , Induced Drag D_L and Lift L	55
2.8.2	Profile Drag D_{F0}	56
2.8.3	Interference Drag D_{INT}	57
2.8.4	Hull Interference Drag D_{IH}	59
2.8.5	Strut Drag D_{ST}	60
2.9	Cavitation and Ventilation	61
3	Model Testing and Scaling	62
3.1	Introduction	62
3.2	Surface Tension	63

<i>CONTENTS</i>	xi
3.3 Cavitation	64
3.4 Air Resistance	65
3.5 Reynolds Number Effects	65
3.5.1 Effect on Drag Coefficient	68
3.5.2 Effect on Lift Coefficient	69
3.5.3 Free Surface Effects on Viscous Corrections for 3-Dimensional Hydrofoils	74
3.5.4 Freestream Turbulence	78
3.5.5 Turbulence Stimulation	80
3.5.6 Experiments with Turbulence Stimulation	82
3.6 Scaling of Model Test Results	86
3.6.1 Correlation Method	87
3.6.2 Correlating Model Test Data Measured without Turbulence Stim- ulation	91
4 Theoretical Design Methods	93
4.1 Introduction	93
4.2 Requirements for a Suitable Design Tool for Hydrofoil-Assisted Cata- marans	95
4.3 Review of Existing Computational Methods	96
4.3.1 Viscous Flow Methods	96
4.3.2 Potential Flow Methods	96
4.4 Mathematical Modeling	97
4.4.1 Potential Flow Formulations for the Planing Phase	98
4.4.2 Potential Flow Formulations for the Displacement and Transi- tion Phase	100
4.5 The Vortex Lattice Method	102
4.5.1 Mathematical Background	104
4.5.2 Discrete Vortex Free Surface Model	106
4.5.3 Solution of the Free Surface Boundary Condition	109

CONTENTS

xii

4.6	The Vortex Roll-Up Process	111
4.7	Calculation of Forces	112
4.8	Solution Process for a Lifting Wing under the Free Surface	114
4.9	Mathematical Model for Planing	116
4.10	Application of the Vortex Lattice Method to Planing Hydrofoil-Assisted Catamarans	119
4.10.1	Calculating Hydrofoil-Assisted Catamarans that consists of a Rear Planing Surface in Combination with a Hydrofoil	120
4.10.2	Validation of Planing Computational Method	122
4.10.3	Optimization using Computational Model for Planing Hydrofoil- Assisted Catamarans	125
4.11	A Free Surface Model for Displacement and Transitional Speeds	129
4.11.1	Two Dimensional Spray Jet Model	129
4.11.2	Numerical Simulation of 3-Dimensional Problems with Jet Spray	133
4.11.3	Results and Comparison with Experiment	139
4.12	Closure	142
5	Hydrofoil Design	146
5.1	Introduction	146
5.2	Primary Hydrodynamic Considerations	147
5.2.1	The Load Distribution and Interactions between Hull and Hy- drofoils	147
5.2.2	Dynamic Stability Considerations	162
5.3	Hydrofoil Design Features	165
5.3.1	The Profile Shape	165
5.3.2	Planform Considerations	167
6	Hull Design for Hydrofoil Assistance	169
6.1	Introduction	169
6.2	Asymmetrical Hullforms	170

CONTENTS

xiii

6.3	Symmetrical Catamaran Hullforms	173
6.3.1	Round-Bilge and Hard Chine Hull Forms	174
6.3.2	The Influence of Aft Buttock Shape and the Position of the LCG180	
6.4	The Influence of Hullform Parameters on Design	190
7	Conclusions	198
7.1	Main Conclusions	198
7.2	Detailed Conclusions	199
7.3	Recommendations for Future Work	201
A	Convergence of Numerical Schemes	202
A.1	Introduction	202
A.2	Application of AUTOWING for Hydrofoils	202
A.2.1	Numerical Convergence	203
A.3	Validation of AUTOWING for Planing Hulls	209
A.4	Application of Transition Speed Model	211
B	Numerical Results Spreadsheet	213
C	Efficiency of some High-Speed Craft	218

List of Figures

1.1	No. of hydrofoil-assisted fast ferries launched in the last decade, given as percentage of conventional fast ferry catamarans.	3
1.2	Two hydrofoil-assisted fast ferries. The upper 32m vessel (Autojet) is capable of 45 knots and has two canard foils located under the bow of each hull. The lower 40m low wash catamaran is capable of 45 knots and uses a University of Stellenbosch, Hysuwac foil system.	4
1.3	A 22m motor yacht capable of 45 knots (left) and a 12m, 42 knot motor boat (right), both assisted by Hysucat hydrofoil systems designed by Prof. K.G. Hoppe at the University of Stellenbosch.	5
1.4	A 22m coastal patrol catamaran using a Hysucat hydrofoil system. The vessel is capable of 36 knots.	5
1.5	Resistance tendencies of high-speed craft	7
1.6	Resistance tendencies of early Soviet hydrofoil-assisted semi-planing catamarans	8
1.7	Hycat layout and resistance	9
1.8	Layout of the Hysucat design	10
1.9	Resistance tendency for a Hysucat	10
1.10	Layout of Chinese channel hydrofoil boats	11
1.11	Resistance comparison for Chinese channel hydrofoil planing boat with $L/\nabla^{0.33} = 7.2$	12
1.12	Hitachi Superjet30 and its hull-foil configuration	14
1.13	Hitachi Superjet model test result	14
1.14	Hyundai hydrofoil-assisted catamaran hull and foil layout	15

LIST OF FIGURES

xv

1.15	Resistance comparison based on model test data. Data without foils is shown as a black line. Data with foils is given for fixed even running condition (blue line) and at a fixed trim angle of 2 degrees (red line) . . .	15
1.16	Daewoo hydrofoil-assisted catamaran with an illustration of the mono-foil	16
1.17	Resistance comparison for Daewoo F-CAT40	17
1.18	Model of the Autojet hydrofoil system	18
1.19	Layout of the Hysuwac foil design	19
1.20	A typical Hysuwac resistance tendency	20
1.21	Summary of foil configurations currently in use	21
1.22	Number of research papers published per year	22
1.23	Transport efficiency of fast craft in relation to some hydrofoil-assisted catamarans	24
1.24	A motion control T-foil fitted to the bow of a catamaran demi-hull developed by Maritime Dynamics Inc.	25
1.25	Vertical accelerations on the Hyundai hydrofoil-assisted catamaran with active and passive hydrofoil assistance	26
2.1	Performance tendencies for hydrofoil-assisted catamarans	31
2.2	Examples of a model test for the three phases of operation	32
2.3	Transom stern flow at $Fn_{\nabla} = 1.5$ for a semi-displacement hull with and without foils	34
2.4	The NPL hullform	36
2.5	Pressure along a streamline on an NPL hullform at B/4	37
2.6	Lift ratio between total dynamic lift forces and hydrofoil lift forces . . .	38
2.7	Changes in pressure on a hull due to a single foil. h/c refers to the separation distance between hull and foil	39
2.8	Resistance, trim and rise tendencies for a typical semi-displacement catamaran with Hysuwac foil system illustrating tendencies at the transition to planing ($V = 4.5m/s$)	41
2.9	Air-water mixing layer on a hydrofoil close to the free surface	43
2.10	The resistance components of hydrofoil-assisted catamarans	44
2.11	Comparison of measured wetted areas for two different foil configurations	47

LIST OF FIGURES

xvi

2.12	Wave-making interference for a catamaran demi-hull as a function of length Froude number: $Fn_L = \frac{V}{gL_{WL}}$	51
2.13	Lift interference between two flat surfaces planing side by side	52
2.14	Interference resistance as a function of Volumetric Froude number	53
2.15	Friction drag of a plano-convex circular arc profile, including free surface effect, relative to flat plate drag, based on equation 2.9	58
3.1	Spray rails for a Hysuwac model. Also shown are the turbulence stimulators on the hull (black strips).	64
3.2	Air resistance of a 2.5m model	66
3.3	Paint trace test showing separation on an 8% thickness foil at $Rn = 8 \times 10^4$ (leading edge at top)	67
3.4	Foil drag coefficients (based on planform area as a function of submergence)	69
3.5	Viscosity effect on the lift curve slope for profiles with leading edge turbulence stimulation	71
3.6	Potential flow pressure distributions including free surface effect for a symmetrical and asymmetrical profile at $\alpha = 0.0$ degrees	77
3.7	The effect of freestream turbulence on an 11% circular arc section	79
3.8	Initial results using wire freestream turbulence stimulation	83
3.9	Arrangement of wires for turbulating the freestream ahead of the model	84
3.10	Comparison of model resistance and trim for improved turbulence stimulation	85
3.11	Illustration of the effect of Reynolds number of the lift of hydrofoils	90
3.12	A resistance comparison for a 40m Hysuwac tested with and without turbulence stimulation	92
4.1	Comparison of AUTOWING results (no leading edge or side edge model) with those of Lai and Savitsky.	99
4.2	Comparison between KELVIN, MICHLET and measurements for a semi-displacement catamaran	103
4.3	Discretization scheme for ring vortex panels	106
4.4	Illustration of free surface mesh panels	110

LIST OF FIGURES

xvii

4.5	Flowchart illustrating the computational steps followed to solve the free surface boundary condition	115
4.6	Illustration of planing surface discretization	118
4.7	Paint trace showing asymmetrical wetted area for a demi-hull planing in the wake of a forward foil	118
4.8	A longitudinal strip of a planing surface showing the free surface rise ahead of the bow	119
4.9	Picture of the SD6 model with F2 foil system	122
4.10	AUTOWING prediction of resistance, displacement and center of pressure	124
4.11	Illustration of the three longitudinal foil positions calculated	125
4.12	Lift to drag ratio as a function of LCG position with displacements as the curve parameter for $Fn_{\nabla} = 2.8$	126
4.13	Upwash averaged along the rear foil chord. Zero on the abscissa axis corresponds to the longitudinal symmetry plane of the vessel.	127
4.14	Wetted area for the 3 different cases calculated	128
4.15	Computational domain and discretization of the 2-dimensional impact problem	132
4.16	The pressure distribution on the wedge for different deadrise angles . .	133
4.17	Influence of Froude number on the impact process and free surface elevation	134
4.18	Influence of non-linearity on the free surface elevation for large Froude numbers	135
4.19	Free surface mesh around a body piercing the free surface	136
4.20	Approximation of the continuous vortex sheet by a set of closed vortices	137
4.21	Directions of the approximation procedure for calculating circulation intensities	137
4.22	Illustration of free surface penetrating a surface piercing body during calculation of free surface elevations	138
4.23	Illustration of the hull paneling scheme. Rectangular elements are used along the hull and triangular elements near the bow	139

LIST OF FIGURES

xviii

4.24	SD6 hull w/o foils, comparison of vortex lattice method AUTOWING with experimental results and also with the numerical predictions of KELVIN and MICHLET.	140
4.25	Free surface elevations for the SD6 catamaran without hydrofoils	141
4.26	Comparison of AUTOWING with experiments for speeds covering the transition phase of the SD6 Hull with foil system F2.	143
4.27	Free surface mesh and deformation calculated with AUTOWING	144
4.28	The symmetrical half of the SD6 Hull (wetted area only) showing the dynamic pressure distribution at $Fn_{\nabla} = 2.3$. The effects of the hull and hydrofoil design on the pressure are pointed out.	145
5.1	The SD8 body plan.	150
5.2	Hull resistance as a function of LCG position	151
5.3	The SD8 hull with Hysuwac foil system	152
5.4	Hump speed ratio of resistance with foils against the resistance without foils as a function of rear hydrofoil lift.	153
5.5	Improvements in resistance as a function of total hydrofoil lift at $Fn_{\nabla} = 1.50$	154
5.6	Improvements in hump resistance for different hull forms as a function of hydrofoil lift fraction. Results are given for the SD8 hull as well as a semi-displacement design [MH00], a high hump resistance planing hull design [Mig97].	155
5.7	The effect of front foil angle of attack on transition hump resistance characteristics	157
5.8	Resistance, trim and rise for a hydrofoil system optimized for the displacement phase	158
5.9	SD8 Hysuwac, resistance improvements as a function of the foil lift fraction for the transition phase Froude number, $Fn_{\nabla} = 2.3$	161
5.10	Porpoising starts with tips of the bow foil emerging from the water (A). Loss of foil lift results in the vessel pitching down. The main foil impacts the water which is associated with strong spray from the leading edge of the foil (B). The vessel continues its downward motion (C) until the front foil lift is restored after which the bow begins to rise again (D) to repeat the cycle	164
5.11	A circular arc type hydrofoil being manufactured	166

LIST OF FIGURES

xix

5.12	Hydrofoil hull connection showing ideal connection	168
6.1	A Prout catamaran with a Hysucat foil system and an asymmetrical hull design	171
6.2	Comparison of the resistance-displacement ratio for symmetrical and assymetrical demi-hulls	172
6.3	A towing tank model showing a symmetrical bow which terminates in a vertical step.	173
6.4	Resistance displacement ratio comparison of a round-bilge and hard chine hull form	175
6.5	Body plans of investigated catamaran demi-hulls	177
6.6	Resistance comparison for similar round-bilge and hard chine hull forms with hydrofoil assistance	178
6.7	Illustration of chine tripping	179
6.8	Schematic pressure distribution on curved surfaces	181
6.9	Hydrodynamic principle of a trim tab and interceptor	183
6.10	Resistance and attitude of a semi-displacement hull showing the influence of a transom wedge. The bare hull includes the wedge.	185
6.11	Buttock lines of SD6 and SD7 hard chine hull designs	186
6.12	Resistance comparison for SD6 and SD7 hullforms with and without hydrofoil assistance.	187
6.13	The effect of forward shifts in LCG on resistance, trim and rise	189
6.14	Tandem body hydrofoil-assisted catamaran proposed by Shin et al.	190
6.15	Resistance and trim tendencies of tandem body catamaran with hydrofoils tested by Shin et al. [SYK96]	191
6.16	Residual resistance coefficient for semi-displacement catamarans	192
6.17	Comparison of L/D for different length-displacement ratios	193
6.18	Comparison of length-displacement ratios for conventional catamarans (solid line) and hydrofoil-assisted catamarans (dashed line and squares)	194
6.19	Resistance and trim comparison for the HC200A model	195
A.1	Drag coefficient as a function of span and chord panel density	204

LIST OF FIGURES

xx

A.2	Lift coefficient as a function of span and chord panel density	205
A.3	Lift and drag as a function of chordwise panel density and submergence.	206
A.4	Lift and drag as a function of spanwise panel density and submergence.	207
A.5	Variation of drag coefficient with panel size	208
A.6	Variation of lift coefficient with panel size	209
A.7	C_D , C_L and LCP as a function of chord-wise panel density for planing hulls	210
A.8	Drag, lift and centre of pressure as a function of span wise number of longitudinal strips	211

List of Tables

1.1	Speed regimes for high-speed craft	6
1.2	Hydrofoil-assisted catamaran ferries	13
2.1	Hulls with hydrofoil assistance model tested in this study	30
2.2	Form factors for mono-hulls and catamarans	46
3.1	Profiles used for investigating viscous effects	72
3.2	Comparison of lift curve slope correction factors	72
3.3	Comparison of zero-lift angle of attack	73
3.4	Particulars of hydrofoils used for investigating 3-dimensional viscous and free surface effects.	75
3.5	Viscous correction factors for wings under the free surface	75
3.6	Separation bubble sizes with and without turbulence stimulation	86
4.1	Main particulars of the SD6-F2 Hysuwac	123
4.2	Calculated results for cases 2 and 3 in relation to case 1	128
6.1	Main particulars of the SD7 and SD8 hulls	176
6.2	Main hull particulars of SD6 and SD7 hulls	184
C.1	Transport efficiency for conventional hydrofoil craft	219
C.2	Efficiencies of some designed and existing hydrofoil-assisted catama- rans. Those vessels marked with a '*' are designs that were developed from findings in this study.	220
C.3	Efficiencies of some existing hydrofoil-assisted mono-hulls	220

LIST OF TABLES

xxii

C.4 Efficiencies for some existing catamarans of different sizes 221

Nomenclature

$(1 + k)$	Form factor [-]
A_{FS}	Hydrofoil wetted area [m^2]
A_V	Frontal area exposed to wind [m^2]
B	Beam [m]
B_T	Tunnel beam [m]
c, C	Hydrofoil chord length [m]
C_A	Roughness addition [-]
C_{AA}	Air resistance coefficient [-]
C_B	Block coefficient [-]
C_{DF}, C_X	Hydrofoil drag coefficient [-]
C_{Dt}	Viscous interference resistance coefficient of hull on hydrofoils [-]
C_{F0}, C_F	Friction resistance coefficient [-]
C_L, C_y	Hydrofoil lift coefficient [-]
$C_{L\alpha}$	Hydrofoil lift curve slope [rad^{-1}]
C_P	Coefficient of pressure [-]
C_P	Prismatic coefficient [-]
C_R	Residual resistance coefficient [-]
D	Draft [m]
D_F	Total hydrofoil resistance [N]
D_{F0}	Hydrofoil profile drag [N]
D_{IH}	Hull interference drag [N]
D_{INT}	Hydrofoil interference drag [N]
D_L	Induced drag [N]
D_S	Spray drag [N]
d_s	Thickness of spray sheet [m]
D_{ST}	Strut drag [N]
D_W	Hydrofoil wave drag [N]
ep	Power ratio [-]
f	Hydrofoil camber [m]
Fn_L	Length Froude number [-]
Fn_{∇}	Volumetric Froude number [-]
F_0	Freestream velocity [m/s]
f_t	Lift curve slope correction factor due to foil thickness [-]
f_{α}	Lift curve slope reduction factor due to viscosity [rad^{-1}]
g	Acceleration due to gravity [m/s^2]

NOMENCLATURE

xxiv

h	Hydrofoil submergence below free surface, measured from quarter chord [m]
h_{sep}	Separation distance between bottom of hull and top of hydrofoil [m]
i_e	Half angle of entrance [deg]
k	Roughness height [m]
k_{corr}	Correlation coefficient
LCG	Longitudinal center of gravity [m]
L_{OA}	Overall length [m]
L_{PP}	Length between perpendiculars [m]
L_{WL}	Waterline length [m]
M	Spanwise number of panels
M_Z	Moments about z-axis [Nm]
N	Chordwise number of panels
\vec{n}	Unit normal vector
p	Pressure [Pa]
P_b	Brake power [W]
$p.c.$	Overall propulsive coefficient [-]
q	$0.5\rho V^2$
R_{AA}	Air resistance [N]
R_F	Friction resistance [N]
R_H	Hull resistance [N]
R_{ICAT}	Demi-hull interference resistance [N]
R_{IF}	Hydrofoil interference resistance [N]
r_{le}	Leading edge nose radius [rad]
Rn, Rn_L, Rn_c	Reynolds number, based on waterline length, based on chord length [-]
R_P	Hull Pressure Resistance [N]
R_{PI}	Pressure Interference resistance [N]
R_{PV}	Viscous pressure resistance [N]
R_R	Residual resistance [N]
R_S	Spray resistance [N]
R_{SR}	Spray rail resistance [N]
R_T	Total resistance [N]
R_{TM}	Model total resistance [N]
R_V	Hull viscous resistance [N]
R_W	Wave-making resistance [N]
R_{WB}	Wave-breaking Resistance [N]
R_{WI}	Wave interference resistance ([N])
R_{WP}	Wave-pattern resistance [N]
R_{WPr}	Hull pressure Resistance [N]
S_W	Hull wetted area underway [m^2]
t	Hydrofoil maximum thickness [m]
TF	Transport factor [-]
V	Velocity [m/s]
v	Perturbation velocity [m/s]

NOMENCLATURE

xxv

V_M	Model speed [m/s]
V_R	Wind or air speed [m/s]
V_{SR}	Mean velocity of spray sheet [m/s]
W	Impact velocity [m/s]
Wn	Weber number [-]
y	Height [m]
z	Lateral Distance [m]

Greek Symbols

α	Angle of attack [rad, deg]
α_0	Zero-lift angle of attack [rad, deg]
β	Deadrise angle [rad, deg]
Δ	Displacement mass [kg]
Δ_{hull}	Effective hull displacement when under hydrofoil assistance [kg]
$\Delta\alpha_0$	Free surface correction factor to α_0 [rad, deg]
ε	Resistance displacement ratio [-]
γ	Vortex sheet intensity per unit area [m^2/s]
Γ	Vortex intensity [m^4/s]
λ	Model to prototype scale ratio L/L_M
∇	Displacement volume [m^3]
ϕ	Angle between wind direction and direction of motion [deg]
ϕ	Velocity potential [m^2/s]
ρ	Density [kg/m^3]
σ	Water surface tension [N/m]
τ_{te}	Hydrofoil trailing edge closure angle [deg]
ν	Kinematic viscosity [m^2/s]

Subscripts

m	model
h, H	hull
a	atmospheric
S	surface
b	body
M, m	model scale
0	without hydrofoils
F	with hydrofoils
DH	demi-hull

Chapter 1

Introduction

Abstract

The hydrofoil-assisted catamaran is a hybrid craft consisting of a catamaran hull form assisted by hydrofoils mounted in the tunnel or underneath the hulls. Hydrofoil assistance is currently being applied and further researched for improving sea-keeping, wake wash as well as speed and efficiency of high-speed catamarans. The various craft that are currently in operation show considerable variation in design. This study attempts to clarify the hydrodynamic design for improving speed and efficiency of hydrofoil-assisted catamarans.

1.1 General

The design of hydrofoil-assisted catamarans is one of many developments in high-speed sea transportation that are currently being pursued worldwide. Initially, the catamaran hull form gained popularity in the early 70's, for vessels that were light weight, required large deck areas, improved sea-keeping and had a design speed requirement that fell within the semi-displacement to semi-planing speed ranges, where the catamaran's lower resistance could be utilized [FG72]. The most notable application of these vessels is the fast ferry industry.

The fast ferry industry is responsible for the majority of sales of high-speed catamarans worldwide and is the principle market for which the larger hydrofoil-assisted catamarans are being developed. The rapid expansion of the high-speed catamaran industry [Jef98] is resulting in it absorbing a larger share of the ferry market. Other notable markets for catamarans are high-speed pleasure craft and military patrol craft. Catamarans for these applications tend to be smaller vessels than their fast ferry counterparts and operate at higher Froude numbers. While catamaran ferries

are designed primarily on semi-displacement craft guidelines, the smaller patrol and pleasure craft tend to use semi-planing and planing, hard-chine deep-V hulls.

The concept of hydrofoil assistance is not new. It is based on the idea that the efficiency of a hydrofoil is far greater than that of any hull. It should therefore be possible to improve the efficiency (i.e. reduce the resistance) of a fast vessel if the hull is assisted partially by hydrofoils. Physically, hydrofoil assistance manifests itself as a decrease in draft for the hull, this in turn decreasing the wave-making and friction resistance of the vessel.

Based on this idea, patents for hydrofoil-assisted mono-hulls were entered as early as 1948 in the United States. Application of hydrofoil assistance for catamarans is slightly more recent. The idea was proposed by Turner et al. [TT68] in an early paper but no investigations were reported. Initial investigations of hydrofoil assistance were performed by the Soviets (see for example [YATR76]) from 1972 to 1981 for small craft operating at high Froude numbers. Hydrofoils are well known to have superior efficiency over planing hulls for volumetric Froude numbers:

$$Fn_{\nabla} = \frac{V}{g\nabla^{\frac{1}{3}}} \geq 2.5 \quad (1.1)$$

Therefore hydrofoils mounted in the tunnel between two planing demi-hulls of a catamaran, could easily provide better performance for planing speeds than an equivalent planing mono-hull.

In the sections that follow, the application of hydrofoil assistance for ferries, patrol craft and pleasure craft is discussed in more detail.

1.1.1 Fast Ferry Catamarans

Since 1981, hydrofoil assistance has been considered for the larger semi-displacement type catamarans of the fast ferry industry. To date a fair number of fast ferry catamarans have been either built or retrofitted with hydrofoil assist systems. Figure 1.1 shows the number of catamaran ferries launched with hydrofoil assistance during the last decade in relation to the number of conventional catamaran ferries. The large development effort in the early nineties by a number of countries aimed at developing hybrid-hydrofoil applications (see for example: [Mey92]) resulted in a peak in the production of hydrofoil-assisted catamarans. Subsequent discontinuation of some designs has led to the decline in the number of hydrofoil-assisted ferries being built.

The hydrofoil-assisted ferries in operation today are in the range of 18m to 45m in length and travel at speeds up to 45 knots. Investigations have been done for vessels over 100m in size and also for vessel speeds up to 60 knots.

Figure 1.2 shows two examples of hydrofoil-assisted catamaran ferries. The upper

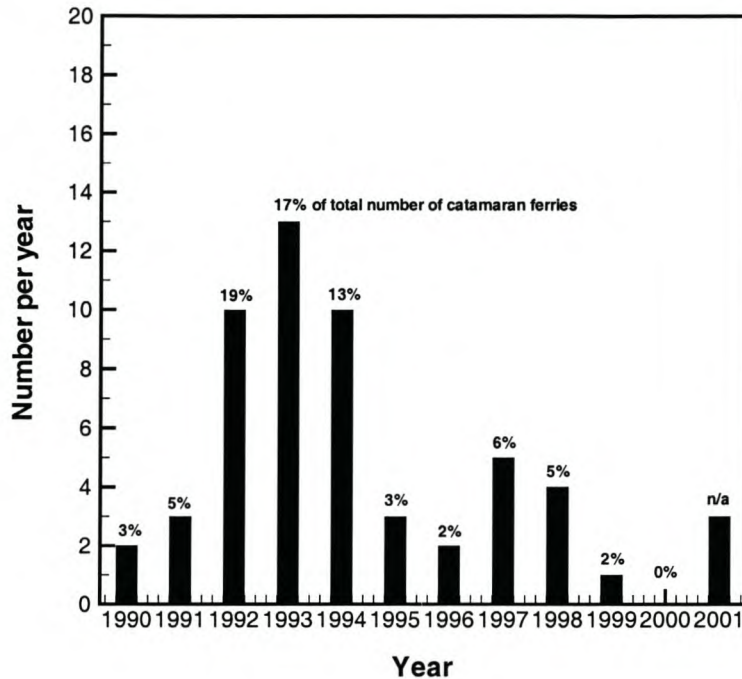


Figure 1.1: No. of hydrofoil-assisted fast ferries launched in the last decade, given as percentage of conventional fast ferry catamarans.

vessel has two canard foils located under the bow of each hull. On the after part, the vessel is planing on the hulls. The lower vessel shows an example of a low-wash semi-displacement catamaran fitted with a Hysuwac foil system¹, designed at the University of Stellenbosch.

1.1.2 Pleasure Craft

In the pleasure craft industry, hydrofoil assistance is seeing some application for smaller ski-boat type pleasure boats (5m to 12m) (see for example: [Hop99]) and also for some top-end motor yachts (20m-40m)(see for example: [Woo93]), primarily for increased speed and sometimes for improved efficiency. Application to motor yachts is still relatively recent and most vessels use a Hysucat² foil system. The numbers being built are few, as the market for these expensive vessels is small. Hydrofoil assistance has seen much more extensive application (350+ vessels) for the smaller (5m to 12m) planing type catamarans, also mainly using the Hysucat foil system. Figure 1.3 shows

¹The Hysuwac foil system is explained in more detail in Section 1.4.5

²The Hysucat development is explained in section 1.3.3

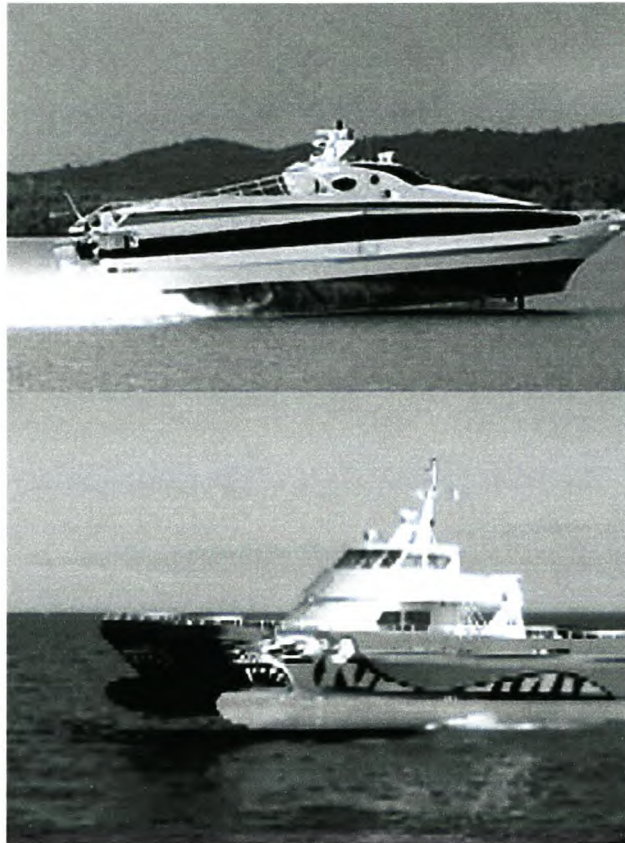


Figure 1.2: Two hydrofoil-assisted fast ferries. The upper 32m vessel (Autojet) is capable of 45 knots and has two canard foils located under the bow of each hull. The lower 40m low wash catamaran is capable of 45 knots and uses a University of Stellenbosch, Hysuwac foil system.

examples of two pleasure craft for which hydrofoils have been designed by Prof. K.G. Hoppe at the Mechanical Engineering Department of the University of Stellenbosch.

1.1.3 High-Speed Patrol Craft

To date the military of South Africa, Thailand, China and Israel [shi98] are using hydrofoil-assisted catamarans for patrol craft applications. With the exception of China, all these countries make use of Hysucat craft designed at the University of Stellenbosch. Hydrofoil assistance is well suited for this application. The long range and good seakeeping characteristics that are required of these vessels is well provided for by hydrofoil assistance. Figure 1.4 shows an example of a South African coastal patrol hydrofoil-assisted catamaran.

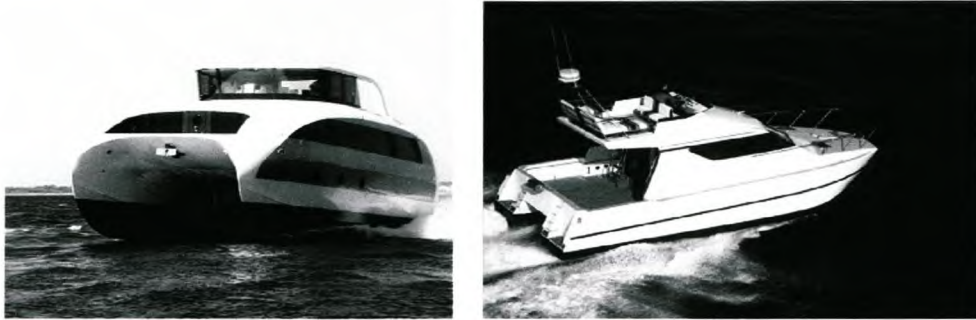


Figure 1.3: A 22m motor yacht capable of 45 knots (left) and a 12m, 42 knot motor boat (right), both assisted by Hysucat hydrofoil systems designed by Prof. K.G. Hoppe at the University of Stellenbosch.



Figure 1.4: A 22m coastal patrol catamaran using a Hysucat hydrofoil system. The vessel is capable of 36 knots.

1.2 Past, Present and Future Developments

Hydrofoil-assisted catamarans can be classed as one of three types [BLSZ95a] according to their foil design:

- Fixed fully submerged foils for seakeeping and resistance improvements
- Surface piercing hydrofoils fully unloading the hull at top speed only
- Active fully submerged foils for resistance and seakeeping improvements.

Of these, the first and third types have found commercial application to date. To gain a better understanding of the development and application of hydrofoil-assisted catamarans, it is useful to review the variety of hydrofoil-assisted catamaran designs that are in use. The sections that follow present examples of each. These vessels are

discussed in some detail, as they will often be referred to in this text for the purpose of example. Many other hull-foil combinations than those mentioned here exist and have been patented. Only those designs that have had significant bearing on current successful developments are included.

It is often useful to compare different vessels by plotting the resistance curves in relation to general tendencies for high-speed craft. Figure 1.5 [Sch73] shows such a diagram of resistance tendencies of high-speed craft. Included are the general tendencies for hydrofoil craft, semi-displacement craft and planing craft. It is also useful to know the basic speed regimes that drive the basic hull shape choice (i.e semi-displacement, semi-planing or planing). The literature shows some variation in definitions for semi-displacement, semi-planing and planing Froude numbers. The notation used throughout this study is one adopted from Almeter [Alm93] and is summarized in Table 1.1.

Regime	Fn_{∇}	Support
Semi-Displacement	$1.5 < Fn_{\nabla} < 2.5$	mostly buoyancy
Semi-Planing	$2.5 < Fn_{\nabla} < 4.0$	buoyancy & dynamic forces
Fully Planing	$Fn_{\nabla} > 4.0$	almost entirely dynamic forces

Table 1.1: Speed regimes for high-speed craft

Figure 1.5 shows the superiority of the catamaran hull form for $1.5 < Fn_{\nabla} < 2.5$. Both hard chine deep-V and semi-displacement catamarans are superior over their mono-hull counterparts due to their slender hull form minimizing wave-resistance. The slender semi-displacement catamaran is one of the most efficient hull forms for semi-displacement vessels³. For the semi-planing range, catamaran and mono-hull designs are in use and most are of the hard chine deep-V type, taking advantage of some dynamic lift. For planing speeds $Fn_{\nabla} > 4.0$, the hard chine deep-V mono-hull form is superior over other basic hull types. The complete superiority of hydrofoils for $Fn_{\nabla} \geq 2.5$ is also clearly apparent and intuitively indicates that, combined with the correct hull form, they can improve the performance of a conventional hull.

1.3 Early Developments

1.3.1 Pioneering Soviet Research

Initial investigations into the concept of assisting a catamaran hull with hydrofoils, started in the USSR in 1972 [YATR72, YATR76]. Tests were conducted for catamarans with plane internal sides. Between one and three hydrofoils were placed in the

³Trimarans can offer better resistance characteristics in some cases.

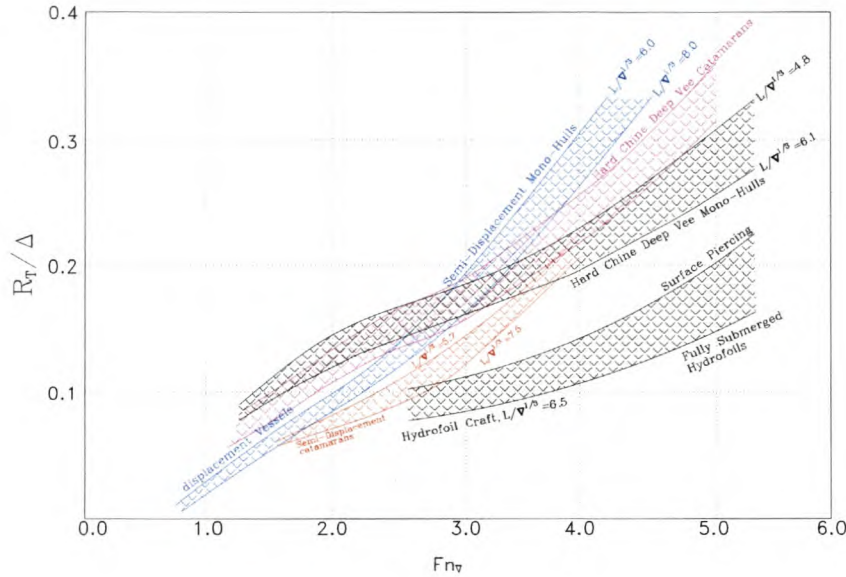


Figure 1.5: Resistance tendencies of high-speed craft

tunnel and optimized. Initial tests were carried out for heavily loaded semi-planing hulls that were typical of that time ($L/\nabla^{1/3} = 3.1 - 5.0$). Russian semi-planing and planing hulls were based on the MBK and BK series mono-hulls [EBS78] and these early tests on hydrofoil assistance used the MBK series hulls that were split along the symmetry plane to form two asymmetrical planing demi-hulls. Very little information is given in the literature on the foil particulars, but the results show that hydrofoil assistance proved to be successful in improving the resistance of the vessels for $Fn_{\nabla} \geq 1.2$, using two or three foils that are of similar type to those used on conventional Russian hydrofoil craft, i.e. circular arc type profiles. Figure 1.6 shows the resistance comparison. Further research was conducted in the 1990's to extend the designs to improve the sea-keeping characteristics of catamarans [Kru95].

1.3.2 The Hycat Development

The Hycat is a design of Prof. D.E. Calkins in the U.S.A. based on model tests conducted in the early 80's [Cal81, Cal84]. The Hycat design is interesting in the sense that it incorporates a hull specifically designed to suit its hydrofoil system that

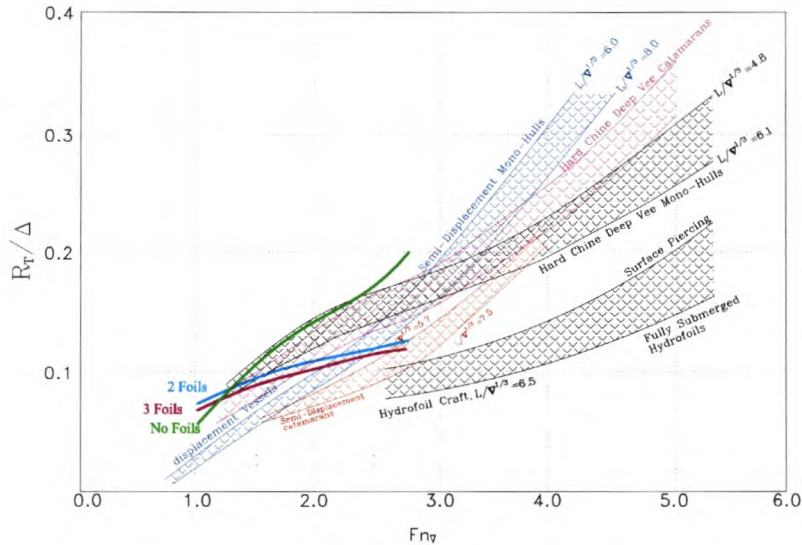


Figure 1.6: Resistance tendencies of early Soviet hydrofoil-assisted semi-planing catamarans

has been derived from the slender SES⁴ hull form. The vessel was designed for semi-planing speeds so the hull is a hard-chine deep-V type, with extended keels, so that the foils can operate more deeply submerged. The idea is sound but unfortunately the measured vessel performance was very poor. This is partially due to incorrect towing tank measurement techniques of that time⁵. Figure 1.7 shows the principal layout and its resistance comparison.

1.3.3 The Hysucat Development

In 1979, Prof. K.G. Hoppe initiated the Hysucat development [Hop80] at the University of Stellenbosch in South Africa, launching the world's first hydrofoil-assisted catamaran prototype in 1982. Since then over 350 Hysucats have been built ranging from 5.5m to 36m. The Hysucat design has been patented [Hop82] internationally. The basis of this study is formed largely on the experience gained out of the Hysucat development. Of all the early developments described in this section, the Hysucat

⁴Surface effect craft.

⁵Chapter 3 examines the problems and complexity of model test procedures for hydrofoil-assisted craft.

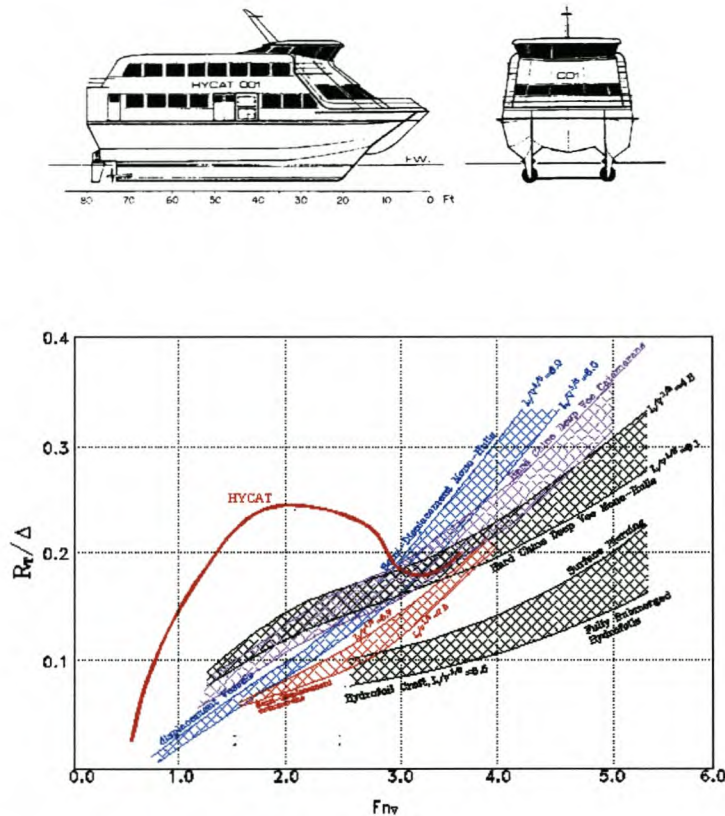


Figure 1.7: Hycat layout and resistance

development is still ongoing and the most successful today. It is therefore appropriate to give a detailed review of this successful design.

Figure 1.8 shows the original principle configuration for the foils and Figure 1.9 a typical resistance tendency. The system was developed for use on semi-planing and planing catamarans and consists of a main foil just ahead of the longitudinal centre of gravity (LCG) and usually one or two stern trim foils operating close to the free surface. The main foil is usually located at keel depth and the stern foils some distance above the keel. The stern foils provide trim stability by utilizing the free surface effect and their positioning above the keel ensures that the correct trim is taken up by the vessel. Both foils consist of circular arc profiles. At semi-planing and planing speeds the main foil is designed to carry between 40% and 75% of the weight, depending on size and displacement of the vessel.

Hysucats usually utilize fully asymmetrical hulls⁶ with plane internal sides. This allows a more even flow over the foils. A hard chine deep-V hull form has been designed

⁶The system has been successfully applied to a number of symmetrical planing catamaran hull designs as well.

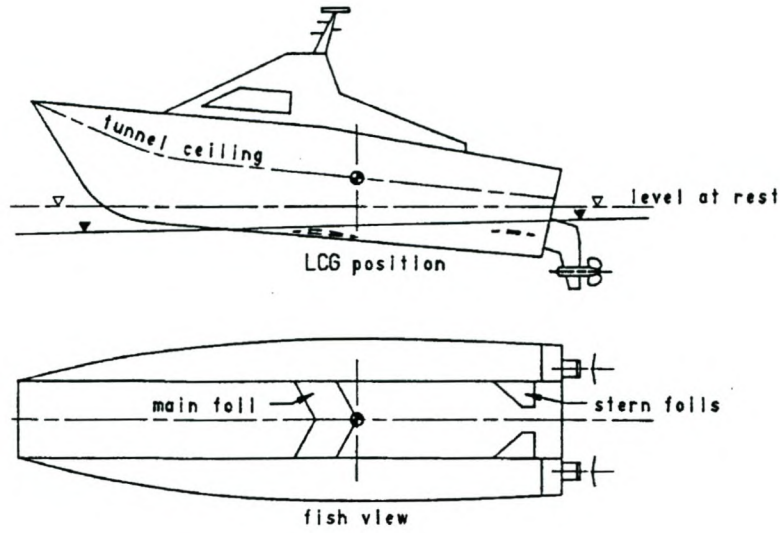


Figure 1.8: Layout of the Hysucat design

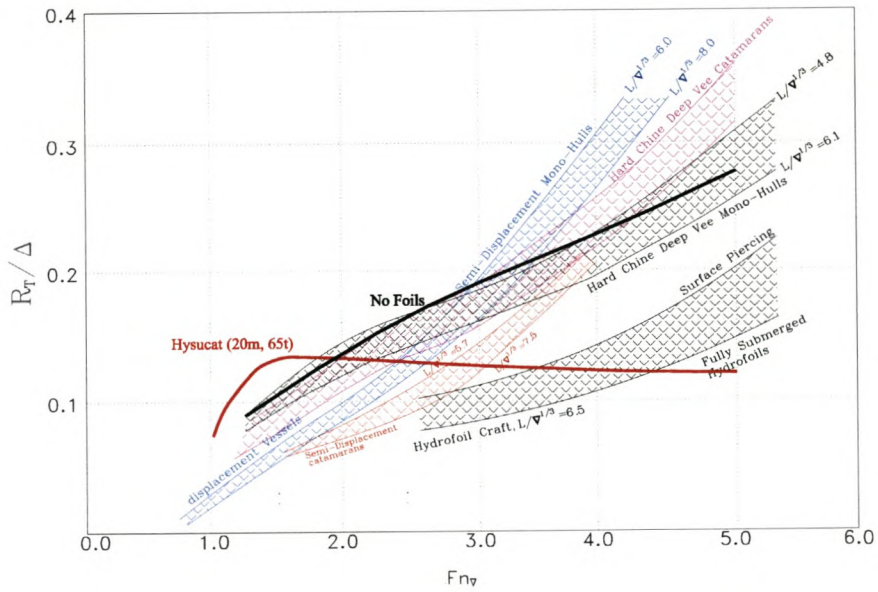


Figure 1.9: Resistance tendency for a Hysucat

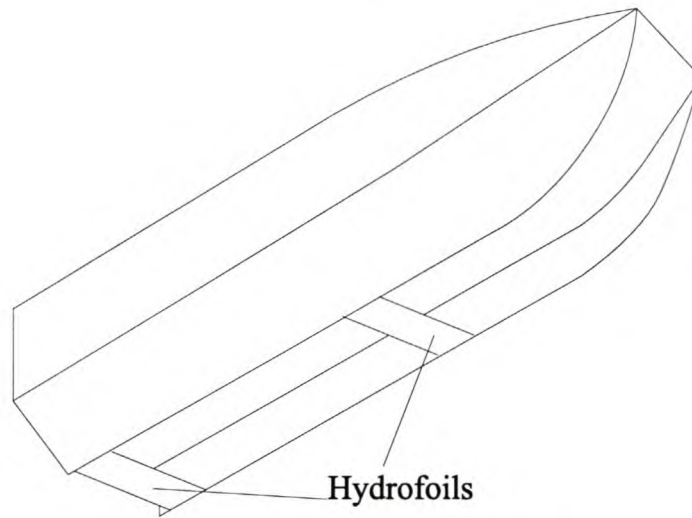


Figure 1.10: Layout of Chinese channel hydrofoil boats

and optimized by Prof. K.G. Hoppe specifically for the Hysucat. It incorporates novel ideas into the tunnel shape, spray rail design and bow sections of the hull. Results obtained during the development show that resistance improvements of up to 40% are achievable with the foil system for semi-planing and planing speeds. The low lift carrying capability of the foils at semi-displacement speeds, results in a slight increase in resistance in the lower speed range. The speed where the foils generate enough lift to improve resistance is usually at $Fn_{\nabla} \approx 2.2$.

1.3.4 Chinese Channel Hydrofoil Boats

China has adopted a very similar development to that of the Hysucat since 1989. The vessels are known as channel hydrofoil boats [Zha94, ZLH97] and make use of asymmetrical planing hull forms very similar to the Hysucat, but use two tandem hydrofoils located at keel depth as shown in Figure 1.10.

Model tests were performed at the Jinmen towing tank in China for various tunnel widths and displacements representing length-displacement ratios $L/\nabla^{0.33} = 6.3 - 7.2$ and for Froude numbers, $1.25 \leq Fn_{\nabla} \leq 6.0$. The tunnel width of the design is narrow at 70% of the demi-hull beam. Two identical foils with circular arc sections were tested corresponding to 50% and 20% of the chine length from the transom.

The narrow tunnel results in these vessels having a high hump resistance without hydrofoils. With hydrofoil assistance, resistance improvements are obtained across the whole measured speed range including the hump resistance speed, which is achieved

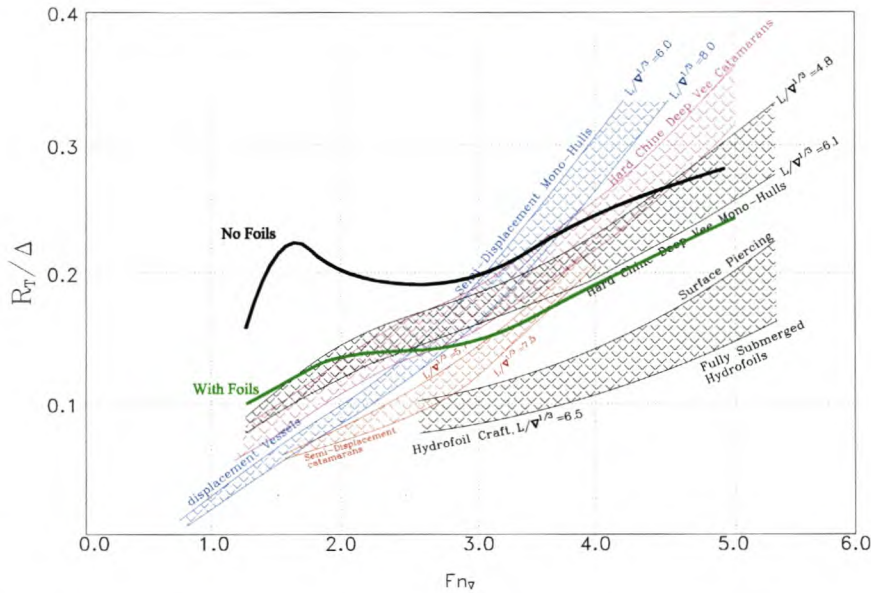


Figure 1.11: Resistance comparison for Chinese channel hydrofoil planing boat with $L/\nabla^{0.33} = 7.2$

by optimizing the hump trim angle with adjustable trim tabs. A representative model test result is shown in Figure 1.11.

1.4 Recent Developments

The 1990's saw the development of the first hydrofoil-assisted catamarans designed for operation in the semi-displacement speed range. Additionally, a number of large (30m+) hydrofoil-assisted catamarans were developed to operate at semi-planing speeds as well. These vessels were developed for the fast ferry industry. Japan, Norway, Russia, South Africa, USA and South Korea were the main players in this initiative. A summary of the vessels currently in operation is given in Table 1.4 and a technical review of the vessels given in the subsections that follow.

1.4.1 The Hitachi Zosen Development

The "Hydrofoil Catamaran" (HC series) was developed by Hitachi-Zosen in conjunction with the University of Tokyo, based on Hitachi's experience and technology building Supramar surface piercing hydrofoils. A large number of publications are available on these vessels (see for example [Miy89, AMKH93]). The basic design is currently available as 30m (40 knots) and 40m (45 knots) fast ferries which have achieved great

Vessel	First Launched	L_{OA}	Speed	Power[kW]
Hitachi-Zosen Superjet 30	1992	32 m	34 knots	3680
Hitachi-Zosen Superjet 40	1996	40 m	42 knots	4046
Hyundai	1994	46 m	35 knots	6122
Daewoo F-CAT 40	1994	40 m	40 knots	4000
MTD Canard-Interceptor	1998	32 m	45 knots	2940
Waterfront Charters/T-Craft	1999	20 m	35 knots	2000
Halter Marine E-Cat	1999	40 m	45 knots	4000

Table 1.2: Hydrofoil-assisted catamaran ferries

success in the high-speed ferry industry in Japan with nine vessels currently in operation. Figure 1.12 shows the basic outline of the design plus a photo of a model test. Figure 1.13 shows the resistance comparison for a model test and clearly indicates the efficiency of the foil system at semi-displacement speeds. The data is not correlated to prototype scale, so the viscous resistance deduction is not included. The design is characterized by its use of very slender demi-hulls similar to those used on SES craft. A wide tunnel width is utilized, allowing high aspect ratio foils to be fitted in the tunnel. This slender hull shape with V-shaped cross-sections, reduces the wave-making resistance of the hull and minimizes the flow disturbance to the foils.

Up to four circular arc type hydrofoils in tandem were model tested during the development of these vessels. Later a half scale sea-going test vessel was built and evaluated [KMYT91]. The final design utilizes two foils that span the hulls at keel level in tandem and ninety percent of the vessel's weight is carried by the foils at design speed. The design shows substantial improvement in resistance for the vessel with foils for $Fn_{\nabla} \geq 1.5$ giving the vessel good performance in the semi-displacement speed range. Based on the success of the design, China has since 1994 followed a similar line of development, designing ferries for its inland waterways [LLYY94].

1.4.2 The Hyundai Development

Hyundai Heavy Industries of Korea have developed a semi-displacement hydrofoil-assisted catamaran for long range and high-speed use [Min91, Min92]. The foils were intended to provide improved resistance and sea-keeping characteristics. Round-bilge hull forms are used with tandem hydrofoils placed in extreme positions fore and aft to improve the sea-keeping characteristics. Figure 1.14 shows the basic hull and foil layout and Figure 1.15 the published resistance data. The figure shows data for hull without foils and the hull with foils for two fixed trim conditions (0 and 2 degrees). The data are for the foils carrying 70% of the load at a design speed of 40 knots. The final design used foils carrying 40% of the displacement at design speed.

INTRODUCTION

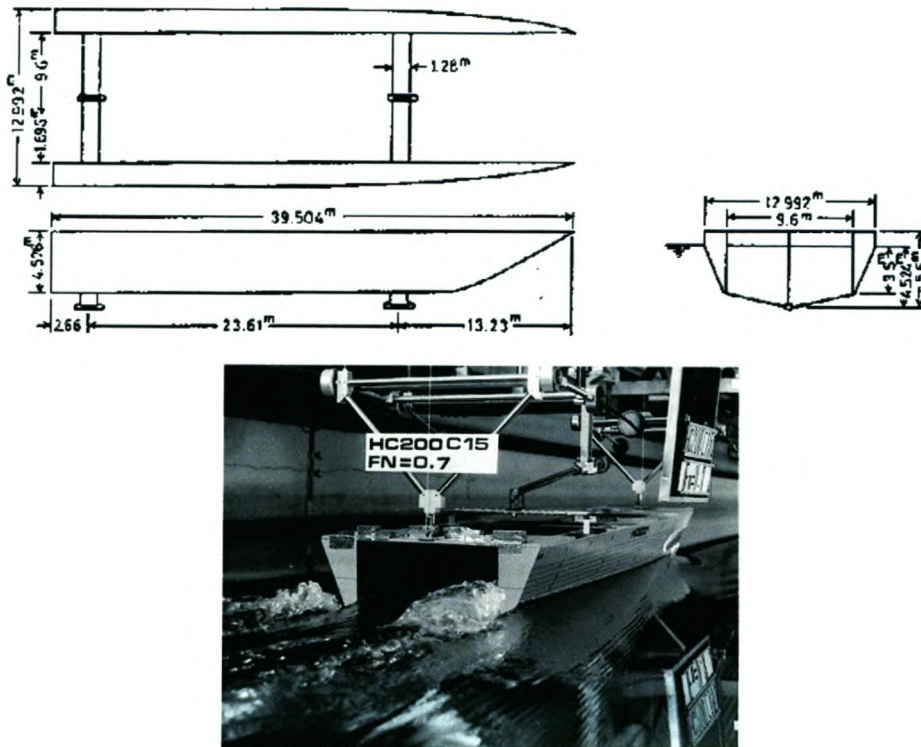


Figure 1.12: Hitachi Superjet30 and its hull-foil configuration

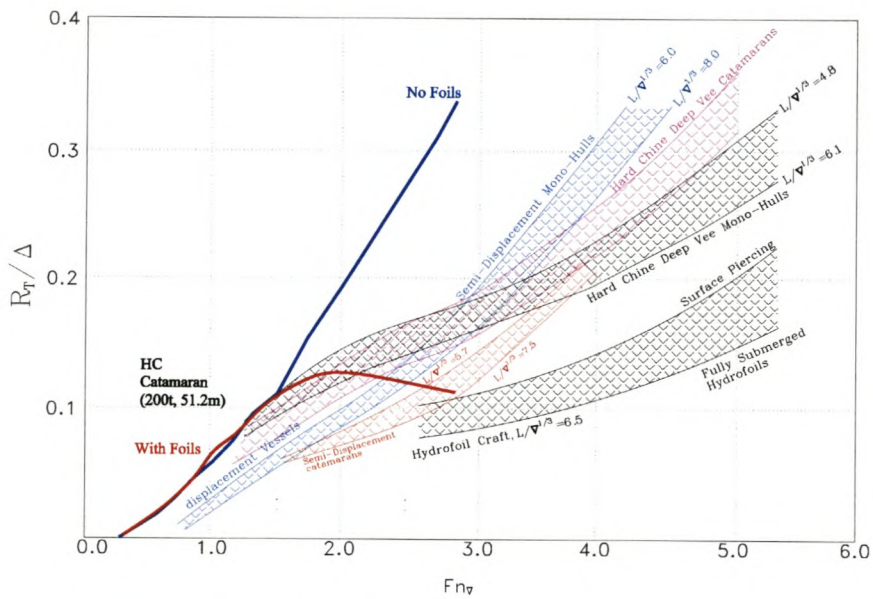


Figure 1.13: Hitachi Superjet model test result

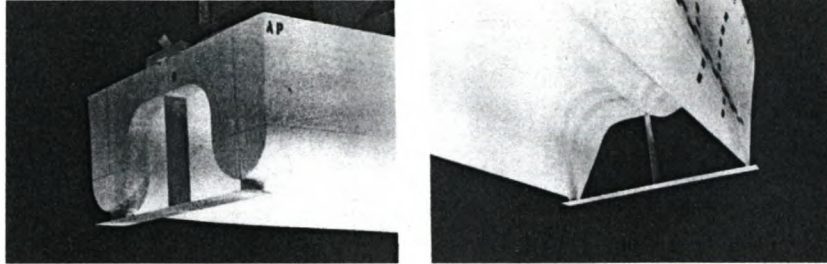


Figure 1.14: Hyundai hydrofoil-assisted catamaran hull and foil layout

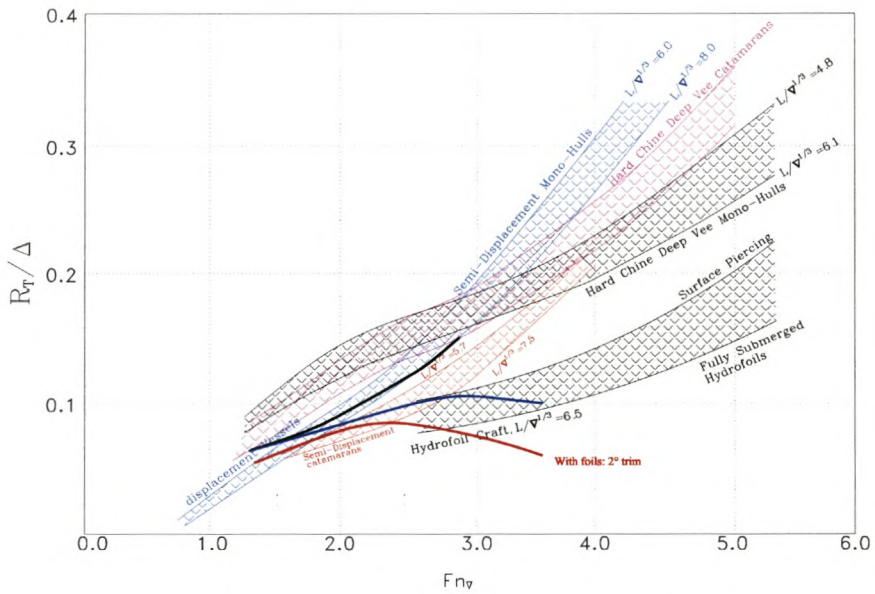


Figure 1.15: Resistance comparison based on model test data. Data without foils is shown as a black line. Data with foils is given for fixed even running condition (blue line) and at a fixed trim angle of 2 degrees (red line)

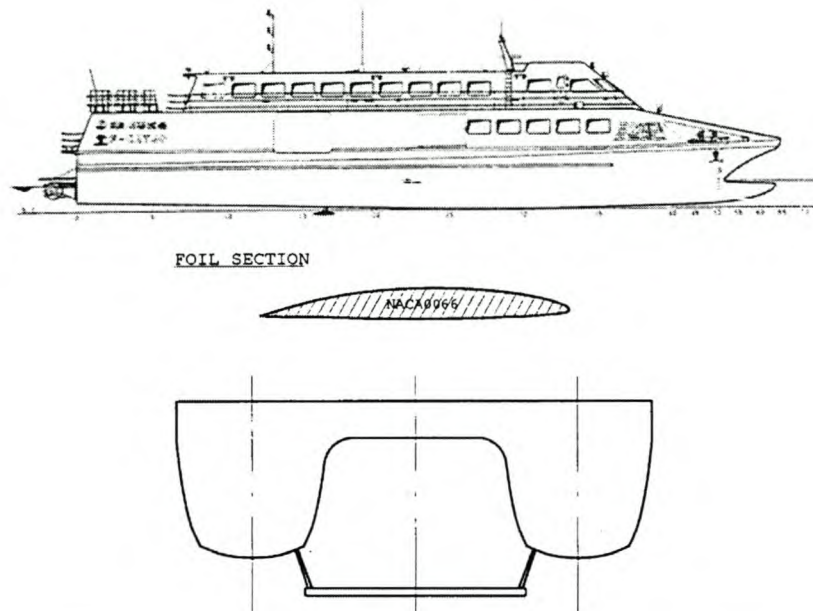


Figure 1.16: Daewoo hydrofoil-assisted catamaran with an illustration of the mono-foil

1.4.3 The Daewoo Development

Daewoo Shipbuilding of Korea has developed a hydrofoil-assisted catamaran (F-CAT 40) [KYS⁺93] that uses a single passive hydrofoil (NACA 66 section) just aft of the LCG below keel depth. The foil develops lift equal to 25% of the displacement and decreases the resistance by 15% at design speed. This allows an increase in speed of about 2.5 knots for the 42m vessel, bringing its maximum speed to 40 knots which corresponds to a volumetric Froude number, $Fn_{\nabla} = 2.8$.

The vessel and its foil system are shown in Figure 1.16. Daewoo compared a number of hull designs and found that a hard chined hull gave better resistance characteristics than the round-bilge form. Comparisons for the various hulls with and without foils show that the resistance is higher for the vessel with foils over a large portion of the speed range. The foil brings improvements from about 29 knots onward. This is understandably similar to the Hysucat resistance tendencies shown in Figure 1.8 as a single foil is not capable to provide the necessary lift at low speeds. The resistance data is shown in Figure 1.17.

1.4.4 The Canard-Interceptor Hydrofoil-Assisted Catamaran

One of the most recent additions (1998) to the hydrofoil-assisted catamaran range is the canard-interceptor concept pictured in Figure 1.2. The vessel is designed for



Figure 1.18: Model of the Autojet hydrofoil system

catamarans and is designed to minimize hull-foil and fore-aft foil interference effects. The efficiency of this design was proved by several series of model tests and further through industrial applications, all of which have formed part of this study.

Figure 1.19 shows the preferred foil layout of a Hysuwac application for a car ferry. The lower vessel (the Halter Marine E-Cat) pictured in Figure 1.2 on page 4 is an example of a craft using Hysuwac foils. The system makes use of one or two bow foils⁷ mounted underneath the tunnel and a stern foil mounted in the tunnel. The system is advantageous in reducing the hump resistance and achieving an efficient high-speed resistance. Figure 1.20 presents a typical resistance tendency for an optimized Hysuwac vessel.

1.5 Current and Future Research

In reviewing the developments that have taken place up to the present time, the variety of designs is quite obvious. The basic foil configurations that have proven successful are summarized in Figure 1.21.

There is on-going research effort by several teams worldwide to improve on the current state of the art. The main players in this effort are commercial and research institutions in Australia, Norway, Russia, China, Germany, Japan, South Korea, South Africa, New Zealand and the United States. Most of these developments are aimed at the fast ferry industry. The smaller planing type craft for military and pleasure craft are easier to design and this technology is well established. At the University of Stellenbosch the level of expertise has been reached that allows designs for such craft to be made without the need for model tests [Hop99] in many cases as a theory

⁷Two foils would be arranged with one underneath each hull.

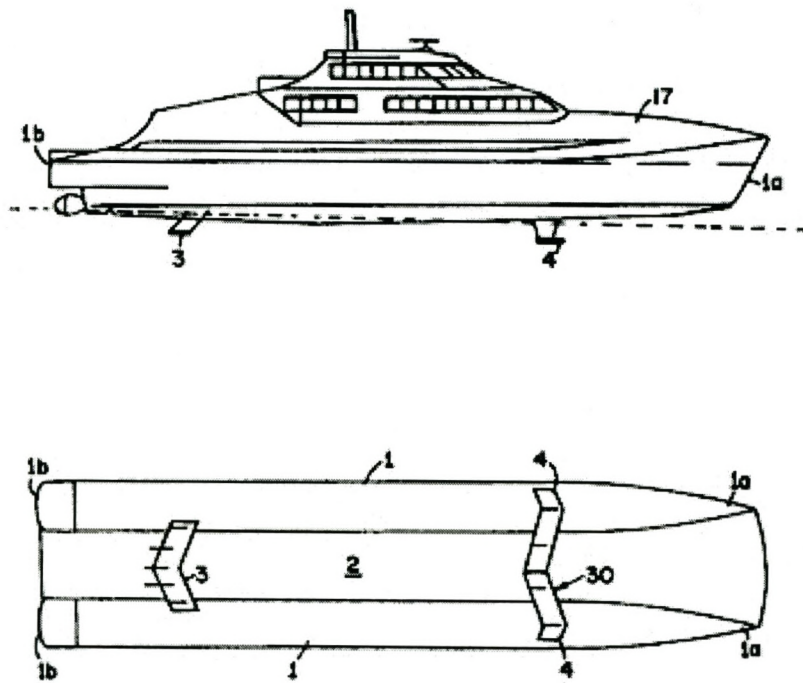


Figure 1.19: Layout of the Hysuwac foil design

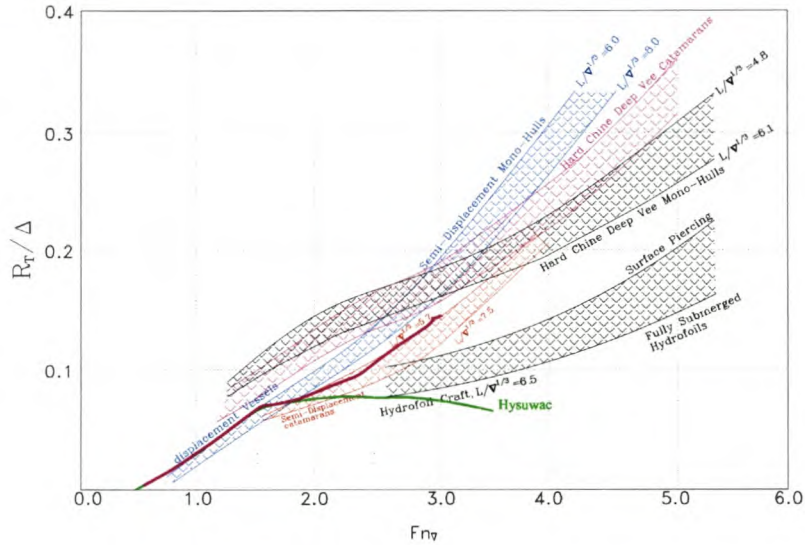


Figure 1.20: A typical Hysuwac resistance tendency

has been developed for Hysucats and implemented as a computerized model. The technology for the large (30m+) semi-displacement and semi-planing vessels is still under development and needs further research.

Figure 1.22 gives an indication of how research and development has progressed over the last decade, from which it is clear that the approximate number of research papers published per year for the last decade and clearly indicates that initial development peaked in 1993. A drop off in the development took place during 1994-2000.

2001 has been some renewed interest in the concept. The fast ferry industry is realizing the potential benefits⁸ that hydrofoil assistance can potentially supply: greater capacity, improvements in speed, range, fuel consumption, a reduction in wave-wake generation as well as improved transport efficiency and sea-keeping. Each of these issues is discussed in more detail in the sections that follow.

1.5.1 Speed, Range and Efficiency

These three factors are considered together because they are inextricably linked. Fast ferry, pleasure craft and military craft markets have shown requirements for increased

⁸Many of these would equally apply to the large pleasure craft and military craft as well

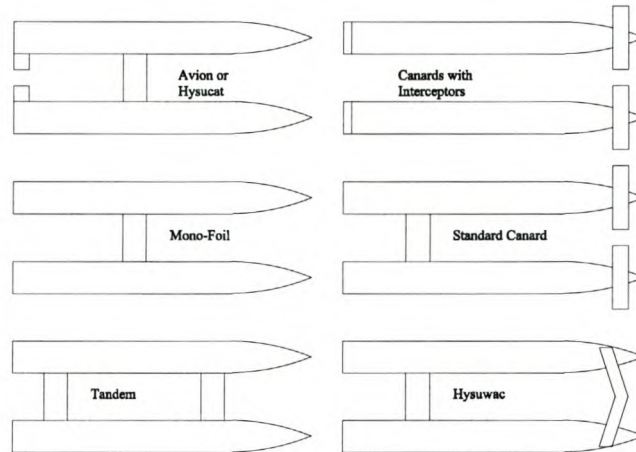


Figure 1.21: Summary of foil configurations currently in use

speed capability [Jef98]. For military craft this is closely linked with the need for long range. Fast ferries are usually more concerned with efficiency to minimize operating costs.

Efficiency can be presented in terms of some form of transport efficiency for a vessel. A number of different ways of defining transport efficiency exist. A useful dimensionless form [Hop91c, Hop91d, KLT98] is the one defined by the equation:

$$ep = \frac{1}{TF} = \frac{P_b[kW]}{g[m/s^2] \cdot V[m/s] \cdot \Delta[t]} = \frac{\varepsilon}{p.c.} \quad (1.2)$$

where ep is the so-called power ratio, which represents a non-dimensional relationship between weight, design speed and the installed power of a craft. A number of studies [Hop91c, Hop91d, McK97, KLT98, Hop99, MHK01] have been done that investigate transport efficiency for both commercial and military applications. Plotting transport efficiency as a function of the Froude number provides a useful means of comparing the efficiency of different craft. Figure 1.23, developed from the data available in

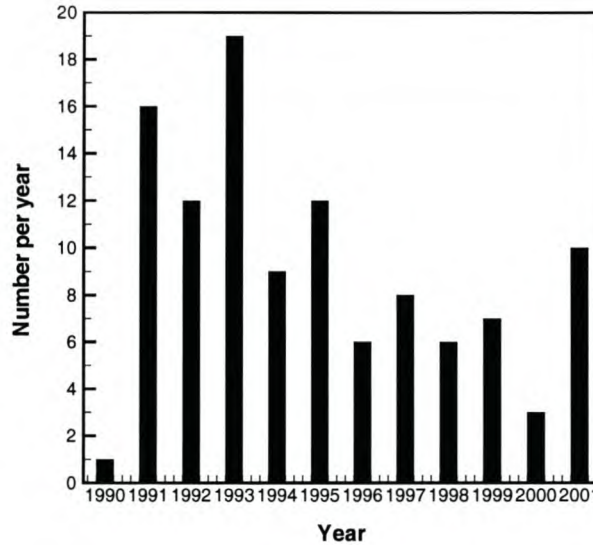


Figure 1.22: Number of research papers published per year

the public domain, shows the typical tendencies for different vessel types including semi-displacement mono-hulls and catamarans and planing craft. For these vessels, the main parameter influencing efficiency is the length-displacement ratio, $L/\nabla^{1/3}$, therefore efficiency tendencies are presented as a function of this parameter.

Also included in the figure is the curve of what was considered 'state of the art' for semi-displacement and semi-planing vessels (including multi-hulls) in 1997 [McK97]. For comparison, the transport efficiency of some existing catamarans, hydrofoils and hydrofoil-assisted catamarans is plotted in the figure. These include available data from the public domain as well as Hysucat and Hysuwac vessels based on prototype and model test data collected during this study. To date only one conventional catamaran has surpassed the state of the art curve for semi-displacement and semi-planing craft through use of a novel propulsion arrangement [SE95] for high efficiency.

The data of some of the craft used in the figure are given in Appendix C. From this data the state of the art tendencies for hydrofoil craft and hydrofoil-assisted catamarans can be constructed. It can be seen that the majority of hydrofoil-assisted catamarans offer better efficiencies than the state of the art for semi-displacement and semi-planing craft including catamarans. Further it can be seen that the state of the art for hydrofoil-assisted catamarans is superior to that achievable by conventional hydrofoil craft.

Comparing passenger catamarans, which are shown as green squares in Figure 1.23, with hydrofoil-assisted catamarans (also passenger vessels) one sees that hydrofoil-

assisted catamarans offer superior efficiency to passenger catamarans for $Fn_{\nabla} \geq 2.0$ and it can therefore be said that based on current technology hydrofoil assistance is a viable option for catamarans if the design speed and displacement fall within the range $Fn_{\nabla} \geq 2.0$.

1.5.2 Wake Wash

Wake wash is a recent problem encountered by the high-speed ferry industry and has become an issue of contention in Denmark, Sweden, Ireland, Australia, New Zealand, England, Germany, Portugal and the United States [Jef98]. Wake wash refers to wave height and energy of the wave train originating from a vessel. In sensitive areas it has been found that the wave wake from high-speed vessels is severely damaging the coastline and poses a danger to small boat users and children on beaches.

A number of catamaran manufacturers now offer low wake ferry designs for operation in sensitive areas, although their effectiveness has not been proven at the time of this writing. Hydrofoil-assisted catamarans can potentially be designed to fulfill many of these requirements as well. Because the foils lift the hull partially out of the water (i.e. reduced transom immersion and waterline length) the wave generation from the hulls can be reduced. There is of course the additional waves generated by the hydrofoils to be considered.

Preliminary investigations by Washington State Ferries [Stu00], Halter Marine and the University of Stellenbosch show that hydrofoil assistance is beneficial to reducing catamaran wake wash. The wake wash of the 45m vessel, pictured in Figure 1.2, was measured before and after being fitted with a Hysuwac hydrofoil system. Improvements of 19% and 21% in wash height and energy density respectively were obtained. This is significant as the foil system was optimized for increasing the speed of the vessel and not for wash reduction. So far no research has been done on optimizing hydrofoil systems for wake wash and developments in this field are still in their infancy. Research is hampered by the fact that wake wash cannot be measured in a standard towing tank and needs specialized wide model basins with large models or prototype testing. It is therefore not considered further in this study.

1.5.3 Sea-Keeping

Improvements in sea-keeping using hydrofoils is well known (see for example [MYS93, BLSZ95a, Kru95, Wel98a]) and a number of companies worldwide specialize in providing high-speed craft with computerized ride control systems making use of small hydrofoils. T-foils mounted forward which use incidence control, active flaps or a combination of both provide motion control. Figure 1.24 shows a typical active T-Foil installation on a large catamaran.

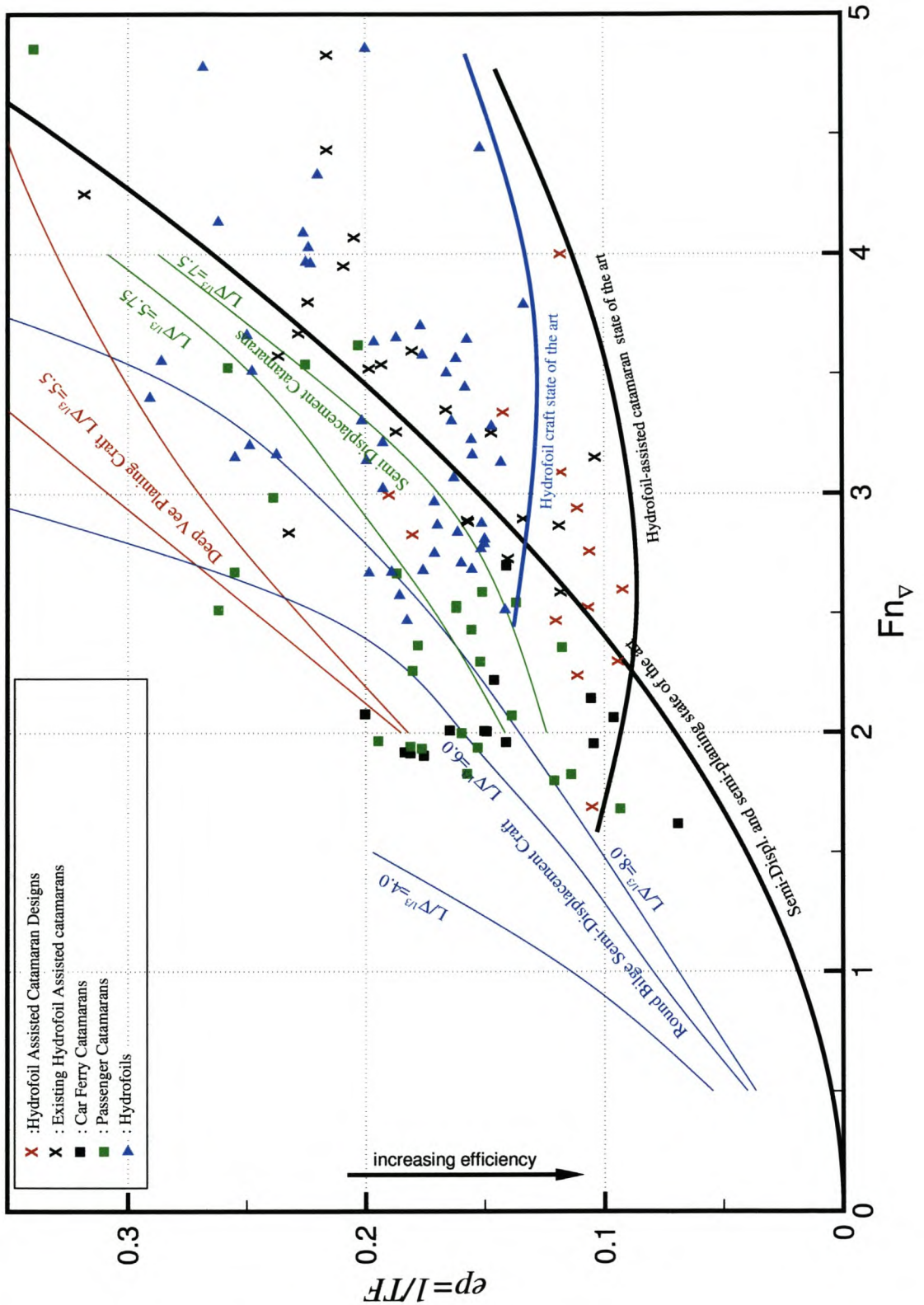


Figure 1.23: Transport efficiency of fast craft in relation to some hydrofoil-assisted catamarans



Figure 1.24: A motion control T-foil fitted to the bow of a catamaran demi-hull developed by Maritime Dynamics Inc.

These ride control foils are usually small in relation to the vessel size and are often detrimental in terms of resistance. In some cases [Min92, AYTS93, Min93] the ride control system has been incorporated into a set of larger high lift foils designed to also reduce resistance, although this is done at the expense of significant extra complexity. This is justified by the dramatic difference in vertical accelerations and motions between active and passive foils. Figure 1.25 shows the difference in accelerations for the Hyundai hydrofoil-assisted catamaran discussed in Section 1.4.2, comparing the unassisted catamaran with passive and active hydrofoils [Ada95].

The main design effort for seakeeping foils is design of the mechanical systems and the computer control system coupled with the hydrofoils to reduce motions. Hydrodynamic design is mainly limited to avoidance or minimization of cavitation. The design of motion control foils is very much a speciality that is a well developed industry and is not considered further in this study.

1.6 Design of Hydrofoil-Assisted Catamarans

The technical developments in hydrofoil-assisted catamarans and application of these vessels clearly shows that the uses for hydrofoil assistance are numerous but the lack of knowledge and understanding amongst designers, particularly for semi-displacement and semi-planing vessels, has limited the number of vessels being produced to a handful each year in relation to the number of conventional catamarans being built. All the vessels designed and built have been the result of an extensive development effort, often including manned models to verify design predictions. Much research, design and operational experience is still necessary for these vessels to become established and be designed with relative ease.

There are two potential design types for hydrofoil assistance: firstly, new vessels, where the foil system and hull are designed to match, and secondly, hydrofoil retrofits to existing vessels. In the latter case, the hydrofoil has to be designed to match an existing hull. This usually results in a less than optimal foil system but one that can

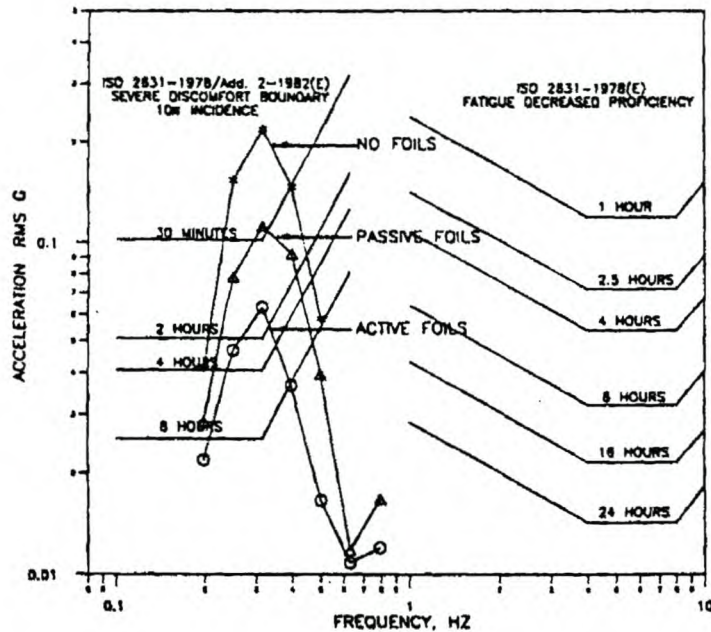


Figure 1.25: Vertical accelerations on the Hyundai hydrofoil-assisted catamaran with active and passive hydrofoil assistance

nevertheless bring substantial improvements in efficiency, sea-keeping etc. For new vessels, where the hull and hydrofoil can be designed to match, there is much more scope for variation of foil and hull parameters to achieve the optimum solution.

To date very little published information is available that specifically focus on hydrodynamic design principles for hydrofoil-assisted catamarans, which could provide guidelines for designers. This lack in information is in spite of quite a large body of literature (in excess of 100 papers) that is publically available on hydrofoil-assisted catamarans and is primarily due to three reasons. Firstly, the competitive nature of the industry at present and the value of this type of research to industry, secondly, the cost of doing basic research into the development of these vessels and thirdly, the hydrodynamic complexity of the problem.

At present it is not easy to design these vessels with any certainty in their performance without extensive model testing. Model testing is required not only for performance prediction, but is a necessary design tool in many cases. New hydrofoil systems usually need to be matched to a hull design through systematic optimization that is often only possible in the towing tank. In some cases it is desirable to test large manned models

as model tests cannot always be considered as very reliable⁹.

1.6.1 Objectives

Of the three main areas of research (speed and efficiency, sea-keeping and wake-wash), this study focuses on the *hydrodynamic design of hydrofoil-assisted catamarans for improvements in speed and efficiency*. Focus is placed on *modern high-speed symmetrical catamarans* operating at *semi-displacement* and *semi-planing* Froude numbers. These vessels and Froude numbers cover the majority of catamarans in operation today. Smaller asymmetrical planing catamarans will be covered in less detail as their use and design has been covered by Hoppe in various publications [Hop80, Hop91a, Hop91b, Hop99]. Attention is placed on fixed, passive (as opposed to actively controlled) hydrofoils as the hydrodynamic principles governing these craft can be investigated sufficiently without introducing the extra complication of actively controlled foils.

The main objectives are:

1. To investigate the suitability of hydrofoil-assistance for use on semi-displacement and semi-planing type catamarans as there is limited knowledge on the use of hydrofoil-assistance for these vessels.
2. To improve the current understanding of the hydro-mechanics governing the performance of hydrofoil-assisted catamarans. Such knowledge will allow more efficient design so that new ships can be designed with efficiencies that are close to 'state of the art'.
3. To further improve and develop experimental techniques of suitable accuracy for design. Research relies heavily on experimental techniques and therefore their accuracy should be as good as possible.
4. To develop a suitable theoretical method that can be used as a design tool. To date there has been little success in modeling hydrofoil-assisted catamarans in a general manner and such a tool would form an important part of future designs.
5. To define the most important geometric parameters governing the design of both hulls and hydrofoils of semi-displacement and semi-planing type hydrofoil-assisted catamarans. To date there have been no thorough investigations for establishing of these parameters.

The objectives of this study are pursued, firstly by gaining a thorough understanding of the hydrodynamic principles involved. This knowledge is applied to develop suitable experimental techniques and computational design tools. Both of these are later

⁹The problems of model testing are discussed in Chapter 3

applied to investigate the hydrodynamic design and optimization of both hulls and hydrofoil systems. Other aspects of design closely tied with the hydrodynamics, such as structural requirements, propulsion design, and operational requirements are considered only secondarily by following current and predicted trends and will be referred to in cases where they constrain the hydrodynamic design.

In the next chapter the basic hydrodynamic principles of hydrofoil-assisted catamarans is covered in detail. The main hydrodynamic parameters affecting performance as well as the different resistance components are covered. In Chapter 3 model testing techniques are discussed. Chapter 4 focuses on the development of theoretical methods needed for design purposes. Existing empirically based and computational methods are investigated and ways of modeling the important hydrodynamic phenomenon are discussed and applied in the development of a suitable computational model using the vortex lattice method. Design principles for the foil and hull systems are presented in Chapters 5 and 6 respectively. Finally Chapter 7 presents the conclusions drawn from this study concerning the hydrodynamic design of these vessels.

Chapter 2

Hydrodynamics and Resistance

Abstract

The hydrodynamics and resistance of hydrofoil-assisted catamarans are reviewed. The three different phases of operation are identified as the displacement, transition and planing phases. For each phase the main hydrodynamic phenomena are discussed and the main resistance components identified, including the hull-foil interactions and the interference resistance components. It is shown that the hydrodynamics for each phase have important differences and that the magnitude of the different resistance components changes in each phase.

2.1 Introduction

In this section the main hydrodynamic aspects of hydrofoil-assisted catamarans are reviewed. These aspects have been touched upon in the previous chapter, but are described here in much more detail as they eventually lead to the objectives of this study: successful hydrodynamic design of hydrofoil-assisted catamarans for speed and efficiency. During this study a number of hullforms and hydrofoil systems were investigated experimentally; they form the basis for the information given in this chapter. Table 2.1 lists the particulars of these hulls, all of which have fixed foil systems. Even though some hydrofoil-assisted catamarans make use of actively controlled foils, the hydrodynamic principles of fixed foils apply equally to active foil systems.

Based on these experimental results as well as the results obtained from the literature, general tendency curves have been constructed, which cover the performance of hydrofoil-assisted catamarans. These are shown in Figure 2.1. In relation to the resistance tendency for a conventional catamaran (red line), the resistance tendencies for hydrofoil-assisted catamarans are shown (grey and black lines). Further, a

No.	Name	L_{WL}	Disp.	No. of Foil Systems tested	Reference
1	SD1	32m	160-180t	2	[MH01]
2	SD3	30m	180t	1	[Mig97]
3	SD6	36m	161t	4	[MH01]
4	SD7	36m	140-188t	1	[MH01]
5	SD8	36m	161t	1	[MH01]
6	KingCat	19.5m	73.5t	1	[MH99b]
7	VII	22m	64-68t	1	[MH00]
8	F22	22m	53.6t	1	[MH98]
9	K55	72m	633t	2	[Hop98]

Table 2.1: Hulls with hydrofoil assistance model tested in this study

representative propulsor thrust curve is shown in green.

From Figure 2.1 three different hydrodynamic phases can be identified in the operational speed range of hydrofoil-assisted catamarans:

- the displacement phase
- the transition phase
- the planing phase

Similar phases have been described by Sottorf [Sot37] in 1937, concerning the different speed ranges during the take-off of sea planes and also by Egorov et al. [ES65] concerning the different phases of operation of conventional hydrofoil craft. The tendencies in attitude and resistance are remarkably similar for these different types of craft even though the hull shapes and form of lift generation are different. The similarity is nevertheless well founded, since all three types of craft are subject to a continuous redistribution of weight from hull to foils (airfoils or hydrofoils), as speed increases.

It is difficult to assign specific Froude numbers to each phase as the boundaries of each phase are a function of foil and hull design as much as of speed. Figure 2.1 nevertheless shows approximate volumetric Froude numbers for each phase that are representative of the data collected in this study. The borders do nevertheless vary quite substantially. The border between the displacement and transition phase may be as early as $Fn_{\nabla} = 1.0$ or as late as $Fn_{\nabla} = 2.5$. Similarly planing may start at $Fn_{\nabla} = 2.5$ or at $Fn_{\nabla} = 3.5$. depending on the hull design and the amount of lift provided by the foils. In comparison to the regimes given in Table 1.1 (page 6) for conventional craft, true planing generally starts earlier for hydrofoil-assisted craft.

The hydrodynamics of each phase are quite different and the influence of foils and hull

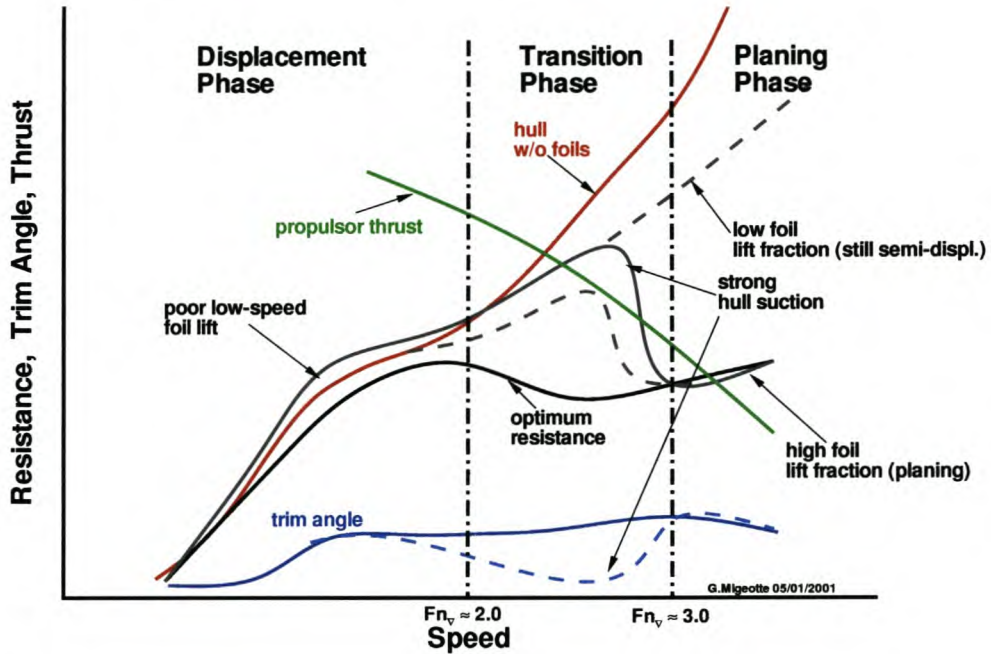


Figure 2.1: Performance tendencies for hydrofoil-assisted catamarans

design on resistance and attitude is decidedly different for each phase. The pictures in Figure 2.2 show the three different phases of operation for a Hysuwac vessel. The displacement phase is characterized by the presence of the strong wave-making which is clearly visible in the first picture. By the time the transition phase is reached, visible waves have practically disappeared and the hull is much higher out of the water but the running trim remains low. Once planing has been reached, there is no visible wave from the hull as it is fully planing. The running trim angle is also higher. The best efficiencies for hydrofoil-assisted catamarans are obtained in the planing phase. The behavior of other foil configurations is similar. The differences lie mainly in the resistance tendencies of the transition phase and in particular, the magnitude of the resistance hump found there.

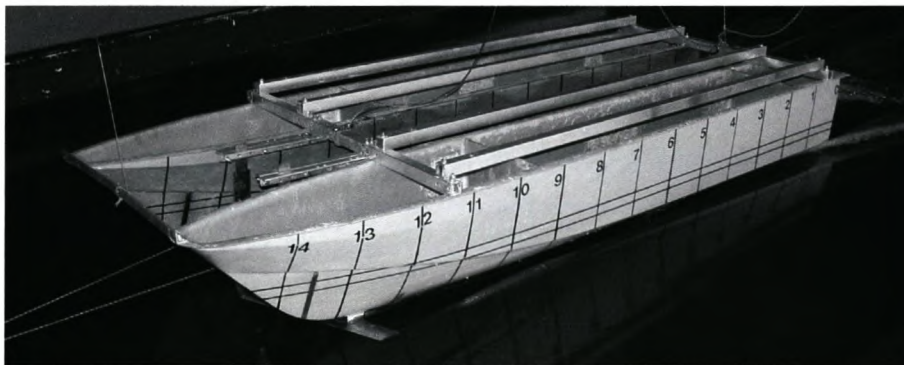
In the sections that follow, each phase of operation is discussed in more detail, including mention of the important resistance components and hydrodynamic phenomena. It is important to note that the total resistance of high-speed craft and especially hydrofoil-assisted catamarans include more resistance components than that of displacement vessels. Familiarity with these components of resistance is necessary as their relative importance changes with speed and for each phase. They are therefore discussed in some detail for each of the three phases.



Displacement Phase



Transition Phase



Planing Phase

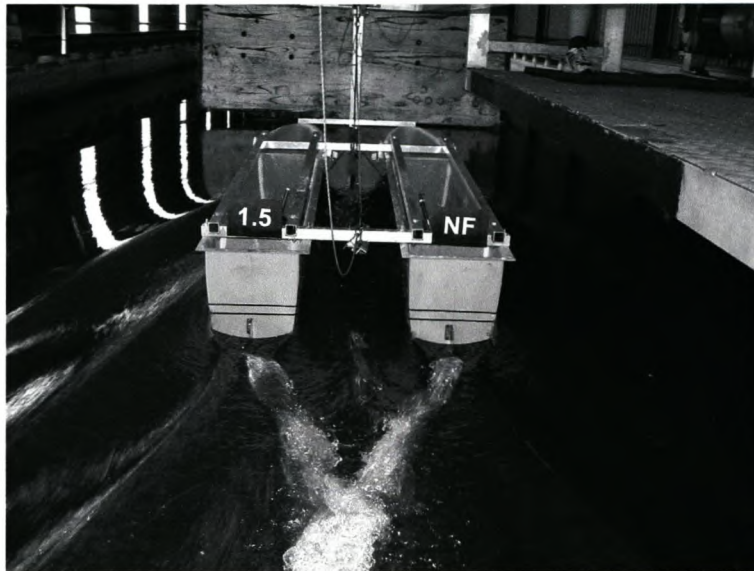
Figure 2.2: Examples of a model test for the three phases of operation

2.2 The Displacement Phase

Experiments show that at displacement speeds there is not much difference hydrodynamically between a hydrofoil-assisted catamaran and a conventional catamaran. Neither the hull nor the hydrofoils produce much dynamic lift and the phase is characterized by buoyant forces supplying most of the lift. The first picture in Figure 2.2 shows this condition. In this phase, 60% or more of the vessel weight is supported by hull buoyancy. For $Fn_{\nabla} \leq 0.8$ the transom stern is wet. As speed increases, clean separation of flow takes place at the transom. The normal displacement hump resistance occurs at $1.0 \leq Fn_{\nabla} \leq 1.5$ and is often associated with the highest trim (1.5° to 4°), the maximum sinkage and a steep resistance increase for the vessel.

Hydrofoil assistance does influence the resistance somewhat at hump speed and the foils may increase or decrease the total vessel resistance when comparing resistances for the same hull with and without foils. Often passive hydrofoil assistance will increase the resistance (approx. 10%) for the same hull at displacement speeds as indicated in the resistance tendencies of Figure 2.1. This is due to the added resistance of the foils that cannot be offset by reductions in hull resistance because of the limited lift of the foils at low speeds. Only under special conditions, using highly efficient foils, some experiments have shown that the resistance can be reduced in the order of about 10-15% at best (see Chapter 5). Any improvements in resistance are due to a reduction in wave-making resistance of the hull. The limited lift of hydrofoils¹ prevents significant reduction in viscous resistance as the wetted area of the hull cannot be significantly reduced at these speeds with practical foil configurations. A hydrofoil system spanning the tunnel between the demi-hulls is beneficial for wave cancellation in the tunnel. The downwash from the foils in general cancels any wave build up in the tunnel. Tao [Tao00] has found that at displacement speeds there is wave cancellation between the hull wave system and the foil wave system that is also beneficial to reduce wave-making resistance. As speed increases to transitional speeds and higher, the wave lengths of the hull and foils differ to the extent that beneficial wave interference is not possible. Figure 2.3 compares the flow behind the transom and in the tunnel between the demi-hulls for a hydrofoil-assisted catamaran. Some wave-cancellation effect in the tunnel is visible, as well as the reduced transom wave generation.

¹Lift is proportional to the square of the linear dimensions, while displacement is proportional to the cube of linear dimensions. This means that at low speeds impractically large hydrofoils are needed to provide high lift.



No Foils



Hysuwac Foils

Figure 2.3: Transom stern flow at $Fn_{\nabla} = 1.5$ for a semi-displacement hull with and without foils

2.3 The Transition Phase

The transition phase is the most complicated hydrodynamically with various interactions taking place between hull and foils. In this phase, the hydrofoil forces are large enough to influence the attitude and resistance quite substantially. For hydrofoils designed to carry only a small fraction of the vessel weight ($\leq 40\%$) at design speed, the transition phase is characterized by a transition from the foils increasing resistance, to a situation where they now reduce resistance compared with the same hull without foils.

Hysucat planing designs often show this tendency as indicated in Figure 1.9. There are usually no large changes in resistance, trim or rise during transition. Improvements in resistance are due to a reduction in wetted area for the hull, decreased wave-making and partially attributed to beneficial hull-foil interactions.

Similar resistance tendencies to that of the Hysucat have been found for Daewoo F-CAT40 semi-displacement catamaran using a single foil, whose resistance tendency is shown in Figure 1.17. The vessel uses a single foil and shows slight improvements in resistance over the unassisted hull at transitional speeds, $Fn_{\nabla} \geq 2.2$. The same positive foil-hull interactions are most likely present.

Foil systems designed to carry a large fraction of the vessel weight (70-100%) suffer from more complicated transition phase hydrodynamics. At transition speeds, foil lift forces are of the same order of magnitude as dynamic suction forces acting on the hull and there is strong interaction between the two. The result of this interaction is that there are often very sudden and large changes in resistance when transition to planing takes place. This is illustrated in Figure 2.1.

An important point worth mentioning is the strong correlation between the magnitude of the transition hump resistance and the running trim angle. Low running trim angles at transition speeds are invariably associated with a high hump and the lowest resistance is achieved by ensuring that relatively high running trim angles are maintained.

The magnitude of the dynamic suction on the hull is largely responsible for the behaviour of the vessel and the resulting transition hump resistance tendencies, including the magnitude of the maximum resistance of the vessel. Dynamic suction forces on the hull are due to two principle factors, the underwater shape of the hull and the foil-hull interactions.

2.3.1 The Hull Shape

Modern high-speed catamaran hullforms designed for semi-displacement speeds, $1.5 \leq Fn_{\nabla} \leq 2.5$ are characterized by the incorporation of rocker into their buttock lines,

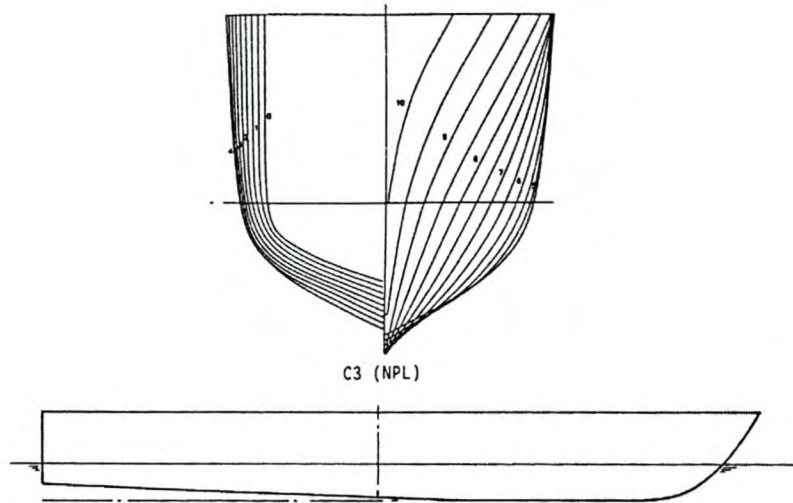


Figure 2.4: The NPL hullform

as this is beneficial for reducing wave-making resistance. This gives the buttock lines a decidedly rounded or convex shape. Chapter 6 analyzes these hulls in detail. Figure 2.4 shows the body plan and keel section of a hull form of this type (the NPL hull [IM91]). At speeds $Fn_{\nabla} \geq 2.0$, the flow around such a shape generates negative (suction) pressures on the hull. Figure 2.5 shows the pressure distribution for the NPL hull form [IM91, Arm99]. The initial positive pressure at the bow is followed by a large region of negative pressure associated with the rounded buttock lines of the hull. Later as the flow approaches the transom, negative dynamic pressures diminish again and the pressure returns to almost atmospheric at the transom stern.

The hull shape is therefore an important parameter influencing hull suction. Slender hulls such as the Hitachi Zosen Superjet 30² shown in Figure 1.12 suffer much less from suction than the beamier conventional hullforms [Miy89]. As a result the resistance tendencies for the Superjet30 shown in Figure 1.13 shows very gradual changes in resistance in the transition phase.

2.3.2 Foil-Hull Interactions

Foil systems designed to carry a large portion of the vessel weight often make use of foil configurations where the foils are located below keel depth. The vessels shown

²This vessel does not have a typical semi-displacement hull shape but rather an asymmetrical deep-V shape.

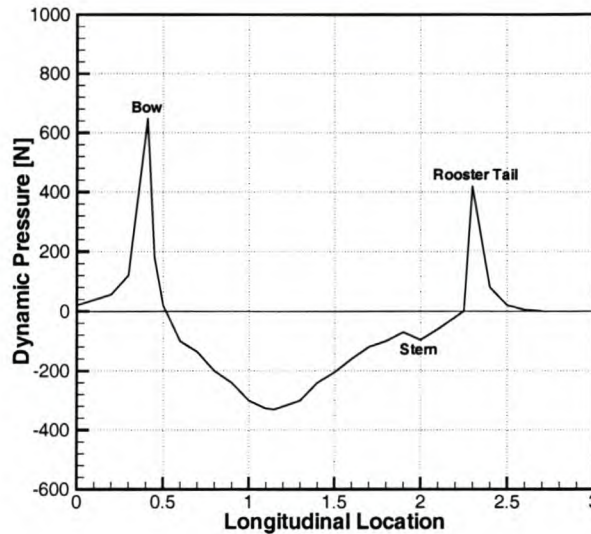


Figure 2.5: Pressure along a streamline on an NPL hullform at B/4

in Figure 1.2 are examples. Investigations of the foil-hull interactions [Ish92, Kat96] for such configurations have shown that foils located below keel depth contribute significantly to the dynamic suction forces on the hull. The amount of interaction depends on the spacing between the hull and the foils. Ishikawa [Ish92] found that for a catamaran with three tandem foils evenly spaced (forward, midships and aft) and mounted half a chord length below the keel, the suction pressure on the hull due to foils in close proximity cancelled anything from 25% to 60% of the foil lift forces. Figure 2.6 shows the experimentally measured ratio of total hydrodynamic lift force versus foil lift force as a function of volumetric Froude number. The fact that this ratio is less than 1.0 indicates that the hydrodynamic lift force on the hull is negative.

Further results of Ishikawa's calculations showed that the foils influence the hull pressures for separation distances between foil and keel, $h_{sep}/c \leq 2.0$. Figure 2.7 shows similar calculated bottom pressure variation for a single foil amidships underneath a typical round-bilge hull characteristic of catamaran ferry demi-hulls using the vortex lattice method described in Chapter 4. The pressure coefficient is given as a function of separation distance between the upper surface of the foil and the keel. From the figure it can be seen that a single foil disturbs the pressure on the hull for approximately two chord lengths ahead and one chord length behind the foil for all the separations. There is a severe drop in pressure on the hull close to the leading edge of the foil, particularly for small separation ratios.

Numerical investigations done by van Walree [Wal99] on the hull-foil interactions of conventional hydrofoil craft (mono-hulls) before take off at $Fn_{\nabla} = 1.5$, have shown

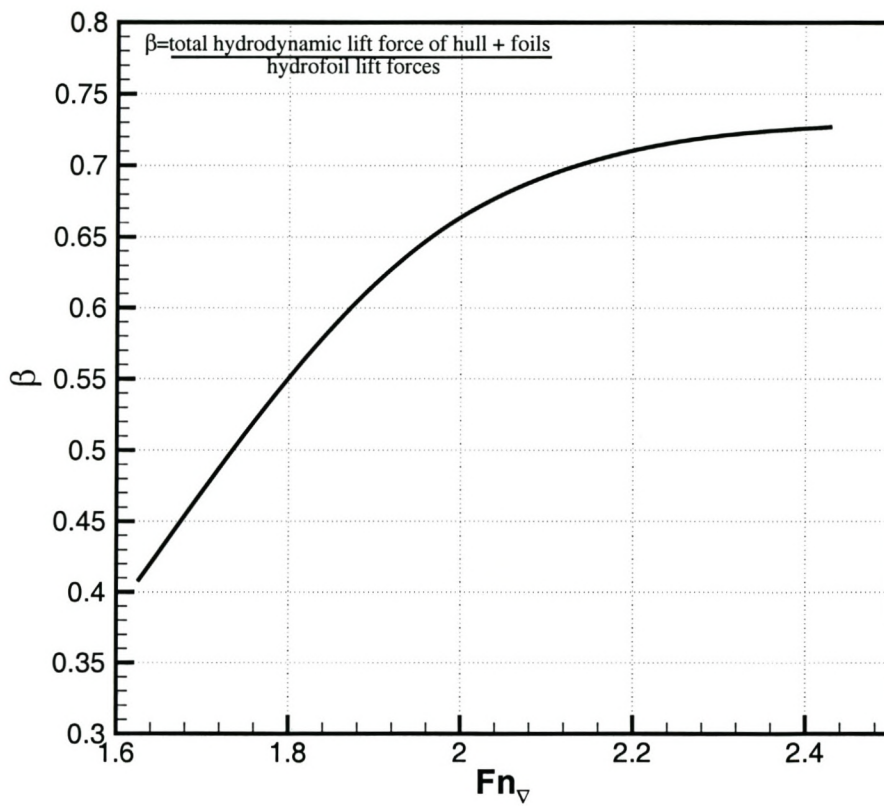


Figure 2.6: Lift ratio between total dynamic lift forces and hydrofoil lift forces

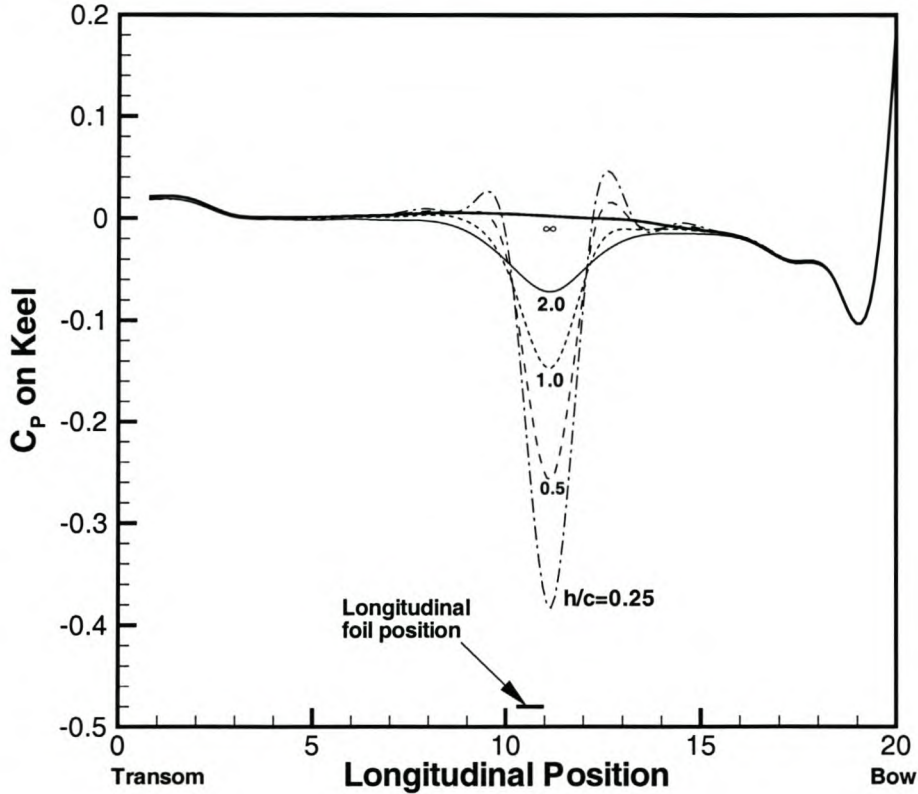


Figure 2.7: Changes in pressure on a hull due to a single foil. h/c refers to the separation distance between hull and foil

that the trailing vortices from a foil at the bow induce suction forces on the hull. For the case examined by van Walree, the suction forces were in the order of 10% of the vertical forces on the hull and seemed to increase with speed. Kornev [KT99] has indicated that the trailing vortices of shallowly submerged hydrofoils follow an inward (convergent) and upward motion towards the free surface, meaning that the tip vortices will move towards the hull. Van Walree found that the reduction in pressure is mainly on the aft sections of the hull; this seems to indicate the importance of the paths of the tip vortices on the hydrodynamics of these vessels.

The effect of suction pressure changes on the hull forces is of course dependent on the shape of the hull. For a foil located near the bow where the body sections are sharp, such pressures will have little effect on the lift force. Aft of amidships, where the typical section shape is quite full, the suction pressures will have maximum effect on the suction force.

2.3.3 Transition to Planing

At the top end of the transition phase, when the foil lift does overcome dynamic suction on the hull, transition to planing takes place. Resistance drops and the maximum resistance is often located at the top end of transition Froude numbers. Out of a practical design point it must be kept in mind that if transition takes place at too high a speed, the vessel will "get stuck" on the hump due to lack of power and planing conditions will not be reached. Figure 2.1 illustrates this situation. A typical propulsor thrust curve in relation to the maximum resistance is shown in the figure and it can be seen that a too high maximum transition resistance will limit the vessel to transitional speeds even though planing speeds could be sustained with the available power if the hump could be overcome. The first canard-interceptor hydrofoil-assisted catamaran (see Section 1.4.4) experienced this problem and the foil system had to be abandoned as unsuccessful.

Often at speeds just before transition takes place, observations during model tests and during sea trials have shown that vessels suffer from directional instability associated with low or even negative trim angles. Figure 2.8 shows an example of measured results [MH01] for a high-speed catamaran with a passive Hysuwac foil system and shows the relation between resistance, trim and rise as the sudden transition to planing takes place. Similar results have been found with a canard system [Mig97]. The low trim angle and loss of lateral area due to rise reduces the directional stability.

Once the foil forces properly overcome the hull suction, the trim angle increases rapidly, reducing suction forces even faster. A form of pitch-up instability therefore exists which is eventually dampened out when the forwardly located foil loses lift in close proximity to the free surface and the vessel settles to a new equilibrium position with the front foil very close to the free surface, and the hull planing with a relatively high trim angle.

It is possible to avoid the negative effects of hull suction and reduce the resistance to an optimum value. The resistance curve considered optimum is shown in Figure 2.1 and has a flat resistance curve with no apparent change in resistance as transition to planing takes place. In essence, this resistance tendency is obtained when the hull design and foil arrangement is such that it does not generate strong suction forces and also the lift of the hydrofoils is strong enough to overcome these weaker suction forces early during the transition phase. Such foil and hull designs are covered in Chapters 5 and 6 respectively.

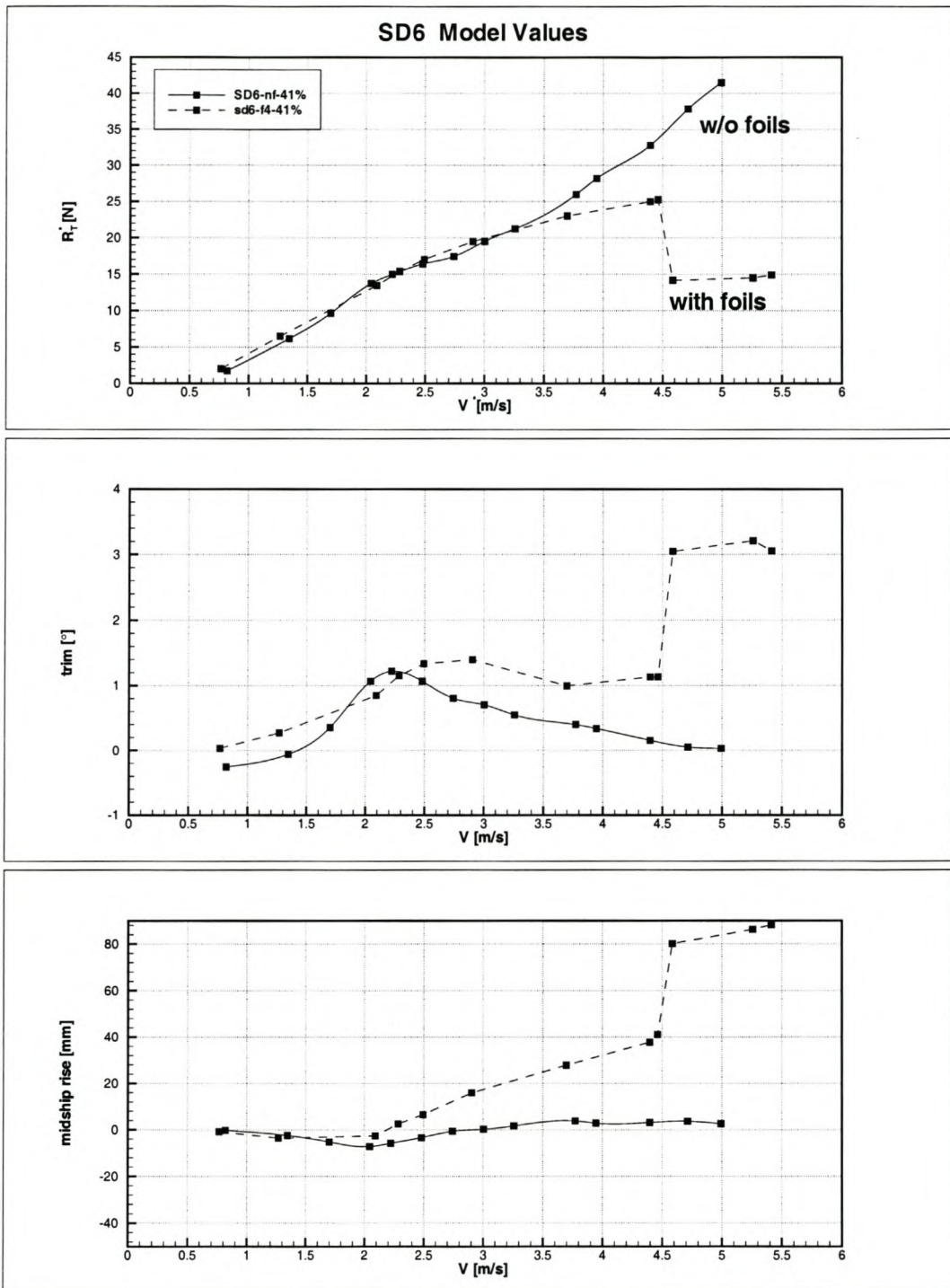


Figure 2.8: Resistance, trim and rise tendencies for a typical semi-displacement catamaran with Hysuwac foil system illustrating tendencies at the transition to planing ($V = 4.5\text{m/s}$)

2.4 The Planing Phase

The planing phase is characterized by its very low resistance and higher trim compared with the same hull without foils. Hysucat type vessels achieve planing as much due to their foil assistance as due to their hard chine planing hull forms. Asymmetrical hard-chine deep-Vee hulls such as those used on the Hysucat, are "assisted onto the plane" by the hydrofoils and because the hulls still provide significant dynamic lift, such craft are to some extent very similar to planing catamarans. In general, those foil systems which are mounted at keel depth experience slightly higher resistance displacement ratios during planing than those vessels with foils mounted below the keel. This is due to the higher wetted area of the former as the hull is not lifted as high out of the water.

For the slender symmetrical hull forms of larger catamarans, planing takes place for high-lift foil systems that allow a high trim angle to be taken up by the hull. This constraint makes systems with a bow foil submerged below the keel ideal for achieving planing. In planing conditions, the hull is largely out of the water and the parts in water contact develop positive lift, aiding the foils. Suction forces have disappeared and buoyancy forces are small. Wave-making of the hull has also effectively disappeared. Figure 2.2 shows this condition. In general, the foil forces dominate and attitude is largely dictated by the foil forces. For fixed hydrofoil systems, foil submergences are usually small as the bow foil invariably stabilizes itself just below the free surface at speed. Trim and rise of the hull is therefore influenced to a large extent by the location of the bow foil on or under the hull. A bow foil located deeper under the keel therefore implies that at planing speeds the trim angle will be higher as the bow is lifted higher out of the water as the foil stabilizes itself just under the free surface. Based on experiments [Mig97, MH01, MH00] it was found that for those cases where the foil remained deeply submerged for $Fn_{\nabla} \geq 3.0$, it was because the vessel remains in semi-displacement mode due to domination of hull suction. Experiments [MH01] have shown that there is a quite inflexible rule governing low resistance: a relatively high trim angle, greater than 1.5 degrees, is needed.

Observations during tank testing have shown that for passive Hysuwac and canard foils tested in this study, the bow foils submerge themselves very close to the free surface, $h/c \leq 0.1$, irrespective of the position below the keel. In some cases the foil is actually above the undisturbed free surface, but because of the wave crest over the foil it remains submerged. In reality, for full scale ships the turbulence level is much higher and this thin layer of water breaks up into an air-water mixing layer. Figure 2.9 shows a picture of such a mixing layer taken during sea trials of a 40m Hysuwac vessel. Since the foil is so close to the free surface, the upper side of the foil no longer contributes much lift, so there is little or no detrimental effect on lift caused by the mixing layer. On the contrary, such a mixing layer has been found to be beneficial to reducing or eliminating the detrimental effects of cavitation on hydrofoils [LT01].

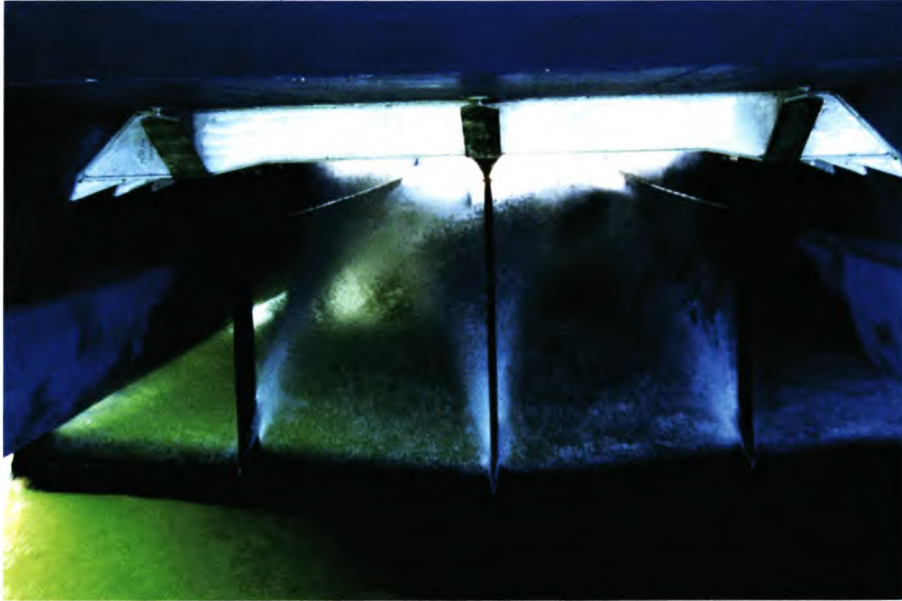


Figure 2.9: Air-water mixing layer on a hydrofoil close to the free surface

Resistance in the planing phase is usually fairly constant with speed as seen in the tendencies of Figure 2.1 and Figure 2.8. This is due to the hull rising higher out of the water as speed increases, reducing the wetted area of the hull proportionally to speed. The top speed of the vessel is usually limited either by some form of instability or propulsor ventilation problem linked to the vessel being lifted too high out of the water. The most common instability is the most forward foil breaking through the free surface and a pitch-heave instability similar to porpoising of planing hulls takes place, with the forward foil breaking through the free surface and then re-submerging to repeat the cycle³. Controllable pitch foils do of course not suffer from such problems as the lift can be regulated to avoid instability.

If instability does not occur, top speed is often limited by ventilation of the waterjets or propellers. Most high-speed catamarans make use of waterjet propulsion and it is known that even small amounts of air ingestion results in a substantial drop in thrust and efficiency and therefore speed.

2.5 Resistance Components

The total resistance of hydrofoil-assisted catamarans contains more resistance components than conventional ships and often more than usually found on most high-speed

³This instability is explained in more detail in Chapter 5

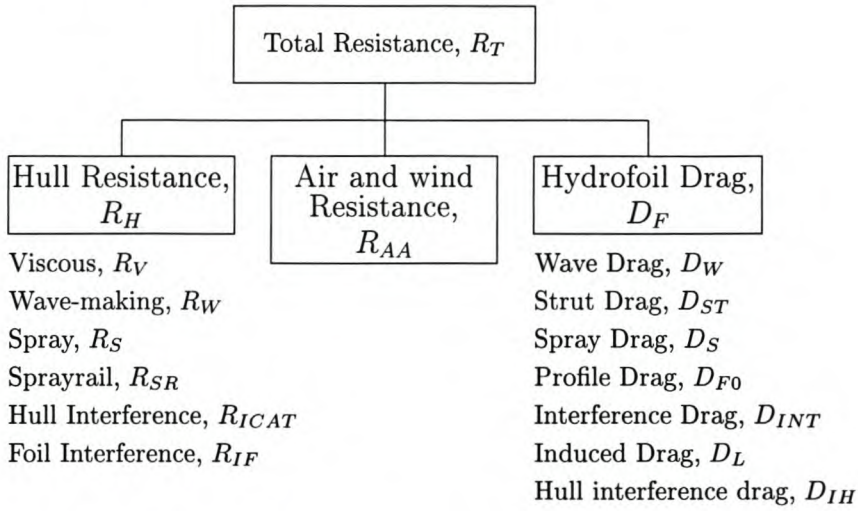


Figure 2.10: The resistance components of hydrofoil-assisted catamarans

marine vehicles. To optimize a design it is necessary to have fundamental knowledge of all the resistance components and their causes. For performance prediction, it is necessary to consider each component and estimate its importance as accurately as possible. A simple resistance breakdown for the hydrofoil-assisted catamarans is presented in the flow chart of Figure 2.10. Distinction is made between the primary resistance components namely: hull resistance, hydrofoil drag and air resistance. Additionally for final resistance prediction one would need to consider appendage drag⁴ as well. The relative importance of the different components change with speed and in the sections that follow these components are discussed.

2.6 Hull Resistance

Hull resistance refers to all those components of resistance that are generated due to the bare hull being in water contact. This includes the resistance of spray rails and interference resistance from the foils over and above normal residual and friction resistance components.

2.6.1 Hull Viscous Resistance R_V

Hull viscous resistance, R_V is composed of mainly friction, R_F and viscous pressure resistance, R_{PV} .

⁴Appendage drag is not discussed in any detail as the associated hydrodynamics are not fundamental to the design of hydrofoil-assisted catamarans and common to all ship types.

Friction Resistance R_F

Friction resistance being a very fundamental component of resistance for all ship types resulting from the shear forces within the boundary layer of the hull needs to be considered for all three phases of operation. It is the dominant component of resistance at high-speed (i.e. the upper end of transition and also the planing phase of operation).

Friction resistance R_F , is dependent on the Reynolds number, Rn and is commonly determined in dimensionless form for a smooth surface using the ITTC-1957 friction equation:

$$C_{F0} = \frac{0.075}{(\log_{10} Rn - 2)^2} \quad (2.1)$$

C_{F0} is based on the effective hull wetted area underway, S_W . Reducing the friction resistance can therefore effectively be achieved by reducing the wetted area. Since hulls are in general not hydrodynamically smooth due to surface roughness, a roughness allowance, C_A is commonly added. For typical aluminum catamaran hulls, $C_A = 0.0001$ is appropriate [MG97b]. In many cases values up to $C_A = 0.0004$ are used to account for other factors such as the effect of the 3-dimensional shape of the hull that Equation (2.1) does not fully account for. Alternatively, a form factor, $(1 + k)$ is often used in conjunction with Equation (2.1) to account for these 3-dimensional form effects. The total friction resistance is then:

$$C_F = (1 + k)C_{F0} + C_A \quad (2.2)$$

where C_{F0} is calculated from Equation 2.1 and C_A is the roughness addition. So far there is little agreement in the literature concerning the most accurate method of determining the form factor for high-speed catamarans since it cannot readily be determined from model tests for transom stern vessels. The general consensus is that it is greater than one [CMAU97, SRZM99] and that values are generally higher for catamarans than mono-hulls due to viscous interference between the demi-hulls [IM91]. Even accounting for viscous interference between the demi-hulls, it is felt [Arm99] that the form factor accounts for other components of resistance that are usually not considered. In particular, hydrostatic (transom) resistance and viscous pressure resistance.

The form factor is therefore a factor correcting for a number of different errors introduced during development of friction drag formulations. It has been found to be independent to demi-hull separation for the normal range of separation values of catamarans and is mainly a function of the demi-hull slenderness. The values listed in Table 2.2 are recommended [CMAU97] for high-speed catamarans.

At present it is unknown how hydrofoil assistance would change the form factor. It is

	$(1 + k)$	
$L/\nabla^{1/3}$	mono-hull	Catamaran
6.3	1.35	1.48
7.4	1.21	1.33
8.5	1.17	1.29
9.5	1.13	1.24

Table 2.2: Form factors for mono-hulls and catamarans

unlikely that hydrofoil assistance would have a significant influence in the displacement phase as the hydrofoils do not change the flow nor the turbulent boundary layer much. Once transition and planing phases are reached the hull comes substantially out of the water, effectively increasing its slenderness and reducing hydrostatic transom resistance and friction resistance (see paragraph that follows). The values in Table 2.2 may then be conservative and it is better to use only a roughness addition and not a form factor.

Hydrofoil assistance does affect the viscous resistance through the wetted area. It allows the hull to lift partially out of the water, meaning a reduction in wetted area. This is one of the main mechanisms that allow hydrofoil-assisted catamarans to achieve their low resistance at high speed. In the displacement phase, the reduction in wetted area is small or non-existent as it is directly related to the lift-carrying capacity of the foils. As speed increases to transitional speeds, useful wetted area reduction is achieved [MH99a].

Figure 2.11 is a plot of measured wetted area versus volumetric Froude number for a semi-displacement catamaran with and without hydrofoil assistance. The increase in wetted area for the hull without foils at the higher Froude numbers is associated with increased sinkage due to suction forces on the hull as well as an increase in wetted area due to spray. For both foil systems shown, there is (in this case) useful wetted area reduction from $Fn_{\nabla} = 1.5$, approximately the beginning of the transition phase. For the high-lift Hysuwac foil system, Figure 2.11 shows the large reduction in wetted area that is achievable at planing speeds as the sudden transition to planing takes place.

Viscous Pressure Resistance R_{VP}

The other component of hull viscous resistance is viscous pressure resistance. It is caused by viscous effects on the hull shape and by flow separation and eddy-making. It is directly linked with the growth of the boundary layer along the hull.

As boundary layers are thicker for lower Reynolds numbers, viscous pressure resistance has been found to be significant for speeds below $Fn_L = 0.6$ ($Fn_{\nabla} \approx 1.5$) [MG97b] for

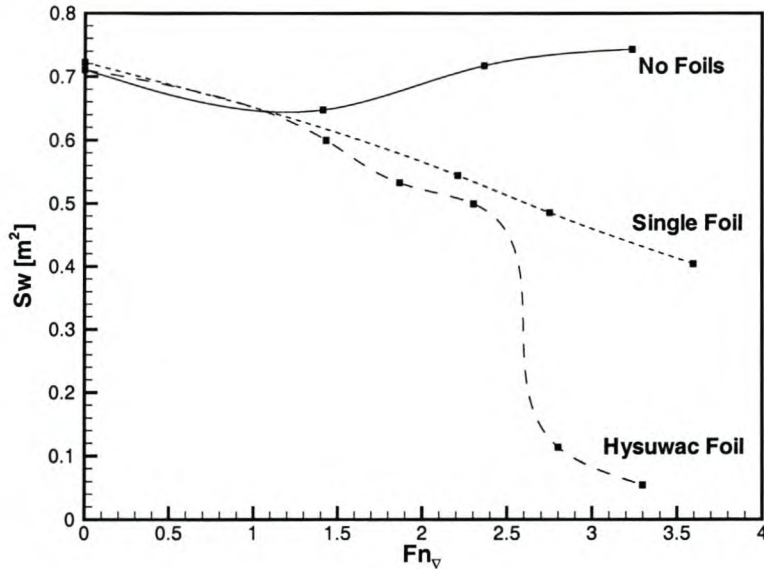


Figure 2.11: Comparison of measured wetted areas for two different foil configurations

high-speed ships and above this speed it can be neglected. As there is no simple way of determining viscous pressure resistance, it is corrected for using the form factor or considered as a part of the residual resistance and during model testing and is scaled according to Froude scaling laws. This is thought to lead to conservative model test estimates for resistance.

For hydrofoil-assisted vessels, one would ideally need to consider viscous pressure resistance for the displacement phase. At transition and planing speeds the reduction in wetted area and the higher Reynolds numbers means viscous pressure resistance is less important especially for planing type hulls [MG97b].

In determining the viscous resistance of hydrofoil-assisted catamarans, the displacement phase can be treated in a similar manner to conventional catamarans, using a form factor and roughness addition. In the transition and planing phase, it is important to obtain accurate estimates of the wetted area reduction, which should be used in conjunction with an appropriate roughness addition.

2.6.2 Hull Wave-Making Resistance R_W

Wave-making resistance refers to the loss of energy due to the generation of waves by the hull. It consists of three main components: wave pattern resistance, wave breaking resistance and hull pressure resistance. Wave-making resistance is the major

component of resistance for displacement ships. For slender catamarans it is a smaller part of the total resistance and is mainly significant in the displacement phase and to a lesser extent in the transition phase. At planing speeds hull pressure resistance dominates and is not associated with much wave generation. When wave-making is determined from model tests, it is included in the residual resistance with all other parts of non-viscous resistance such as spray etc. listed in the flow chart in Figure 2.10.

Wave-Pattern Resistance R_{WP}

A number of thorough investigations into the wave-making resistance of high-speed catamarans are available [IM91, MWC96]. These investigations show that speed and length-displacement ratio, $L/\nabla^{1/3}$, are the predominant factors influencing wave-pattern resistance. Resistance decreases with increasing length-displacement ratio and speed (when $Fn_{\nabla} \geq 1.5$). For high-speed craft, the appropriate speed parameter is the volumetric Froude number, Fn_{∇} . For such craft, where $L/\nabla^{1/3}$ is not constant for the hull, it is appropriate to define an effective Froude number based on the hull displacement:

$$Fn_{\nabla_e} = \frac{V}{\sqrt{g\nabla_{hull}}} \quad (2.3)$$

where ∇_{hull} refers to the fraction of the displacement carried by the hull.

As the load carried by the foils increases with speed, ∇_{hull} decreases, meaning that as speed increases the effective Froude number of the hull increases with approximately V^2 . Using the effective Froude number, Fn_{∇_e} and the hull length-displacement ratio $L/\nabla_{hull}^{1/3}$, it is possible to approximately predict the wave-making resistance for a hydrofoil-assisted hull.

The difficulty in separating the various residual resistance components from wave-pattern resistance means that resistance prediction methods based on model tests mostly refer only to residual resistance. A number of publications [Wer90, MWC96, MG99b] provide simple methods for estimating the residual resistance of slender catamarans (both hard chine and round-bilge). Alternatively, demi-hull wave-making resistance can typically be estimated using the Series 64 experimental data [Yeh65] together with a suitable wave interference factor (see Section 2.6.3).

The usefulness of applying existing experimental data to hydrofoil-assisted catamaran performance predictions is somewhat questionable as the hull is being unloaded by the foils. The effective hull length-displacement ratio, $L/\nabla_{hull}^{1/3}$ is often outside the experimental range of data for conventional catamarans. Numerical methods provide an alternate means to determine the wave-pattern resistance and provide reliable

estimates for this [BBC⁺98]. Numerical methods are the subject of Chapter 4.

Wave-Breaking Resistance R_{WB}

Wave breaking resistance is primarily due to the breaking bow wave at Froude numbers, $Fn_{\nabla} \geq 1.4$, and also the rooster tail behind the transom. For hydrofoil-assisted catamarans wave-breaking resistance is therefore of primary importance in the displacement phase and the transition phase. At planing speeds the breaking bow wave has thinned to form an overturning bow spray sheet at lower planing speeds and at higher speeds a spray jet. The difficulty in determining wave-breaking resistance means that it is usually included as a part of the residual resistance estimation using model test data. Estimating it accurately using numerical methods is often unsuccessful.

Hull Pressure Resistance R_P

Hull pressure resistance is the main residual component governing planing hull resistance. During planing, the hydrodynamic pressure acting on the planing hull responsible for lift is also responsible for hull pressure resistance and is therefore a form of induced planing drag.

Planing is governed to a large extent by the same parameters that govern lifting surfaces such as hydrofoils. It has been shown [Wag32] that a planing surface has similar hydrodynamic characteristics to the pressure side of a corresponding wing and that the lift of a planing surface is exactly half that of this corresponding wing. While resistance of semi-displacement craft depends mainly on $L/\nabla^{1/3}$, that of high-speed planing hulls depends on several parameters, including LCG location and the relation between planing bottom area and volumetric displacement at rest, $A_p/\nabla^{2/3}$ (the wing loading).

Numerous different methods (dozens!) are available to estimate planing hull resistance and the pressure drag. Most commonly used are planing hull series and prismatic equations, both of which are summarized in detail by Almeter [Alm93] and Payne [Pay95]. The prismatic equations of Savitsky [Sav64] have been successfully applied by Hoppe [Hop95a] in conjunction with simple foil theory, to predict the performance of planing hydrofoil-assisted catamarans such as the Hysucat. The method of Savitsky is particularly useful as it allows the solution of the dynamic equilibrium, given the LCG and the thrust and has been used to model a similar problem: the take-off regime of hydrofoil craft [Kar76].

For non-prismatic shapes that are common of modern planing hull designs, numerical methods have also been applied. Numerical methods are particularly useful for resistance estimation of hydrofoil-assisted planing catamarans where it is necessary to

determine the demi-hull interactions and the foil-hull interactions. Numerical methods for modeling planing and their application to planing hydrofoil-assisted catamarans are explained in detail in Chapter 4.

2.6.3 Hull Interference Resistance R_{ICAT}

Hull interference resistance, R_{ICAT} refers to the wave and pressure interference between the demi-hulls. Wave interference dominates in the displacement phase and pressure interference in the planing phase. The transition phase suffers to some extent from both.

Wave Interference R_{WI}

Everest [Eve68] has shown that at displacement speeds, beneficial partial wave cancellation is obtained between the diverging wave systems originating from each demi-hull, whereas adverse wave interference arises from interaction of the transverse wave system. Müller-Graf [MG97b] provides data to estimate the wave interference factor for round-bilge and hard chine catamaran hulls and shows that the demi-hull interference can be as high as 1.6 times the sum of the total demi-hull wave resistance for small separation distances, ($B_T/L_{WL} = 0.1$) making it an important factor to consider. Figure 2.12 [IM91] illustrates how the interference effect changes with Froude number. In general, positive wave cancellation is achieved in the displacement phase, at speeds $0.32 \leq Fn_L \leq 0.4$ and negative interference occurs at higher speeds [TT68, MG97b]. Once $Fn_L \geq 0.8 - 1.0$ (approx. $Fn_{\nabla} = 2.5$) wave interference disappears as the bow waves are swept back forming a small enough angle so that they no longer reflect off the other demi-hull. Only for very small demi-hull spacing do the effects then remain significant. The generation of dynamic lift through hydrofoil assistance and the associated reduction in wave generation most likely has significant effects on the interference [Lew88] so, for hydrofoil-assisted catamarans it is probable that the wave interference will be reduced and one can ignore it at Froude numbers lower than for the same hull without foils. The volumetric Froude number considering only the hull displaced volume, $Fn_{\nabla hull} = 2.5$, could be used as a guideline for determining the wave interference of the demi-hulls.

Pressure Interference R_{PI}

According to the wing analogy of Wagner [Wag32], a planing hull behaves similarly to the same wing. Well known from aeronautical practice is the beneficial situation created by two high aspect ratio wings in flight, side by side. The trailing vortices of each wing induce upwash and increase the effective incidence angle for the other

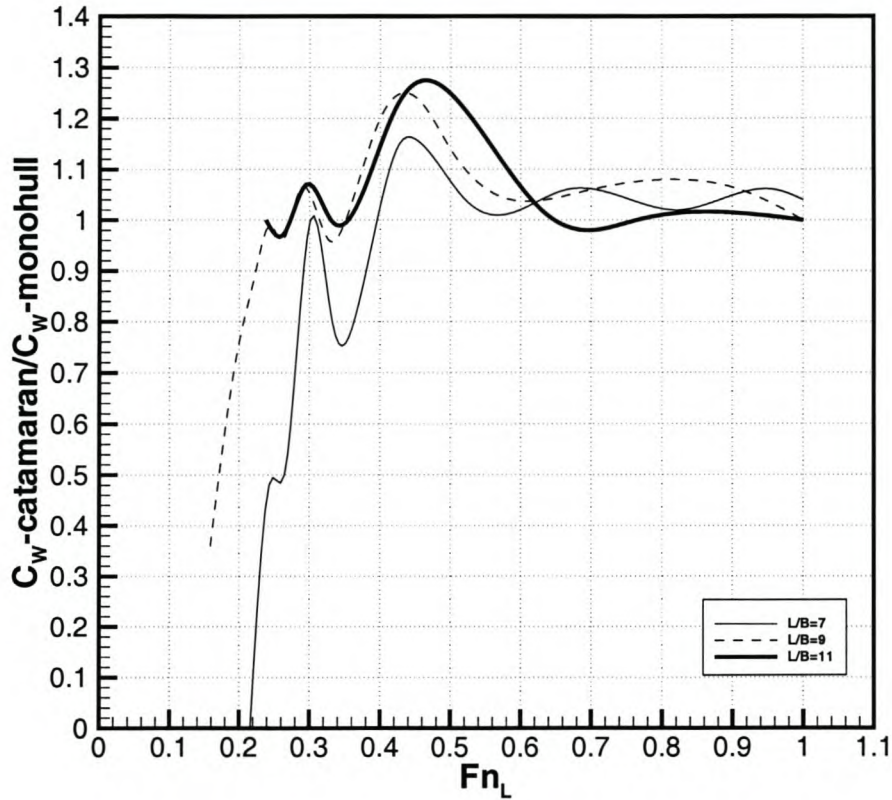


Figure 2.12: Wave-making interference for a catamaran demi-hull as a function of length Froude number: $Fn_L = \frac{V}{gL_{WL}}$

wing resulting in better efficiency. Lift increases as the separation distance between the two wings decreases.

An analogous situation occurs for two planing hulls side by side, as in a catamaran configuration. Experiments by Savitsky et al. [SD54] have shown that for two planing plates side by side (i.e. like a catamaran) the lift is markedly increased as separation distance diminishes. Lee [Lee82] has shown that the drag follows a similar tendency and is applicable to surfaces with deadrise as well. Figure 2.13 [SD54] shows how the lift⁵ varies with separation distance. It is expected that the relation presented in Figure 2.13 will not change much for hydrofoil-assisted hulls. Rather, the importance of this effect will diminish with increasing lift by the foils as the hull lift fraction and hence the interference lift becomes less.

⁵Pressure resistance follows a similar tendency.

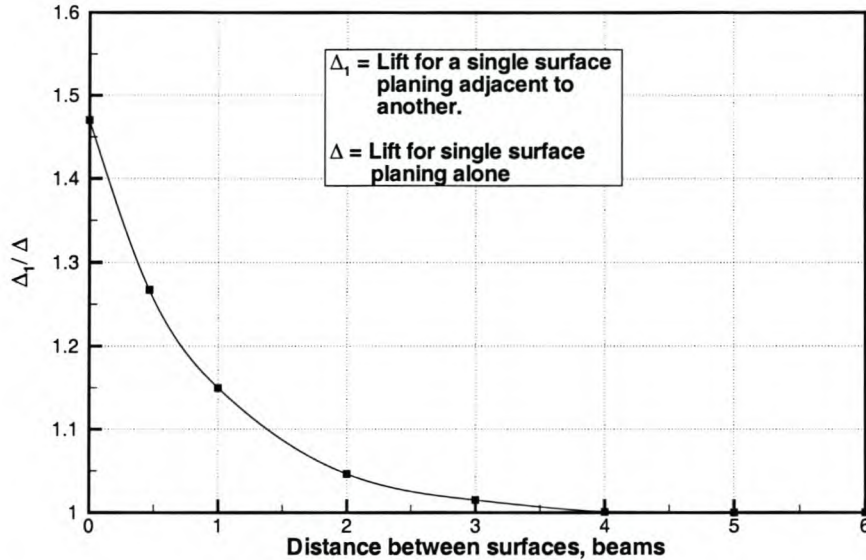


Figure 2.13: Lift interference between two flat surfaces planing side by side

2.6.4 Foil Interference Resistance R_{IF}

Foil interference resistance refers to the component of hull resistance due to foils in close proximity. It is closely related to hull suction due to the hydrofoils as explained in Section 2.3.2. The increased suction on the hull causes the vessel to squat increasing wave-making and wetted area. For the setup where a hydrofoil is located in the tunnel between the demi-hulls, as in the Hysucat configuration for example, the hull acts as an end-plate and benefits from the positive pressure on the underside of the foil which creates extra lift for the hull that is beneficial, but also results in foil interference resistance. Kaji et al. [KMY91] have investigated the foil-hull interactions for tandem hydrofoils located in the tunnel between the two demi-hulls for semi-displacement speeds $1.8 \leq Fn_{\nabla} \leq 2.6$. By measuring the foil and the catamaran hull resistance independently and also together as a hydrofoil-assisted catamaran, they found that the foil interference resistance is strongest at low Froude numbers and decreases with speed. Their results further show that the aft foil causes most of the interference resistance, while the forward closer to the slender bow only has a minor contribution to the interference resistance. This is in line with the earlier findings concerning hull suction: the pressures induced on hull by hydrofoils is of importance for the fuller sections away from the bow.

Similar experiments to those of Kaji et al. have been carried out by Hoppe [Hop80] for mono-foil assisted asymmetrical planing hulls at speeds corresponding to $2.6 \leq$

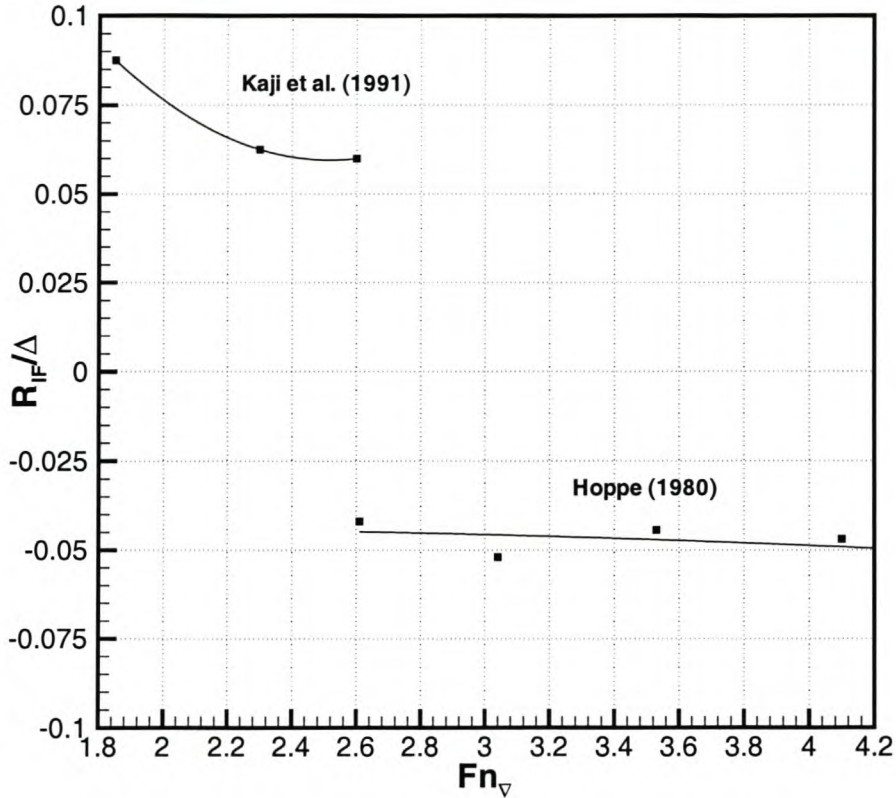


Figure 2.14: Interference resistance as a function of Volumetric Froude number

$F_{n_{\nabla}} \leq 4.2$. At these speeds, Hoppe found that the foil interference resistance is negative and of the same order or larger than the foil resistance. Figure 2.14 shows the results of Hoppe and Kaji et al. for the interference resistance. The hydrofoil resistance was not measured by Hoppe, so it is estimated theoretically.

The results of Kaji et al. and Hoppe differ fundamentally in the sense that Hoppe's results show beneficial interference and those Kaji et al., detrimental interference. The difference is mainly due to the foil layout. In Hoppe's case the mono-foil was operating in the freestream while the rear foil of Kaji et al. (found to cause most of the interference resistance) operates in the downwash of a forward foil. The rear foil produces much less lift and therefore does not create as much positive pressure on the hull, but rather disturbs the flow around the hull increasing the hull resistance.

Given that the foil-hull interference resistance can be positive or negative and is a function of foil layout and possibly the hull shape, there is no simple method to determine it. One is required to take the full geometry of the vessel and the influence

of the wake from forward foils into account to be able to estimate it. Model tests or advanced numerical methods offer the only alternatives to determine it.

As pointed out by Egorov et al. [ES65], hydrofoils in close proximity to the hull also cause an increase in the level of turbulence in the flow around the hull, the degree of which is unknown. Foil interference resistance is therefore a partially viscous phenomenon. It can be expected that standard methods for determining hull friction will be less reliable because of this.

2.7 Air and Wind Resistance R_{AA}

Air resistance due to the exposed parts of the hull as well as the superstructure account for a important percentage (up to 30%) of the total resistance for high-speed craft such as hydrofoil-assisted catamarans where the hull is to a large extent out of the water. Air resistance is usually determined based on the frontal area of the vessel and calculated from the following simple relation:

$$R_{AA} = 0.5\rho_A \cdot V_R^2 \cdot A_V \cdot C_{AA} \quad (2.4)$$

The air resistance coefficient, C_{AA} is typically around 0.42 – 0.7 [Wer90, MG97b] for catamarans. For hydrofoil craft in foilborne mode, values are in the range: $C_{AA} = 0.6 – 0.9$ [MG97b]. For hydrofoil-assisted catamarans, the value would be somewhere in between these two, given that the hull is partially lifted out of the water and is therefore very dependent on design.

The maximum air and wind resistance usually occurs when the angle between wind direction and the direction of motion is $\phi = 20 – 30^\circ$. In this case the area, A_V in equation 2.4 should be the area exposed to the wind and would thus include the tunnel area plus a part of the lateral area. As a measure of safety it is worthwhile to include the area of the tunnel in the frontal area when determining air resistance. Because the tunnel is small in relation to the frontal area it often blocks up forcing the flow of air around the superstructure instead of through the tunnel. In this study the frontal area included the tunnel area and an air drag coefficient of $C_{AA} = 0.5 – 0.7$ was used to determine air resistance, keeping in mind that the exposed area increases with speed as the hull is lifted higher out of the water.

2.8 Hydrofoil Drag D_F

Hydrofoil drag consists of the components listed in the flowchart in Figure 2.10 on page 44. Of these components, profile drag, wave drag and induced drag make up the

largest part. Interference drag refers to the interference between multiple foils and is due to the vortex-wave wake shed from forward foils affecting downstream foils. Hull interference is the component of drag due to the hull in close proximity.

2.8.1 Wave Drag D_W , Induced Drag D_L and Lift L

The non-viscous components of hydrofoil drag, namely wave drag and induced drag are inextricably linked to the lift generation of the foils and are therefore considered together with lift. Hydrofoil theory for predicting these forces is well developed and a number of different methods exist to model hydrofoil lift and drag in similar ways to aeronautical practice. These include lifting line theories (for example [WC58]) and extensions of thin foil theory. Simple empirical relations exist to correct results for planform, taper, dihedral and sweep etc. Additionally for hydrofoils, the free surface in close proximity to the foil needs to be considered. The theoretical general solution to this problem was originally obtained by Kochin [Koc49] by modeling the foil as a single vortex below the free surface. The complexity of the solution resulted in simplification of the theory for high speeds - the limiting case of an infinitely large Froude number. This simplification has been found valid for chord based Froude numbers, $F_{n_C} \geq 4.0$ which, considering that hydrofoil craft usually operate at higher chord Froude numbers, is a practical solution. For hydrofoil-assisted catamarans this criteria is usually fulfilled for transition and planing speeds. The solution of the high-speed free surface problem can then be simplified to considering the effect of an image vortex system without the need to consider the free surface deformation. This method is applied to 2-dimensional as well as finite aspect ratio problems. Simple equations for the lift, induced drag and wave drag have been derived using this method (see for example [Das00]) and are in common use. Because the theory is linear, lift, induced drag and wave drag are treated separately and the drag components are simply added together.

Physically, the presence of a deformable free surface in close proximity to the foil results in curvature of the flow over and past the hydrofoil. This effectively decreases the camber of the profile and also the effective angle of attack. The final result of these two effects is that the zero-lift angle is shifted to higher values and the lift curve slope is decreased. Physically, these effects manifest themselves as a pressure increase on the upper side of the foil, with the pressure on the lower side remaining almost unchanged compared with deep submergence [ES65].

While simple methods based on the high-speed approximation provide reasonably good predictions of lift and drag for single foils of regular shape, it is often appropriate to consider more modern numerical methods as fewer of the simplifying assumptions are introduced in the solution process. Such methods allow one to model the complex hydrofoil geometries usually found in practice and also model the foil interference effects when considering multiple hydrofoils. In this study, the non-linear vortex

lattice method (NVLM) implemented in the commercial code AUTOWING has been used for hydrofoil calculations. The method is explained in detail in Chapter 4, and has formed the basis for further development of the vortex lattice method generalized for hydrofoil-assisted catamarans.

2.8.2 Profile Drag D_{F0}

Profile drag refers to the viscous component of drag that is a function of the state of the boundary layer (laminar or turbulent), the Reynolds number and the profile geometry. Profile drag is composed of friction drag, viscous pressure drag as well as any separation drag that may be present.

Friction drag is usually calculated using friction drag formulas based on flat plate drag and corrections are introduced for the increased fluid velocity around the profile and the additional pressure and separation drag. Hoerner [Hoe65] presents empirical correlations for the profile drag of streamlined sections. For sections with the maximum thickness located at approximately 30% chord length from L.E. the following equation applies:

$$C_{F0} = C_F \left(1 + 2\frac{t}{c} + 60\left(\frac{t}{c}\right)^4 \right) \quad (2.5)$$

where, $2\frac{t}{c}$ represents the drag increment due to the increase in velocity and $60\left(\frac{t}{c}\right)^4$ represents the increment due to pressure and separation drag. For profiles with the maximum thickness at 40% to 50% of the chord from the leading edge the following equation is proposed by Hoerner:

$$C_{F0} = C_F \left(1 + 1.2\frac{t}{c} + 70\left(\frac{t}{c}\right)^4 \right) \quad (2.6)$$

Such equations have been developed from experimental data for symmetrical sections not generating any lift and are based on the wetted area of the hydrofoil. An extra increment of profile drag is needed for lifting surfaces. It can be approximated by [Lew88]:

$$\delta C_{F0} = 0.005 C_L^2 \quad (2.7)$$

Alternatively an equation that takes all the above factors into account has been presented by van Walree [Wal99]

$$C_{F0} = C_F \left(1 + 1.2\frac{t}{c} + 60\left(\frac{t}{c}\right)^4 + 120\left(\frac{t}{c} + 0.2C_L\right)^4 \right) \quad (2.8)$$

Such equations assume that the angle of attack is small, that turbulent flow prevails and that the foil is operating in an unbounded fluid. When applied to actual hydrofoils, these equations are typically valid for submergences: $h/c \geq 3$ [ES65]. For shallower submergences the free surface affects the pressure distribution on the upper

surface of the foil and this is known to decrease the friction drag [ES65]. In some cases the reduction in friction drag can be larger than the increase in wave drag close to the free surface, so that the total hydrofoil drag will decrease as the free surface is approached [SS57]. At deep submergences, $h/c \geq 3$ the friction drag is 10% to 20% greater than flat plate drag for normal hydrofoil sections. As the foil approaches the free surface, the increase in pressure on the upper surface alters the boundary layer. Egorov et al. [ES65] points out that as a hydrofoil (at small angles of attack) approaches to within $h/c = 0.2$, the friction drag approaches that of a flat plate to within 1.5%. As the submergence decreases, the difference diminishes even more remarkably. Egorov et al. presents the following formula for determining the profile drag taking the free surface into account:

$$C_{F0} = C_F \left(1 + \left[(m_p + 0.5) \frac{\varphi}{k_\varphi} - 0.5 \right] C_L \right) \quad (2.9)$$

m_p is an empirical correction factor and varies within the limits 0.5 – 0.75. Its smaller value correspond to $C_L = 0.175$ and its larger value to $C_L = 0.55$. A linear interpolation can be done for other C_L values. φ is a free surface correction factor for the decrease in pressure drop on the upper side of the foil:

$$\varphi = 1 - e^{-2\left(\frac{h}{c}\right)^{0.6}} \quad (2.10)$$

k_φ is a correction factor for the lift curve slope of the foil:

$$k_\varphi = 1 - \left(0.5 + \frac{t}{c} \right) \cdot e^{-2\left(\frac{h}{c}\right)^{0.6}} \quad (2.11)$$

Figure 2.15 shows the typical profile drag tendencies for a plano-convex⁶ circular-arc profile calculated using Equations (2.9) to (2.11).

Hydrofoil-assisted catamarans often make use of passive foils where the foils operate in extreme free surface effect: $h/c < 0.1$, so it is important to include the free surface effect on friction. From Figure 2.15 one can see that for typical hydrofoil thicknesses (6 - 12%), the drop in friction resistance is important for $h/c \leq 1.0$.

2.8.3 Interference Drag D_{INT}

Interference drag refers to the interference between multiple foil systems. A shallowly submerged hydrofoil introduces a vortex-wave wake into the downstream flow. The wave wake and the vortex wake can have positive or negative effects on resistance.

⁶A circular arc profile with flat underside.

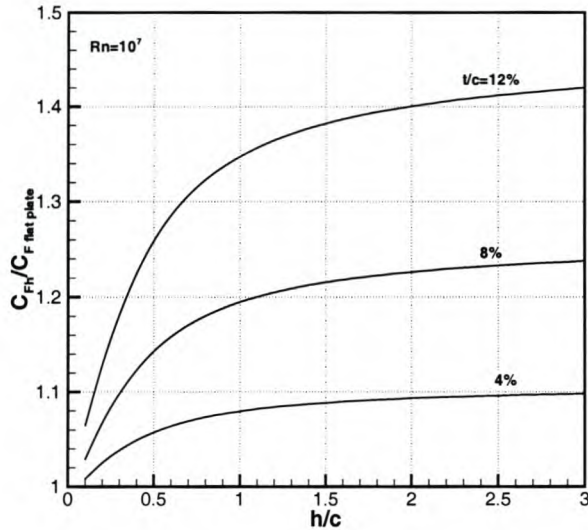


Figure 2.15: Friction drag of a plano-convex circular arc profile, including free surface effect, relative to flat plate drag, based on equation 2.9

Wave Wake

The wave wake created by a forward foil causes downstream foils to either operate in wave induced downwash or upwash. Simple empirical equations such as those of Li [Li81] have been developed to determine the free surface elevation and downwash angle at downstream locations and can be used to correct lift and drag calculations for hydrofoils in the wake of a forward foil. Accuracy of total drag predictions using such equations are in the range of 10 - 30% [Wal99]. Conventional hydrofoil craft endeavor to space the foils so that rear foils operate in positive upwash from the forward foils [MM00]. Forward foils do not experience any interference from downstream foils unless the separation distance between the foils is less than about 4 chord lengths [MT90].

For hydrofoil-assisted catamarans operating in the planing phase, the wave wake will in general result in a loss of efficiency for downstream foils arranged in practical configurations. At high speed, the wave length from the forward foil is large (a few boat lengths) and the downstream foils are in a region of wave downwash thus reducing the submergence and lift. At displacement and transitional speeds the wave length is less and it is possible to design to take advantage of induced upwash [MM00] to improve the lift to drag ratio of the rear foils. As shown by Miyata et al. [MT90] this improvement can be quite large at semi-displacement speeds, in the order of about a 30% increase in lift to drag ratio for an aft foil mainly as a result of reduced drag, but also some increased lift.

Vortex Wake

The trailing tip vortices strongly influence the induced flow field in the wake. The tip vortex induces upwash on its outer side and downwash on its inner side. The tip vortices are often a cause for concern because they induce strong changes in inflow angles to downstream foils close to the vortices. The result can be cavitation, ventilation and an increase in drag.

Given the difficulty in determining interference drag, model tests and numerical methods are the most suitable for estimating this drag component. Feifel [Fei81] describes a vortex lattice method to determine the influence of tip vortices on the lift and drag of downstream foils. More advanced vortex lattice methods have been applied by Morch [Mor91] and van Walree [Wal99] in design of hydrofoil craft considering a deformed free surface. More recently Kornev et al. [KMHN01] have used vortex lattice theory for optimizing the design of hydrofoil-assisted catamarans by modeling the path of the tip vortices and determining the influence of the deformed free surface on the lift forces of the hull and downstream hydrofoils and show very good agreement with experiments. Such a method considering all vortex-wave wake interactions is the preferred method for determining foil interference forces.

2.8.4 Hull Interference Drag D_{IH}

Hull interference drag refers to the effects of the hull on the foils. These effects are both wave-making and viscous in nature. At displacement speeds and during transition, the waves from each demi-hull reflect off the opposite hull creating disturbed inflow conditions for the foils thus reducing their efficiency. Van Walree [Wal99] has done some preliminary numerical investigations into this effect and shows that the lift reduction of the foils due to the hull is not so significant for deeply submerged foils. For the foils 2 to 3 chord lengths below the hull, the loss in lift was 3.4% for the low speed case ($Fn_{\nabla} = 1.4$) examined and less for the higher speeds. Ishikawa [Ish92] presents similar results for foils up to half a chord length below the hull. This loss in lift would result in a small decrease in induced drag for the foil, but this is most likely negligible compared with the increase in resistance for the hull associated with the suction.

For foils that are located at keel depth for example in a Hysucat configuration, the end plate effect of the hull on the foils improves the efficiency of the foils. Numerical computations⁷ [KMHN01] show that the rear foil drag can be reduced as much as 45% due to the end plate effect.

Viscous interference effects between hull and foils are also present. The foils change the velocity field around the hull causing changes in the boundary layer and increased

⁷Presented in Chapter 4.

friction for the hull and foils. This is particularly true in the corners formed by the attachment points of the foils with the hull. In these corners, the boundary layer of the hull combines with the boundary layer of the foils resulting in viscous interference drag. According to Hoerner [Hoe65], the extent is dependent on the foil thickness to chord ratio and the angle formed between the foil and the hull. In general the viscous interference resistance increases dramatically as the angle decreases below 90 degrees. For a 90 degree intersection one can use the following equation [Hoe65] to estimate the value of this component:

$$C_{Dt} = 0.75 - \frac{0.0003}{(t/c)^2} \quad (2.12)$$

Comparisons with the foil drag show that this interference drag is in fact negligible at displacement speeds (2% of foil drag). With increasing speed it becomes important and needs to be considered at transition and planing speeds (10% of foil drag).

2.8.5 Strut Drag D_{ST}

Strut drag comprises of wave-making drag, spray drag and friction drag. As speed increases above a chord Froude number $Fn_C = 0.7$, the wave-making drops off rapidly. For this reason it need not be considered for hydrofoil-assisted catamarans. Of primary importance is the spray drag D_S of the strut. Hoerner [Hoe65] has analyzed much of the available experimental data on spray drag of struts and points out that it is a function of the forebody thickness ratio (the ratio of maximum thickness to the position of the maximum thickness along the chord from the leading edge), t/x :

$$D_S = 0.12q \left(\frac{t}{x} \right)^2 \quad (2.13)$$

when $t/x \leq 0.4$. Zhu et al. [ZG90] show that this equation is only approximate and for circular arc struts often used for hydrofoil applications the data of Chapman [Cha72] may be more useful. Chapman proposes the use of the following equations:

$$\begin{aligned} D_S &= qct(0.003 + 0.06t/c) \text{ when } x/c = 65\% \\ D_S &= qct(0.011 + 0.08t/c) \text{ when } x/c = 50\% \\ D_S &= qct(0.009 + 0.13t/c) \text{ when } x/c = 35\% \end{aligned} \quad (2.14)$$

These equations are used in the present study for estimation of spray drag of struts. Values for other thicknesses can be interpolated from the equations.

2.9 Cavitation and Ventilation

Major factors in the design of hydrofoil vessels of any kind is the limitation in performance imposed by cavitation and ventilation. Cavitation causes a large increase in drag and decrease in lift. Cavitation invariably occurs in conventional hydrofoil craft above a certain operating speed (typically around 50 knots but can be delayed to 60 knots). When the vapor bubbles caused by cavitation collapse in the water, they produce strong shock waves. If the collapse occurs in the vicinity of the foil, the shock waves not only produce unpleasant noise and vibrations (and subsequent fatigue problems), but can also physically damage the foil of the craft through pitting.

Cavitation needs consideration mainly in the planing phase for hydrofoil-assisted catamarans. It usually occurs in the form of an attached sheet starting at the leading edge and covering a substantial portion of the suction side of the foil. Alternatively, cavitation may start at mid-chord position close to the point of maximum thickness of the foil. Care has to be taken particularly in the vicinity of struts and near trailing edge flaps [NGF79]. The prediction of the susceptibility of a foil design to cavitation requires determining the pressure distribution over the foil including free surface effects, foil-hull interaction as well as fore-aft interactions between multiple foils [Fei81, Mor91]. This prediction can be done with sufficient accuracy using numerical methods [NGF79, Wal99].

Furthermore, tip vortex cavitation can occur [YHTC94] or the tip vortices can connect with the free surface [KT99] which can lead to ventilation of the vortex core and possibly of the foil. Numerical investigations [KMHN01] have shown that there is strong interaction between the tip vortices and the hull. Often the tip vortices are located very close to the hull surface, so that there is a risk that such vortices may interfere with the propulsor and cause waterjet or propeller cavitation.

As most hydrofoils are designed to avoid cavitation and ventilation it is not necessary to consider the drag due to these factors in any detail. Chapter 5 presents details on hydrofoil design to avoid cavitation.

Chapter 3

Model Testing and Scaling

Abstract

Model testing and scaling of model test data of high-speed craft and in particular hydrofoil-assisted catamarans introduces significant inaccuracies to the conventional Froude scaling method. Model testing small models of high-speed craft requires special attention to be paid to the generation of spray, air resistance and, particularly important for hydrofoil-assisted catamarans, viscous scale effects. It is shown that viscous scale effects cannot be properly accounted for in the scaling procedure for hydrofoil-assisted catamarans if small models are used. This is due to laminar flow effects that reduce the lift of the hydrofoils. It is found that with the use of proper turbulence stimulation and large models, one can improve the accuracy and reliability of scaling procedures for model test data of hydrofoil-assisted catamarans.

3.1 Introduction

Model testing of hydrofoil-assisted catamarans poses a much more serious challenge than tests for conventional displacement vessels where Froude's hypothesis for correlating model test results is well established. According to Froude [Fro55], the total resistance consists of frictional resistance and residual resistance. Frictional resistance is a function of the Reynolds number (see Equation 2.1) and is proportional to the wetted surface of the hull. Residual resistance encompasses all the remaining resistance components including wave-making, eddy-making, spray etc. Residual resistance is proportional to the wetted surface of the hull, and the residual resistance coefficient, C_R , which is the same for the model and the full scale ship provided the Froude number of both is the same and the boundary layer is turbulent.

A number of important complications are introduced when applying Froude's hypoth-

esis to model testing and scaling of high-speed craft. These are due to factors that cannot be practically scaled without violating some dimensional scaling laws during model tests. The development of a suitable correlation procedure for hydrofoil-assisted catamarans therefore requires one to do a much more thorough breakdown of the resistance components. This way, the necessary corrections due to scaling can either be introduced theoretically into the correlation method or by means of changes in the test procedures introduced to improve the accuracy of scaling for high-speed craft.

The resistance components of hydrofoil-assisted catamarans have been discussed in detail in Chapter 2. Those components that are affected by model scaling are discussed in detail in this chapter.

3.2 Surface Tension

At high speed, the effect of surface tension becomes significant as it is associated with the generation of spray [JF91, Gri97]. Surface tension is a function of the Weber number, W_n :

$$W_n = \frac{V_{SR}^2 d_s \rho}{\sigma} \quad (3.1)$$

To achieve equal Weber numbers, the model speed must be scaled up with $\sqrt{\lambda}$. This cannot be practically implemented without violating the Froude scaling laws. The nature of spray and the spray wetted area will therefore be different on the models. It is a coherent sheet of water at model scale instead of a jet of droplets. The spray therefore only separates from chines and spray rails at higher speeds than Froude scaled speeds and reattachment may occur downstream. This results in an undesirable increase in wetted area. The friction coefficient of the wetted area of the spray sheet is also larger than that appropriate to the rest of the hull [MG97a]. These effects on resistance cannot be determined experimentally or analytically at present.

To minimize this added model spray friction resistance it is usually recommended that spray rails be used. To ensure separation of flow from spray rails, the rail angle needs to be made very sharp and should also be enlarged [Gri97] compared with spray rails used on full sized vessels. Figure 3.1 shows the spray rails of models used in this study where spray resistance was considered important. Spray rails were designed according to the guidelines of Müller-Graf [MG89]. Observations during model tests show that these rails suitably separate the coherent spray sheet.

The errors resulting from the effects mentioned above are fortunately not very large, so with the use of spray rails these effects are minimized so that model tests provide a useful result.



Figure 3.1: Spray rails for a Hysuwac model. Also shown are the turbulence stimulators on the hull (black strips).

3.3 Cavitation

The cavitation number of hydrofoil craft cannot be scaled properly without reducing the ambient pressure. This means that hydrofoil cavitation inception and the associated loss of efficiency of the foil cannot be captured experimentally using standard towing tank facilities. Loss of lift due to cavitation can reach 80% and the increase in drag is in the order of 100%. Cavitation characteristics can only be investigated in special cavitation tunnels, where the pressure can be suitably reduced. For the case of hydrofoils operating close to the free surface this ideally needs a free surface cavitation tunnel such as available at the Technical University of Berlin¹ and in Ede in the Netherlands.

Cavitation can usually be fairly accurately predicted using theoretical methods. In this study cavitation limits for hydrofoils were calculated using the AUTOWING software [Kor98]. The pressure distribution calculated by means of the vortex lattice method provides the ability to determine the presence of cavitation for a 3-dimensional wing including the effect of the free surface. If the cavitation limits for a particular foil configuration are known one can design to avoid cavitation, making it unnecessary to consider cavitation during model testing.

¹Versuchsanstalt für Wasserbau und Schiffbau, Technische Universität Berlin

3.4 Air Resistance

High-speed ships experience a significant amount of their resistance due to air resistance (up to 30%), which is proportional to the frontal area of the ship. Models usually don't include the vessel superstructure, so this introduces significant errors in the final resistance prediction if it is not accounted for. The most accurate way of determining the air resistance, is by testing the scaled emerged parts of the vessel in a wind tunnel and measuring the air resistance component directly.

For determining the air resistance in the towing tank, two techniques were applied and compared in this study. Firstly, a model was towed through the air hanging just above the water and the resistance measured. An error in the air resistance is introduced due to the whole hull being out of the water which is not the case in reality, but nevertheless gives an indication of the air resistance component. A second air resistance measurement was done by towing the same model through the water behind a screen blocking the air flow. The difference in resistance between testing the model firstly with the screen in place and later without the screen, gives the air resistance component of the model. The result will still include some minor error as the screen can never block the air flow completely.

Figure 3.2 shows the comparison between the two methods of determining the air resistance for a 2.5m model. In dimensionless form the curves convert approximately to an air resistance coefficient, $C_{AA} = 1.4$, based on the frontal area of the model. As mentioned in Section 2.7, prototype C_{AA} values are typically around 0.42 – 0.7, substantially lower than that for the model. A major reason for this is the non-streamlined shape of the model framework.

Based on these measurements and results, the following scheme has been adopted to correct for the model effect. The model resistance is measured in the towing tank using the screen to eliminate air resistance². The measured resistance is then scaled up using Froude's scaling laws giving the prototype resistance without any air resistance. A prediction of the prototype air resistance is then done based on the frontal area of the vessel, including superstructure, using a drag coefficient of $C_{AA} = 0.5 - 0.7$ (a partially streamlined body).

3.5 Reynolds Number Effects

The differences in Reynolds numbers between full-scale and model-scale result in differences in the boundary layer between model and full scale. The thicker and sometimes laminar boundary layer at model scale results in a different pressure distribution

²This method is consistent with the procedures used in other towing tanks (e.g. The Krylov Institute, David Taylor Model Test Basin) for model tests of high-speed craft.

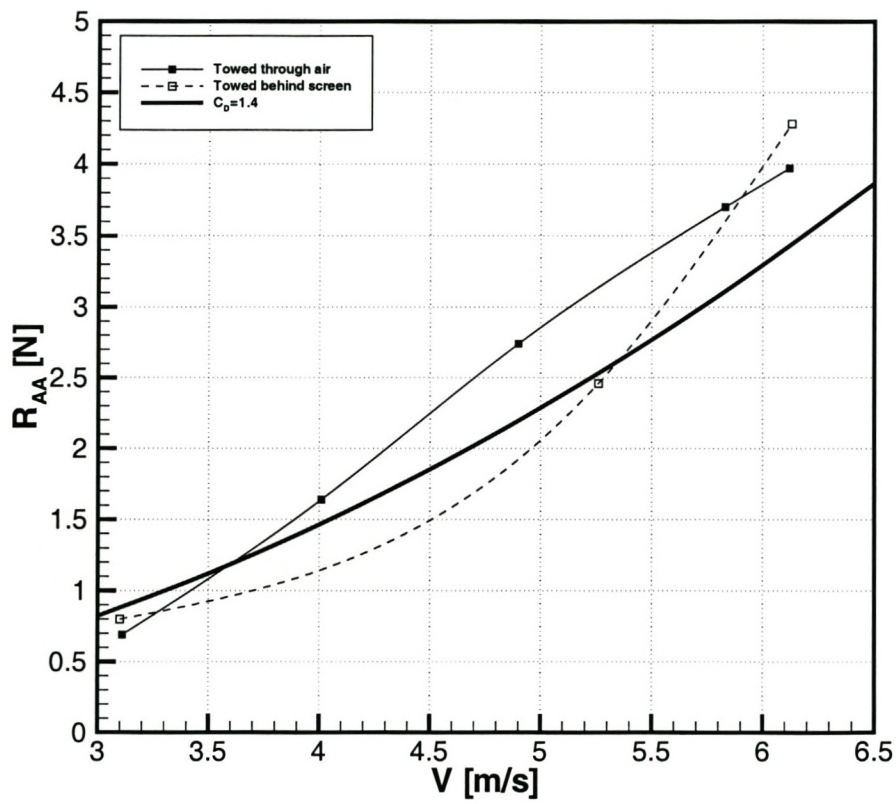


Figure 3.2: Air resistance of a 2.5m model

on both the hull and the foils. The thicker boundary layer at model scale means that models experience extra viscous pressure drag. Resulting speed predictions for conventional high-speed catamarans based on model tests can err as much as 10% due to this effect [Arm99]. Trim can also be over-predicted by as much as 1 degree. For model hydrofoils the situation is more severe as a large part of the foil operates in laminar flow. To achieve similar lift and drag characteristics on model and full-scale foils that can be scaled using normal Froude scaling, one would require testing in turbulent flow. For hydrofoil-assisted vessels this is difficult to achieve. Reynolds numbers of at least 5×10^5 are needed to ensure turbulent flow with turbulence stimulation. For the University of Stellenbosch towing tank, which has a carriage speed of 8.5 m/s, this would lead to model sizes too large for the tank if blockage and shallow water effects are to be avoided. Based on model sizes of 2m, typical of the models used in this study, the hydrofoils operate between $3 \times 10^4 < Rn < 2 \times 10^5$, while the hulls are at $1 \times 10^6 < Rn < 3 \times 10^6$. Effective turbulent stimulation can ensure that the hull boundary layer will be turbulent, it cannot be ensured at the Reynolds numbers of the foils. Laminar flow tells on both the drag and lift coefficient as laminar separation takes place on the suction side. Figure 3.3 shows the typical laminar separation by means of a paint trace on a model hydrofoil as observed during model tests conducted in this study.

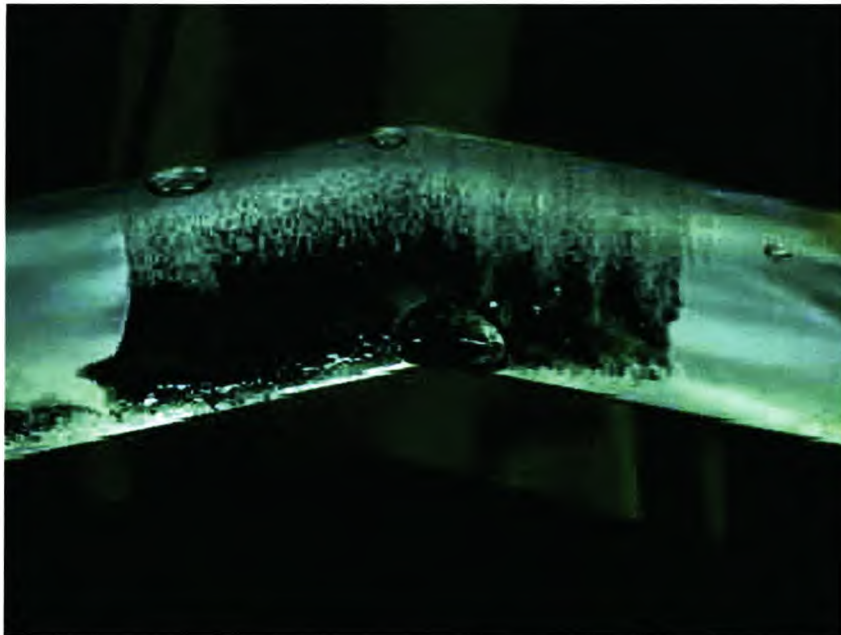


Figure 3.3: Paint trace test showing separation on an 8% thickness foil at $Rn = 8 \times 10^4$ (leading edge at top)

The effect on lift is less pronounced yet still significant. Viscous and separation effects reduce the lift curve slope of the foil. The lower lift produced by model foils means

that the attitude of the whole vessel will be different, influencing the wetted area, wave-making as well as the induced drag of the foils. The following sections explain these effects in more detail and how one can take them into account in correlating hydrofoil data at low Reynolds numbers.

3.5.1 Effect on Drag Coefficient

To satisfactorily correlate hydrofoil resistance the laminar flow and separation of flow over the foils need to be accounted for. Laminar separation has been shown to increase the drag of non-lifting streamlined sections by an order of about two for $Rn \leq 5 \cdot 10^5$. Kirkman et al. [KK80] have developed the following empirical relations for estimating the drag as a function of Rn , which include the effect of laminar separation.

$$\begin{aligned}
 & \text{For } Rn < 5 \times 10^4 : \\
 C_{D_0} &= 1.46Rn^{-0.507} \\
 C_{D_{20}} &= 0.466Rn^{-0.259} \\
 & \text{For } 5 \times 10^4 \leq Rn \leq 5 \times 10^5 \\
 C_{D_0} &= 0.172Rn^{-0.310} \\
 C_{D_{20}} &= 181Rn^{-0.810} \\
 & \text{For } 5 \times 10^5 < Rn < 1 \times 10^7 \\
 C_D &= 2.93 \times 10^{-3} \left[1 + 2\frac{t}{c} + 60 \left(\frac{t}{c} \right)^4 \right] \\
 & \text{For } Rn > 1 \times 10^7 \\
 C_D &= 0.03Rn^{-0.1428} \left[1 + 2\frac{t}{c} + 60 \left(\frac{t}{c} \right)^4 \right] \tag{3.2}
 \end{aligned}$$

All drag coefficients are based on twice the plan form area of the foil. C_{D_0} represents values for $t/c = 0$ and $C_{D_{20}}$ values for $t/c = 0.20$. Values for other thickness to chord ratios can be linearly interpolated from these. Equation 3.2 allows one to determine the friction deduction for laminar flow and laminar separation drag while using standard Froude scaling.

These equations do not take into account the friction reduction close to the free surface and it can be assumed that they are valid for $h/c \leq 3.0$ similar to the turbulent flow foil friction drag equations given in Section 2.8.2. For hydrofoils close to the free surface, it is more suitable to approach estimation of the friction and form drag in a similar manner to that proposed by Egorov et al. [ES65] described in Section 2.8.2, which is a function of the submergence of the foil. The experimental results of Schuster and Schwaneke [SS60] reproduced in Figure 3.4 illustrates how the total foil drag decreases

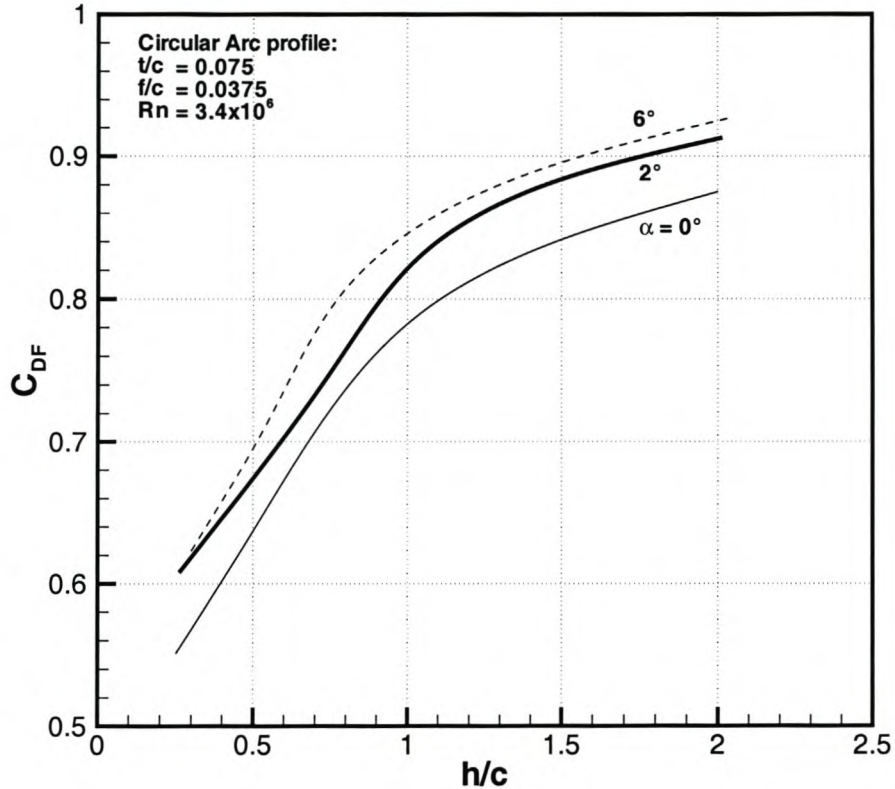


Figure 3.4: Foil drag coefficients (based on planform area as a function of submergence)

as the foil approaches the free surface. This is in spite of increased wave drag close to the free surface. This implies a reduction in the form drag close to the free surface.

3.5.2 Effect on Lift Coefficient

It is well known that viscosity in general affects hydrofoil lift in two ways. Decreasing Reynolds number reduces the lift curve slope and increases the zero-lift angle. This leads to increasing lift force at lower angles of attack and decreasing lift at higher angles.

As the foil Reynolds number increases with speed, the effects of viscosity become less and less, making it possible to predict foil characteristics at prototype Reynolds numbers with reasonable accuracy using potential flow theory although it is still ben-

essential to introduce some viscous corrections [Wal99]. At lower model scale Reynolds numbers, the viscosity effect on the foil lift can be investigated using empirical or theoretical methods. Van Walree [Wal99] found that a 2D panel method incorporating boundary layer theory such as XFOIL [Dre89] is suitable to determine the viscosity effect on the lift curve slope of foil sections provided that $Re > 5 \times 10^5$. Even though this is a 2-dimensional calculation, the corrections on the lift curve slope were found to be applicable in 3-dimensions as well and can be used to predict viscosity effects during model testing.

The viscosity effect on the 2D lift curve slope is a function of Reynolds number, the state of the boundary layer (laminar or turbulent) and the closure angle of the foil trailing edge. Both Martin [Mar63a, Mar63b] and Egorov et al. [ES65] present empirical methods to correct for viscosity effects. Martin presents a lift curve slope reduction factor due to viscosity, f_α :

$$f_\alpha = \frac{C_{L\alpha v}}{C_{L\alpha p}} \quad (3.3)$$

$$C_{L\alpha p} = 2\pi f_t \quad (3.4)$$

$$f_t = (1 + 0.80(t/c)) \quad (3.5)$$

where $C_{L\alpha v}$ is the lift curve slope in viscous flow. Martin's values are shown in Figure 3.5. $C_{L\alpha p}$ is the 2 dimensional potential flow lift curve slope which is greater than 2π (thin foil theory) due to non-linear effects caused by the thickness of the foil section (f_t). Martin provides a useful equation for determining the thickness effects empirically with Equation (3.5). Alternatively one can also use the theoretically derived equation [ES65]:

$$f_t = \frac{1}{1 - \frac{2t/c}{\pi}} \quad (3.6)$$

For turbulent flow Reynolds numbers, the increase in lift due to thickness (f_t) is cancelled by viscous reduction in lift (f_α), meaning that thin foil theory often provides reliable predictions of lift without the need for correction of viscous effects [MKS98, Wal99].

Unfortunately Martin's curves (shown in Figure 3.5) are only applicable for $Re > 1 \times 10^6$ but give a clear indication for the magnitude of viscous effects. For large trailing edge closure angles at a Reynolds number of 10^6 the loss in lift can be as high as 30%. As mentioned, model tests of hydrofoil-assisted catamarans typically have Reynolds numbers in the range of $3 \times 10^4 < Re < 2 \times 10^5$ and Figure 3.5 does not provide data. XFOIL provides an alternate means to determine f_α for these Reynolds numbers.

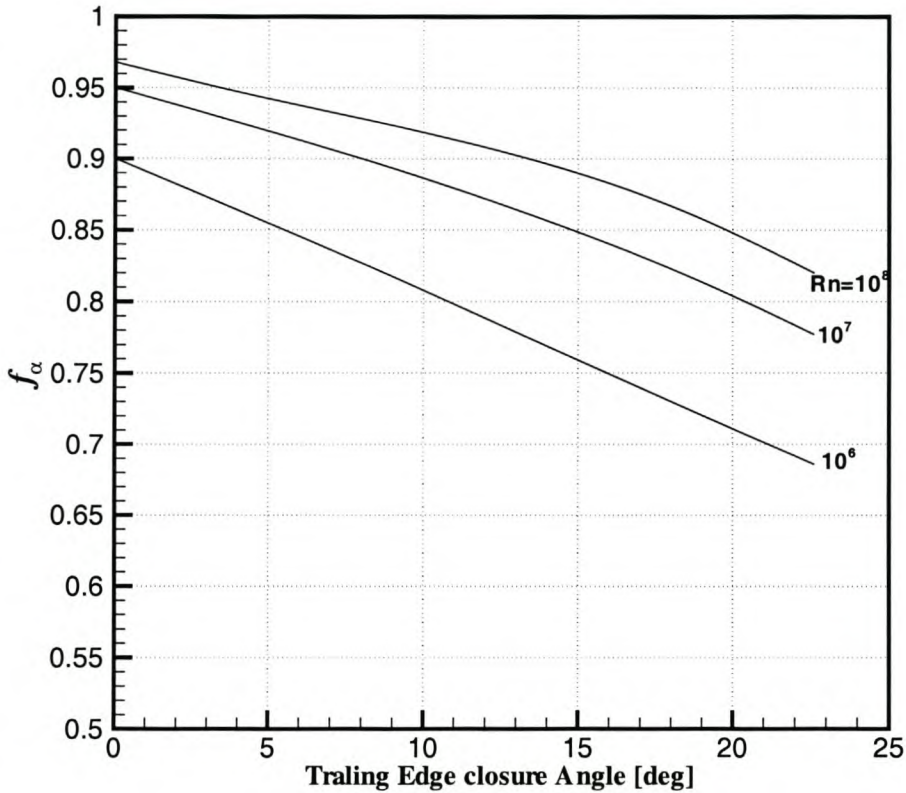


Figure 3.5: Viscosity effect on the lift curve slope for profiles with leading edge turbulence stimulation

To determine the accuracy of XFOIL in predicting f_α , XFOIL results were compared with experiments for some hydrofoil profiles and also a number of airfoils. These are listed in Table 3.1. Unfortunately no test data for typical hydrofoil profiles at Reynolds numbers below 5×10^5 are available, so instead, wind tunnel data for a number of low speed airfoils, listed on the NASG airfoil database [Gro01] were used. Fluid dynamic forces measured in water differ somewhat to those in air [HB75] due to higher wind tunnel freestream turbulence. The use of wind tunnel data for airfoils are therefore not ideal for investigating the abilities of XFOIL for hydrofoils, but will nevertheless give a good indication of the XFOIL's abilities.

Table 3.2 shows the comparisons of the lift curve slope for different Reynolds numbers based on experimental data and XFOIL calculations. The empirical values of Martin's Equation 3.3 are also given. All foils apart from the YS920 (which had leading edge turbulence stimulation) had free transition to turbulence.

Profile	t/c	f/c	r_{te}	τ_{te}	how tested	turb. stim.
YS 920 [She85]	0.0905	0.0214	0.0018	5.02	towing tank	leading edge
DAE51 [Gro01]	0.0938	0.0403	0.0088	7.79	wind tunnel	none
AQUILA [Gro01]	0.0939	0.0399	0.0078	10.24	wind tunnel	none
SPICASM [Gro01]	0.1172	0.0462	0.0128	15.13	wind tunnel	none
CR001 [Gro01]	0.0733	0.0406	0.0059	18.19	wind tunnel	none

Table 3.1: Profiles used for investigating viscous effects

Type	Rn	f_{α} -exp	f_{α} -XFOIL	f_{α} -Martin
YS 920	2.5×10^6	0.885	0.880	0.801
	1×10^7	-	0.938	0.892
DAE 51	101 400	0.837	0.998	-
	153 500	0.817	0.907	-
	203 200	0.817	0.929	-
	310 400	0.817	0.928	-
	1×10^6	-	0.925	0.86
AQUILA	101 500	0.770	0.872	-
	150 500	0.790	0.883	-
	203 900	0.809	0.895	-
	301 100	0.813	0.894	-
SPICASM	202 300	0.839	0.887	-
	301 500	0.839	0.896	-
CR001	199 000	1.167	1.087	-
	298 800	0.985	0.970	-

Table 3.2: Comparison of lift curve slope correction factors

Type	Rn	α_0 -exp.	α_0 -XFOIL	α_0 -Egorov	α_0 -PT
YS 920	2.5×10^6	-2.15	-2.17	-2.18	-2.74
	1×10^7	-	-2.23	-2.49	-2.74
DAE 51	101 400	-4.27	-3.67	-3.02	-4.15
	153 500	-5.34	-4.52	-3.16	-4.15
	203 200	-5.34	-4.55	-3.26	-4.15
	310 400	-5.34	-4.37	-3.40	-4.15
	1×10^6	-	-4.38	-3.80	-4.15
AQUILA	101 500	-4.70	-4.08	-2.66	-3.40
	150 500	-4.62	-3.96	-2.84	-3.40
	203 900	-4.45	-3.83	-2.98	-3.40
	301 100	-4.48	-3.85	-3.15	-3.40
SPICASM	202 300	-2.24	-4.59	-3.12	-4.23
	301 500	-2.30	-4.50	-3.38	-4.23
CR001	199 000	-3.30	-3.86	-2.24	-4.90
	298 800	-4.26	-4.60	-2.56	-4.90

Table 3.3: Comparison of zero-lift angle of attack

The experimental results show that f_α is significant for all the profiles, with as much as a 23% loss in lift. The results show that in general, XFOIL underpredicts the loss in lift. The difference between XFOIL and experimental values is quite large (14%) for Reynolds numbers around 200000, and become less as the Reynolds number increases. For those profiles with higher trailing edge closure angles (SPICASM and CR001) the discrepancies are smaller (5% and 1% respectively) between XFOIL and experiments. Once turbulent flow conditions prevail XFOIL is in good agreement with experimental values for the hydrofoils examined. Van Walree [Wal99] found similar results for his tests at $Rn \geq 5 \times 10^5$.

As mentioned earlier, Reynolds number scaling also affects the zero lift angle of the foil. Egorov et al. [ES65] found that the zero-lift angle (in degrees) can be determined through the following empirical relation:

$$\alpha_0 = 100 \frac{f}{c} - 0.1\tau(6.3 - \log Rn) \quad (3.7)$$

where f is the maximum camber, c the chord and τ is closure angle (in degrees) of the trailing edge. The influence of viscosity on the zero-lift angle of attack can also be investigated with XFOIL. Table 3.3 shows the results for the same foils given in Table 3.1. The zero lift angle according to potential flow XFOIL (PT) calculations are also given.

The viscosity effect on the zero-lift angle is clear from the experimental results and

calculations. Both XFOIL and Egorov et al.'s empirical equation have trouble in predicting the correct zero-lift angle for laminar flow Reynolds numbers. The potential flow solution always overpredicts the experimental value quite substantially and the thickest profile tested is also the one that is worst predicted by both XFOIL and Egorov et al. This is most likely due to laminar separation effects taking place over the foil that are not fully captured by XFOIL and not considered in Equation 3.7. For turbulent flow Reynolds numbers, the situation improves dramatically with both the equation of Egorov et al. and XFOIL being in good agreement with experiments for the case examined.

3.5.3 Free Surface Effects on Viscous Corrections for 3-Dimensional Hydrofoils

The free surface effect changes the pressure distribution particularly on the suction side of the foil profile. This will influence the boundary layer as the pressure gradients and lift contribution of the suction side are less. Very little experimental data are available investigating this fact. Min et al. [MKS98] gives some comparisons between various potential flow methods and experimental results for two different profiles in turbulent flow. The results indicate that potential flow methods consistently overpredict the lift. It is not clear whether this is a viscous effect or computational error. 3-dimensional viscous effects of wings was investigated by van Walree [Wal99] in the development of his numerical methods. It was found that 2-dimensional viscous predictions were sufficient to predict 3-dimensional viscous effects but no mention is made of how free surface effects influence the viscous correction. To investigate this, experimental data for three different hydrofoils were compared with theoretical predictions.

The hydrofoils used in the development of the Hysucat and Hysuwac foil systems typically make use of circular arc profiles. These differ substantially from those given in Table 3.1. Unfortunately no experimental data examining Reynolds number effects on these profiles are available. Three wings for which experimental data are available were investigated to get an idea of 3-dimensional and free surface viscous effects on the lift characteristics of a hydrofoil. Table 3.4 gives the particulars of the wings investigated. The first two represent typical asymmetrical hydrofoil profiles, the third is symmetrical profile thicker than what is used on typical hydrofoil craft. The Göllk profile was tested without turbulence stimulation. The NACA 23-008 profile made use of a trip wire stimulator to turbulate the flow ahead of the foil. The NACA 16-012 profile made use of Hama strips attached to the suction side near the leading edge.

The 3-dimensional potential flow solution was calculated with the vortex lattice method of AUTOWING (AW) (explained in Chapter 4). AUTOWING has been validated for hydrofoil calculations under the free surface [KT99]. Experimental (exp) lift curve slope correction factors (f_α) were calculated for the 3-dimensional foils and compared with the 2-dimensional result of XFOIL for different submergences. Table 3.5 contains

Profile	t/c	f/c	r_{le}	τ_{te}	Rn	h/c
mod. Gö11K [Hop90]	0.077	0.0380	0.0075	17.00	0.69×10^6	0.06 - 1.5
NACA 23 008 [EB68]	0.080	0.0800	0.0070	10.68	0.25×10^6	0.2 - 2.0
NACA 16 012 [Yam93]	0.120	0.0000	0.0070	15.81	0.68×10^6	0.125 - 1.0

Table 3.4: Particulars of hydrofoils used for investigating 3-dimensional viscous and free surface effects.

Profile	h/c	f_α -exp	f_α -XFOIL	α_0 -exp	α_0 -AW	α_0 -XFOIL
Gö11k	0.125	1.010	0.824	-4.10	-4.02	-3.128
	0.25	0.944	0.824	-4.50	-4.41	-3.487
	0.5	0.747	0.824	-4.70	-4.81	-3.788
	1.0	0.817	0.824	-4.80	-4.85	-4.003
	1.5	0.772	0.824	-4.80	-4.85	-4.086
NACA23008	0.1	1.007	0.851	+0.35	-0.25	-0.061
	0.2	0.954	0.851	-0.40	-0.30	-1.000
	0.3	0.933	0.851	-0.75	-0.59	-1.206
	0.5	0.907	0.851	-1.00	-0.88	-1.431
	1.0	0.865	0.851	-1.30	-1.10	-1.656
NACA16012	0.125	0.723	0.746	2.42	2.60	1.844
	0.25	0.704	0.746	1.60	1.40	1.205
	0.5	0.679	0.746	0.95	0.39	0.683
	1.0	0.670	0.746	0.60	-0.16	0.315

Table 3.5: Viscous correction factors for wings under the free surface

the results. Also included are comparisons for the zero-lift angles. As the free surface effect influences the zero lift angle, the XFOIL result is corrected using the following empirical equation [ES65].

$$\Delta\alpha_0 = \frac{t/c}{2} \left(\frac{1}{k_\phi} - 1 \right) \quad (3.8)$$

$$k_\phi = 1 - (0.5 + t/c) \exp(-2(h/c)^{0.6})$$

in the formula $C_L = C_{l\alpha}(\alpha + \alpha_0 - \Delta\alpha_0)$ with $\Delta\alpha_0$ in radians.

The clear tendency that emerges from Table 3.5 is that as the foil approaches the free surface, f_α tends towards one, indicating that viscous effects play a smaller role. This makes good sense as viscous effects are important mainly on the suction side of the foil, where the adverse pressure gradients are found. Close to the free surface, the suction side of the foil contributes only a small fraction of the lift. The pressure side of the foil has favorable pressure gradients and thus the boundary layer is less

effected by the Reynolds number. Comparing pressures on the under-side of the foil for potential and viscous flows at Reynolds numbers as given in Table 3.4, very little or no difference in the pressures can be found. Experimental investigations [ES65] have shown that this holds true under the free surface as well.

As explained in Chapter 2, the free surface effect does reduce the friction drag coefficient. As both friction drag and f_α are related to boundary layer effects and Reynolds number, this reduction of friction drag close to the free surface supports the result of Table 3.5. For the two asymmetrical thinner profiles (7.7% & 8%), f_α is negligible for the shallowest submergences. For the thicker 12% foil, f_α follows the same tendency but is still significant close to the free surface. This is most likely due to the thicker profile having larger induced velocities that are stronger than the free surface effect and also the profile being symmetrical means that the pressure side also experiences adverse pressure gradients that would lead to separation. The work of Gebhardt [Geb68], who investigated the friction resistance of a 30% thick symmetrical hydrofoil under the free surface, substantiates this. Gebhardt showed that the free surface has little effect on the friction resistance for his thick profile. The thick symmetrical profile is shown to suffer high pressure gradients on the pressure side.

Figure 3.6 shows a comparison of the potential flow pressure distributions for the Gö11k profile and the NACA 16012. One can clearly see how the upper side of the profile is influenced by the free surface, while the lower surface remains largely unaffected. Notice that at the shallowest submergence ($h/c = 0.1$) there is actually a favorable pressure gradient on the upper surface from mid-chord towards the trailing edge. The freedom of the free surface to deform makes the flow over the upper part of the foil conform to the foil shape. This allows the downstream end of the flow to accelerate and to become thinner creating the favorable pressure gradient, which in turn affects the boundary layer in a positive way. In contrast, the under side of the asymmetrical foils have a practically flat distribution in relation to the upper side. Potential flow investigations show that this remains so for all reasonable attack angles. Without pressure gradients the viscous effects on lift and drag are less severe. The symmetrical NACA 16012 profile is quite different therefore the findings are similar to those found by Gebhardt.

Table 3.5's result further show that AUTOWING's predictions of the zero-lift angle, without viscous correction, are in quite good agreement with experimental values for the 3-dimensional wings, with the largest errors occurring at the shallowest submergences. This result seems to indicate that the viscous effect is less severe on zero-lift angle for 3-dimensional hydrofoils and can for engineering purposes be ignored, especially for the typical hydrofoil thickness ratios, which is not in line with findings for deeply submerged foils from which Equation 3.8 was developed. Further basic research is needed to clarify this effect.

The results presented in this section nevertheless clearly indicate that viscous effects have an important effect on hydrofoil lift, and that they are a function of Reynolds

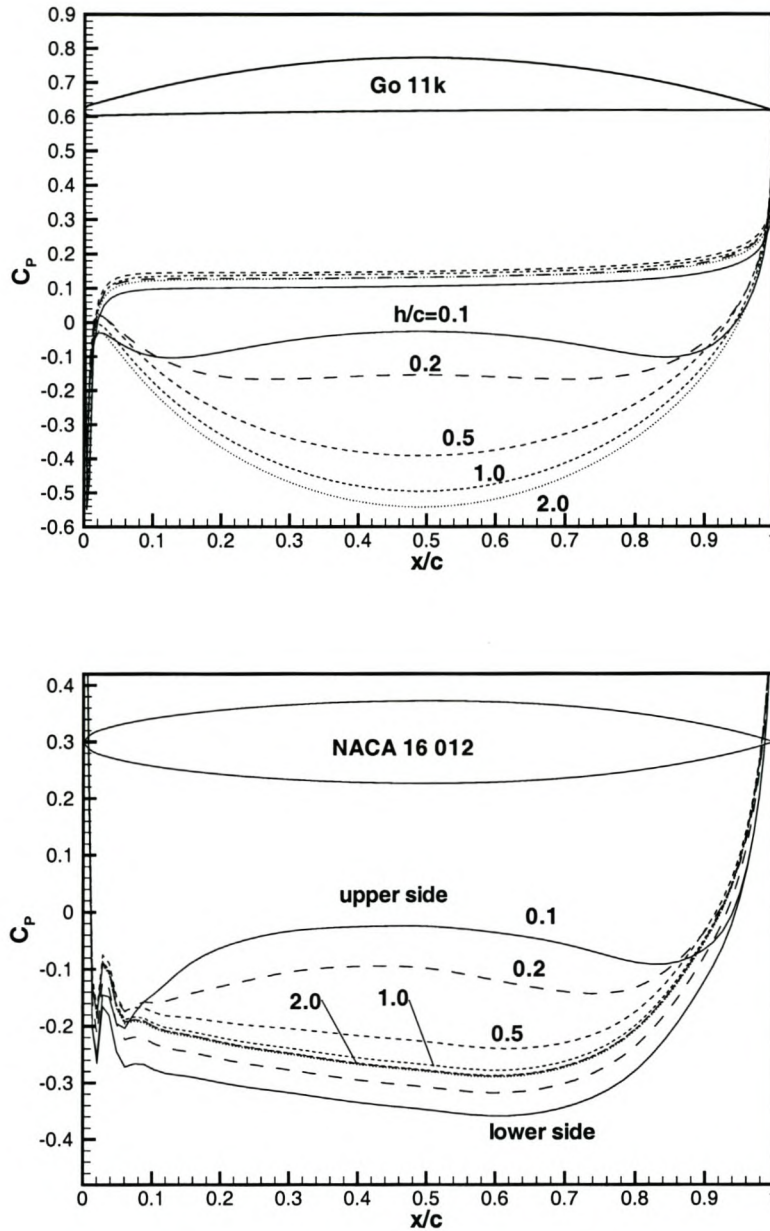


Figure 3.6: Potential flow pressure distributions including free surface effect for a symmetrical and asymmetrical profile at $\alpha = 0.0$ degrees

number, hydrofoil submergence and the profile geometry. For thin asymmetrical profiles (7%-8%) typical of practical hydrofoils, viscous effects can be ignored at very shallow submergence, seemingly irrespective of Reynolds number. For deeper submergences and thicker profiles one needs to correct for its effect. The results given in Tables 3.2, 3.3 and 3.5 indicate that there is no easy way to theoretically predict the lift characteristics of foil sections operating in laminar or transitional flow regimes. XFOIL offers more reliable results than the empirical equations, but still not completely satisfactory results. The conclusion of van Walree [Wal99] concerning viscous effects on hydrofoils is echoed here: "Laminar flow is undesirable because its occurrence and extent are difficult to predict and therefore difficult to correct in the extrapolation of model test results to full scale values." Some effort should therefore be made to eliminate laminar flow during model testing through effective turbulence stimulation. Before examining turbulence stimulation in detail it is necessary to discuss freestream turbulence and its influence on the boundary layer.

3.5.4 Freestream Turbulence

Freestream turbulence hastens the transition process from laminar to turbulent flow. It is defined as root mean square (RMS) of the fluctuating velocities in reference to the mean free stream velocity. The effect of freestream turbulence on transition is strong, at 0.35% freestream turbulence, the transition Reynolds number has dropped 50% from its "quiet value" [Whi91].

The effect of freestream turbulence was investigated with XFOIL for a circular arc profile typical of those used and tested in this study. XFOIL uses the e^n method [Whi91] to predict transition. n specifies the level of turbulence. Drela [Dre96] recommends values of $n \leq 1$ ($n = 1$ corresponds to 1.9% freestream turbulence) for very high levels of turbulence. To obtain some idea of the sensitivity of the lift to freestream turbulence, calculations were done for different values of free stream turbulence: 0.07%, 0.6% and 1.9% freestream turbulence. 0.07% is considered as standard low turbulence conditions found in an average wind tunnel. Figure 3.7 presents the results for the profile.

The figure shows a lot of variation in lift especially in the $-1 \geq \alpha \geq 3$ range. The humps and hollows in the lift curve are due to boundary layer effects associated with transition from laminar to turbulent flow. The same tendencies have been found experimentally on other hydrofoil profiles [JM79, SIS01] and is well known for low Reynolds number airfoils [SDF89]. The effect is due to the size and position of the separation bubble, which is influencing the lift (and drag) of the foil [SDF89]. These humps are generally minimized and shifted to lower angles of attack by increased free stream turbulence. For $Rn = 1 \times 10^6$ the maximum difference in C_L is about 18% between low (0.07%) and high (1.9%) freestream turbulence conditions. For $Rn = 1 \times 10^5$, the maximum difference is about 10%. For higher angles of attack: $\alpha \geq 3$

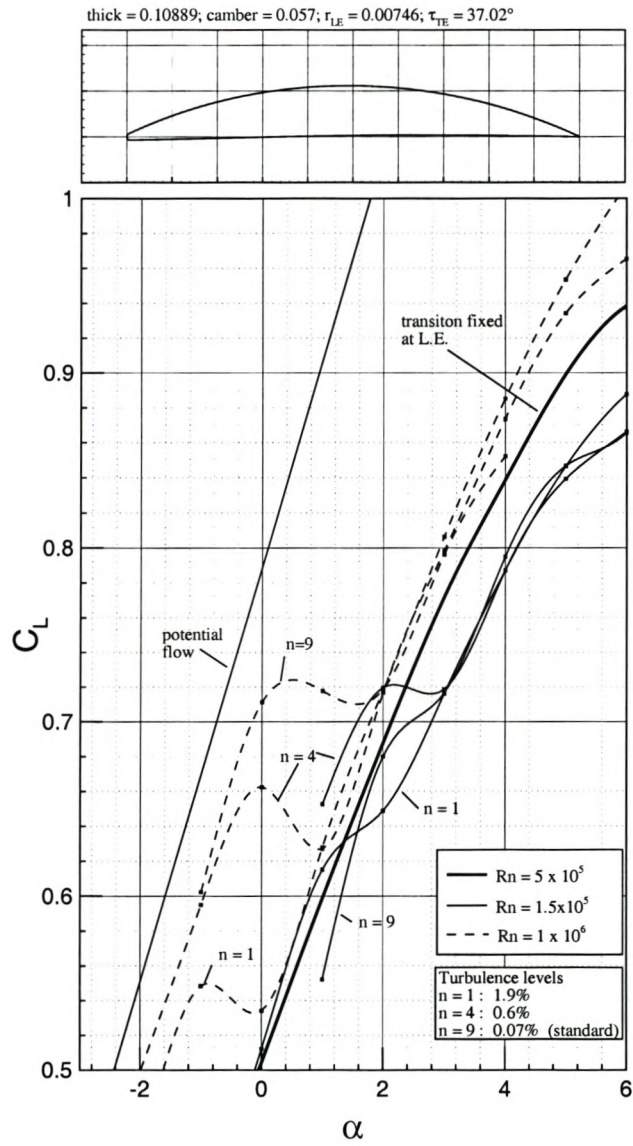


Figure 3.7: The effect of freestream turbulence on an 11% circular arc section

freestream turbulence has negligible effect for model scale and full scale Reynolds numbers until such angles that turbulent separation becomes important.

The result confirms the need to avoid laminar flow conditions over the foils. To illustrate this further, the much 'nicer' result, free of transition humps and hollows (for the profile at $Rn = 5 \times 10^5$ with leading edge transition) is included in Figure 3.7 for comparison.

3.5.5 Turbulence Stimulation

By inducing turbulent flow over the hydrofoil the negative effects associated with transition and laminar separation can be avoided or at least minimized. The result of XFOIL given in Figure 3.7 as well as results of various investigators [JM79, Lew89, Wal99] show that more predictable lift characteristics can be obtained under turbulent flow conditions induced by turbulence stimulators. A number of different turbulence stimulation techniques have been used with varying success during hydrofoil testing. The use of mechanical turbulators or trips (sand grains, zig-zag tape etc.) are the most obvious solution, but their use for Reynolds numbers of interest in this study is controversial. Very little information is available on turbulence stimulation for hydrofoils. Some sources recommend turbulence stimulation for hydrofoil tests above $Rn = 5 \times 10^5$ [Wal99], while others mention that it is not practicable at all [MG81].

Mechanical turbulence stimulation has nevertheless been extensively used for airfoils at low Reynolds numbers (down to $Rn = 4 \times 10^4$) [Pre86], to reduce profile drag due to separation and also increase the lift in some cases. It is therefore worth investigating for hydrofoil applications as well. Turbulence trips have been found to have beneficial or detrimental effects on lift [SDF89]. A number of investigations concerning their use nevertheless indicate that turbulence stimulation does have the desired effect of eliminating a non-linear lift curve slope [Pre86, Lew89]. The effectiveness of turbulence trips depends to a large extent on the profile shape and the magnitude of the pressure recovery gradient on the aft part of the profile. Aeronautical experience has shown that turbulence trips are particularly useful if a profile has a large laminar separation bubble and the Reynolds number is $Rn \leq 3 \times 10^5$. The turbulence trip alleviates adverse effects by shortening the length of the bubble. The shorter bubble leads to reduced drag for the profile and a more linear lift curve slope. This is ultimately desirable for accurate correlation of model test results and an accurate prediction of viscous scale effects on lift. If the profile has a small bubble the trip generally increases the drag, as its own drag is higher than that of the bubble.

Mechanical turbulence trips can take the form of discrete trips or distributed roughness. Both require a certain minimum height to be effective. This height depends on the position of the trip as the boundary layer grows in thickness and with increasing chord position. A transition critical Reynolds number can be defined, which links the

critical roughness height to the flow conditions [Sch79]:

$$Rn_{crit} = \frac{V_k \cdot k}{\nu} \quad (3.9)$$

where V_k is the velocity at roughness height, k in absence of roughness. For a rough surface a value $Rn_{crit} = 120$ is supposed to induce turbulent flow [Sch79] but for completely turbulent flow the ITTC [ITT90] recommends $Rn_{crit} = 450$. This value has been found [Yam93] to be insufficient for chord based Reynolds numbers of $Rn \leq 2.2 \times 10^5$ for hydrofoils and more recent investigations by Semionicheva et al. [SIS01] have shown that ITTC recommendations are unsuitable for chord based Reynolds numbers up to $Rn = 1 \times 10^6$. Aeronautical experience [HM86] on low Reynolds number airfoils ($Rn = 1 \times 10^5$) shows that $Rn_{crit} = 600$ is a more suitable conservative value and is adopted for the current investigations.

Equation 3.9 essentially links the roughness height k to the boundary layer thickness through the velocity V_k . Practically, for $Rn_{crit} = 600$ this equation results in the critical roughness height k being close to the boundary layer displacement thickness. The freestream velocity can therefore safely be substituted for V_k .

The addition of mechanical turbulators results in additional drag for the profile. This drag is difficult to estimate. For small aspect ratio wings (1.0 to 2.0) it has been found that Hama strips³ have a drag coefficient of $C_D = 1.25$ based on the frontal area of the strip [Lew89].

Equation 3.9 gives a critical height of 0.6mm for a speed of 1m/s, typically the lowest speed where turbulence stimulation is needed for test conditions of this study. Using $C_D = 1.25$ and a typical foil size for a 2m model this results in about a 85% increase in drag for the foil. This seems somewhat too large to allow for an accurate resistance prediction and correlation of model test results.

To avoid the problem of additional drag from a mechanical turbulator, one can consider methods of turbulating the water ahead of the foil. This has to be done with care, so not to induce any significant flow wake velocity into the water from the turbulating device. Thin wires located at a distance of a few dozens of chords in front of the leading edge of a foil can be used [Gre64, EB68] and are effective to turbulate the water. The wires oscillate with frequency of a few thousand Hertz, turbulating the flow intensively.

For a non-oscillating wire, a critical Reynolds number, based on the diameter of the trip wire, k , is needed to trip the flow into turbulent flow [Whi91].

$$Rn_{crit} = \frac{V \cdot k}{\nu} \approx 850 \quad (3.10)$$

³A specific zig-zag type strip that creates 3D vortex loops within the boundary layer leading to laminar-turbulent breakdown, with minimal parasitic drag.

To cover the full speed range, $V \geq 1\text{m/s}$ during model testing, a trip wire diameter of 0.9mm is required.

3.5.6 Experiments with Turbulence Stimulation

Experiments were conducted using 1mm wire turbulators for a 2m hydrofoil-assisted catamaran model with a Hysuwac foil system [MH01], which is shown in Figure 5.3 on page 152. Usually one uses a single wire located ahead of the leading edge of the foil at the same submergence as that of the foil. As the submergence of the foils of a hydrofoil-assisted catamaran continually changes with speed, a grid of horizontal 1mm wires, spaced 1cm apart located approximately 1.5m ahead of the model were used. It was felt that this would allow the induced turbulence to spread and cover the whole submergence range of interest. The shallowest wire was located only a few millimeters below the free surface. Observations and initial tests with this system showed that the wires suitably turbulated the flow ahead of the model. The main problem encountered was that for speeds above $V_M = 3\text{m/s}$, the flow separates from the wire closest to the free surface, disturbing the free surface to an undesirable extent.

Figure 3.8 presents the resistance and rise for the model with (TS1) and without (no TS) the turbulence wires present. Interestingly and importantly for speeds $2.2 \leq V_M \leq 3.3$, the front foil rises higher with turbulence stimulation and the resistance is reduced. This indicates that the front foil is generating more lift. For model speeds, $V_M \geq 3.3$ the resistance of the vessel is increased due to the free surface disturbances caused by the wires. At these speeds the forward foil is very close to the water surface and is negatively influenced by these free surface disturbances. Observations further showed that the closely spaced wires were inducing a small mean wake velocity into the flow but it is felt this has a minor effect, since the lift of the front foil is increased. The front foil lift, being proportional to V^2 , would be very sensitive to such velocity changes and would decrease the front foil lift if this was significant.

To try and improve on the initial system, a number of different wire setups were tried. The submergence and spacing of the wires were varied to try and reduce the free surface disturbance for high speeds and secondly to reduce the wake effect from the wires. While in most cases the results were similar to those given in Figure 3.8, the best system using 5 wires with the shallowest wire submerged 25mm below the surface gave the most consistent results.

To solve the problem of the free surface disturbance, the wires were placed much farther ahead (2.5m) of the model and their span increased from 0.9m to 2m, so that the free surface disturbances had some time to settle before the model passed. Figure 3.9 shows the setup of the turbulence stimulators lifted out of the water.

Observations with this system, for the top wire submerged 25mm below the free surface, showed that the front foil lift became much stronger and the hull is lifted out

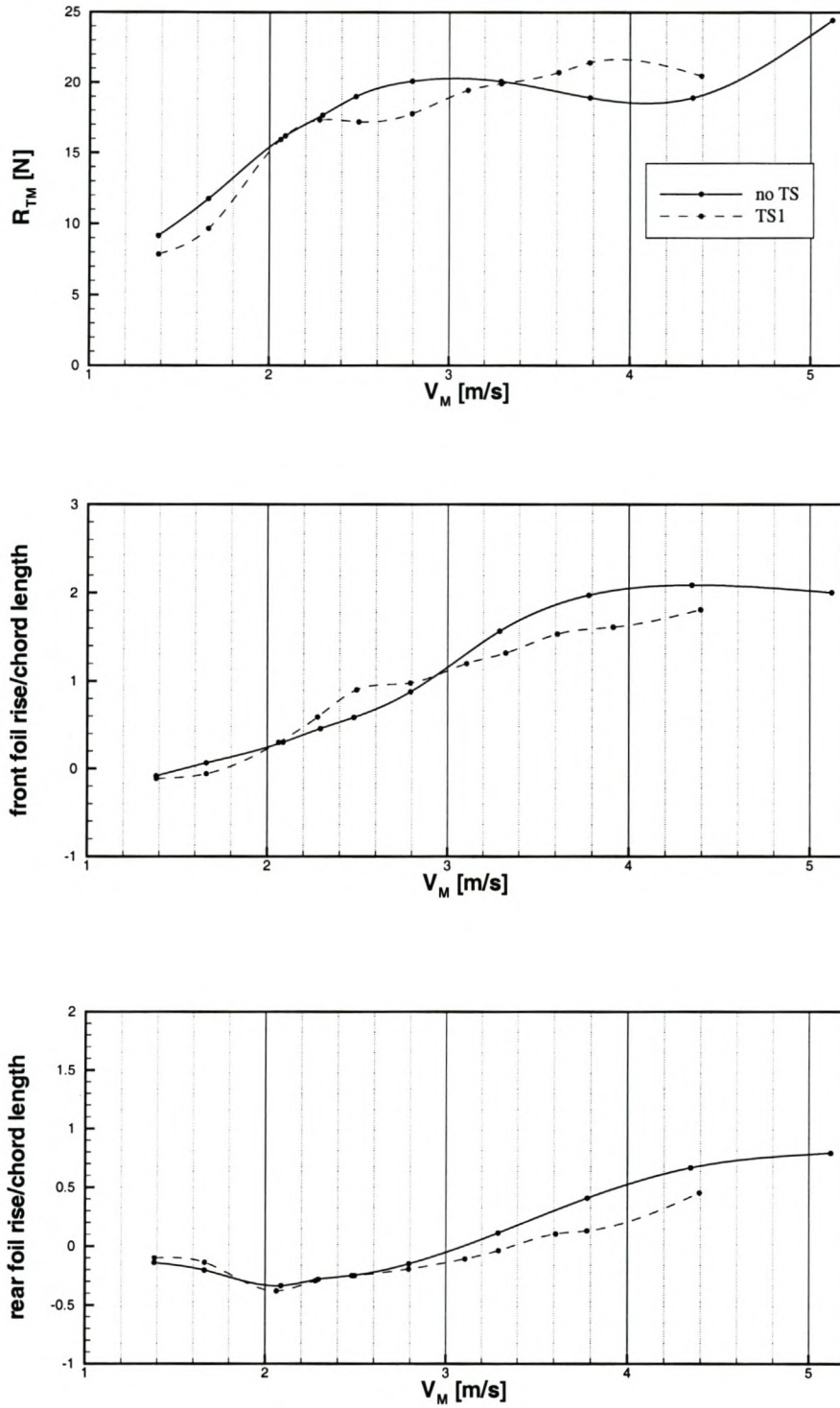


Figure 3.8: Initial results using wire freestream turbulence stimulation



Figure 3.9: Arrangement of wires for turbulating the freestream ahead of the model

of the water at lower speeds. Figure 3.10 shows this result in comparison with the previous one. The most obvious difference shown in the figure lies in the much higher front foil rise (i.e. stronger lift) compared to previous results. The rear foil is affected relatively little, most likely due to a combination of the following effects. Firstly, the stronger downwash from the front foil because of its higher lift means that the rear foil "suffers" less lift. Second, even without turbulence stimulation the rear foil operates in disturbed flow conditions originating from the wake of the front foil and also flow disturbances from the hull, meaning that the rear foil will be less sensitive to any changes in the flow turbulence level from the wires. No visible effect of the turbulence stimulation could be seen on the hulls. As turbulence trips are already used on the hull (see Figure 3.1 on page 64 for example), it is expected that the effect on the hull will be minimal.

At hump speed, the higher rise on the front foil leads to a higher trim angle at hump speed and thus increases the hump resistance over previous results. The high-speed resistance shows much more satisfactory results with the larger stimulators with only a slight increase in resistance, most likely not so much due to a free surface disturbance but due to the front foil submerged somewhat shallower than before and thus has a lower efficiency. Observations showed that there was very little free surface disturbance with the wires spanned wider and further forward.

Observations and measurements of the sizes of separation bubbles with and without turbulence stimulation were conducted to obtain an idea of how strongly the turbulence wires were influencing the boundary layer on the foils. Systematic paint trace tests were conducted on the front and rear foils of the model for a number of important

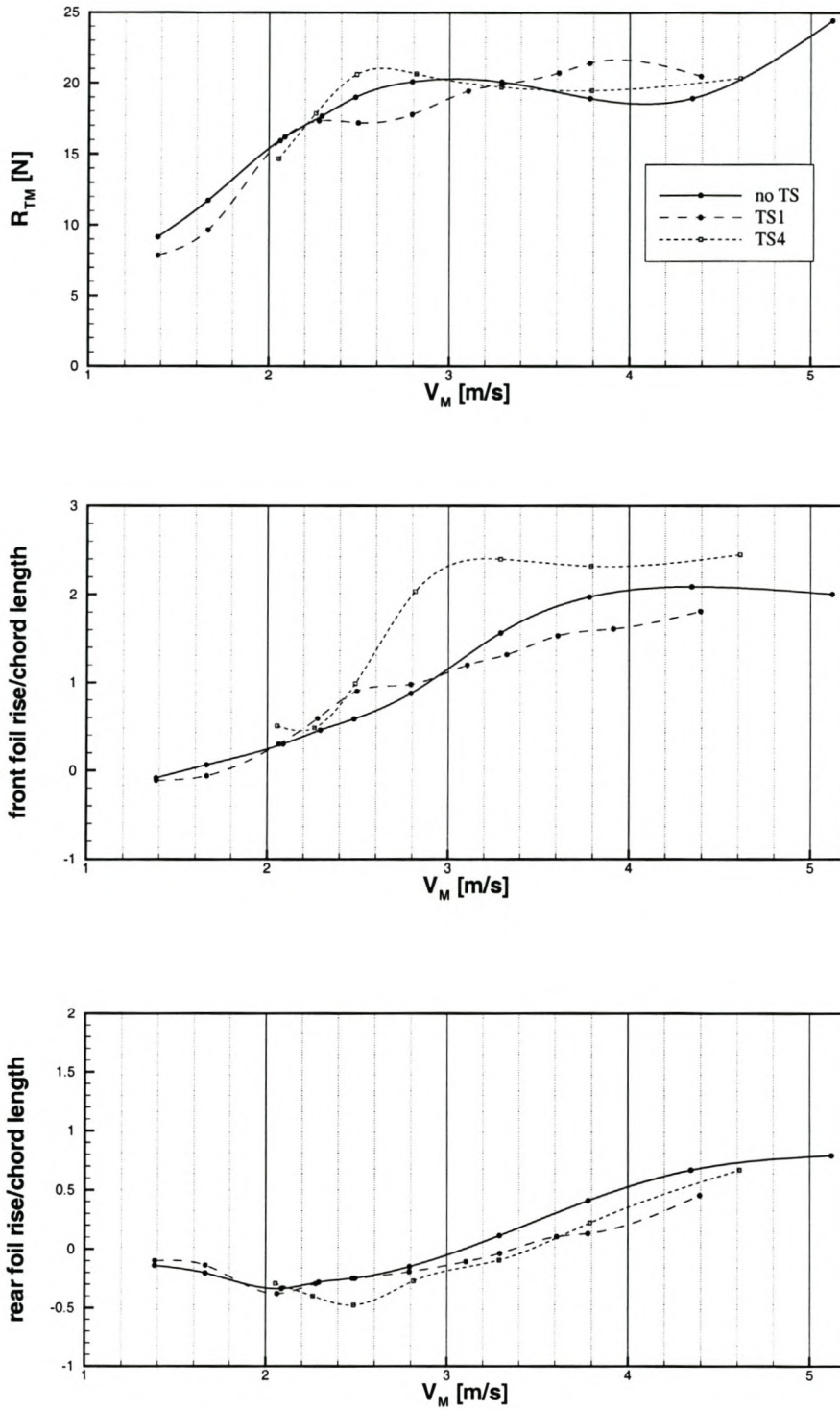


Figure 3.10: Comparison of model resistance and trim for improved turbulence stimulation

speeds with and without turbulence stimulation and the separation and reattachment points recorded. Table 3.6 gives the measured separation bubble sizes.

V_M [m/s]	w/o turbulence stimulation		with turbulence stimulation	
	separation	reattach	separation	reattach
1.7	0.56c	none	0.61c	none
2.1	0.63c	none	0.61c	none
2.5	0.59c	none	0.61c	none
2.8	0.93c	none	0.84c	none
3.3	T.E.	none	T.E.	none
3.8	T.E.	none	T.E.	none
4.4	T.E.	none	T.E.	none

Table 3.6: Separation bubble sizes with and without turbulence stimulation

The measurements do show some small variations in the separation point. Turbulence stimulation induces separation 1-2% later on average, with little effect on reattachment. Given that the submergences for the two cases differ, as given in Figure 3.10, it is difficult to draw conclusions from the data. It can only be said that the length of the bubble does not seem to play an important role in this case. The increased lift seems therefore be due to a different effect, possibly the height of the separation bubble and the level of separation taking place which is lower for the turbulated conditions. No measurements were made of the forces on the foils, so the exact effect on the lift coefficient is unknown. The increased lift on the front foil nevertheless allows one to assume with reasonable certainty that the turbulence stimulation reduces the viscous effect and will make XFOIL predictions more accurate and are recommended for model tests of hydrofoil-assisted catamarans to improve the scaling of model test data.

3.6 Scaling of Model Test Results

The previous sections have covered the different scaling errors introduced during model testing of high-speed craft and in particular hydrofoil-assisted catamarans. It has been shown that it is not possible to eliminate or correct for all the scale effects introduced during model testing. The most important scale effect being due to Reynolds number. To eliminate this problem, one has to resort to use of large models (6m+). In some cases manned sea-going models have been used for final verification of performance for hydrofoil-assisted catamarans (e.g. the Hitachi and MTD developments summarized in Chapter 1).

3.6.1 Correlation Method

A suitable correlation procedure has been developed based on previous works of Hoppe that are partially published in [Hop95b]. Correlating model resistance requires a modification to standard Froude scaling methods to correct for the differing hull and foil friction forces. The development of a correlation factor relating the resistance displacement ratio, ϵ to the model resistance-displacement ratio ϵ_m is given below.

Development of a Correlation Factor

A correlation factor k_{corr} can be defined as follows:

$$\epsilon = k_{corr} \cdot \epsilon_m \quad (3.11)$$

where $\epsilon = R_T/\Delta$.

According to Froude, vessels operating at the same Froude numbers have the same residual resistance. For craft such as hydrofoil-assisted catamarans it is appropriate to use the volumetric Froude number, $Fn_{\nabla} = \frac{V}{\sqrt{g\nabla^{1/3}}}$.

The total resistance R_{Tm} consists of three main components which are different functions mainly of Froude (Fn_{∇}) and Reynolds numbers (Rn):

$$R_{Tm}(Fn_{\nabla}, Rn_{Lm}, Rn_{cm}) = R_{Rm}(Fn_{\nabla}) + R_{Fhm}(Rn_{Lm}) + R_{F0m}(Rn_{cm}) \quad (3.12)$$

From this equation the residual resistance R_{Rm} follows as the difference between the total and friction resistance components:

$$R_{Rm}(Fn_{\nabla}) = R_{Tm}(Fn_{\nabla}, Rn_{Lm}, Rn_{cm}) - R_{Fhm}(Rn_{Lm}) - R_{F0m}(Rn_{cm}) \quad (3.13)$$

and the model residual resistance coefficient C_{Rm} may be expressed as

$$C_{Rm} = \frac{R_{Rm}}{0.5\rho_m V_m^2 S w_m} = \frac{R_{Tm} - R_{Fhm}(Rn_{Lm}) - R_{F0m}(Rn_{cm})}{0.5\rho_m V_m^2 S w_m} \quad (3.14)$$

The coefficients of the individual resistance components are:

the total resistance coefficient of the hull

$$C_{Tm}(Fn_{\nabla}, Rn_{Lm}, Rn_{cm}) = \frac{R_{Tm}}{0.5\rho_m V_m^2 S w_m} \quad (3.15)$$

the friction resistance coefficient of the wetted hull

$$C_{Fhm}(Rn_{Lm}) = \frac{R_{Fhm}(Rn_{Lm})}{0.5\rho_m V_m^2 S w_m} \quad (3.16)$$

the pseudo friction coefficient C_{F0m}^* of the foil

$$\begin{aligned} C_{F0m}^* &= \frac{R_{F0m}(Rn_{cm})}{0.5\rho_m V_m^2 A_{FSm}} \cdot \frac{A_{FSm}}{S w_m} \\ &= C_{F0m}(Rn_{cm}) \cdot \frac{A_{FSm}}{S w_m} \end{aligned} \quad (3.17)$$

C_{F0m} is the friction coefficient of the foil which is a function of Rn_{cm} only.

Replacing the dimensional quantities in Equation 3.14 by their non-dimensional coefficients, this equation changes into

$$C_{Rm}(Fn_{\nabla}) = C_{Tm}(Fn_{\nabla}, Rn_{Lm}, Rn_{cm}) - C_{Fhm}(Rn_{Lm}) - C_{F0m}(Rn_{cm}) \cdot \frac{A_{FSm}}{S w_m} = C_R \quad (3.18)$$

According to Froude's law this equation is valid for model and full scale.

The total resistance of the full scale prototype, $R_T = R_F + R_R$ in coefficient form (omitting reference to Froude and Reynolds number) is then:

$$R_T = 0.5\rho V^2 S w \left[C_{Fh} + C_A + C_{Tm} - C_{Fhm} + \frac{A_{FS}}{S w} (C_{FO} + C_{Af} - C_{F0m}) \right] \quad (3.19)$$

The correlation factor $k_{corr} = \frac{\epsilon}{\epsilon_m}$ is then

$$k_{corr} = \frac{\frac{0.5\rho V^2 S w}{\Delta} \left[C_{Fh} + C_A + C_{Tm} - C_{Fhm} + \frac{A_{FS}}{S w} (C_{FO} + C_{Af} - C_{F0m}) \right]}{\frac{0.5\rho_m V_m^2 S w_m}{\Delta_m} C_{Tm}} \quad (3.20)$$

This equation reduces to

$$k_{corr} = 1.0 - \frac{C_{Fhm} - C_{Fh} - C_A}{C_{Tm}} - \frac{A_{FS}}{S w} \frac{C_{F0m} - C_{FO} - C_{Af}}{C_{Tm}} \quad (3.21)$$

For a hull with multiple foils it can be shown that the following modification applies:

$$k_{corr} = 1.0 - \frac{C_{Fhm} - C_{Fh} - C_A}{C_{Tm}} - \sum_i \frac{A_{FS_i}}{S_w} \frac{C_{FOm_i} - C_{FO_i} - C_{Afi}}{C_{Tm}} \quad (3.22)$$

Equation (3.22) does include the foil form and friction drag, C_{FO_i} separately, so one can take the laminar separation drag into account. Laminar separation drag can be estimated empirically by making use of Equation (3.2) given by Kirkman and Kloetzli [KK80] or more accurately calculated using boundary layer theory with XFOIL and then introducing free surface corrections. Equation (3.22) does not include the influence of air resistance of the vehicle. If it is a small component as is the case at low speeds it can be treated as a part of the residual resistance, or as is done in this study, models are tested behind a screen to eliminate air resistance and it is empirically determined and added to the prototype resistance.

The scale effects of surface tension and cavitation are also not considered in the correlation model as their effect can be minimized or avoided during testing as explained in Sections 3.2 and 3.3. Based on Equation (3.22), a model to prototype correlation program was developed using Microsoft Excel. The hull friction resistance components are determined according to the ITTC-1957 or form factor method as explained in Section 2.6.

Reynolds number scale effects on lift are approached in the different manner. Under the assumption that laminar flow effects have been largely eliminated during the model test by using turbulence stimulation, it is a reasonable assumption that the hydrofoil lift curve slope is linear. The viscous lift reduction factor, f_α and profile drag can then be calculated accurately using XFOIL⁴. According to Table 3.5 the XFOIL result is applicable at foil submergences $h/c \geq 1.0$. At shallower submergences f_α tends to 1.0 as the free surface is approached. This fact means that it is not possible to account for Reynolds number scale effects accurately for the whole speed range of a hydrofoil-assisted vessel. One is forced to adopt different strategies for deep and shallow foil submergences.

Deeply Submerged Foils: $h/c \geq 1.0$

If the foils remain deeply submerged for the whole speed range of interest, one can account for f_α in a number of ways. The simplest of these is to adjust the foil angles of attack for the prototype, so that its lift coefficient corresponds to that at model scale for design speed. Such a correction will only be correct at design speed. Figure 3.11 illustrates the lift curves for high and low Reynolds numbers including the influence of zero-lift angle. From the figure one can see that the discrepancy between the two curves grows with increasing angle of attack. It is clear that any deviation from the design point, the angle of attack correction will be too large or too small.

⁴Equations (3.2) are not applicable under these conditions.

This compromises the accuracy of the model test and runs the risk that at maximum resistance speed⁵ the correction will be too large and that foil lift will then be too low and the full scale maximum resistance hump may be higher than predicted in the model test. If no correction is introduced the foil lift will be larger and one risks the vessel being unstable in some way because of excessive foil lift. It may therefore be useful to test a range of different lift coefficients during the model test to establish resistance tendencies as a function of lift coefficient and make an estimate based on the result.

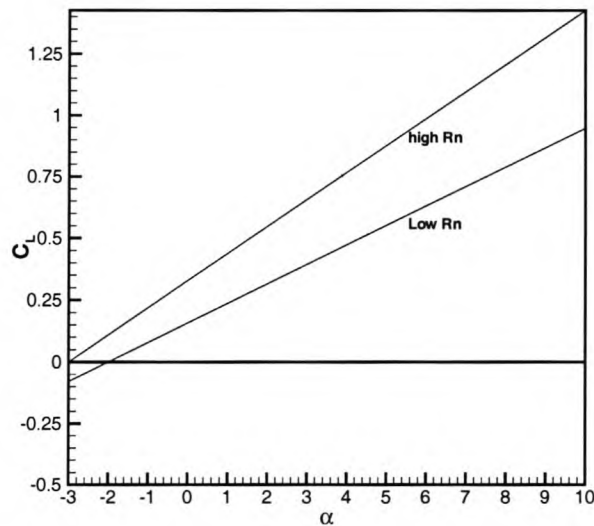


Figure 3.11: Illustration of the effect of Reynolds number of the lift of hydrofoils

Shallowly Submerged Foils: $h/c \leq 1.0$

Shallowly submerged foils for hydrofoil-assisted catamarans often make use of the free surface effect to stabilize the vessel and suffer the added complication that viscous effects on lift and drag change with submergence. This means that the total resistance prediction method based on model tests for hydrofoil-assisted catamarans will be subject to greater inaccuracy as errors in the foil lift will result in differences in hull wetted area and attitude for the vessel. It is therefore important to try and minimize the viscous effect. Making use of different foil profiles for model and full scales would make sense. This way one can better guarantee the same lift curve slope [MG81]. One needs to consider variations in the foil thickness, camber and trailing edge closure

⁵As explained in the previous chapter, maximum resistance often occurs at lower speeds to the design speed.

angle to try and obtain a lift curve slope and zero-lift angle that corresponds as close as possible to the prototype foil's lift characteristics. The simple relations given in Section 3.5.2 that relate lift curve slope and zero-lift angles to the foil geometry that can be used to initially modify a foil profile.

3.6.2 Correlating Model Test Data Measured without Turbulence Stimulation

To date, a lot of experimental data has been collected in this study and by others that has not made use of turbulence stimulation or alternative profiles. Practically, there is no way of determining the scale effects accurately for these tests. The correlated resistance (including air resistance) for a 40m Hysuwac type hydrofoil-assisted catamaran is compared in Figure 3.12 for model tests with and without turbulence stimulation. Table 3.6 shows that separation is still present on the foils, so it was deemed suitable to use the method of Kirkman and Kloetzli for the correlation of the foil friction resistance components⁶. From the figure it can be seen that the main effect of turbulence stimulation is to increase the hump resistance by 13%, which in this case, happens to be the maximum resistance further emphasizing the importance of viscous effects. As expected, at planing speeds there is very little difference in resistance, when the hydrofoils are close to the free surface.

For model test data collected without turbulence stimulation a rough correction would be to increase the transition phase resistance in the order of 13% for a foil system comprising of two foils and perhaps slightly less for single foils. Single foils and multiple foils will most likely have similar differences in resistance as downstream foils operate in disturbed freestream conditions and therefore turbulence stimulation will have less effect on them.

The error in model test results for high-speed vessels is in the range of 2% to 10% [MG97a, Ber00] and for hydrofoil-assisted catamarans could be as high as 15% if the Reynolds number scale effects on the foils are not considered. By taking Reynolds number scale effects into account in the approximate manner outlined, accuracies are most likely in the range similar to that for other high-speed vessels.

The value of model tests even with the difficulties involved should not be disregarded. It is the only tool available so far to predict resistance for hydrofoil-assisted craft and will remain so until a fully validated theoretical tool is developed. One must also keep in mind that the geometric accuracy to which high-speed ships are built is in the range of 4 - 5% [MG97a] and more accurate resistance predictions are practically not needed.

⁶This will lead to a over prediction of the resistance at high speed when the foils are in extreme free surface effect.

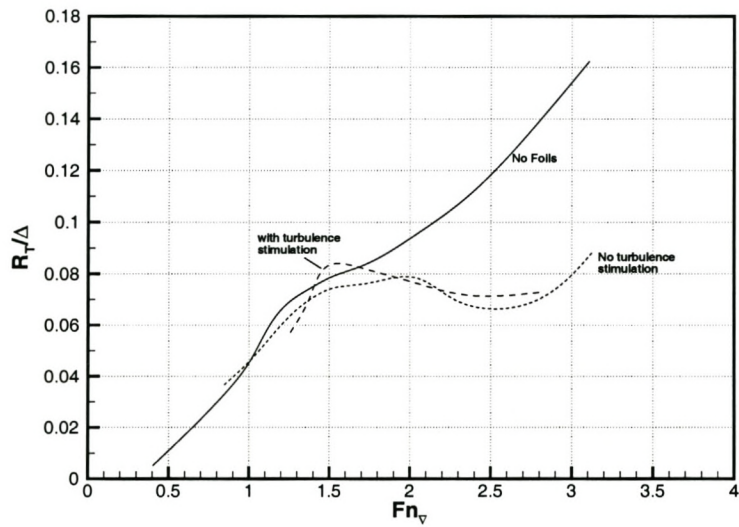


Figure 3.12: A resistance comparison for a 40m Hysuwac tested with and without turbulence stimulation

Chapter 4

Theoretical Design Methods

Abstract

A large variety of performance prediction methods exist that can be applied to hydrofoil-assisted catamarans. With recent developments in computational fluid dynamics, it is now possible to model the complex flows about such vessels with reasonable accuracy using potential flow and viscous formulations. Given the hydrodynamic complexity of the problem, potential flow methods at present offer the best compromise between time, numerical complexity and accuracy. For modeling hydrofoil-assisted catamarans a suitable potential flow method was developed by considering the mathematical modeling, experimental experience as well as other qualitative considerations. Initially the source panel method KELVIN was applied to semi-displacement speeds and the suitability of the numerical method proven for semi-displacement speeds. The vortex lattice method, AUTOWING, was successfully applied to semi-planing and planing speeds. Based on effective practical testing and the experience gained with KELVIN, AUTOWING was further developed to model the displacement and transition phases of operation. Final agreement is found to be similar to that obtained with KELVIN, but scope exists for some refinement of method which will improve predictions somewhat.

4.1 Introduction

Theoretical methods for modeling hybrid vessels such as hydrofoil-assisted catamarans are not new. The similar problem of modeling conventional hydrofoil craft in the hull borne mode has received considerable attention. Early theoretical methods for modeling such craft often made use of the planing formulations of Savitsky [Kar76] together with simple hydrofoil theory. Others [LB93] have made use of systematic series data obtained from hydrofoil craft. These methods neglected the effect of hull-foil interactions. Hoppe [Hop95a] has applied Savitsky's method to model

hydrofoil-assisted catamarans and has included empirically based factors to account for interference between the hull and foils. In general, such methods provide reliable predictions for certain cases: the method of Hoppe has reached a level of reliability that allows the design and performance prediction of Hysucat type hydrofoil-assisted catamarans without the need for model testing [Hop99]. It is more difficult to develop empirically based models as a general design tool for arbitrary speeds and foil hull combinations. Computational methods offer a better possibility of successfully developing such a tool.

There have been significant advances in computational fluid dynamics (CFD) for ship hydrodynamic applications that now also allows one to consider them in the design process of high-speed vessels such as hydrofoil-assisted catamarans. Advancements are being made in both potential flow methods and in the more complex viscous flow methods. Bertram [Ber00] gives a detailed account of the present capabilities of CFD in the design process.

Most of the literature concerned with computational methods for ship design focuses on the displacement speed range ($Fn_{\nabla} < 1.5$), as these ships represent the bulk of the tonnage in operation. Today's computational state of the art methods can predict steady resistance to within 5% of measured values for displacement speeds [Soe99b], $0.1 \leq Fn_L \leq 0.4$.

Numerically, higher speeds pose a more complicated problem, as at these speeds attitude and resistance is governed to a larger extent by hydrodynamic pressures on the hull and these are usually associated with wave-breaking and spray, particularly in the region of the bow. For speeds representing $Fn_{\nabla} \geq 1.5$, the breaking bow wave forms a spray sheet that affects the resistance of the vessel. Resolving it computationally poses a formidable problem as it is a highly non-linear phenomenon that results in a breakdown of numerical calculations. An additional problem is the flow behind the transom stern: breaking waves (wetted transom or rooster tail) occurring in the vicinity of the transom are difficult to resolve [Kri92, CMAU97]. Fortunately as speed increases, the rooster tail that develops behind the transom shifts farther astern and its effect on the vessel becomes less, allowing computations to be made with more ease, by limiting the computational domain to the area behind the transom ahead of the rooster tail.

At semi-planing speeds ($2.5 \leq Fn_{\nabla} \leq 4.0$) buoyant lift and the effects of gravity become less as dynamic forces (from hull and hydrofoils) reduce the buoyant forces and wave generation. The bow spray sheet from the hull also becomes much thinner and by the time fully planing conditions are reached ($Fn_{\nabla} = 4.0$), buoyancy forces, gravitational effects and the bow spray sheet can be neglected from a computational point of view [KT01] if the trim angle remains relatively small ($\tau \leq 10^\circ$). In general, modeling the planing regime is therefore somewhat simpler than modeling the displacement, semi-displacement and semi-planing speed regimes as planing can be satisfactorily modeled without the need to enforce complex free surface boundary con-

ditions or model breaking waves. A simple linear kinematic boundary condition (i.e. no flow through the undisturbed free surface) [Kor98, LT96, CW94] is suitable.

In addition to modeling the hull, one needs to consider modeling the hydrofoils under the free surface as well as the foil-hull interactions. Due to the complexity of the hydrodynamics, most pure numerical investigations of hydrofoil-assisted catamarans have focused on a particular aspect of the hydrodynamic problem. Ishikawa [Ish92] made useful calculations of the foil-hull interactions using a panel method with simplified free surface boundary conditions. Others [Mor91, SMFI93] focused on determining foil forces and foil interactions not considering the influence of the hull. Li et al. [LLYY94] describes the use of a source panel method to determine the wave-making resistance - including hull-foil interaction - for a slender hydrofoil catamaran design at low speed where wave breaking is limited. Kataoka [Kat96] investigated the hydrodynamic interaction between hulls and hydrofoils using a combination of source panel and vortex lattice methods for a simplified Wigley¹ hull form. More recently, Kornev et al. [KT99] have investigated the effect of planing surfaces operating in the wake of hydrofoils using a non-linear vortex lattice method.

These simplifications limit the effectiveness of the present methods as effective design tools. To develop a suitable computational method the exact requirements of such a method for design purposes need to be established.

4.2 Requirements for a Suitable Design Tool for Hydrofoil-Assisted Catamarans

A suitable design tool requires a combined theory to model hydrofoils and catamaran hulls for semi-displacement speeds up to planing speeds, $1.5 \leq Fn_{\nabla} \leq 4.5$. The resulting numerical model must allow one to size and position hydrofoils on hulls of varied geometry estimating the performance of the proposed design in at least a qualitatively reliable fashion so that the proposed design can be optimized.

The three phases of operation of hydrofoil-assisted craft have been outlined in Chapter 2. Given the differences in the hydro-mechanics governing each phase, one cannot expect a single theory to cover all speed ranges equally well. Suitable models for each phase need their own simplifying assumptions valid only for that particular phase. The requirements for a computational model nevertheless are similar for each. Ideally, one should be able to complete the following with at least qualitative reliability and in an amount of time that is reasonable for design purposes:

- predictions of performance and attitude

¹A simple mathematical hullform construct out of parabolic sections and waterlines.

- sizing and positioning of hydrofoils on a hull
- calculating the effect of hull shape on performance and attitude
- optimizing of hydrofoils on the hull
- calculation of the interactions between hull and hydrofoils and the free surface

Focusing on these requirements, existing computational methods can be reviewed.

4.3 Review of Existing Computational Methods

The literature reveals that a significant amount of research has been devoted to development of theoretical tools for hydrofoils and other high-speed vessels including catamarans. These methods range in complexity from relatively simple potential flow methods (e.g. [Pay88, Soe99b]) to very complex viscous flow methods solving Reynolds Averaged Navier-Stokes (RANS) equations for fluids with free surfaces and breaking waves (e.g. [HHH91, KKT95, OM97, Shi00]).

4.3.1 Viscous Flow Methods

The advantage of these methods is that one is solving the "exact" problem. With the state of the art methods of today, it is possible to resolve the flow, including breaking waves and separation, with reasonable accuracy in many cases. If one examines the complexity and computation times of these methods, it is quickly seen that very large computation times (in order of 30 to 100 hours per calculation) are required [OM97]. The high level of complexity means that a large time input as well as significant user experience is needed to set up the computation. For the high Reynolds numbers associated with high speed ship flows, there are various problems that still need solving, the most important being the need for better turbulence modeling and the complex mesh requirements for computations [Ber99a]. For hydrofoil-assisted catamarans, being geometrically and hydrodynamically complex, it would take a significant time investment, beyond what is required for this study, to gain enough experience to accurately model such vessels. It is also doubtful that the large computation times would allow for design optimization within a practical time frame. For this reason these methods will not be considered further in this study.

4.3.2 Potential Flow Methods

Potential flow methods are considerably less complex, requiring only a maximum of a few hours of computation time with much simpler user inputs. The relative simplicity

of the methods mean that their applicability is not as general as viscous flow methods. Nevertheless, inviscid computations still represent the majority of CFD calculations performed for ship hydrodynamic problems [Ber99a]. The simplicity and accuracy of results that can be obtained with these methods make them more applicable for general design purposes than viscous flow computations. Today's state of the art methods can model the displacement speed range [Soe99b] and also the planing speed range [LT96, Kor98] with sufficient accuracy for design purposes. There is also extensive experience in modeling lifting flows in hydrofoil and propeller applications (e.g. [Thi97, AMN98, Kor98]).

For the semi-displacement speed range, potential flow methods have seen more limited application as the highly non-linear characteristics of the bow spray sheet and the flow behind the transom stern (both of which contribute significantly to the resistance [TH86, WSM95]) can only be modeled in an approximate sense, compromising accuracy somewhat. The wave-making resistance (wave-breaking and spray not included!) and the form of the wave-wake can nevertheless be accurately predicted [BBC⁺98] making qualitative comparisons possible. The difficulty in obtaining quantitative resistance data from theoretical methods, forces one to rely on some empirical input usually as form factors of different kinds [Doc98, SRZM99] to obtain the required accuracy.

The literature nevertheless indicates that potential flow theory has reached a sufficient level of capability to warrant further development as a general design tool for hydrofoil-assisted craft. In the application of such methods the accuracy of the final result depends on some discipline being introduced between the aspects of mathematical modeling and practical testing. This chapter focuses on development of suitable mathematical models, which have been developed based on experimental hydrodynamic experience of hydrofoil-assisted catamarans built up during this study.

4.4 Mathematical Modeling

A mathematical model must include all the relevant equations, initial conditions and boundary conditions in their exact sense, which follow from physical laws or, if this is not possible due to complexity, in a way that physical phenomena are at least qualitatively correct. In the scope of the present research this refers to correct modeling of the fluid, boundary conditions and attitude of the vessel using potential flow formulations. The different phases of operation for hydrofoil-assisted catamarans have been explained in Chapter 2. Of most interest for design purposes is the transition phase and the planing phase and to a much lesser extent the displacement phase. Given the simplifications introduced in potential flow theory and the large differences in hydro-mechanic principles governing behaviour and performance for the different phases, the displacement and transition phases are considered as a separate problem

to the planing phase. The planing phase can be separated from the two lower speed phases because both wave-making and wave-breaking can be ignored during planing. Based on solution of the simpler planing problem, development of a method for modeling hydrofoil-assisted catamarans for the lower speeds covering the transition and displacement phases is undertaken.

4.4.1 Potential Flow Formulations for the Planing Phase

Investigation of the literature on numerical methods for planing indicate that there are a number of methods varying in complexity that are currently in use to model the planing hydrodynamics. The simplest of these are the added mass theories (see for example: [Pay88, Soe99b]) where a planing hull is modeled as a large number (> 300) of 2 dimensional cross-sections. The force on each section is calculated by the change in momentum of the added mass of that particular section. The forces for each section can then be integrated to provide the force over the whole length of the hull. Added mass theory, while suitably developed to model planing, is still somewhat crude to model hydrofoils [Das00]. The method could be used in combination with a simple foil theory (e.g. lifting line theory) to model hydrofoil-assisted planing catamarans if one is content to ignore the interaction effects between hull and hydrofoils.

An advancement on the simple added mass theories are the water impact theories that also include the effects of flow separation, spray and sometimes wave making [ZFH97, FC97, XT99]. A valid simplification in planing hydrodynamic theory is that the longitudinal perturbations can be neglected in comparison with the transverse ones in the vicinity of the ship. This allows one to solve the flow field as a 2-dimensional problem for a number of cross-sections of the ship. By solving the exact free surface boundary condition, it is possible to model the bow spray sheet. Results for planing problems are usually in good agreement with experiments. The limitation of the method is that it cannot easily be extended to include hydrofoils in close proximity to the hull as hydrofoils introduce significant longitudinal perturbations into the flow. This limits the slender ship theory's applicability to hydrofoil-assisted vessels somewhat. It is therefore preferable to apply a 3-dimensional model to the problem.

Two 3-dimensional potential flow approaches have been developed that can model planing: the variable pressure element method [CW99] and the vortex lattice method [LT96, Kor98]. The variable pressure method adopts a pressure distribution on the free surface of the water that represents the wetted area of a planing hull. An integral equation is then established which relates the unknown pressure distribution with the displacement of the hull. The disadvantage of this approach is that the method tends to predict pressure oscillations along the hull that are unrealistic. As a result the method has seen limited application for only very simple geometries with results that are not very satisfying [CW94, CW99].

The vortex lattice approach has been applied with more success. It has already found commercial² application [BEKM00] in design for planing WIG³ craft and hydrofoil-assisted catamarans. The application of the vortex lattice method stems from the discovery of Wagner [Wag32] that the flow beneath a planing hull is the same as the flow on the bottom of the same wing (in planform and curvature) except for the leading edge and the generation of spray at the side edges. Vortex lattice theory can therefore be effectively used to model a planing lifting surface. The discrepancies due to the flow in the vicinity of the leading and side edges are usually small and can either be ignored [BEKM00] with little loss of accuracy or modeled using complex non-linear boundary conditions (Lai, [LT95, LT96]) to represent the jet spray. Figure 4.1 shows a result comparing the two different methods for modeling the leading and side edges and demonstrates its suitability for modeling planing. The results are presented in comparison to Savitsky's [Sav64] empirical method.

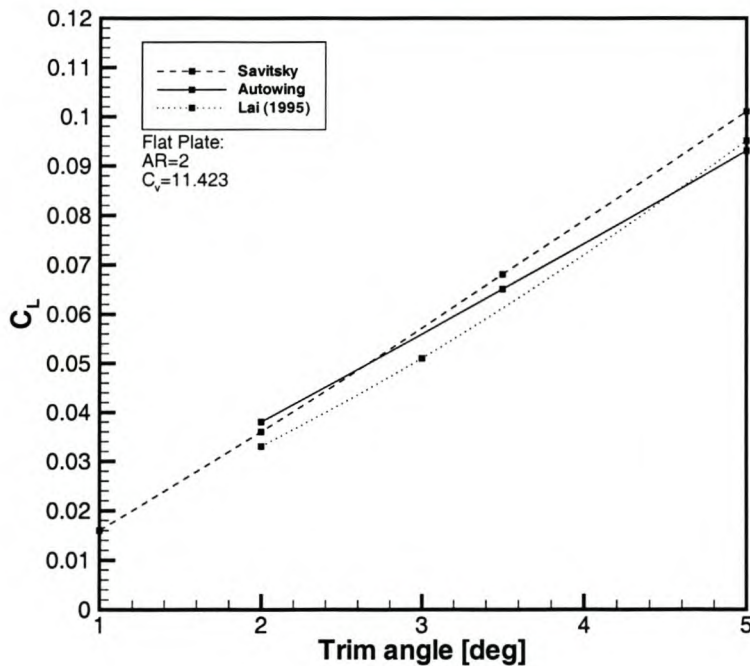


Figure 4.1: Comparison of AUTOWING results (no leading edge or side edge model) with those of Lai and Savitsky.

Vortex lattice theory has also been validated for hydrofoil applications under the free surface. The combination of lifting surfaces and the vortex wake is treated in the

²The commercial code: AUTOWING [KT]

³Wing in ground effect craft or Ekranoplans.

most simple and natural way within the framework of vortex methods. It is therefore well suited to modeling planing hydrofoil-assisted catamarans as vortex panels can be used to model hull, hydrofoils, free surface and importantly the hull-foil interactions by implementing a vortex roll-up model. As explained in Chapter 2, it is necessary to model the vortex roll-up process and path of the tip vortices to capture the vortex interactions with the hull and downstream foils [Mor91, Wal99].

The generalization of vortex lattice theory for free surface problems concerned with *lifting surfaces* has been performed by Kornev [Kor98] and implemented in the commercial software package AUTOWING [KT]. Generalization and further development of the vortex lattice theory for application to *hydrofoil-assisted catamarans* (a hydrodynamically different object with complicated interactions between multiple hydrofoils and multiple hulls!) has been performed during this study by the author in collaboration with Prof. N.V. Kornev and use of the AUTOWING package. This work is reported in this chapter.

4.4.2 Potential Flow Formulations for the Displacement and Transition Phase

From a computational viewpoint, the displacement and transition phases fall into what is typically considered as semi-displacement speeds for conventional vessels. The difficulty of modeling the semi-displacement regime accurately is evident in the literature by the lack of success by most in achieving reliable quantitative resistance predictions. It is known that the difficulty lies in modeling the free surface in the vicinity of the bow and behind the transom stern as the flows there are wave-breaking in nature.

For transom stern flow, the determining parameter is the Froude number based on the immersion of the transom (including trim and sinkage): if this Froude number is below 2.5, it is troublesome to numerically resolve the transom stern flow; if it is below 2.0, it is impossible within the potential flow framework without a wave-breaking model. This is connected with the fact that in a 2-dimensional case a solution with a dry transom does not exist if the Froude number is less than $\sqrt{5}$ [Bro80, Hau80]. Wave-breaking, associated with the closure of the transom hollow and the resulting rooster tail, is then required to dissipate the excess energy that the waves cannot transport away. In 3-dimensions, the limits are slightly different, but similar. For practical catamaran hulls, a transom submergence Froude number of 2.5 is in the region $0.8 \leq Fn_{\nabla} \leq 1.6$ depending on the hull design. It is therefore usually only a problem for the less important displacement phase.

The second difficulty in numerical simulation lies in modeling the wave formed at the bow. The bow wave of a ship increases steadily in height and gradient as speed increases. At $Fn_{\nabla} \approx 1.0$, ($Fn_L \approx 0.4$), the wave becomes sufficiently steep to break

and complicate the numerical solution of the free surface boundary condition. Once planing speeds are reached the breaking bow wave has thinned and transformed into a jet of water (spray) separating from the hull⁴. Special numerical treatment of the jet and wave-making phenomena is then required.

For displacement ships it is a necessary condition for accurate resistance prediction that the fully non-linear free surface boundary condition is implemented when calculating the wave-making resistance [Ber99b]. This boundary condition results in numerical divergence as soon as any wave-breaking takes place. To sidestep this problem a linearized form of the free surface boundary condition is usually applied to semi-displacement speeds. This boundary condition, while prone to wave damping (amplitude) and dispersion (wave-length) errors, is numerically much more resistant to numerical instability due to wave-breaking. Investigations of semi-displacement catamarans (for example: [BBC⁺98, CMAU97]), has shown that the linear free surface condition is suitable to model the wave-making component of resistance of catamarans, but under-predicts the total resistance because wave-breaking resistance is not being considered.

In computational methods for modern catamarans, the assumptions that the demi-hulls are slender⁵ (slender ship theory [WSM96, SRZM99]) or thin⁶ (Michel's thin ship theory [Mic98, Doc98]) is often applicable. These assumptions are generally not suitable for modeling hydrofoil-assisted catamarans as their assumptions are not consistent with solving the foil-hull interactions. Similar to simple planing theories, slender ship theory ignores longitudinal perturbations [Ogi77]. Thin ship theory suffers the inability to model a transom stern, therefore the hollow behind the transom must be modeled in some approximate manner as an extension to the hull [DD97]. With empirical corrections these methods can predict vessel resistance with reasonably good accuracy [SDR99]. For the case of hydrofoil-assisted catamarans this is not practical as the size and shape of the transom hollow is influenced not only by the size of the transom but also by the wave-wake of the hydrofoils. The downwash from the foils changes the shape of transom hollow. This means the shape of the transom hollow will be a function of speed, foil configuration and foil loading. It is most likely difficult to develop suitable empirical factors for such varied conditions and would lower the reliability of such a method for general design purposes.

To gain some experience of the abilities of different potential flow methods, some investigations were carried out using the thin ship code, MICHLET [Laz97] and also the non-linear panel method KELVIN⁷ [Soe99a] for three catamaran hulls (non-foil-assisted) tested in this study [MH01]. Figure 4.2 is representative of the results found for all three hulls. MICHLET uses an artificial hull extension to model the

⁴The breaking bow wave and the development of the jet can partially be seen in Figure 2.2.

⁵The hull beam and draft are assumed small in relation to its length.

⁶The beam of the hull is assumed small in relation to the length.

⁷KELVIN is the property of the SVA-Potsdam.

transom hollow, while KELVIN can model the free surface both with linear and fully non-linear free surface boundary conditions. MICHLET has the disadvantage that it is not capable of predicting trim and sinkage. It is possible to determine trim and sinkage theoretically within the framework of thin ship theory, but the linearities introduced into the theory result in the resistance being independent of sinkage and trim [Weh73]. The effects of trim and sinkage can be taken into account by re-entering the hull geometry for the theoretically trimmed and sunk hull. If the transom hollow is modeled as an extension to the hull it is doubtful if the trim will then be accurately predicted, especially for high-speed catamarans where the transom is large (and thus the hollow also).

Figure 4.2 indicates that both KELVIN (linear) and MICHLET resistance predictions are reasonably good, but under-predicting the resistance somewhat. Surprisingly, MICHLET predicts the hump resistance slightly better than KELVIN. Nevertheless, KELVIN's ability to predict the trim and sinkage reasonably well makes the method substantially superior to MICHLET.

KELVIN's poor trim prediction at higher speeds is most likely due to inequalities between the KELVIN calculation and the experimental setup. The towing harness of the model causes a bow-down moment, thus decreasing the trim of the vessel. The bow down moment is proportional to vessel resistance and thus speed. This was not accounted for in the KELVIN calculation and thus higher trim is predicted. The non-linear KELVIN results, as expected, diverge for $Fn_L \geq 0.4$ ($Fn_{\nabla} \geq 1.0$) due to the breaking bow wave.

With such results, one can predict with relative certainty that a panel method and a linear free surface boundary condition will provide reasonably good results for hydrofoil-assisted catamarans at semi-displacement speeds. When the hull is increasingly dynamically unloaded with speed by hydrofoils, the wave-breaking will be less, and likely improve the prediction if the hydrofoil model is accurate. Unfortunately at the time of conducting this research, KELVIN had no suitable hydrofoil model. The development of suitable panel method with the ability to model hydrofoils was undertaken within the framework of AUTOWING, using vortex lattice theory.

4.5 The Vortex Lattice Method

The vortex lattice method within the potential flow framework, makes use of discrete vortices in the form of horseshoe vortices or vortex rings [BL93] to model the hydrodynamics of lifting surfaces. Sections 4.5.1 to 4.6 summarize the mathematical background and implementation of the vortex lattice method in AUTOWING for modeling planing and hydrofoil lift. This theory forms the basis for generalization of the vortex lattice method (presented later in this chapter) for modeling hydrofoil-assisted catamarans. Vortex lattice theory is well known for modeling lifting surfaces,

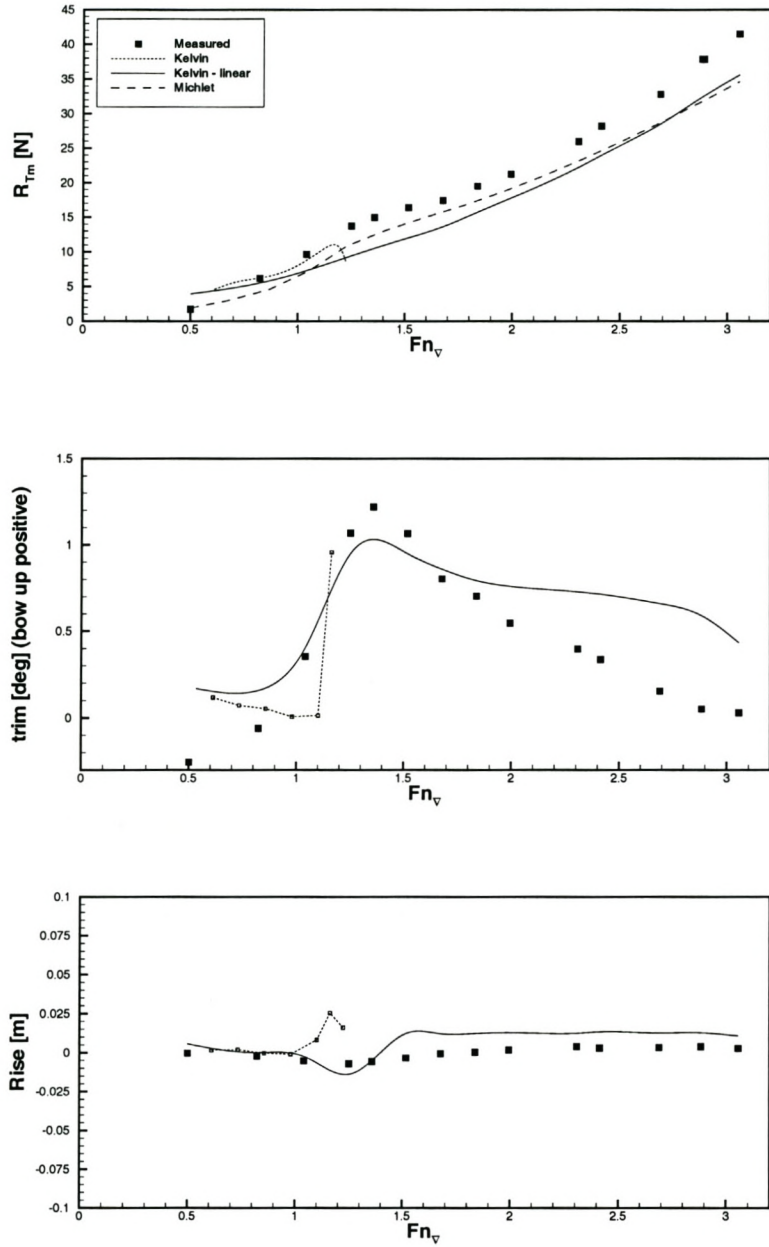


Figure 4.2: Comparison between KELVIN, MICHLET and measurements for a semi-displacement catamaran

but is relatively unknown for modeling free surfaces because publications describing this application are difficult to obtain. The theory used in the present method is therefore repeated here. It is applied to model first, the simpler planing phase of hydrofoil-assisted catamarans (Sections 4.8- 4.10) and later, the theory is extended to include models for calculation of the more complex transition phase hydrodynamics (Sections 4.4.2 - 4.11.3) of hydrofoil-assisted catamarans.

4.5.1 Mathematical Background

In essence, the vortex lattice method uses a set of discrete vortices to model the continuous vortex sheet generated by a lifting surface and its downstream wake within the framework of potential flow. AUTOWING uses discrete vortex ring elements for this.

Defining x in the direction of motion of a wing, y as upward and z to starboard and assuming irrotational, inviscid and incompressible flow - assumptions that are valid outside the boundary layer and wake generated by the lifting surface - the flow can then be represented by a velocity potential ϕ which satisfies the Laplace equation:

$$\frac{\partial^2 \phi}{\partial x^2} + \frac{\partial^2 \phi}{\partial y^2} + \frac{\partial^2 \phi}{\partial z^2} = 0 \quad (4.1)$$

where the velocity components are:

$$v_x = \frac{\partial \phi}{\partial x}; \quad v_y = \frac{\partial \phi}{\partial y}; \quad v_z = \frac{\partial \phi}{\partial z} \quad (4.2)$$

For solving the flow field around a hydrofoil-assisted catamaran allowing one to determine the required parameters for design, requires setting up a system of discrete vortices to model each lifting surface and its downstream wake. This includes both hydrofoils, struts and the planing demi-hulls. Solution of the flow field is through a system of algebraic equations that is set up based on the boundary conditions that apply.

Boundary conditions

For a fixed body in a moving fluid, the body kinematic boundary condition specifies that the flow must be tangential to the body surface:

$$\frac{\partial \phi}{\partial \vec{n}} = 0 \quad (4.3)$$

where n is the normal vector to the surface of the body. This body boundary condition is usually applied on the mean camber line for a wing and the thickness effect is either

ignored (thin wing theory) or accounted for through a combination of sources and sinks on the mean camber line, which have strengths proportional to the thickness gradient of the hydrofoil. This allows one to determine the pressure distribution on the foil with more accuracy for cavitation prediction. For planing surfaces of hydrofoil-assisted catamarans it is most appropriate to enforce the body boundary condition on the hull surface itself. Linearizations of the body kinematic condition [Lai94] to the undisturbed free surface do not make sense for modeling hydrofoil-assisted catamarans as it cannot be assumed that the planing hull is operating on an undisturbed free surface.

The radiation condition requires that there is no flow perturbation in the far field except in the region of the wake.

$$\nabla\phi \rightarrow 0, \text{ at infinity} \quad (4.4)$$

This condition is satisfied automatically using discrete vortices.

The Kutta condition prescribes that the flow must leave the trailing edge smoothly, implying that the velocity at the trailing edge is finite:

$$\nabla\phi \leq \infty, \text{ at the trailing edge} \quad (4.5)$$

Hydrodynamic pressure

Once the vorticity distribution on the lifting surface has been determined, it is straightforward to obtain the velocity distribution. Bernoulli's equation is then used to compute the pressure. Integrating the pressures over the whole surface area provides the lift and moments on the lifting surface. Bernoulli's equation is:

$$p = f - \rho \left(\frac{\partial\phi}{\partial t} - \vec{F}_o \vec{v} + \frac{1}{2} |\vec{v}|^2 + gy \right) \quad (4.6)$$

Discretization

The body surface is divided into a mesh of trapezoidal panels, on each of which, a vortex element is placed and the body boundary condition is enforced. In AUTOWING, trapezoidal vortex panels containing closed vortex ring elements are used for representing the lifting body as well as the wake. The boundary conditions are also applied on the actual wing surface and not on the camber line. A system of linear algebraic equations is developed from the boundary conditions based on the discretization scheme that is implemented.

Rigorous theoretical analysis by Belotserkovsky [BL93] as well as numerical investigations by Hough [Hou73] have shown that if the system of algebraic equations is to

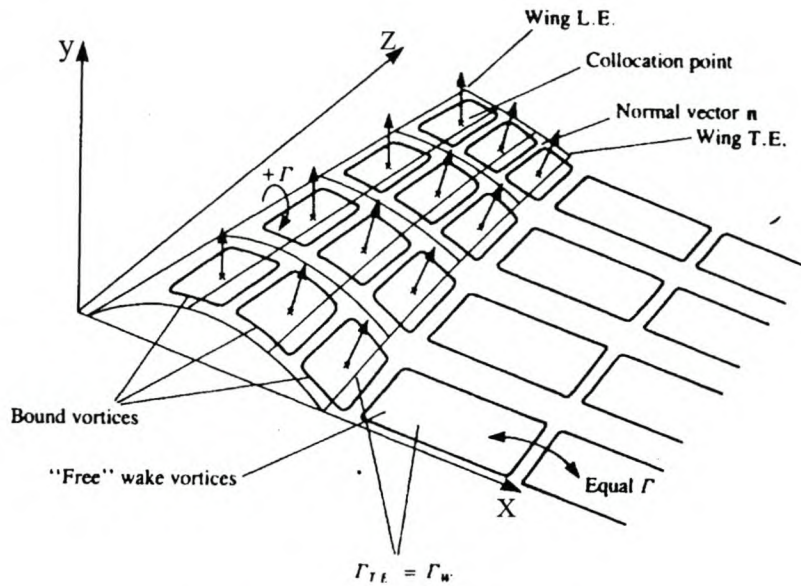


Figure 4.3: Discretization scheme for ring vortex panels

be well conditioned and have optimum convergence the leading segment of the vortex ring should be located at the quarter chord and the collocation point - where the boundary condition is satisfied - should be located at the three-quarter chord of each panel. Furthermore, discrete vortices and collocation points must be located near the leading and trailing edges respectively as is shown in Figure 4.3.

Standard texts on the vortex lattice method (for example: [KP91, BL93]) provide details for implementing the method for aerodynamic applications. Application of the vortex lattice method for hydrodynamic applications including modeling of the free surface is less well-known and is presented in more detail in the sections that follow.

4.5.2 Discrete Vortex Free Surface Model

Considering only gravity forces, two non-viscous flows with a common surface can be described by the Bernoulli equation in a similar manner to (4.6):

$$p_{1,2} = f_{1,2} - \rho_{1,2} \left(\frac{\partial \phi_{1,2}}{\partial t} - \vec{F}_0 \vec{v}_{1,2} + \frac{1}{2} |\vec{v}_{1,2}|^2 + gy \right) \quad (4.7)$$

Solution of this equation on the surface separating the two fluids additionally requires the following radiation conditions to be considered on the free surface:

The perturbation velocities should disappear at infinity:

$$\vec{v}_{1,2}(x \rightarrow \pm\infty) = 0 \quad (4.8)$$

Waves do not propagate ahead of the body and disappear at infinity:

$$y(x \rightarrow -\infty) = 0 \quad (4.9)$$

The pressure on the free surface should be atmospheric:

$$p_{1,2}(x \rightarrow \pm\infty) = p_a = f_{1,2} \quad (4.10)$$

Since no pressure jump exists at the interface of the two fluids, i.e. $f_1 - p_1 = f_2 - p_2$ the Bernoulli equations (4.7) are equal for both sides which results in

$$\rho_1 \left(\frac{\partial \phi_1}{\partial t} - \vec{F}_0 \vec{v}_1 + \frac{1}{2} v_1^2 + gy \right) = \rho_2 \left(\frac{\partial \phi_2}{\partial t} - \vec{F}_0 \vec{v}_2 + \frac{1}{2} v_2^2 + gy \right) \quad (4.11)$$

For the case of a water-air interface the approximation:

$$\frac{\rho_1}{\rho_2} = 0 \quad (4.12)$$

is valid. Using (4.12), Equation (4.11) can be simplified to the standard form of Bernoulli's equation or the dynamic free surface boundary condition for steady flow conditions:

$$\vec{F}_0 \cdot \vec{v} - \frac{1}{2} |\vec{v}|^2 - gy = 0 \quad (4.13)$$

Mathematical solution of this boundary condition can be achieved by modeling the free surface as a continuous vortex sheet.

Properties of the Free Surface Vortex Sheet

A vortex sheet is a surface across which the tangential velocity changes abruptly. When considering the induced velocities of the free surface vortex sheet, three values are of importance. \vec{V}_0 , the velocity on the free surface, \vec{V}_1 , the velocity just above the free surface and \vec{V}_2 , the velocity just below the free surface. The magnitude of the discontinuity in the tangential velocity distribution is given by [MT96]:

$$\vec{V}_\gamma = \vec{V}_2 - \vec{V}_1 \quad (4.14)$$

The velocity on the free surface (i.e. the vortex sheet) is the mean of velocities just above and just below the free surface:

$$\vec{V}_0 = \frac{1}{2} (\vec{V}_1 + \vec{V}_2) \quad (4.15)$$

The velocities induced by the vortex sheet in the fluid below the free surface can be rewritten from (4.14) and (4.15) as:

$$\vec{V} = \vec{V}_2 = \vec{V}_0 + \frac{1}{2}\vec{V}_\gamma \quad (4.16)$$

The magnitude of the velocity below the free surface can therefore be determined as a function of \vec{V}_0 and \vec{V}_γ :

$$|\vec{V}|^2 = |\vec{V}_0|^2 + \vec{V}_\gamma \cdot \vec{V}_0 + \frac{1}{4}|\vec{V}_\gamma|^2 \quad (4.17)$$

If $\vec{\gamma}$ is the vortex sheet intensity per unit area then

$$\begin{aligned} \vec{\gamma} &= \vec{V}_\gamma \times \vec{n} \\ \vec{V}_\gamma &= \vec{n} \times \vec{\gamma} \end{aligned} \quad (4.18)$$

where $\vec{\gamma}$ is tangential to the free surface vortex sheet and \vec{n} is a unit vector normal to the vortex sheet.

Using (4.18) the dynamic free surface boundary condition (4.13) can be rewritten in the form

$$\vec{F}_0 \cdot \vec{V}_\gamma = |\vec{V}_0|^2 + \vec{V}_\gamma \cdot \vec{V}_0 + \frac{1}{4}|\vec{V}_\gamma|^2 + 2gy - 2\vec{F}_0 \cdot \vec{V}_0 \quad (4.19)$$

Without loss of generality, $\vec{\gamma}$ can be decomposed into two components, both tangential to the free surface:

$$\vec{\gamma} = \vec{\gamma}_x + \vec{\gamma}_z \quad (4.20)$$

where $\vec{\gamma}_x$ is parallel to the free stream flow and $\vec{\gamma}_z$ perpendicular to $\vec{\gamma}_x$. With the use of (4.18), the left hand side of (4.19) can be written as:

$$\vec{F}_0 \cdot \vec{V}_\gamma = \vec{F}_0 \cdot (\vec{n} \times \vec{\gamma}) = |\vec{F}_0| \vec{\gamma}_z \quad (4.21)$$

Defining the Froude number, F_n and a unit vector, \vec{f}_0 :

$$\begin{aligned} F_n &= \frac{|\vec{F}_0|}{\sqrt{gL}} \\ \vec{f}_0 &= \frac{\vec{F}_0}{|\vec{F}_0|} \end{aligned} \quad (4.22)$$

where L is a reference length, equation (4.19) can now be rewritten using Equations (4.20-4.22) in the form:

$$\bar{\gamma}_z = |\bar{V}_0|^2 + (\vec{n} \times \bar{\gamma})\bar{V}_0 + \frac{1}{4}|\bar{\gamma}|^2 + 2\frac{\bar{y}}{F_n^2} - 2\bar{f}_0\bar{V}_0 \quad (4.23)$$

where: $\bar{\gamma} = \frac{\vec{\gamma}}{|\vec{F}_0|}$; $\bar{V}_0 = \frac{\vec{V}_0}{|\vec{F}_0|}$ and $\bar{y} = \frac{y}{L}$.

Equation (4.23) represents the basic equation for implementation of the vortex lattice method to solve the fully non-linear dynamic free surface boundary condition. The linearized form of (4.23) is given by:

$$\bar{\gamma}_z = 2\frac{\bar{y}}{F_n^2} - 2\bar{f}_0\bar{V}_0 \quad (4.24)$$

4.5.3 Solution of the Free Surface Boundary Condition

Solution of the dynamic free surface boundary condition, (4.23), requires three unknowns to be solved for, the free surface velocity \vec{V}_0 , the surface vorticity: $\vec{\gamma}$ and the free surface elevation: y . \vec{V}_0 can be calculated using the Biot-Savart law which is a function of the vorticity, $\vec{\gamma}$.

$$\vec{V}_0(\vec{x}) = \frac{1}{4\pi} \int \frac{\vec{\gamma} \times (\vec{x} - \vec{\xi})}{|\vec{x} - \vec{\xi}|^3} dS \quad (4.25)$$

The free surface elevation y can be solved from the free surface kinematic boundary condition representing the free surface as a streamline:

$$\frac{dx}{V_{0x}} = \frac{dy}{V_{0y}} = \frac{dz}{V_{0z}} \quad (4.26)$$

and the zero-divergence of vorticity condition provides a relation between the γ_x and γ_z vorticity components:

$$\frac{\partial \gamma_x}{\partial x} + \frac{\partial \gamma_z}{\partial z} = 0 \quad (4.27)$$

The complete fully non-linear boundary condition can therefore be solved by modeling the free surface as a continuous vortex sheet.

Numerical Method

The free surface vorticity $\vec{\gamma}$ is represented by a number of closed vortex ring elements forming the borders of the free surface panels as shown in Figure 4.4. The longitudinal

and transverse lines forming borders of the free surface panels are parallel to the X and Z axes respectively. Each panel is characterized by:

- the intensity of the vortex ring, Γ_{ij} ,
- the area of each panel: S_{ij} ,
- the radius vector to the left forward corner of the panel: τ_{ij} .

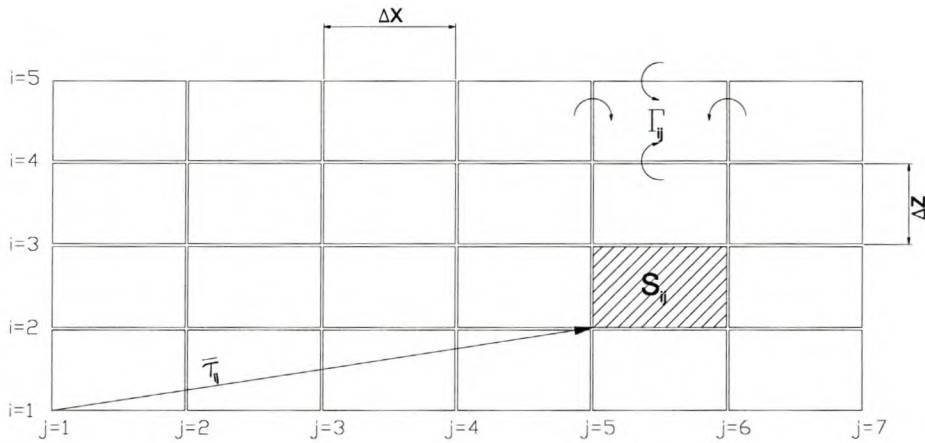


Figure 4.4: Illustration of free surface mesh panels

It is assumed that the vorticity is concentrated in the form of a vortex ring of constant strength along the boundary of each panel. The intensity, Γ_{ij} , of each vortex ring is dependent on the areas of the bordering panels, S_{ij} and S_{ij+1} , in the following manner:

$$\gamma_{zij} \frac{1}{2} (S_{ij} + S_{ij+1}) = \Gamma_{ij+1} - \Gamma_{ij} \quad (4.28)$$

From (4.28) it follows that the vortex intensity of the $(j + 1)$ -th panel in the i -th row can be expressed as a function of the vortex intensity in the previous row (j):

$$\Gamma_{ij+1} = \gamma_{zij} \frac{1}{2} (S_{ij} + S_{ij+1}) + \Gamma_{ij} \quad (4.29)$$

The radiation condition at infinity ($\vec{\gamma} = 0$) can be approximated at the 1st panel row as: $\Gamma_{i1} = 0$. The intensity of all the following panel rows can be calculated using (4.29). The wave elevation can be calculated from the kinematic free surface boundary condition, which can be written as follows for each transverse cross section, j :

$$\vec{\tau}_{ij+1} = \vec{\tau}_{ij} + \frac{\vec{V}}{|\vec{V}|} \Delta l \quad (4.30)$$

where $\vec{\tau}_{ij}$ is the vector from the origin to the bottom left hand corner of the ij -th panel, as illustrated in Figure 4.4 and Δl is a chosen length that reflects the panel size.

Equation(4.30) can be rewritten in terms of the mesh co-ordinates and the panel length ΔX and then simplifies to:

$$\tilde{y}_{ij+1} = y_{ij} + \frac{V_{0y}(x_{ij}, y_{ij}, z_{ij})}{V_{0x}(x_{ij}, y_{ij}, z_{ij})} \Delta X \quad (4.31)$$

$$\tilde{z}_{ij+1} = z_{ij} + \frac{V_{0z}(x_{ij}, y_{ij}, z_{ij})}{V_{0x}(x_{ij}, y_{ij}, z_{ij})} \Delta X \quad (4.32)$$

in the vertical (y) and lateral (z) directions respectively. The collocation point where the velocity in Equations (4.30)-(4.32) is calculated, is at the center of each panel. \tilde{y}_{ij+1} and \tilde{z}_{ij+1} represent the grid co-ordinates for the next iteration. Equation (4.32) causes a lateral shift in each of the grid co-ordinates resulting in a non-orthogonal free surface grid being created after each iteration. A new orthogonal grid can be obtained through a B-spline⁸ interpolation procedure before the next iteration step is performed. By performing these steps in an iterative manner the fully non-linear free surface boundary condition is satisfied.

4.6 The Vortex Roll-Up Process

In many engineering applications it is not necessary to model the vortex roll-up process and straight vortices trailing from the wing suffice to obtain suitable accuracy. As has been discussed in Section 2.3.2, hydrofoil-assisted catamarans suffer from important hull-foil and foil-foil interactions. To be able to accurately determine these, it is necessary to model the wake in an accurate manner by modeling the vortex roll-up process. The shape and position of the vortex wake behind a wing is not known *a priori* and has to be solved, similar to the free surface, through an iterative process.

The requirement for the vortex wake model is that the vortex wake moves with local streamlines and carries no load. This condition leads to a complex rolled-up wake which is physically associated with the formation of the tip vortices. Not often mentioned is that the numerical procedure for solving the roll-up process is unstable. Calculation of the vortex roll-up process is defined as an ill-posed problem. Hadamard [Had32] defines an ill-posed problem as having one or both of the following characteristics:

⁸A spline is a flexible drafting device that is used to construct a smooth curve through a set of data points such as those formed by the free surface grid.

- small perturbations grow very quickly in time
- the solution is not unique

For a slightly disturbed vortex sheet in two dimensions the vortex dynamics have been shown [Mol75] to obey the Laplace equation:

$$\frac{\partial^2 y}{\partial t^2} + \frac{\partial^2 y}{\partial x^2} = 0 \quad (4.33)$$

with the initial condition: $y(x, t) = y_0(x)$. This is the Cauchy problem for the Laplace equation, which is known to be ill-posed due to the first condition above. Characteristics of the 3-dimensional vortex roll-up process is that it is not possible to obtain a converged solution if a high panel density is used [Kor98]. This mathematical instability is due to the discontinuity in the velocity field through the vortex sheet.

An important characteristic of vortex dynamics in actual viscous flows is that the trailing vortex sheet behind a lifting surface has finite thickness and the core radius grows with time. If one makes use of a vortex sheet of finite thickness, using so-called Rankine vortices, it can be shown [BEKM00, Sar89] that the vortex roll-up process is no longer ill-posed, allowing a 3-dimensional solution without numerical instability.

Choice of the appropriate thickness should, strictly speaking, be based on the size of the core radius⁹ calculated using some form of viscous flow calculation or experimental measurement. Investigations by Yang et al. [YHTC94] indicate that the core radius is a function of angle of attack, planform and the profile shape of a hydrofoil. In practice, vortices are very effective in capturing air bubbles in the water, resulting in ventilated cavities inside the core of the tip vortex (see for example: [CCMF97]). Such cavities further influence the size of the core radius. For the sake of simplicity it is therefore easier and more suitable to prescribe a value for the core radius. Within the potential flow framework, this can be done by specifying a cut-off radius based only on the span of the hydrofoil.

4.7 Calculation of Forces

The forces acting on a body can be divided into hydrostatic and hydrodynamic forces. The hydrodynamic force \vec{R} can be determined by integrating the dynamic pressure p , over the surface S , of the hull:

$$\vec{R} = \int_S p \vec{n} dS \quad (4.34)$$

⁹The core radius is defined as the mean distance from the core centre to maximum tangential velocity.

Using the pressure coefficient

$$C_P = \frac{P}{\frac{1}{2}\rho F_0^2} \quad (4.35)$$

the force on the body can be written in coefficient form based on a characteristic length B and the non-dimensional area $\tilde{S} = S/B^2$:

$$\vec{C} = \frac{B^2}{S} \int_S C_P \vec{n} d\tilde{S} \quad (4.36)$$

The dynamic pressure coefficient can be determined from Bernoulli's equation:

$$C_P = 1 - (V/|\vec{F}_0|^2) \quad (4.37)$$

The boundary value of the induced velocity above (+) and below (-) the vortex sheet moving at speed \vec{F}_0 can be written as:

$$\begin{aligned} \vec{V}^- &= \vec{V}_0 - \vec{F}_0 - \frac{1}{2}(\vec{\gamma} \times \vec{n}) \\ \vec{V}^+ &= \vec{V}_0 - \vec{F}_0 + \frac{1}{2}(\vec{\gamma} \times \vec{n}) \end{aligned} \quad (4.38)$$

where \vec{V}_0 is the mean of the velocities above and below the vortex sheet:

$$\vec{V}_0 = \frac{1}{2}(\vec{V}^+ + \vec{V}^-) \quad (4.39)$$

By substituting (4.39) into (4.38) and taking account that $|\vec{F}_0|^2 = 1$ the following are obtained:

$$\begin{aligned} (V^-)^2 &= 1 - 2\vec{F}_0 \cdot \vec{V}_0 + |\vec{V}_0|^2 - (\vec{V}_0 - \vec{F}_0)(\vec{\gamma} \times \vec{n}) + \frac{1}{4}(\vec{\gamma} \times \vec{n})^2 \\ (V^+)^2 &= 1 - 2\vec{F}_0 \cdot \vec{V}_0 + |\vec{V}_0|^2 + (\vec{V}_0 - \vec{F}_0)(\vec{\gamma} \times \vec{n}) + \frac{1}{4}(\vec{\gamma} \times \vec{n})^2 \end{aligned} \quad (4.40)$$

The pressure coefficient is then:

$$\begin{aligned} C_P^- &= +2\vec{F}_0 \cdot \vec{V}_0 - |\vec{V}_0|^2 + (\vec{V}_0 - \vec{F}_0)(\vec{\gamma} \times \vec{n}) - \frac{1}{4}(\vec{\gamma} \times \vec{n})^2 \\ C_P^+ &= +2\vec{F}_0 \cdot \vec{V}_0 - |\vec{V}_0|^2 - (\vec{V}_0 - \vec{F}_0)(\vec{\gamma} \times \vec{n}) - \frac{1}{4}(\vec{\gamma} \times \vec{n})^2 \end{aligned} \quad (4.41)$$

For a body that is completely submerged, there is a difference in pressure on the upper and lower surfaces of vortex sheet. This difference can be written as:

$$\Delta C_P = C_P^- - C_P^+ = 2(\vec{V}_0 - \vec{F}_0)(\vec{\gamma} \times \vec{n}) \quad (4.42)$$

and the force on the body is:

$$\vec{C} = \frac{2B^2}{S} \int_S [(\vec{V}_0 - \vec{F}_0)(\vec{\gamma} \times \vec{n})] d\tilde{S} \quad (4.43)$$

keeping in mind that $(\vec{V}_0 - \vec{F}_0)(\vec{\gamma} \times \vec{n}) = \vec{n}[(\vec{V}_0 - \vec{F}_0) \times \vec{\gamma}]$ and that $(\vec{V}_0 - \vec{F}_0) \times \vec{\gamma}$ is parallel to the normal vector \vec{n} the final expression for the force coefficient is obtained:

$$\vec{C} = \frac{2B^2}{S} \int_S (\vec{V}_0 - \vec{F}_0) \times \vec{\gamma} d\tilde{S} \quad (4.44)$$

In addition to the hydrodynamic forces, one has to take into account the hydrostatic forces acting on the hull, which is proportional to the displaced volume. For a fully submerged body such as a hydrofoil this is easily done. For the case of a surface piercing body (e.g a hull) there is some added difficulty. Strictly speaking, the displaced volume should be calculated in reference to the disturbed free surface, but it is usually sufficient to make use of the mean waterline taking into account the sinkage and trim of the hull. Further, one has to consider the loss of hydrostatic force due to the presence of the transom. The pressure at a ventilated transom is equal to atmospheric pressure and therefore the hydrostatic force acting on the hull is less than that calculated according to Archimedes' principles. Payne [Pay95] has found that this loss of hydrostatic force is proportional to the wetted length to beam ratio of the hull in the following manner:

$$\frac{\text{Actual Buoyancy}}{\text{Archimedes' Buoyancy}} = 1 - \frac{B}{L_{WL}} \quad (4.45)$$

This equation indicates that the loss in buoyancy is particularly strong for hulls with small length to beam ratios. For catamarans, which have large length to beam ratios this correction is not of critical importance. For hydrofoil-assisted catamarans that operate in the condition where the waterline length is significantly reduced (e.g Hysuwac planing phase) this correction becomes more important. For this reason it has been implemented for the calculation of hydrostatic forces acting on hydrofoil-assisted hulls in the present numerical method.

4.8 Solution Process for a Lifting Wing under the Free Surface

The computational steps for solving the free surface boundary condition for a hydrofoil under the free surface are summarized in the flow-chart given in Figure 4.5.

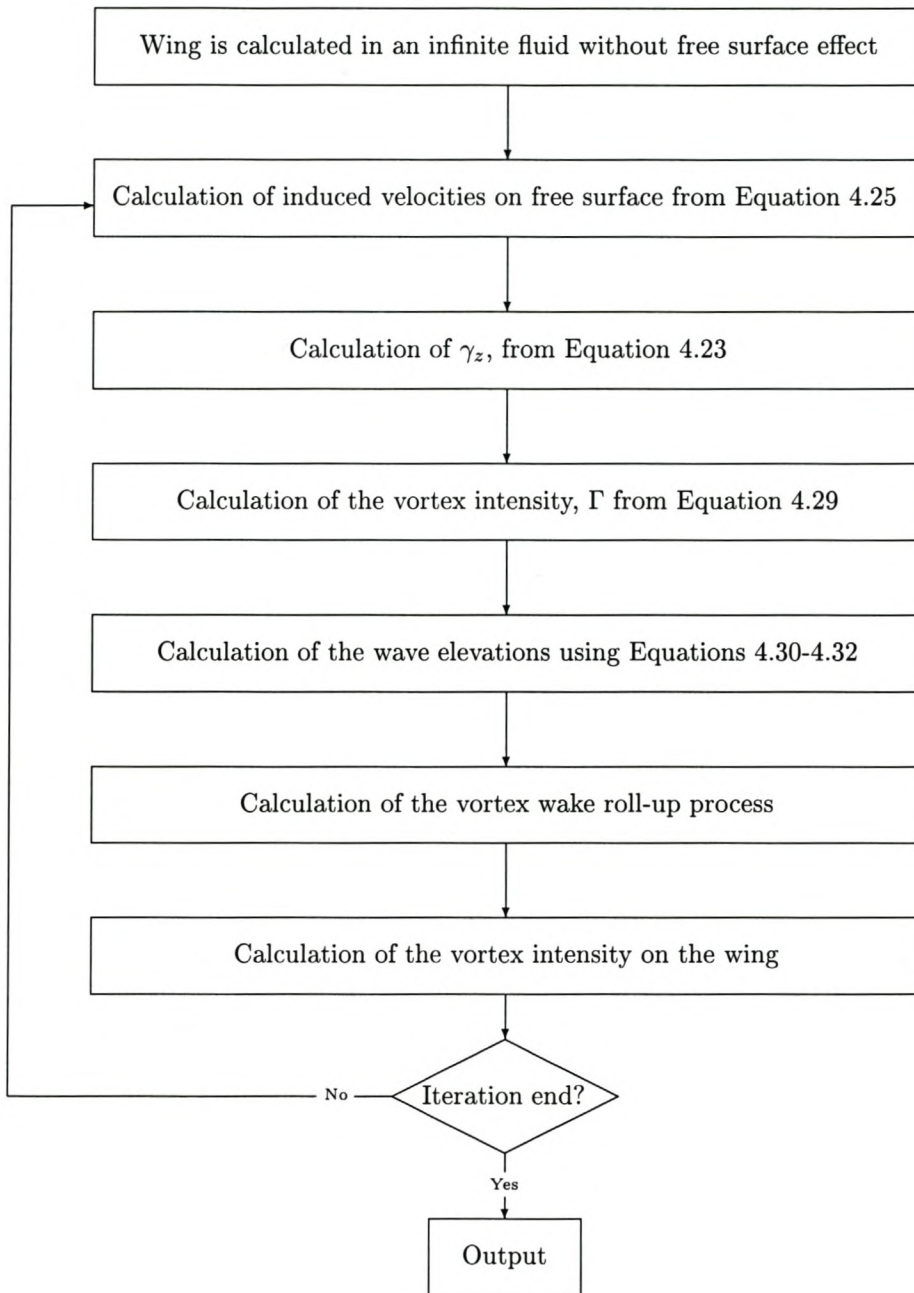


Figure 4.5: Flowchart illustrating the computational steps followed to solve the free surface boundary condition

It requires approximately 30 iterations to obtain convergence for the hydrofoil forces and moments, and 70 iterations to solve the free surface shape accurately. Appendix A presents the details of investigations done to prove convergence.

4.9 Mathematical Model for Planing

The analogy of Wagner [Wag32] allows one to model the planing surface in exactly the same way as a lifting surface with only a few minor differences due to the generation of spray at the leading edge and the formation of the vortex wake. During planing, the hull is treated as a lifting surface planing on the free surface that is either undisturbed or disturbed as a result of the wave wake from forward foils. The latter case would be the situation for the vessel shown in Figure 2.2 in the planing phase.

Boundary Conditions

The same body kinematic boundary conditions (Equation 4.3) apply on the planing surface and the same radiation conditions (Equation 4.4) are valid at infinity. The Kutta condition at the trailing edge (transom) applies in a similar manner to lifting wings, but for the sake of simplicity the vortex wake is prescribed. In the present model the vortex wake is assumed to lie in the plane formed by the chord of the planing surface. Strictly speaking, the vorticity that is shed from the transom must move with the local stream velocity and thus the free surface vortex sheet must follow a similar roll-up process to that of submerged lifting surfaces. Physically this roll-up process results in wave-breaking as the hollow behind the transom closes in on itself. It has been well documented [RTS91, LT96] that the exact shape of the wake at high speeds has little effect on the vorticity distribution on the planing surface and can therefore be modeled in some approximate manner as is done in the present method.

Assuming that the influence of gravity on the free surface boundary condition can be neglected, a number of simplifications can be introduced. The linear combined free surface condition is

$$F_o^2 V_{ox}^2 + g V_{oy} = 0 \quad (4.46)$$

Assuming that gravity is negligible at high Froude numbers, the following simplification results:

$$V_{ox} = 0 \quad (4.47)$$

For a planing surface moving on the undisturbed free surface, it can further be assumed that there is no perturbation far upstream and the equation simplifies to:

$$\vec{\gamma} = 0 \quad (4.48)$$

There is no appreciable free surface elevation until the flow reaches the jet location [Tul56], so it is possible to apply the free surface boundary condition on the free surface undisturbed by the planing hull.

Practically this means the free surface need only be modeled in the wake behind the transom, where according to Equation 4.47 the vortex sheet intensity has the same value as that at the trailing edge of the planing surface and its shape is prescribed. For the case where the planing surface is moving in the wake of upstream hydrofoils, Equation 4.47 applies and the shape of the free surface and its vorticity are obtained from the calculations for the hydrofoils explained in Section 4.8. In practice this means the induced velocities from the front foil vortex-wave wake are considered in determining the forces on the planing surface.

Discretization

Discretization of planing surfaces is done in a similar way as for lifting wings: the surface is divided into trapezoidal elements each representing a vortex ring element. A planing surface is modeled as a set of thin cambered longitudinal strips with rectilinear trailing and leading edges and allows one to model planing surfaces with an arbitrary shape. Each strip is divided into a number of vortex ring elements. The discretization is illustrated in Figure 4.6.

Prediction of the Wetted Area

The wetted area for planing surfaces are often determined through simple equations. Lai and Troesch [LT96, LT95] present a comprehensive review of simple theories, either empirical or based on water impact theory that allow wetted area to be determined for prismatic shaped hulls. Unfortunately the complexity of the wetted surface of hydrofoil-assisted catamarans does not allow use of such simple relations. This is especially true for such cases where the planing surface is influenced by the wave-wake of upstream foils as is often found for hydrofoil-assisted catamarans. Experimental measurements of the wetted surface show it to be asymmetrical for each demi-hull. Figure 4.7 shows the asymmetrical wetted area determined from a paint trace test for a planing Hysuwac model [MH01]. It is therefore more appropriate to make use of a numerical method to estimate the wetted area. The method proposed by Sherglova [She59] and validated by Tikhonov [Tik94] has been implemented in the present method to determine the wetted area numerically.

Considering a longitudinal strip of the planing surface (Figure 4.8), the local free surface elevation close to the bow and the wetted chord can be calculated iteratively in a manner not unlike the method proposed by Zhao and Faltinsen [ZFH97] for solving water impact problems. In the first iteration, the wetted chord is determined

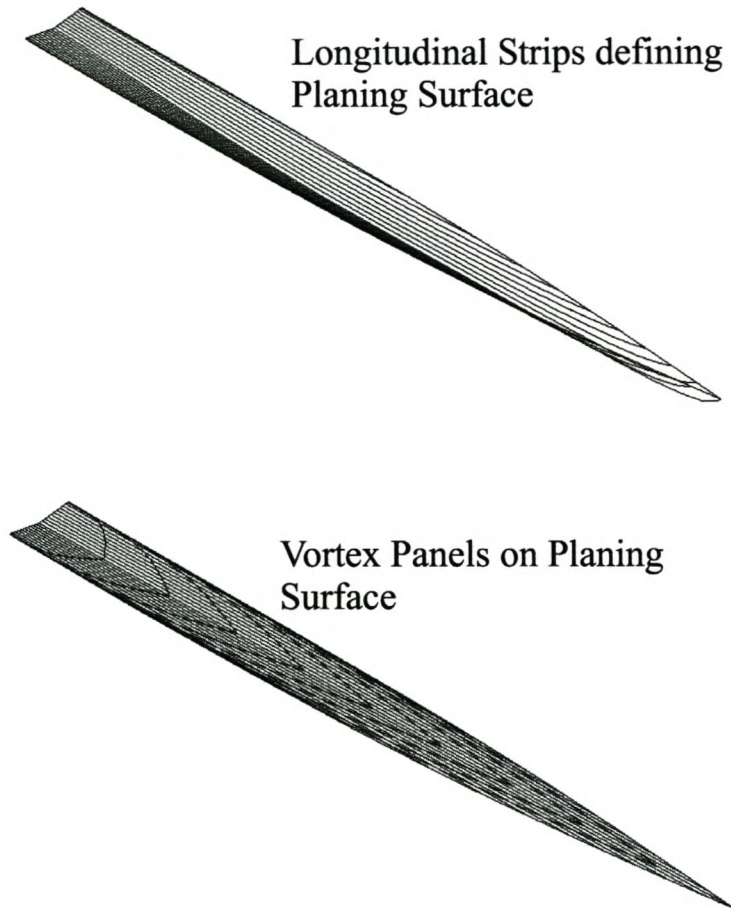


Figure 4.6: Illustration of planing surface discretization

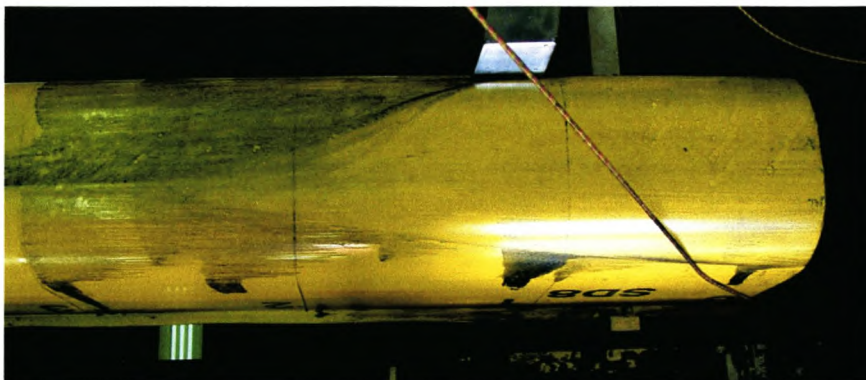


Figure 4.7: Paint trace showing asymmetrical wetted area for a demi-hull planing in the wake of a forward foil

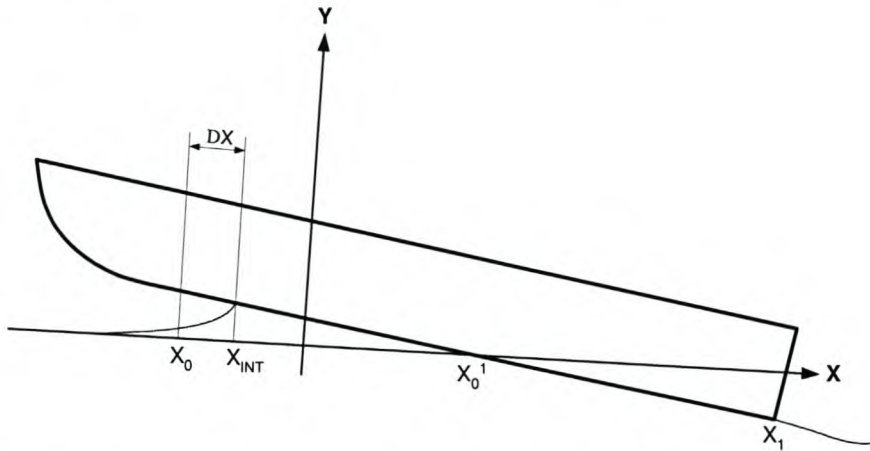


Figure 4.8: A longitudinal strip of a planing surface showing the free surface rise ahead of the bow

as the length measured from the trailing edge to the point of intersection between the keel contour and the free surface (x_0^1), either undisturbed or disturbed by upstream foils. The free surface deformation caused by the planing surface itself can be written in the n -th iteration in the form of the streamline equation

$$y^{<n>} = y(-\infty) + \int_{-\infty}^{x_0^{<n>}} v_y^{<n>}(\xi)/(V_\infty + v_x^{<n>}(\xi))d\xi \quad (4.49)$$

where v_x and v_y are components of the velocity induced by the entire planing surface. They can be obtained using the Biot-Savart law. In the iteration process, the leading edge, x_0^n is shifted towards the bow by adding Δx along the keel contour until the intersection point between the surface streamline (Equation 4.49) and the hull bottom is found. Performing calculations for all sides and strips and connecting the corresponding points, one obtains the wetted area of the planing surface. Obviously the jet flow near the leading edge and sides of the planing hull is ignored in this approach. It should also be noted that the integral of Equation 4.49 only converges in the 3-dimensional case [BEKM00].

4.10 Application of the Vortex Lattice Method to Planing Hydrofoil-Assisted Catamarans

The planing model described in the previous section is well suited to modeling planing hydrofoil-assisted catamarans of the Autojet type shown in Figure 1.2 which consist of forward foils, and planing surfaces aft. The distance between the front foils and the rear planing surfaces are large enough to consider the front foil independently of

the rear planing surface. Considering this, the problem can be simplified into the two following problems:

- Calculation of the front foil and its vortex-wave wake.
- Calculation of the rear planing surface moving in vortex wake generated by the front foil.

Solving the problem in this way, the influence of the forwardly positioned foils on the hull is captured but the influence of the hull on the foils is neglected. This is correct within the linearizations of the planing theory. For a more complex configuration such as the Hysuwac described in Section 1.4.5, one has to consider the aft planing hull together with a rear foil¹⁰. Calculating such a system planing in the wake of the front foil introduces some errors concerning the rear hydrofoil and the free surface boundary conditions:

- The free surface effect on the rear foil lift and drag is not considered.
- The free surface elevation of the rear foil on the planing hull is not considered.

The first point above arises due to the simplifications introduced into the planing model free surface boundary condition, Equation 4.48. The result is that the rear foil, modeled together with the planing hull, is seen as operating in unbounded flow. It is well known that the effect of the free surface is important in determining the lift and drag forces on hydrofoils and modeling the rear foil in the above manner will introduce significant error into the calculation. The second point above is less important as the rear foil is located in the tunnel between the demi-hulls and the hull is thus less affected by the wave-wake of the rear foil (the influence of rolled-up vortex wake from the rear foil is captured).

An alternate calculation procedure was developed within the framework of the current method to model planing hydrofoil-assisted catamarans with other foil configurations, allowing one to include the effect of the free surface on the rear foil.

4.10.1 Calculating Hydrofoil-Assisted Catamarans that consists of a Rear Planing Surface in Combination with a Hydrofoil

The development of the procedure was done by applying it to a planing Hysuwac design [MH01] as this system has been extensively investigated during this study and

¹⁰A similar situation applies to modeling planing Hysucac type and tandem hydrofoil-assisted catamarans illustrated in figure 1.5

the available experimental results could be used for validation purposes. Similarly to the Autojet example, the front foil and the rear lifting system (comprising of the planing hull and rear foil) are located far apart, so there is negligible interference to the front foil from the rear lifting system and one only requires a modification in the method of modeling the hull and rear foil together.

If one linearizes the interactions between the various lifting surfaces and assumes that they can be determined separately and simply be added together, a combination of different calculations allows one to determine the effect of the free surface on the rear foil while capturing the important interactions between the rear foil and the hull. The following five calculations need then be performed:

1. Calculation of the front foil forces and its vortex-wave wake.
2. Calculation of the front and rear foil (w/o hull) together.
3. Calculation of the rear foil only w/o free surface effect.
4. Calculation of the rear lifting system in the vortex-wave wake of the front foil.
5. Calculation of the planing surface in the vortex-wave wake of the front foil.

The first calculation provides the front foil forces and the vortex-wave wake. As explained earlier, there are no interference effects on the front foil as the distances between the front foil and the rear lifting surface is large. Experimental investigations by Miyata et al. [MT90] indicate that this is valid if the rear lifting system is more than four chord lengths behind the front foil.

The second calculation, for the front and rear foil under the free surface, captures the interaction between front foil, rear foil and vortex-wave wake of both foils. The foil interference is therefore captured.

The third calculation considering the rear foil only without consideration of the free surface is necessary, together with the fourth calculation, to determine the influence of the hull on the rear foil. A hull interference factor can be determined and used to correct the rear foil forces calculated for the rear foil under the free surface (the second calculation).

The fourth calculation for the rear lifting system (hull and rear foil) in vortex wake of the front foil allows one to determine the planing hull forces including the interference effects from the front foil and rear foil. The rear foil interference on the hull is somewhat in error as the rear foil forces in this calculation do not include the free surface effect.

A fifth calculation is done for the planing surface only in the vortex-wave wake of the front foil. While this calculation is in essence not required for determining the forces



Figure 4.9: Picture of the SD6 model with F2 foil system

on the hull, it gives useful values for comparison with planing hull calculations with the rear foil present (the fourth calculation). The influence of the rear foil on the hull forces can then be readily determined in the form of an interference factor.

At planing speeds a small amount of wave-making remains [Sav88]. The wave-making resistance component in the scope of the present numerical method is calculated separately using thin ship wave-making theory (MICHLET) as explained in Section 4.4.2.

Each of the five calculations is done for constant speed, vessel trim and sinkage. To determine the equilibrium conditions a matrix of trim and rise variations needs to be computed. The resulting matrix of total vessel forces and moments allow one to determine the running equilibrium for any specified LCG, displacement and thrust that falls within the range of computed trim, rise and speed values.

A similar approach can be used to model other foil configurations such as the Hysucat system. In such cases the foil and hull forces would be modeled in the same way as Calculations 2-4 described above, without the need to consider a forward foil vortex-wave wake.

4.10.2 Validation of Planing Computational Method

To validate the method, a Hysuwac configuration (code-named SD6-F2) for which experimental data exists [MH01] was modeled and the resistance trim and sinkage compared. Figure 4.9 shows a picture of the model and its Hysuwac foil system. Keeping in mind the aim to develop a practical design tool, a satisfying result would be accurate prediction of engineering quantities required for design, in particular, the resistance, lift forces, moments and attitude of the vessel.

Length [m]	40
Δ [tons]	161
LCG [m]	14.84

Table 4.1: Main particulars of the SD6-F2 Hysuwac

A spreadsheet was set up that allows one to enter the force components of each lifting surface after each of the five calculations is completed. The interference factors and final resistance are then calculated and given as output in the spreadsheet. The main parameters of the SD6-F2 model are given in Table 4.1.

Computations were performed for a number of different speeds in the planing phase of motion and compared with experimental results. During planing the foils operate very close to the free surface, so it can be assumed that the viscous scale effects on the lift and drag of the foils are small. Computed values should therefore be in good agreement with measurements. At each speed the trim and rise was specified from experiments in the computation so that the lift, drag and longitudinal centre of pressure could be calculated and compared with measured values¹¹. Figure 4.10 shows the comparisons of computed lift, drag and LCP position (which must correspond to the LCG) against experimental values and it can be seen that the predictions are in reasonably good agreement with experimental values, even in the transition regime. Although measurements were made at higher planing speeds, these could not be calculated directly as the forward foil was in extreme free surface effect, with only a very thin layer of water covering the upper surface at model scale. In reality this thin layer breaks up into the air-water mixing layer pictured in Figure 2.9. The forward foil is actually above the undisturbed free surface but due to the wave formed over the foil, it remains submerged. The highly non-linear behaviour of the flow at such small submergences prevents the vortex lattice method from converging.

It is gratifying to see the good agreement between theory and experiment in Figure 4.10 at transition speeds and that the model shows some indication of the transition to planing. This is in spite of the simple fashion in which the bow spray sheet is modeled (as a local free surface elevation only affecting the wetted area). Predictions of resistance at lower speeds understandably show much poorer correlation with experiments. To model the speeds comprising the displacement and transition phases $1.0 \leq Fn_{\nabla} \leq 3.0$, a more general numerical model is needed to model the free surface boundary condition.

¹¹In actual design problems the inverse would apply, the LCG and displacement would be specified and the resulting trim, rise and resistance calculated.

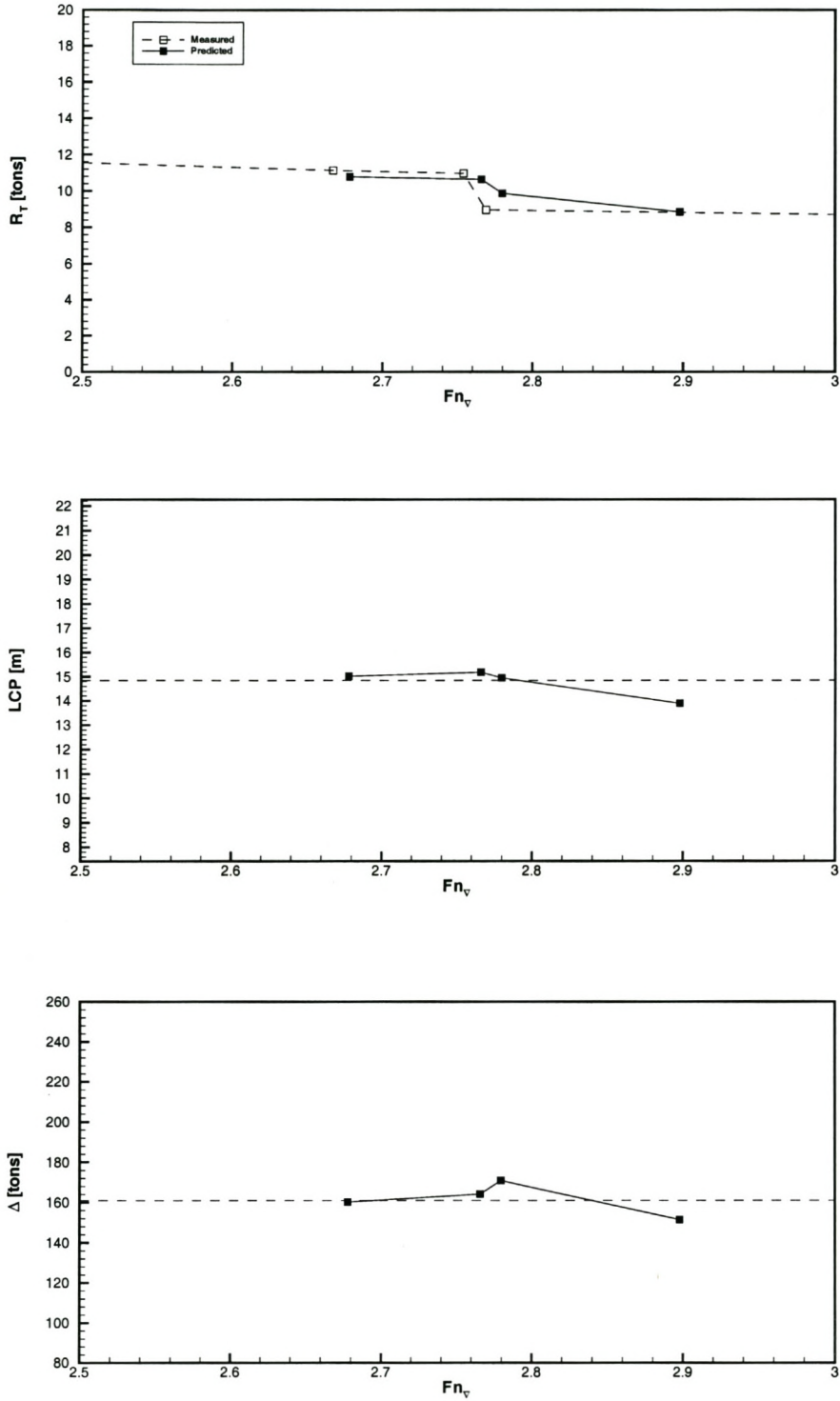


Figure 4.10: AUTOWING prediction of resistance, displacement and center of pressure

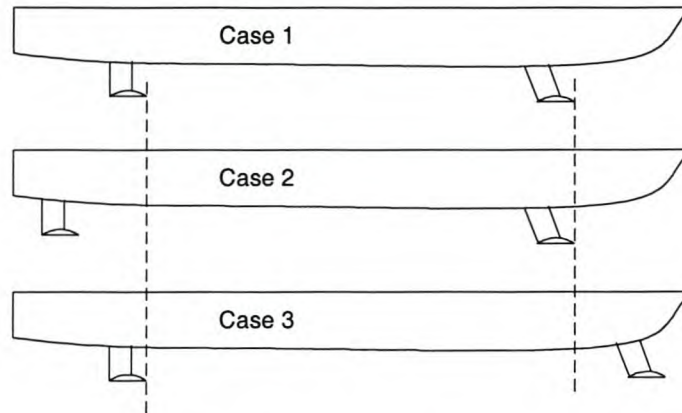


Figure 4.11: Illustration of the three longitudinal foil positions calculated

4.10.3 Optimization using Computational Model for Planing Hydrofoil-Assisted Catamarans

The developed method was used to optimize a Hysuwac type hydrofoil-assisted catamaran with particulars as given in Table 4.1. Focus was on investigating different mutual positions for the foils on the hull, while not changing the hull geometry [KMHN01]. Numerical calculations for a speed of 40 knots ($Fn_{\nabla} = 2.8$) show that optimizing the lateral distance between the hydrofoils is very effective in optimizing the vessel for low resistance. Figure 4.11 illustrates the three conditions that were tested.

Case 1 represents the original configuration which was model tested and compared with model test data in Figure 4.10. Case 2 has the rear foil shifted aft compared to Case 1 and Case 3 the forward foil shifted forward relative to Case 1. Figure 4.12 shows a sample result for the 3 different cases tested. In the figure the lift to drag ratio (L/D) is presented for the three cases as a function of LCG position where the displacement of the vessel is the curve parameter. It can be seen that the method is a useful tool for optimizing the positions of the foils and also the LCG position of the craft to obtain the most efficient operating point. Further the effects of varying displacement are also seen.

From the figure a clear tendency emerges: that increasing the distance between the foils results in an improvement of the L/D ratio. To explain this result, consider Table 4.2, which gives the lift and drag of the hull and foils for Case 2 and 3 relative to that of Case 1.

The table shows that the L/D of the rear foil is substantially increased for Cases 2 and 3. This is due to the rear foil operating in increased upwash as the separation distance is increased between the foils. Figure 4.13 shows the upwash on the rear

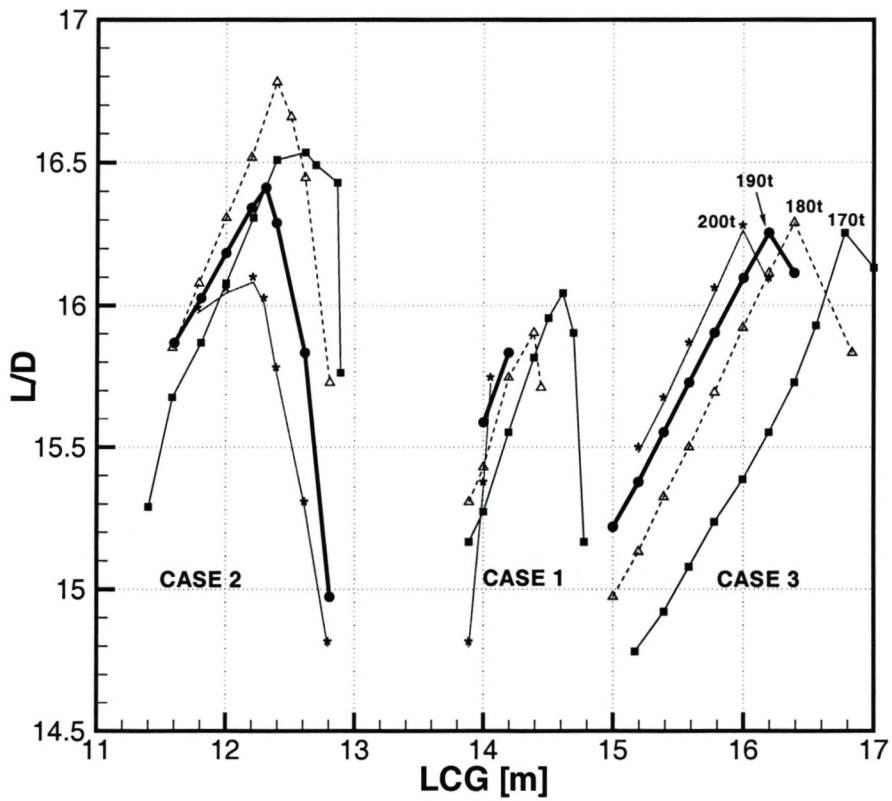


Figure 4.12: Lift to drag ratio as a function of LCG position with displacements as the curve parameter for $F n_{\nabla} = 2.8$

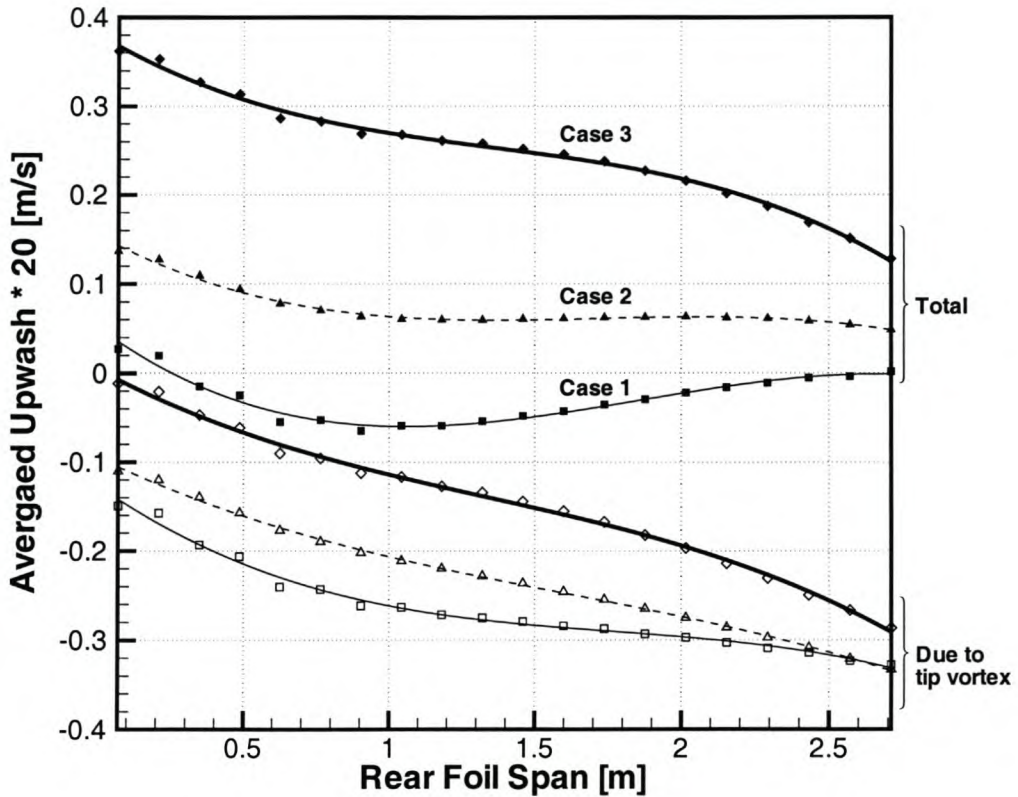


Figure 4.13: Upwash averaged along the rear foil chord. Zero on the abscissa axis corresponds to the longitudinal symmetry plane of the vessel.

foil across the span. It can be clearly seen from the figure that the rear foil enjoys increased upwash for Cases 2 and 3. The rear foil in Case 3 experiences the most upwash and also the highest lift coefficient and L/D for the three cases.

The increase in lift on the rear foil leads to the rear of the ship rising out farther of the water decreasing the wetted area for Case 2. Case 3 has an increased wetted area as the hull is located farther aft in relation to the front foil and therefore is planing close to the wave crest, which increases its wetted area. Figure 4.14 shows the wetted area for the 3 cases. Note the asymmetry in the wetted area similar to that found experimentally (Figure 4.7).

The rear increase in lift leads to a decrease in trim angle for the vessel and in turn, a lower angle of attack and lift coefficient for the front foil. The tip vortex intensity and therefore the downwash experienced by the rear foil is lower and despite the lower trim of the vessel the rear foil lift coefficient increases. Case 2 offers the best L/D

	Basic Variant	The rear foil shifted 3m aft	Both rear foil and hull shifted 7m aft
	Case 1	Case 2	Case 3
Trim angle	2.15	2.08	1.65
Transom submergence	-0.48m	-0.54m	-0.7m
front foil C_L	100%	83.1%	92.5%
L/D of front foil	100%	98.6%	63.8%
rear foil C_L	100%	106%	107.4%
L/D of rear foil	100%	107%	136.9%
C_L of hull + rear foil	100%	102%	103.5%
L/D of hull + rear foil	100%	109%	101.8%
Hull R_W	100%	87%	79.8%
L/D of ship	100%	105%	104.3%

Table 4.2: Calculated results for cases 2 and 3 in relation to case 1

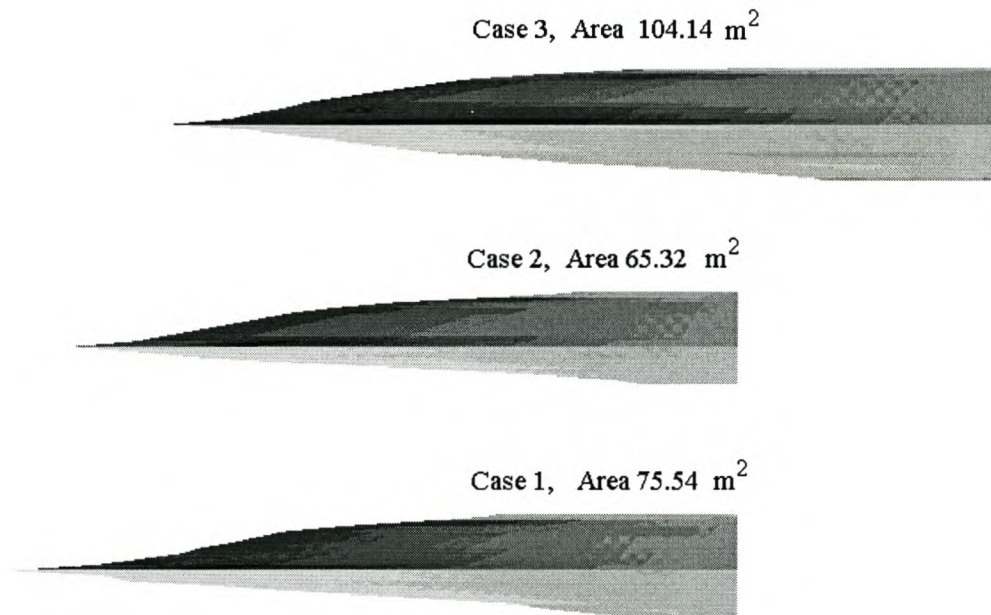


Figure 4.14: Wetted area for the 3 different cases calculated

ratio for the cases tried as the L/D of the rear foil is improved and the wetted area increased. The increase in wetted area of Case 3 offsets the improved efficiency of the rear foil so that there is only a small improvement in resistance over Case 1.

This example shows that the mathematical model provides an effective basis for design of hydrofoil-assisted catamarans in the planing phase. The main interactions between the hull and the hydrofoils as well as between fore and aft hydrofoils are suitably captured. The method is therefore suitable to perform optimization of any geometric parameters pertinent to optimization studies of planing hydrofoil-assisted catamarans.

4.11 A Free Surface Model for Displacement and Transitional Speeds

In Section 4.4.2 the use of a 3-dimensional vortex lattice method to solve the free surface problem for semi-displacement speeds has been outlined. At these speeds, such methods make use solely of linear free surface boundary conditions, often with a relatively coarse panel mesh in the region of the bow, in order to avoid numerical instability arising from the spray jet. In reality the spray jet has a large velocity but small thickness, which causes numerical simulations to break down (see for example: [Fal90]). The result of such approximations in the paneling arrangement cause conventional panel methods to under-predict the resistance as the bow wave together with its associated spray sheet are insufficiently captured. A primary requirement of any further development is therefore to model the spray jet in the region of the bow in more detail.

Implementing such a method to model spray and wave-making within the framework of vortex lattice theory would allow the AUTOWING code to model the displacement, transition and planing phases of operation for hydrofoil-assisted craft as well as capturing all non-viscous interactions between any combination of hulls and hydrofoils.

The development of such a method to model the bow spray sheet in 3 dimensions, started first with solution of the canonic problem of a 2-dimensional wedge impacting the water surface. Solution of this problem serves as validation of the vortex method for problems involved with development of a jet.

4.11.1 Two Dimensional Spray Jet Model

To date 2-dimensional numerical solutions of the water impact problem have relied on source panel methods to model the flow including the jet. To overcome the difficulty of numerical breakdown of the jet spray model, Zhao et al. [ZFA96] proposed simply cutting off the spray jet that forms close to the impacting body from the global flow

in the numerical model. A number of works (e.g. [ZFH97, FC97, XT99]), modeling 2-dimensional impact problems using the jet cut-off, have shown excellent agreement with experiments, even though mass and momentum are no longer conserved. Such 2-dimensional solutions have been successfully applied to modeling planing and slender ship problems (see for example: [FFC00]). Some research [May91] has further shown that such methods for modeling the spray jet are suitable and can be extended to 3-dimensions.

The development of a jet spray model within the framework of vortex lattice theory was undertaken by following a similar line to that presented by Zhao et al. [ZFA96], which is an extension to the theory of Wagner [Wag32]. Kornev and Migeotte have developed the numerical method [KMH01] and validated it against experimental data and other numerical methods for a 45 degree wedge impacting the water. The main points of the method are given in the subsection that follows. Further details can be found in [KMH01].

Mathematical Formulation

The mathematical formulation is based on potential flow assumptions, with the Laplace equation having to be solved at every time instant with the standard boundary conditions:

the kinematic condition on the wedge:

$$\frac{\partial \phi}{\partial \vec{n}} = 0 \quad (4.50)$$

the kinematic boundary condition on the free surface:

$$\frac{\partial \phi}{\partial \vec{n}_1} = \frac{\partial \phi}{\partial \vec{n}_2} \quad (4.51)$$

the dynamic boundary condition on the free surface:

$$p_1 = p_a \quad (4.52)$$

the radiation condition:

$$\nabla \phi \rightarrow 0 \text{ at infinity} \quad (4.53)$$

Similar to the vortex method described earlier in this chapter, use is made of a vortex sheet with unknown intensities, γ_s and γ_b on the free surface and wedge respectively. The kinematic free surface boundary condition is satisfied with a linearized free surface boundary condition assuming that the free surface follows the trajectories of fluid particles lying on the free surface:

$$\frac{d\vec{r}}{dt}(a) = \vec{V}_0(a) \quad (4.54)$$

The dynamic free surface boundary condition is satisfied using Bernoulli's equation which can be written in a reference system moving with the free surface velocity:

$$\frac{D\phi}{Dt} + \frac{\vec{V} \cdot \vec{V}}{2} + gy - \vec{V}_0 \cdot \vec{V} = 0 \quad (4.55)$$

where $\frac{D}{Dt}$ represents the substantial derivative. The velocity and potential under the vortex sheet are satisfied by

$$\phi = \phi_0 - \Gamma/2, \quad \vec{V} = \vec{V}_0 - \vec{s}\gamma_s/2 \quad (4.56)$$

where Γ is the circulation around the tip end of the free surface vortex sheet and ϕ_0 is the direct value of the potential on the free surface:

$$\Gamma = \int_{-\infty}^A \gamma_s ds \quad \phi_0 = \int_{-\infty}^A \vec{V}_0 \vec{s} ds \quad (4.57)$$

By substituting (4.56) into (4.55) and performing the integrations, one obtains an expression for the vortex intensity on the free surface:

$$\gamma_s(s, t) = 2\vec{V}_0 \cdot \vec{s} + \int_0^t \left[-\frac{\partial}{\partial s} V^2 - \frac{\gamma_s}{4} + 2\frac{y}{Fn^2} + (2V_s - \gamma_s) \left(\frac{\partial(\vec{V}_0 \cdot \vec{n})}{\partial s} - \frac{\vec{V}_n \cdot \vec{n}}{\rho} \right) \right] dt \quad (4.58)$$

or its linear analog

$$\gamma_s(s, t) = 2\vec{V} \cdot \vec{s} + \frac{2}{Fn^2} \int_0^t \frac{\partial y}{\partial s} dt \quad (4.59)$$

In (4.58) and (4.59) all lengths are referred to a unit length, L , velocities and γ_s are referred to the impact speed, W and the Froude number is defined as $Fn = W/\sqrt{gL}$. Non-dimensional time is obtained by multiplying by a factor W/L .

Numerical Method

As with the 3-dimensional vortex method described earlier, the free surface and the wedge are represented by a set of straight vortex segments (panels) with a piecewise distribution of the vortex intensity as indicated in Figure 4.15. Numerical implementation of the method was performed by Kornev [KMH01] as follows:

1. Assuming the free surface being known, the intensities, γ_s and γ_b are calculated iteratively from Equations (4.50) and (4.58). The velocities are found from the Biot-Savart law.
2. The free surface elevation is calculated from equation (4.54).

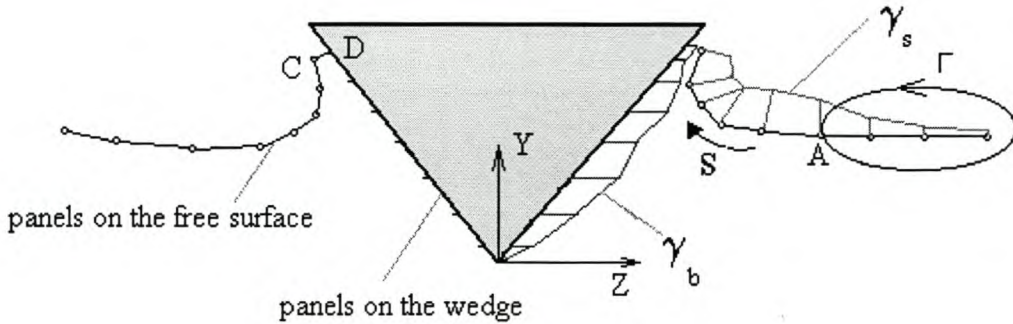


Figure 4.15: Computational domain and discretization of the 2-dimensional impact problem

3. The free surface form is analyzed and smoothed. When solving the non-linear free surface boundary condition, the jet is cut off if the angle between the free surface and the body surface is less than some predefined angle (6°), section CD (Figure 4.15) is introduced as suggested by Zhao et al. [ZFA96].
4. The panels on the free surface are redistributed so that the length of each panel is equal to a given value.

Numerical Results

Numerical results for the pressure distribution and the free surface elevation are in good agreement with those of Dobrovolskaya, Zhao et al. and Mei et al. [Dob69, ZFA96, MLY99] as is shown in Figure 4.16. Further, the method shows the correct limit when the Froude number (based on the impact velocity, and a unit length) tends to zero. Figure 4.17 shows the result for the free surface elevation as a function of Froude number.

It was found that the influence of Froude number has an important effect. At low Froude numbers the impact process is characterized by the formation of detached waves on the free surface as can be seen in Figure 4.17, while for $Fn \geq 1.0$ the influence of Froude number is small. Further, it is gratifying to see that the numerical scheme converges to the correct limit when $Fn \rightarrow 0$, i.e. tends to the undisturbed free surface.

Comparing the numerical results for the linear and non-linear free surface boundary

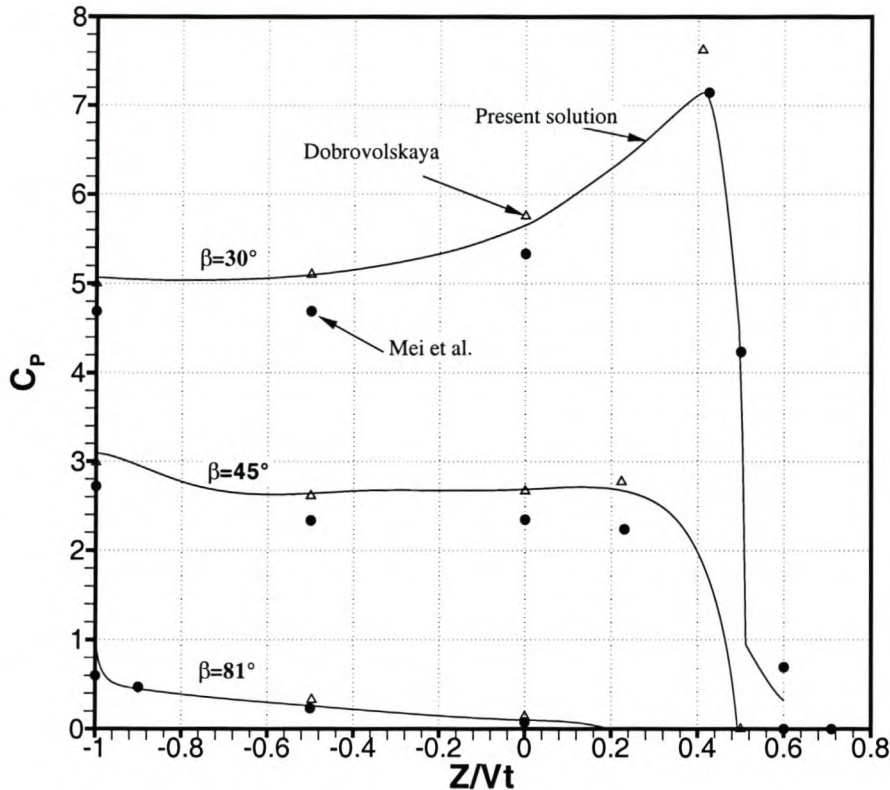


Figure 4.16: The pressure distribution on the wedge for different deadrise angles

conditions, it was found that the non-linear boundary conditions often lead to numerical instability, while its influence is not essential in capturing the water rise close to the hull. Figure 4.18 shows a comparison of results for the linear and non-linear cases.

The results of this 2-dimensional simulation of the impact process including a model for the jet spray have proved the suitability of the vortex method to model the formation of the jet spray and can be further developed for 3-dimensional problems.

4.11.2 Numerical Simulation of 3-Dimensional Problems with Jet Spray

Solution of the 3-dimensional problem follows similar lines for modeling the free surface as explained in Section 4.5 using equations (4.3) - (4.27). The main differences lie in the numerical implementation of the method, which is now more complicated

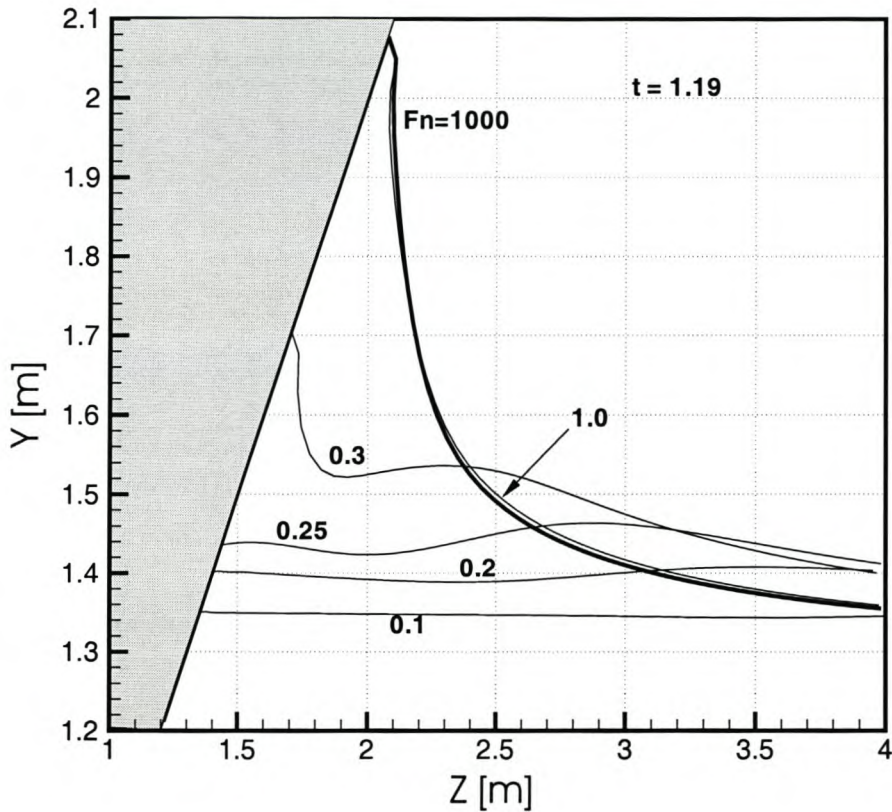


Figure 4.17: Influence of Froude number on the impact process and free surface elevation

as one has to consider a surface piercing body.

Numerical Implementation

In the numerical implementation, the free surface is represented by grid defined within the rectangle x_0, x_1, z_0 and z_1 and the free surface is represented by a number of closed vortex rings. The grid on the free surface consists of two sets of lines: longitudinal lines which are body fitted and lateral lines that are perpendicular to the x -axis. Such a grid is illustrated in Figure 4.19.

Note the difference between the free surface mesh shown in Figure 4.19 and that used previously for the high-speed planing approximation (Figure 4.4). The orthogonal grid used in the previous calculations is convenient for submerged bodies such as

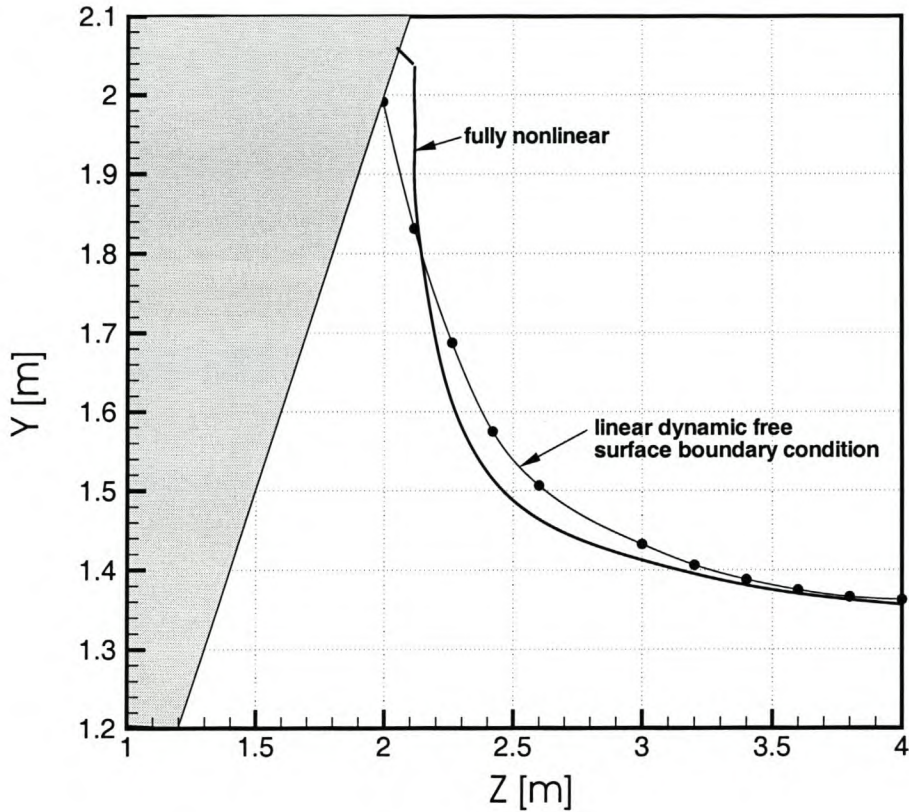


Figure 4.18: Influence of non-linearity on the free surface elevation for large Froude numbers

hydrofoils, but for surface piercing bodies such a grid is complicated and unnecessary.

For the orthogonal grid, approximating the free surface vortex intensity was done using the simple relations given in Equations (4.28) and (4.29). For a non-orthogonal grid the relationships take on a more complicated form. In this case, the vortex sheet intensity vector $\vec{\gamma}_{ij}$ is a function of the following relation:

$$\begin{aligned} \vec{\gamma}_{ij} = & \left[\frac{(\Gamma_{ij} - \Gamma_{ij-1})\vec{\rho}_{ij}}{\Delta_i} + \frac{(\Gamma_{i-1j} - \Gamma_{i-1j-1})\vec{\rho}_{i-1j}}{\Delta_{j-1}} \right] / 2.0 \\ & + \left[\frac{(\Gamma_{i-1j} - \Gamma_{ij})\vec{r}_{ij}}{\delta_j} + \frac{(\Gamma_{i-1j-1} - \Gamma_{ij-1})\vec{r}_{ij-1}}{\delta_{j-1}} \right] / 2.0 \end{aligned} \quad (4.60)$$

When Equation (4.60) is multiplied by a unit vector in the z-direction $\vec{\zeta}$ we get:

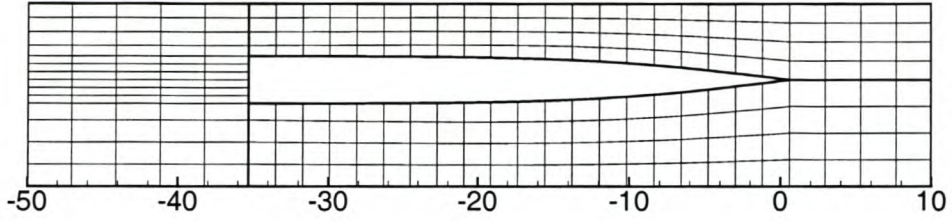


Figure 4.19: Free surface mesh around a body piercing the free surface

$$\begin{aligned} \vec{\gamma}_{ij\zeta} = & \left[\frac{(\Gamma_{ij} - \Gamma_{ij-1})\vec{\rho}_{ij\zeta}}{\Delta_i} + \frac{(\Gamma_{i-1j} - \Gamma_{i-1j-1})\vec{\rho}_{i-1j\zeta}}{\Delta_{i-1}} \right] / 2.0 \\ & + \left[\frac{(\Gamma_{i-1j} - \Gamma_{ij})\vec{r}_{ij\zeta}}{\delta_j} + \frac{(\Gamma_{i-1j-1} - \Gamma_{ij-1})\vec{r}_{ij-1\zeta}}{\delta_{i-1}} \right] / 2.0 \end{aligned} \quad (4.61)$$

where the subscript ζ for every vector denotes the scalar product of this vector with the unit vector $\vec{\zeta}$. The definition of the different vectors are shown in Figure 4.20. This equation provides a relation for the circulation Γ_{i-1j} :

$$\Gamma_{i-1j} = a_{i-1j-1}\Gamma_{i-1j-1} + a_{ij-1}\Gamma_{ij-1} + a_{ij}\Gamma_{ij} + a_\gamma\gamma_{ij\zeta} \quad (4.62)$$

where

$$\begin{aligned} a_{i-1j-1} &= \left(\frac{\rho_{i-1j\zeta}}{\Delta_{i-1}} - \frac{r_{ij-1\zeta}}{\delta_{j-1}} \right) / \left(\frac{\rho_{i-1j\zeta}}{\Delta_{i-1}} + \frac{r_{ij\zeta}}{\delta_j} \right) \\ a_{ij-1} &= \left(\frac{\rho_{ij\zeta}}{\Delta_i} + \frac{r_{ij-1\zeta}}{\delta_{j-1}} \right) / \left(\frac{\rho_{i-1j\zeta}}{\Delta_{i-1}} + \frac{r_{ij\zeta}}{\delta_j} \right) \\ a_{ij} &= \left(-\frac{\rho_{ij\zeta}}{\Delta_i} + \frac{r_{ij\zeta}}{\delta_j} \right) / \left(\frac{\rho_{i-1j\zeta}}{\Delta_{i-1}} + \frac{r_{ij\zeta}}{\delta_j} \right) \\ a_\gamma &= 2\gamma_{ij\zeta} / \left(\frac{\rho_{i-1j\zeta}}{\Delta_{i-1}} + \frac{r_{ij\zeta}}{\delta_j} \right) \end{aligned} \quad (4.63)$$

Equations (4.62) and (4.63) provide an explicit relation for Γ_{i-1j} , allowing one to solve the free surface boundary condition starting from the outer upper side of the free surface grid and moving inside and downstream in the manner illustrated in Figure 4.21. These equations replace the simpler relation of Equation 4.29 used in the orthogonal grid.

The free surface elevation is calculated as before, using the kinematic free surface boundary condition: Equations (4.30) to (4.32). In these equations the free surface

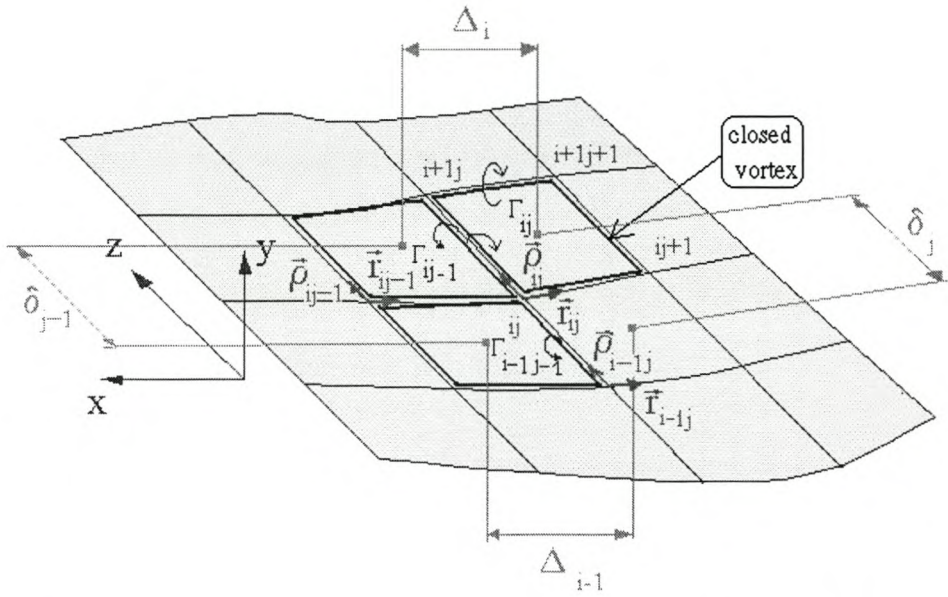


Figure 4.20: Approximation of the continuous vortex sheet by a set of closed vortices

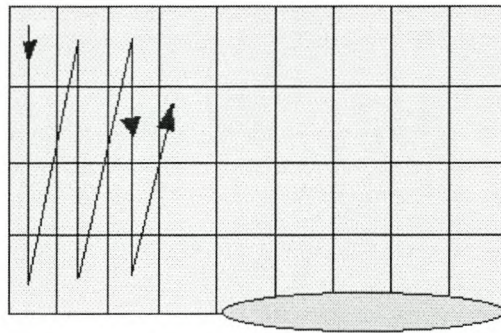


Figure 4.21: Directions of the approximation procedure for calculating circulation intensities

elevation at section $j + 1$ is calculated from the velocities and free surface elevation at section j . This leads to a situation where the free surface penetrates the body at section $j + 1$ as illustrated in Figure 4.22.

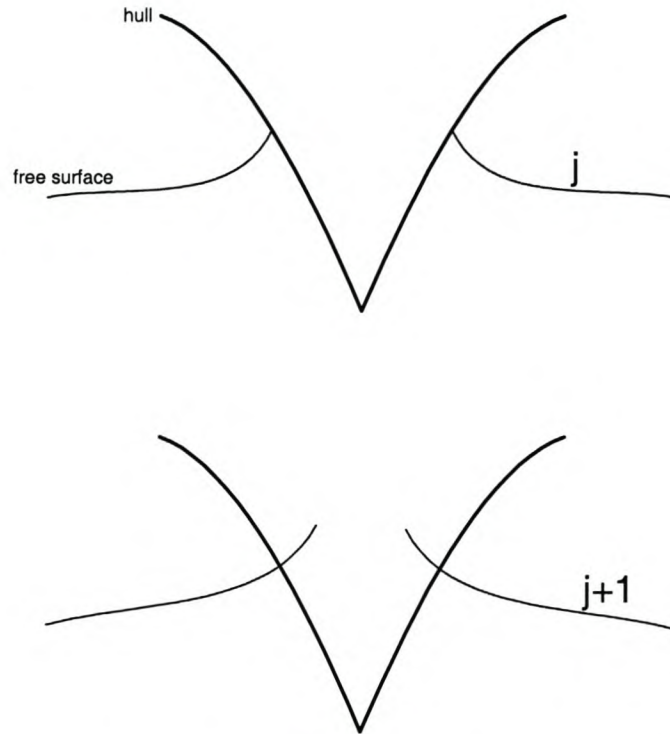


Figure 4.22: Illustration of free surface penetrating a surface piercing body during calculation of free surface elevations

A similar procedure to that implemented in the solution of the 2D wedge impact problem is adopted to solve the flow in the region of the hull:

1. After calculating the free surface elevations, using the kinematic free surface boundary condition, the free surface is cut at the intersection with the hull.
2. The panels on the free surface are redistributed to create a new body-fitted grid with lateral lines perpendicular to the x-axis and body-fitted longitudinal lines (see Figure 4.19).

The hull is paneled using rectangular elements along the hull and triangular elements near the bow. This scheme is illustrated in Figure 4.23. Calculations to establish convergence of the method are described in Appendix A and the next section shows some results obtained with the method including comparison with experiment.

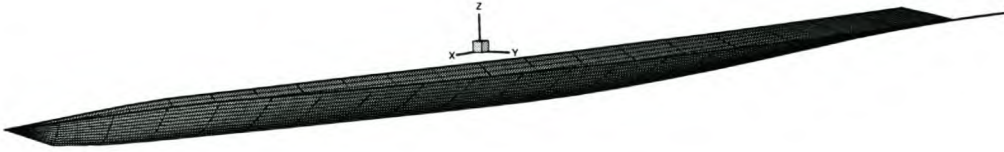


Figure 4.23: Illustration of the hull paneling scheme. Rectangular elements are used along the hull and triangular elements near the bow

4.11.3 Results and Comparison with Experiment

The results of the numerical method were compared firstly with the SD6 hull without foils for the same conditions for which the KELVIN and MICHLET calculations were presented earlier (Figure 4.2). Figure 4.24 shows the results of the present method, AUTOWING against experiment and those found earlier with MICHLET and KELVIN. It is clear that the present method has a similar accuracy to that of KELVIN. The accuracy of MICHLET is slightly better as this code has a number of empirical correction factors which have been introduced to improve its accuracy. All the numerical methods show some under-prediction of the total resistance, which is due to a number of wave-breaking and other parasitic resistance components such as for example resistance due to flow separation from the submerged chines that are not considered.

Figure 4.25 shows the computed free surface mesh and also the height contours for $Fn_{\nabla} = 3.0$. It is seen that the code produces a regular free surface shape, even in the region of the spray jet close to the hull.

To validate the method for a hydrofoil-assisted catamaran problem, the same Hysuwac configuration used to validate the planing model (section 4.10.2) was used and compared with measurement at transition speeds (see Figure 4.9). These experimental results are considered as a suitable validation problem as there is a prominent transition hump resistance. The numerical predictions are not expected to agree as well with experimental results due to experimental error introduced by the viscous scale effects.

Figure 4.26 shows the comparison of the numerical and experimental result of resistance, wetted area and lift. In the calculation the experimentally measured values for trim and rise of the vessel were specified. The results show that resistance and wetted

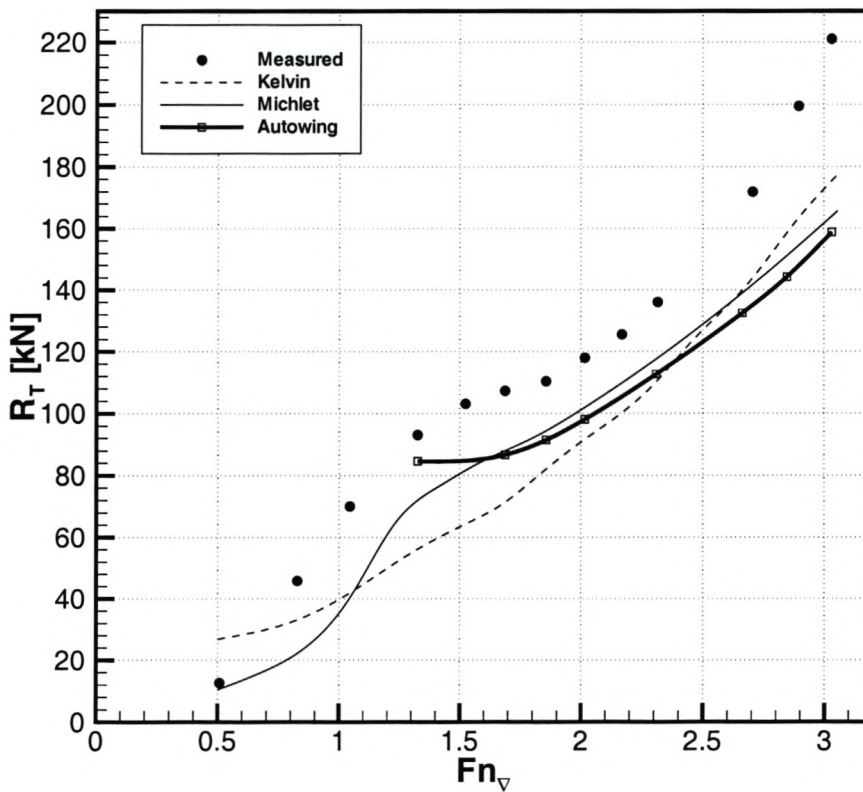


Figure 4.24: SD6 hull w/o foils, comparison of vortex lattice method AUTOWING with experimental results and also with the numerical predictions of KELVIN and MICHLET.

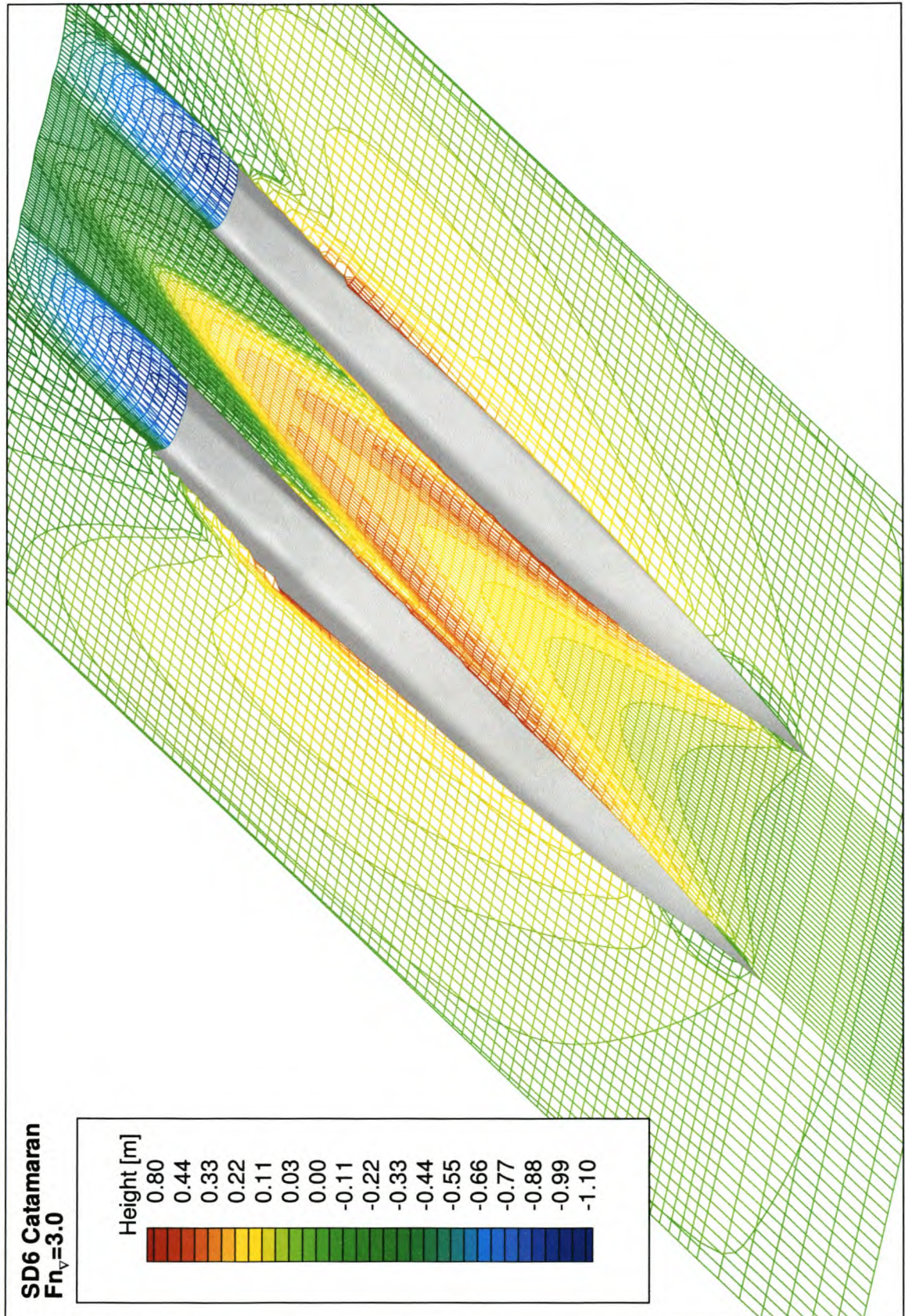


Figure 4.25: Free surface elevations for the SD6 catamaran without hydrofoils

area are over-predicted by about 15% at most but tendencies are well captured even the region of transition to planing where gradients are steep.

The lift at low speed is over-predicted by about 30%, later converging towards the correct values. This increased lift in fact makes good sense: it was found in Chapter 3 that the viscous scale effects result in lower lift for the model foils¹² and as the numerical method does not consider viscous effects of this nature, the lift is over-predicted. The increased drag is therefore most likely due to increased induced and wave-making drag components resulting from the higher lift of the foils. The discrepancies between experiment and numerical predictions are in the order of 15%, which can be considered as within the error range of the model tests as the experimental tests were not conducted with turbulence stimulation for the foils.

Figure 4.27 shows the free surface deformation for the Hysuwac example. The result agrees well with observed free surface deformations. The downwash in the tunnel due to the foils is well captured as well as the free surface shape behind the transom.

Figure 4.28 shows an example of the calculated pressure on the SD6 Hysuwac configuration for $Fn_{\nabla} = 2.3$. The pressure distribution clearly shows that the foils influence the pressure on the hull in the vicinity of the foils, creating areas of low pressures and also high pressures.

4.12 Closure

The details of the numerical methods developed for modeling hydrofoil-assisted catamarans have been included in the most recent version of the AUTOWING code (version 3.0.2) [KT]. This includes the simplified model for modeling the planing phase using Wagner's theory as well as the more complex non-linear model solving the free surface boundary conditions over the whole computational domain for the displacement and transition phases and includes the model for the spray jet. The results that have been presented with the method in its current form indicate that the method gives the correct resistance tendencies in comparison with experiment. This indicates that the fundamental hydrodynamic concepts governing resistance of hydrofoil-assisted catamarans are understood and correctly implemented in the method.

Work is in progress to improve the predictions of resistance in the transition phase further. The following aspects will be considered in future:

- Improved scheme for paneling the hull
- Further validation against experiments
- Implementation of the non-linear free surface boundary condition.
- Introduction of corrections for viscous effects

¹²The higher hydrofoil drag has been corrected for using Equation 3.2.

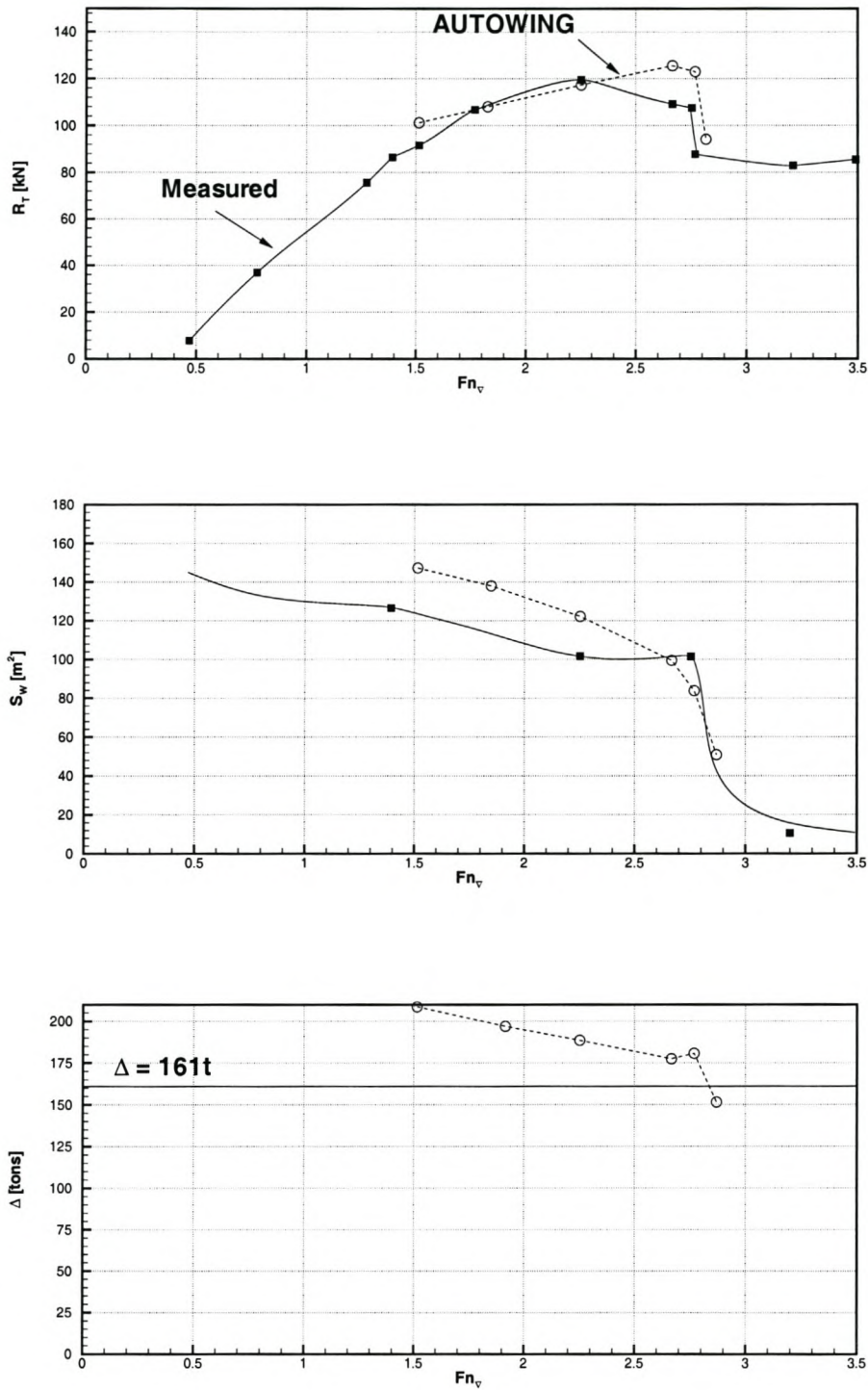


Figure 4.26: Comparison of AUTOWING with experiments for speeds covering the transition phase of the SD6 Hull with foil system F2.

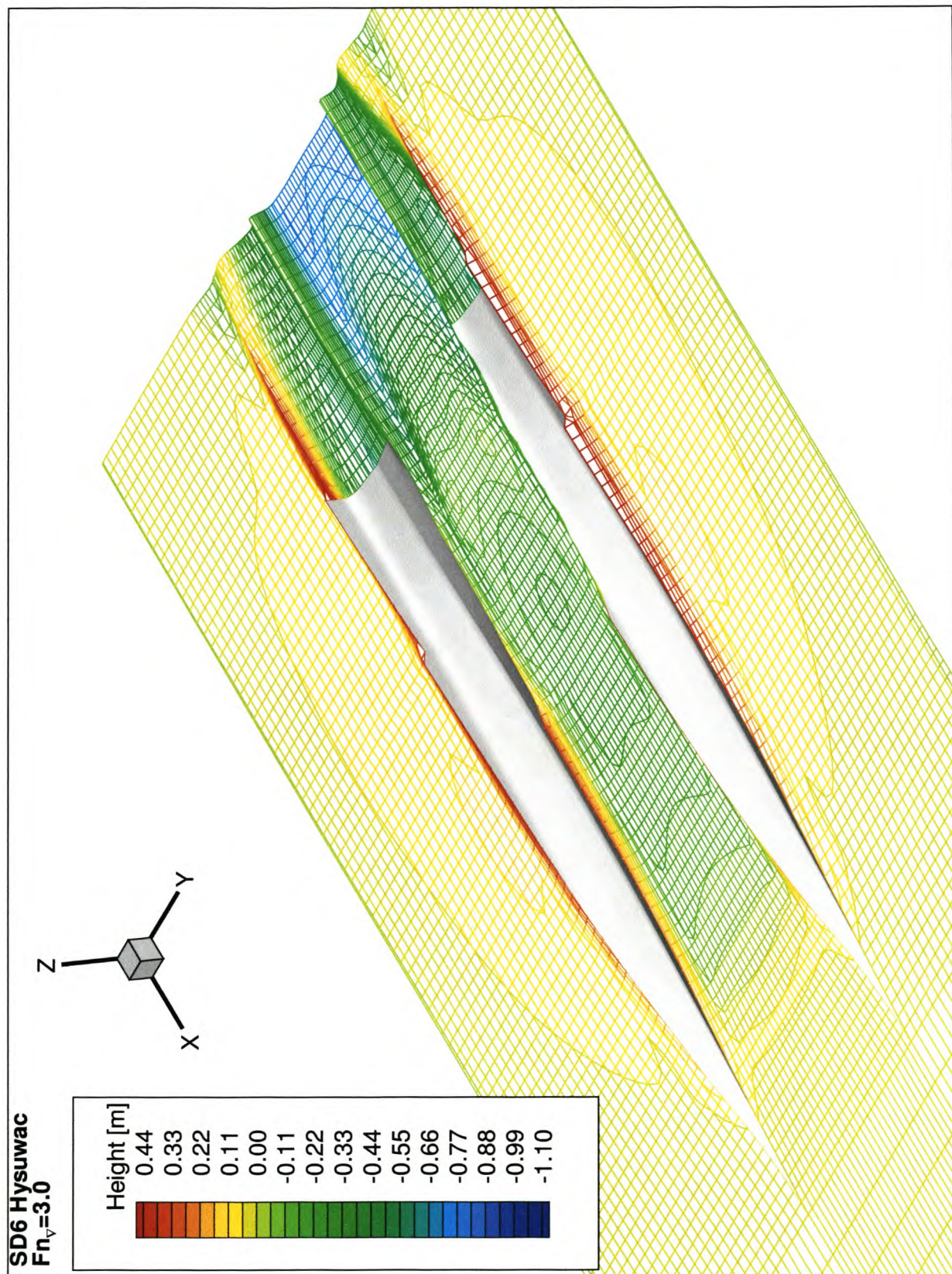


Figure 4.27: Free surface mesh and deformation calculated with AUTOWING

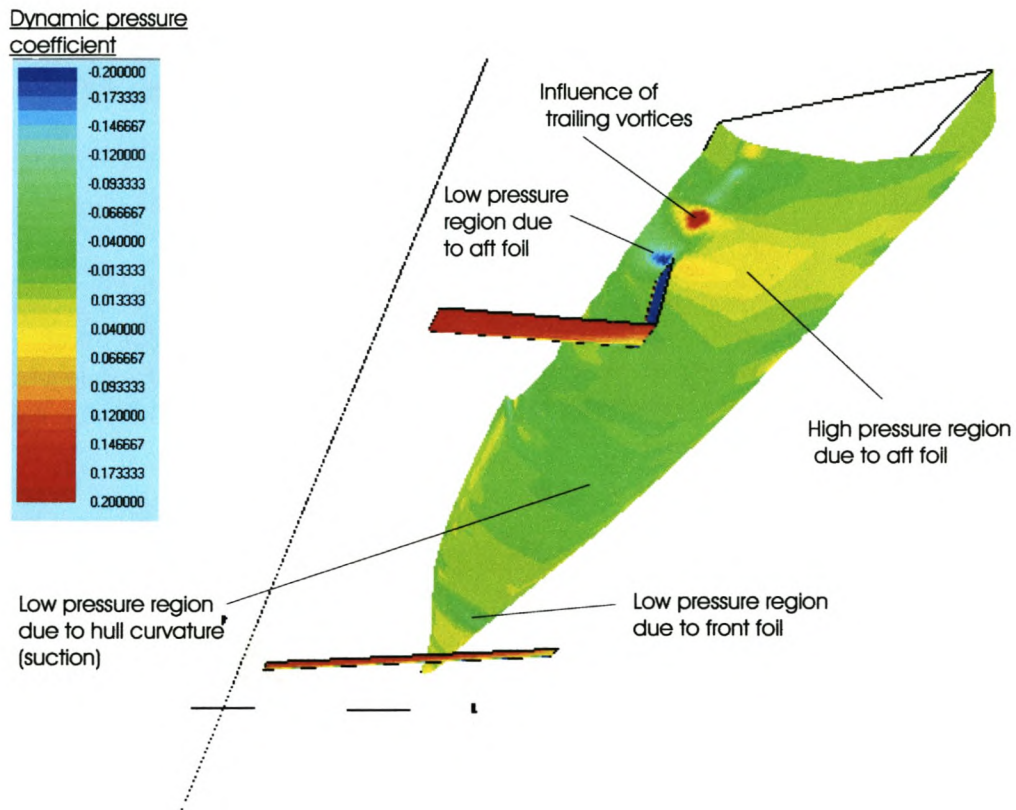


Figure 4.28: The symmetrical half of the SD6 Hull (wetted area only) showing the dynamic pressure distribution at $Fn_{\nabla} = 2.3$. The effects of the hull and hydrofoil design on the pressure are pointed out.

Chapter 5

Hydrofoil Design

Abstract

The design of hydrofoil assist systems for catamarans requires careful consideration of the hydro-mechanics involved. The design is considered separately for each phase of operation as it is shown that there are conflicting requirements for the hydrofoil design in each phase. For the displacement phase, it is shown that hydrofoil lift producing a bow down moment is important for reducing the resistance. In the order of 30% foil lift fraction is needed in the displacement phase to achieve resistance improvements. The optimum foil settings for the transition phase are those that induce a bow-up trimming moment and a large foil lift fraction. The hydrofoil design for the planing phase needs careful consideration of pitch-heave stability, which dictates the foil lift fraction. The requirements for planing are in conflict with the transition phase as settings inducing a bow down moment are again needed. The final foil design is therefore a compromise between the needs for the different phases.

5.1 Introduction

The design of a hydrofoil assist system for a catamaran cannot be considered in isolation without the hull but rather keeping in mind the interactions between the hull and foils. Nevertheless, the basic design principles cover the majority of hull shapes and one can therefore present general design guidelines for the design of assisting hydrofoils. The hydrofoil design requirements can be grouped generically into four topical areas. First, the primary hydrodynamic considerations that provide the major definition of the hydrofoils system:

- The design speed of the vessel

- The load distribution between hull and hydrofoils
- Various interactions between the hydrofoils, demi-hulls and the propulsion system
- Vessel dynamic stability

Second, a number of hydrofoil design features relating to the geometry of the hydrofoil system need consideration:

- The hydrofoil profile shape
- The shape of the plan form

Finally, there are a number of non-hydrodynamic considerations that must be addressed as they influence the hydrodynamic design:

- Structural requirements
- Manufacturing considerations
- Maintenance considerations

In this chapter, prime emphasis is placed on the first two topics, namely the primary hydrodynamic considerations and the hydrofoil unique design features. The third topic will not be considered in any detail.

5.2 Primary Hydrodynamic Considerations

The design speed of a vessel is linked to the three different phases of operation outlined in Chapter 2. The primary hydrodynamic considerations are inextricably linked to the different phases of operation given the varying importance of the different hydrodynamic factors influencing speed, resistance and efficiency. The first three factors are discussed separately for the displacement, transition and planing phases respectively and afterwards dynamic stability is considered.

5.2.1 The Load Distribution and Interactions between Hull and Hydrofoils

The load distribution between the hull and the hydrofoils refers to the amount of support provided by the foils (the hydrofoil lift fraction) and also the resulting position of the longitudinal center of lift of the hydrofoil system in relation to the longitudinal center of gravity of the hull (LCG) as this is important in regulating the running trim of the vessel. This load distribution is primarily a function of the hydrofoil setup,

but particularly for the transition and planing phases, it is also dependent on the interactions and interference effects.

The vessels reviewed in Chapter 1 indicate that the designs already in use for improving the efficiency and speed of catamarans make use of hydrofoils that carry anything from 25% to 100% of the displacement on the foils at design speed, which for hydrofoil-assisted catamarans falls within the transition or planing phases. The displacement phase can nevertheless not be neglected as a hydrofoil-assisted craft can experience its maximum resistance at the displacement hump, not unlike the resistance tendencies of conventional hydrofoil craft.

The Displacement Phase

The design of hydrofoil assistance for the displacement phase is particularly important for vessels that are heavily loaded and exhibit high hump resistances. This is typical of hydrofoil-assisted catamarans with semi-planing and planing hull designs. Semi-displacement hull designs are designed to have low hump resistances as their design speed falls close to the resistance hump, it is only in the overload case, that the hump resistance can become important.

The Froude number range relating to the displacement phase, $Fn_{\nabla} \leq 2.0$ means that the amount of lift that can be carried on the foils is limited. To achieve useful lift at these speeds one needs to make use of a hydrofoil configuration that generates high-lift in an efficient manner. Reviewing the existing craft resistance tendencies given in Chapter 1, it can be seen that it is only those vessels that make use of multiple foils that achieve an improvement in resistance at displacement speeds.

Investigations were performed by Migeotte and Hoppe [MH99b] investigating the effects of hydrofoil design on hump resistance. These model tests for a 21m heavily loaded hard-chined catamaran ($L/\nabla^{1/3} = 4.6$), which makes use of a tandem hydrofoil system mounted at keel depth, made use of an adjustable stern hydrofoil mounted just ahead of the transom to regulate the trim. By increasing the lift of the rear hydrofoil at hump speed the resistance is reduced. This is in effect very similar to the standard use of trim tabs or interceptors to reduce the hump resistance, but importantly indicates that the added drag of a hydrofoil assist system can be offset - even at displacement speeds - by using the stern hydrofoil to regulate the trim so that wave-making is reduced. A maximum reduction of 9% was achieved in hump resistance. This is very similar to that found by Migeotte in earlier investigations [Mig97] with a canard hydrofoil system, for a semi-planing catamaran operating at displacement speeds.

The lift fraction provided by the foils plays an important role in the dynamics of the craft. The trim and resistance of a vessel whose hydrofoil system only carries a small fraction of the load is dictated mainly by the pressures acting on the hull and

vice versa. The use of a high-lift hydrofoil system therefore allows better control of the running trim angle of the vessel. Also, the positioning of the foils on the hull plays an important role in regulating the trim. For example, the Hysucat hydrofoil system illustrated in Figure 1.8 makes use of a main hydrofoil close to the LCG of the vessel while the stern trim foils are located some distance aft of the LCG. Considering moments around the LCG, one quickly sees that the main hydrofoil has limited capability of influencing the trim of the vessel and trim control is provided to a large extent by lift from the smaller trim foils, which at displacement speeds is minimal. Mono-foil systems (effective at transition and planing speeds) do not allow sufficient lift at displacement speeds and usually result in an increase in trim (compared with the bare hull) at displacement speeds (often also found with Hysucat type designs optimized for high speed) [MH98, KYS⁺93], which increases the hump wave-making resistance over that of the bare hull. Their use offers limited means for improving the hump resistance. Similarly the canard foil-interceptor system cannot use hydrofoil lift effectively to reduce resistance at displacement speeds. Trim control is best achieved by tandem foils, spaced some distance fore and aft of the LCG. In choosing the positioning of the foils it is worthwhile considering the hydrofoil interference explained in Section 2.8.3. By spacing the foils correctly one can obtain some wave cancellation between the foils as explained by Matveev [MM00] and also some wave cancellation between the hulls [Tao98].

Furthermore, as explained in Chapter 2 the wave-making resistance of the hull is primarily a factor of the length-displacement ratio of the hull. A high hydrofoil lift fraction is therefore beneficial in reducing the wave-making of the hull. If increased resistance at displacement speeds due to the addition of a hydrofoil system is to be avoided, the hydrofoil system must be effectively used to provide useful lift as well as proper trim control.

It is well known that the required hydrofoil area for constant lift is inversely proportional to the square of the speed. It is therefore clear that reasonably large hydrofoils are required at displacement speeds to generate useful lift. Tandem, canard and Hysuwac arrangements are therefore the most suitable for reducing the displacement speed resistance.

The Hysuwac system was developed by Hoppe [Hop00] specifically with the aim of improving the resistance of semi-displacement type catamarans ($1.5 \leq Fn_{\nabla} \leq 2.5$). The use of the large, high aspect ratio front hydrofoil deeply submerged underneath the hull allows for high lift and a good lift to drag ratio. The stern hydrofoil located between the demi-hulls benefits from the end-plate effect provided by the hulls, which increases its effective aspect ratio and also creates some beneficial pressure increase on the aft part of the hull. The hydrofoils are widely spaced longitudinally so that the foils are effective in controlling the trim and can be used to take advantage of wave cancellation. The Hysuwac can be considered one of the most efficient hydrofoil systems for semi-displacement speeds. Higher efficiencies would require deeper submerged

foils and also higher aspect ratio foils wider than the beam of the vessel, both of which are practically limiting in terms of structural requirements and maneuvering in constricted areas such as harbors.

Resistance improvements gained with the Hysuwac hydrofoil system will therefore be close to the maximum achievable for a practical hydrofoil system. To gain an idea of the maximum improvements possible at hump speed, use was made of a Hysuwac hydrofoil system for experiments investigating reductions in hump resistance. Figure 5.1 shows the body plan of catamaran demi-hull used in the investigations. The demi-hulls are round-bilged and have straight buttock lines towards the transom characteristic of a semi-planing design [Alm93, CCEP89]. By changing the LCG of the vessel forward and aft of even floating the transom submergence is altered, a parameter that is known to affect hump resistance significantly (see for example [GD01]).

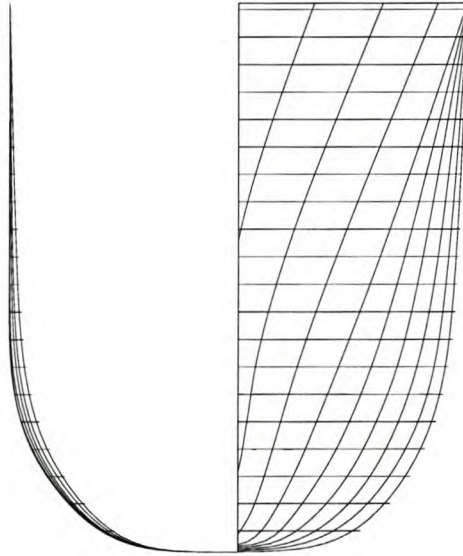


Figure 5.1: The SD8 body plan.

Figure 5.2 shows the resistance tendencies of the SD8 hull without foils for the three LCG positions. By determining the resistance improvements gained for the different LCG positions, one can qualitatively determine resistance improvements for different hull shapes: those with high hump resistance (rear LCG) and those with very slight resistance humps (forward LCG) by simulating the wave-making resistance of different hulls through shifts in LCG position.

The hydrofoil design for the SD8 hull is based on previous experience [Hop98, MH01] designing Hysuwac foils. The sizes and positions of the foils were chosen to be the same as for other hull designs, thus allowing one to determine the effects of hull shape on the attitude and resistance of a hydrofoil-assisted vessel¹. Figure 5.3 shows the

¹Hull design is the focus of Chapter 6.

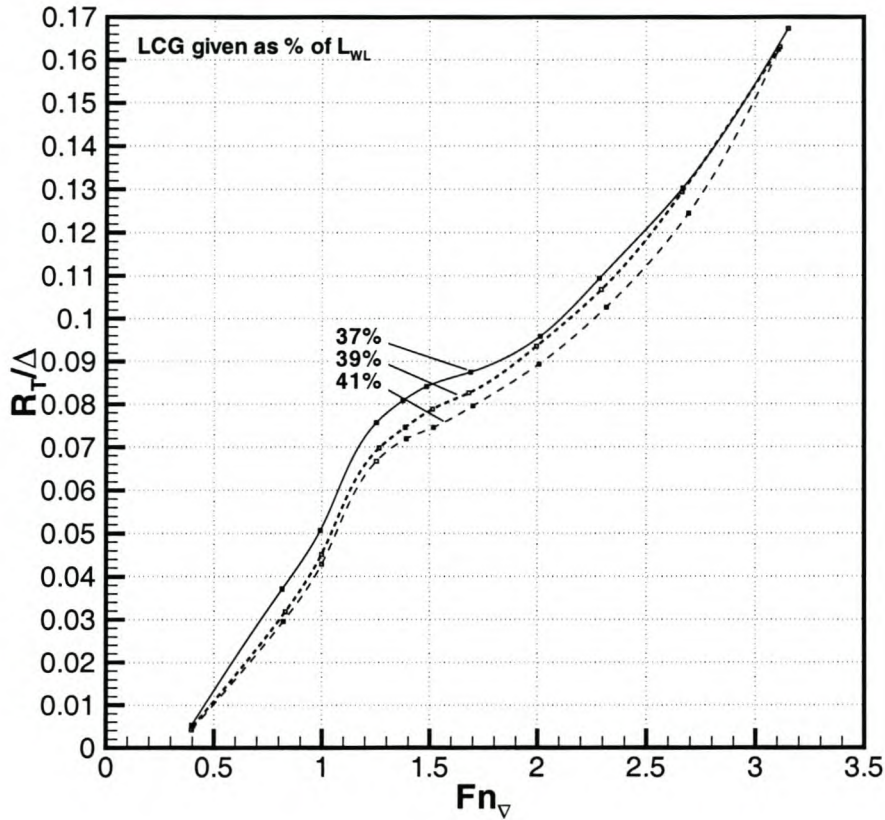


Figure 5.2: Hull resistance as a function of LCG position

Hysuwac hydrofoil system used.

Systematic investigations were done varying the hydrofoil angles of attack while keeping the centre of lift within acceptable limits. Two different regimes were adopted for investigating the effect of hydrofoil lift variations on the hump resistance:

- Systematically varying only the rear hydrofoil attack angle.
- Varying both hydrofoil's attack angles proportionally.

These regimes would indicate what resistance improvements can be gained by trim angle adjustments and what can be gained by increasing total hydrofoil lift.

Measurements for each angle setting were done for the three LCG positions, even floating and $\pm 2\%L_{WL}$ from the even floating position. Figure 5.4 shows the resistance variations at hump speed $Fn_{\nabla} = 1.5$ for the rear hydrofoil lift forces as a fraction of



Figure 5.3: The SD8 hull with Hysuwac foil system

the displacement obtained by adjusting only the rear hydrofoil attack angle. The lift forces of the foils were calculated numerically with AUTOWING and approximately corrected for viscous scale effects on lift according to the results for the Göl1k results of Table 3.5: $f_\alpha = 0.8$ for the submergence $h/c = 1.2$.

The results show that resistance improvement is possible for all the LCG settings, but that the rear LCG position (37%), which has the highest hump resistance, benefits most from increasing the rear hydrofoil lift. The higher lift of the rear hydrofoil lowers the running trim, which in turn lowers the wave-making resistance and also the front hydrofoil lift. Interestingly, Figure 5.4 shows that the total hydrofoil lift for each LCG setting varies very little with changes in rear hydrofoil lift. Also clear from the 39% and 41% LCG settings is that there is a maximum rear hydrofoil lift after which very little or no improvement in resistance is gained. The forward LCG position shows only slight decrease in resistance before the point of maximum improvement is reached. This seems to indicate that resistance improvements are easier to obtain when the hump wave-making resistance is high. Analysis of the resistance data of the Hitachi Superjet (Figure 1.13) is in line with these findings. The very slender hulls produce a small resistance hump and the hydrofoil assistance (using efficient high aspect ratio foils) shows no significant improvement in resistance for most of the displacement speed range.

Further investigations were done with the SD8 Hysuwac model to investigate the effect of increasing the lift of both foils. This was done by increasing both foil attack angles proportionally so that the resultant centre of lift for both foils stayed approximately the same. While the previous investigations varying only the rear hydrofoil angle of attack did not cause a significant change in the total hydrofoil lift, these investigations focus on increasing the total hydrofoil lift substantially. Figure 5.5 shows the resistance improvements for the three different LCG positions as a function of total hydrofoil lift.

The result indicates that the resistance improvement is influenced substantially by the hydrofoil load fraction for all three LCG positions and only a weak dependence on the LCG position. From the figure it can be deduced that in the order of 30% of the

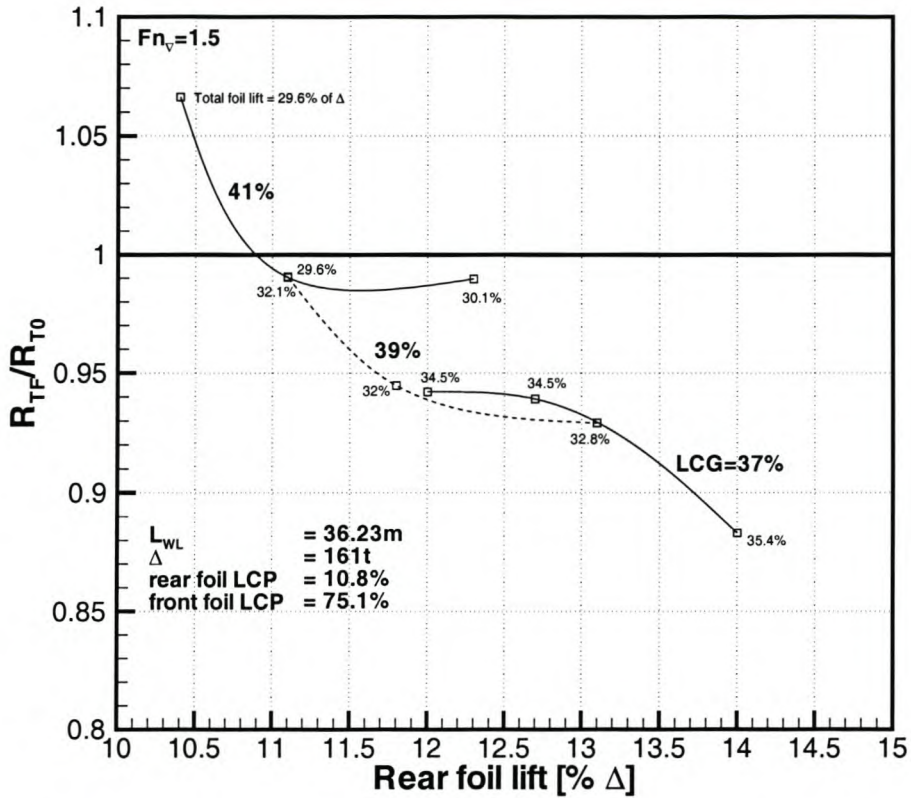


Figure 5.4: Hump speed ratio of resistance with foils against the resistance without foils as a function of rear hydrofoil lift.

displacement weight needs to be carried by the foils if resistance improvements are to be gained and that the maximum attainable improvement in resistance seems to be about 20% with 45% of the load being supported by foils for this hull and hydrofoil system.

To establish a feel of how important the hull shape and the amount of wave-making is on the possible reductions in hump resistance, resistance improvements versus hydrofoil lift fraction were plotted for limited model test data available for vessels ranging from semi-displacement [MH00] to planing catamarans [Mig97] all using variants of the Hysuwac hydrofoil system. Figure 5.6 shows the results in relation to the SD8 results.

It is clear from the figure that there is a lot of variation in the resistance improvements to be gained in the displacement phase and that the hull shape plays an important role. The semi-displacement catamaran analyzed shows very little improvement in hump

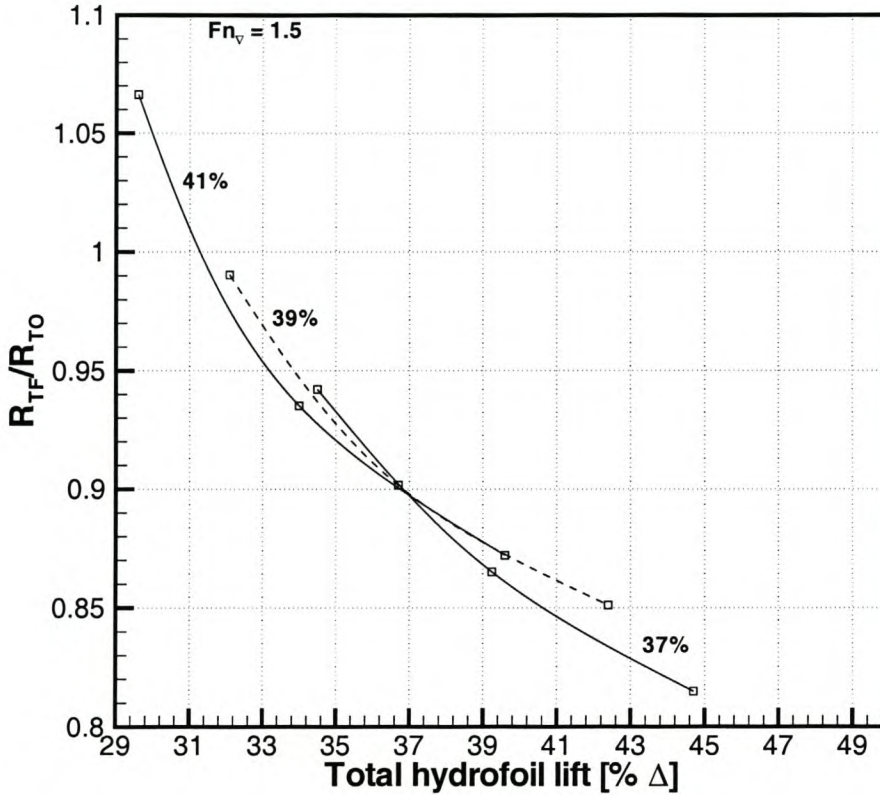


Figure 5.5: Improvements in resistance as a function of total hydrofoil lift at $Fn_{\nabla} = 1.50$

resistance even at relatively high hydrofoil lift fractions of over 40%, while planing catamaran hull forms characterized by their high wave-making at displacement speeds can be improved with lower foil lift fractions.

The Transition Phase

The transition phase is influenced to a large extent by hull-foil interactions relating to suction forces on the hull. This phase is of primary importance for catamarans with semi-displacement and semi-planing type hulls as their design speeds fall within this phase and the nature of their hullforms make them prone to suction. The transition phase is also very important to those hydrofoil-assisted catamarans designed to reach the planing phase by lifting a large fraction of the hull clear of the water such as for instance the vessels shown in Figure 1.2. Such vessels need to overcome the transition

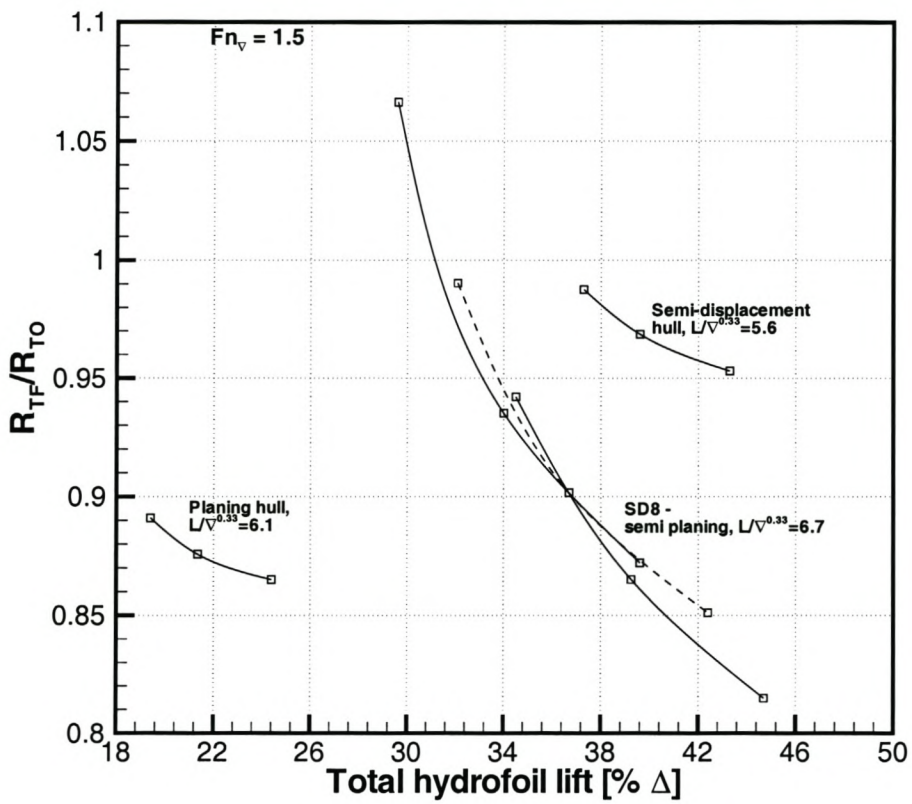


Figure 5.6: Improvements in hump resistance for different hull forms as a function of hydrofoil lift fraction. Results are given for the SD8 hull as well as a semi-displacement design [MH00], a high hump resistance planing hull design [Mig97].

hump resistance.

The design of suitable hydrofoil systems in terms of the load distribution between the hull and the foils for the transition phase therefore differs to some extent from the displacement phase. At displacement speeds it has been shown that high hydrofoil lift and strong rear hydrofoil lift to reduce trim offer the best possibility to minimize resistance. Unfortunately the hydrofoil induced bow-down moments required to counter the natural bow-up trim tendency of the hull at hump resistance speeds, cause the hull to take up negative trim angles at higher speeds, which can result in undesirable directional instability and increased resistance for the vessel. Experimental data shows that the magnitude of the transition hump resistance correlates strongly with the trim angle. Higher bow up trim angles are needed to reduce the magnitude of the resistance in the transition zone. Figure 5.7 shows the resistance for the SD8 hull with Hysuwac foils for two different bow foil angles. The effect of the lower bow foil lift is a lower running trim angle in the transition phase, which relates to a substantially increased transition hump resistance.

This rule applies to those vessels with a prominent transition hump as well as designs which do not exhibit a hump (e.g. Hysucat designs) and has been shown for different types of hull forms and hydrofoil arrangements (see for example [Mig97]). Figure 5.8 shows a typical result for a planing catamaran vessel with a tandem hydrofoil design [MH99b]. In this example the design optimized for displacement speeds makes use of higher angles of attack on the rear hydrofoil to reduce the hump trim angle. As speed increases the strong rear hydrofoil angle now results in the vessel taking very low trim angles which eventually become negative and observations during experiments shown the vessel to be directionally unstable in this condition. Modern catamarans are prone to this instability due to their sharp bows. The design optimized for transitional speeds (lower rear hydrofoil lift and higher front hydrofoil lift) shows the highest hump resistance and trim, but allows higher speeds to be attained without instability.

This example indicates the conflicting requirements in the design of the hydrofoil system for displacement and transitional speeds. At transitional speeds the centre of lift of the hydrofoil system needs to be further forward compared to displacement speeds for efficient operation. Some method of controlling the hydrofoil lift is needed if optimal resistance is to be achieved for both displacement and transitional speeds. Conventional catamarans often make use of trim tabs or interceptors for trim control at speed, and these can also be effectively used in conjunction with a hydrofoil assist system to reduce trim at hump speed and increase it at transition (see for example [THCC01]). Alternatively, an adjustable stern hydrofoil to regulate the stern hydrofoil lift is useful in such cases to allow optimal efficiency in both phases of operation.

While the avoidance of instability is of primary importance, the main consideration and problem of improving the efficiency of hydrofoil-assisted catamarans particularly in the upper end of the transition phase is overcoming the detrimental effects of

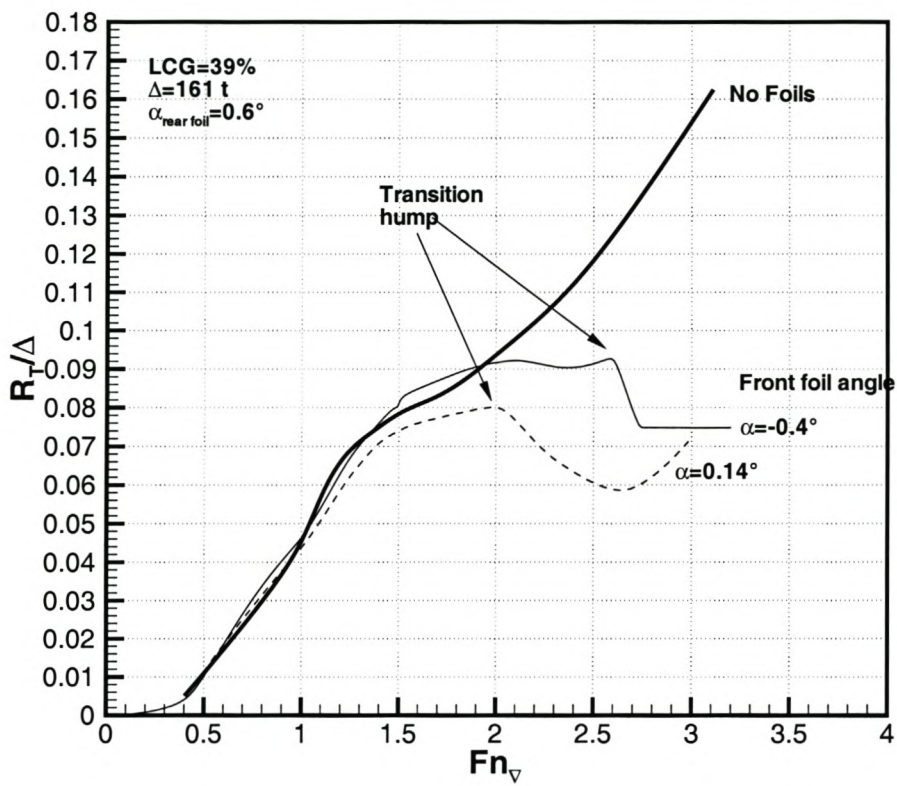


Figure 5.7: The effect of front foil angle of attack on transition hump resistance characteristics

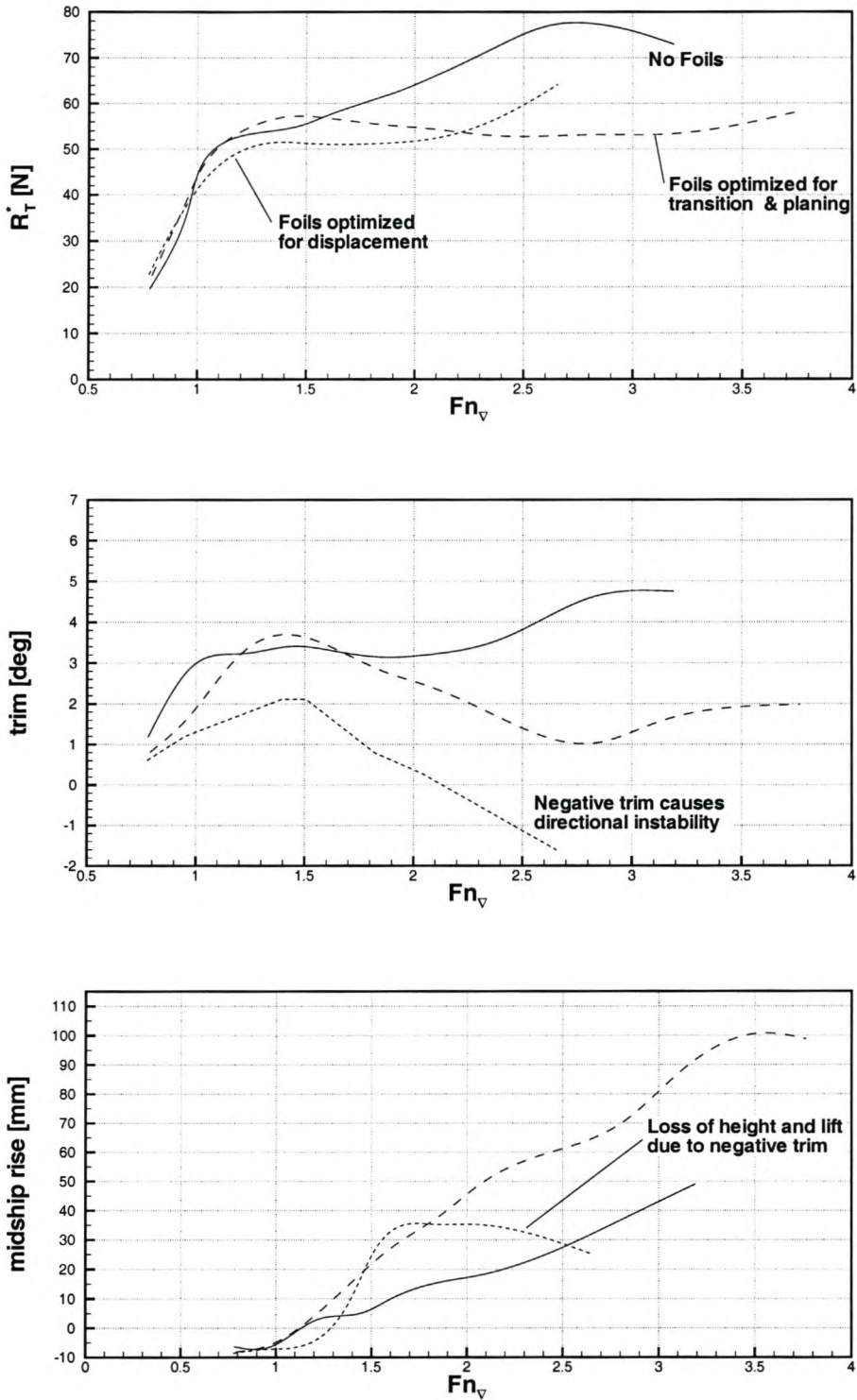


Figure 5.8: Resistance, trim and rise for a hydrofoil system optimized for the displacement phase

suction on the hull, which is due to the hull shape² as well as foil-hull interactions. Chapter 2 has shown that these effects have an important influence on the maximum resistance of the vessel. Certain hydrofoil design principles allow one to minimize the hull suction induced by the hydrofoil system. Chapter 2 has explained that suction due to hull-foil interactions is primarily a problem for hydrofoils located below the keel line. Avoidance of suction therefore requires that the foils under the keel not be placed in areas where the suction pressure will affect the vertical forces on the hull to any great extent. Practically, this limits the positioning of such foils to the bow region³. In other regions of the hull (aft of the bow) one can benefit from positive interference effects by placing the foils in the tunnel between the demi-hulls (see Section 2.6.4 on page 52). In a similar way to the hydrofoil induced suction, the hull will experience extra lift from the increased pressure from the underside of the hydrofoil. The Hysuwac design illustrated in Figure 1.19 shows the optimal use (in terms of hydrodynamic efficiency) of a forward hydrofoil submerged under the keel near the bow, and a rear hydrofoil located between the demi-hulls.

Similarly to the displacement phase, experiments conducted in this study and those of others (see for example: Miyagawa et al. [MTM99]) have shown that increasing the hydrofoil lift fraction (by increasing the angle of attack of the foils) is very effective in overcoming suction on the hull and reducing the resistance at transition speeds. Analysis of data for hydrofoil craft during transition by Lattore [LT92] have found similar results by increasing the hydrofoil area.

In the transition phase it is only of limited value to present resistance improvements as a function of foil lift fraction alone. The presence of the strong suction forces on the hull means that one needs to consider the hull forces in conjunction with the foil forces. The hull forces are largely dependent on the hull shape and the running trim angle taken up by the vessel. These aspects are explained in detail in Chapter 6. Figure 5.9 shows the resistance tendencies for the SD8 Hysuwac in the transition phase. The tendencies are somewhat unclear due to the large number of interacting effects that affect the resistance in the transition phase. In general terms, the figure indicates that the resistance improvements are sensitive to the foil lift fraction as well as the running trim angle of the hull.

The tendencies for the different LCG positions vary as different effects dominate. For the $LCG = 37\%$ case, the resistance improvements are inversely proportional to the foil lift fraction. This is due to the hydrofoils riding close to the free surface with reduced lift to drag ratios (indicated on the figure). Nevertheless the resistance improvements are best for this condition because suction is lower for the high trim angles

²Hull shape considerations are the focus of the next chapter.

³An example of an existing vessel disobeying this rule is the Hyundai hydrofoil-assisted catamaran. While the model test data presented in Chapter 1 show good efficiencies, it is known that the vessel experienced high resistance due to problems with the hydrofoil design [Pet95], possibly due to suction effects.

in this condition and the hull can rise farther out of the water. For the $LCG = 41\%$, the opposite tendency is found: resistance improvements are directly proportional to increasing foil lift fraction. In this condition suction forces are strong due to the relatively low running trim angles and even though the L/D of the foils decreases for the very high foil lift fractions (97%!), the resistance improvements are continually better with increasing foil lift. The resistance improvements are nevertheless less than for the other LCG settings because suction does not allow the hull to lift as far out of the water. The $LCG = 39\%$ condition shows a combination of influences making it difficult to determine proper tendencies.

This experimental result indicates the importance of hull-foil interactions and shows that to achieve the optimum resistance improvements requires the hull design to be considered together with the foil lift fraction and the running trim angle. These aspects are covered in more detail in Chapter 6. The magnitude of foil lift fractions shown in the figures and the resistance improvements gained with the Hysuwac foil system can be considered to be close to the maximum achievable for conventional catamaran hull forms with hydrofoils. Similar results have been achieved using Hysuwac foil systems on a variety of different hullforms tested in this study [MH01].

For foil systems such as mono-foils or Hysucats making use of the main lifting foil at or just ahead of the LCG , the transition phase is also significant as it is in this phase that resistance improvements are achieved over the bare hull. Such foil systems, which usually increase resistance at displacement speeds, now create enough lift to improve the resistance of the bare hull. The Hysucat (Figure 1.8) and Daewoo's mono-foil assisted F-CAT40 (Figure 1.17) are examples of this.

The Planing Phase

The planing phase for hydrofoil-assisted catamarans is characterized by the majority (over 50%) of the lift being supplied by the hydrofoils and almost all the lift being supplied due to dynamic lift⁴. Due to the high foil lift at planing speeds the main parameter influencing the foil lift fraction is dynamic stability⁵ which results in a pitch-heave motion of constant or increasing amplitude, similar to porpoising on planing craft.

For vessels such as the Hysucat or the Chinese channel hydrofoil planing boats, which both have foils at keel depth, the foil load is usually not higher than 70% of the displacement [Hop95a, ZLH97] for stable running designs. For hydrofoil-assisted catamarans, which make use of bow foils under the keel line, such as the Hysuwac stable running conditions can be achieved with up to 95% foil lift fraction, but that sta-

⁴It must be remembered that the effective Froude number of the hull is high, $Fn_{\nabla e} \geq 4.0$ due to the foil lift even though the planing phase starts at $Fn_{\nabla} = 3.0$ which is normally considered semi-planing.

⁵Stability is discussed in detail in the next section.

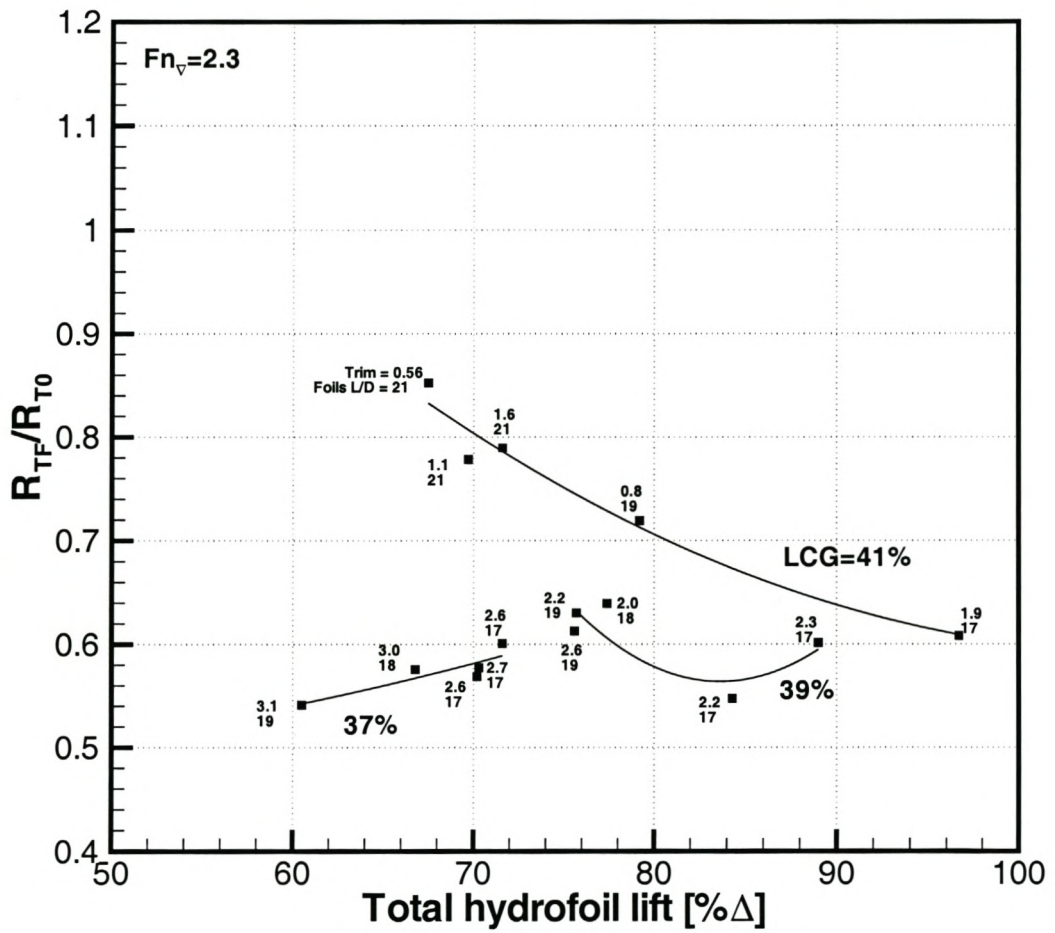


Figure 5.9: SD8 Hysuwac, resistance improvements as a function of the foil lift fraction for the transition phase Froude number, $Fn_v = 2.3$

bility is highly dependent on front foil lift. Model tests have repeatedly shown that at planing speeds vessel stability and attitude are very sensitive to the set-up of the bow foils. This was found for canard bow foils as well as Hysuwac type bow foils [Mig97, MH01].

This brings to light a conflict in hydrofoil design requirements between the transition phase and planing phase for those designs with hydrofoils located under the keel such as the Hysuwac. At transition speeds, a high front foil lift is required to overcome suction, if low resistance is to be obtained in that phase. After the transition to planing, without the suction to balance the high foil lift, the bow foil takes up a position very shallowly submerged under the free surface ($h/c \approx 0.1$ or less!). Observations during model tests show that the forward foil will stabilize itself at the same submergence irrespective of how deep the foil is mounted under the keel. A foil positioned deeper under the keel simply lifts the bow of the vessel higher out of the water, increasing the running trim angle of the vessel.

Hydrofoils operating in such extreme free surface effect have poorer efficiencies compared to deeper submerged foils producing the same lift. Experimental results of this study and of Miyagawa et al. [MTM99] substantiate this. Miyagawa et al. found that by controlling the total lift carried by the foils to about 75% and keeping the trim constant in the planing phase the resistance could be reduced. The running trim for optimum resistance of hydrofoil-assisted catamarans at planing speeds is lower than for transition speeds. It is therefore difficult to choose the foil angles of attack correctly for fixed foils so that the transition hump is overcome, but prevents the bow foil from operating too shallowly submerged. There is therefore a conflicting foil design requirement for the transition and planing phases.

5.2.2 Dynamic Stability Considerations

In the context of hydrofoil-assisted vessels dynamic stability has been found to be mainly a problem associated with the transition and planing phases, although it is known that in some cases, hydrofoil assistance can result in a porpoising like action even at displacement speeds. This situation was realized during the development of the oceanographic research catamaran USNS-Hayes [Cro85], which was fitted with hydrofoils for stability purposes.

Two forms of instability have been identified for hydrofoil-assisted catamarans during this study:

- Directional instability and broaching.
- Pitch-heave porpoising instability.

During model tests conducted in the present study, use was made of a towing harness

which can be seen in Figure 5.10. In all tests the hull mounting points were slightly above the floating waterline and at about $0.66L_{WL}$ measured from the transom. Such a towing system provides a certain amount of directional stability but does not dampen out severe motions and therefore would indicate if any strong directional or other instability is present.

Directional Instability

It is well known that directional stability of high-speed craft is largely related to the submerged lateral area of the hull and that there must be sufficient lateral area abaft of the axis of yaw for the vessel. Hydrofoil-assisted vessels are understandably prone to this problem as their draft continually decreases with speed reducing the lateral area. Hydrofoil designs that make use of foils near the bow are more prone to this problem as the vertical struts supporting the foils increase the lateral area forward and also causes destabilizing moments if any yawing disturbance is encountered. This is also true of the sharp bows characterizing modern high-speed catamaran lines. As pointed out by du Cane [dC72] such instabilities are aggravated on craft that suffer from suction. For semi-displacement and semi-planing catamaran hull forms assisted with hydrofoils, suction has the effect of keeping the running trim angle low and increasing the lateral area forward. Directional stability is understandably a problem in the transition phase where suction is strongest and directional stability problems the worst. Fortunately, directional stability problems are often easily solved with the use of skegs or rudders mounted at the transom. Model tests have shown that demi-hulls fitted with skegs solve even severe course keeping problems.

Pitch-Heave Instability

Hydrofoil-assisted vessels can suffer from the same form of porpoising heave-pitch instability common on planing hull forms. Towing tank observations show that this instability is associated with high-speed (the planing phase) and high foil lift fraction. If the craft is disturbed, bow-up, the main foil lift increases, causing it to break through the free surface (or remain just under the free surface) losing lift. This in turn, results in the hull pitching down and returning to its original position, but due to the downward momentum it pitches down past the equilibrium position, to start the cycle again. Karafiath [Kar74] has investigated the stability limits for a hybrid mono-hull using a single foil at planing speeds and found that instability correlates well to the foil lift fraction as well as the ratio of foil lift moment to weight moment referred to the transom. Values for foil lift fraction exceeding 40% and foil lift moment to weight moment exceeding 50% were found to be suitable values for stability limits for the single foil at the LCG. Such limits obviously differ for different foil configurations and each design would have to be investigated on a case by case basis. Suitable stability

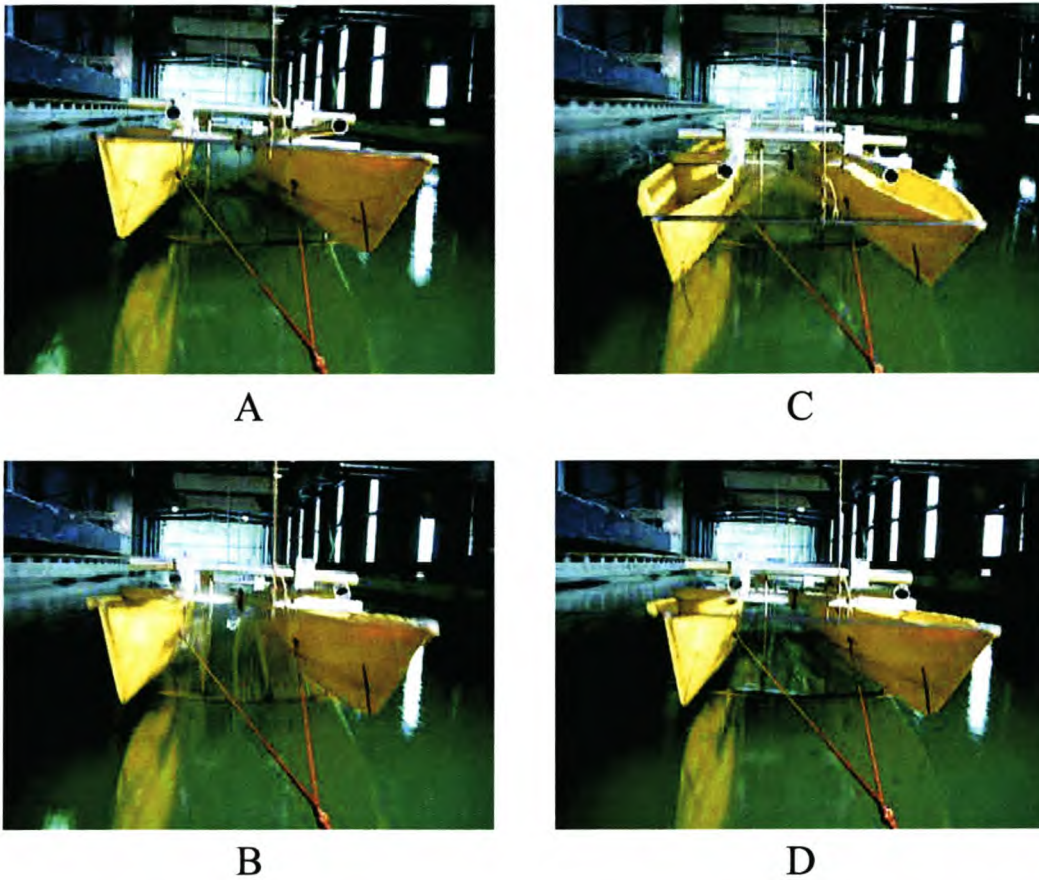


Figure 5.10: Porpoising starts with tips of the bow foil emerging from the water (A). Loss of foil lift results in the vessel pitching down. The main foil impacts the water which is associated with strong spray from the leading edge of the foil (B). The vessel continues its downward motion (C) until the front foil lift is restored after which the bow begins to rise again (D) to repeat the cycle

limits can be established theoretically for foil lift fractions up to 100%. Matveev [MM00] has shown that by considering the lift curve slope of each lifting element relative to pitch as well as relative to heave one can establish proper limits. This theory needs to be extended to hydrofoil-assisted craft.

Model tests in this study found that pitch-heave instability is common to all fixed hydrofoil systems and that the form of the instability is similar for all vessels. For the Hysuwac configuration, instability occurs in a similar manner to that found on Hysucac type craft, but is a phenomenon solely associated with the lift of the bow foil. Figure 5.10 illustrates the situation captured during a model test.

The conflicting requirements for the hydrofoil design for each of the three phases, means that a fixed hydrofoil system cannot provide the optimum solution for all

speeds. The design of a suitable hydrofoil system is therefore a compromise between the requirements for each phase and has to be evaluated on a case by case basis. The use of adjustable hydrofoils provides the best possibility to optimize the hydrofoil system for the complete speed range of interest and the design of these hydrofoils needs to be considered further in future.

5.3 Hydrofoil Design Features

5.3.1 The Profile Shape

Suitable profiles for use on hydrofoil craft have made use of very many different profile shapes. The first profiles for surface piercing hydrofoils were circular arc types [Sot40]. Later with the development of deeply submerged hydrofoils, airfoil profiles such as the NACA-16 and NACA-66 sections (see Abbot and von Doenhoff [Av58]) have as a result been widely used in hydrofoil applications. In general, methods for their design are similar to those used for airfoil design [ES79, ES81] and well-known. Design of modern profile sections for hydrofoils differs somewhat from airfoils in the sense that cavitation is the main parameter being designed for, whereas boundary layer flow is less significant.

Hydrofoil profiles with improved cavitation characteristics have flat suction side pressure distributions, as this maximizes lift while minimizing cavitation over the greatest possible range of attack angles. Design of such profiles is usually done without consideration of the free surface effect (see for example [ES81]), which for conventional hydrofoil craft is often acceptable as the hydrofoils are deeply submerged. Shallowly submerged hydrofoils suffer extra complication due to ventilation, which can occur through surface piercing foils and struts and through tip vortex tubes that vent to the free surface. Hydrofoils for hydrofoil-assisted catamarans, being connected at or only slightly below keel depth of the hull mean that they operate continually in free surface effect with submergence ratios of up to $h/c = 0.1$ and their design needs to consider both cavitation and ventilation.

Of those vessels described in Chapter 1, the majority make use of profile shapes derived from circular arcs with the maximum thickness located close to the mid-chord of the profile and approximately flat or slightly cambered pressure sides. The use of such profiles found popularity originally for surface piercing hydrofoil applications due to their superior cavitation and ventilation characteristics compared with regular airfoil sections such as the commonly used NACA-16 and NACA-66 series. The cavitation characteristics of circular arc sections have been extensively investigated by Walchner [Wal32], and known as the Göttingen K-series profiles (see Riegels [Rie61]). These profiles have been found to have favorable cavitation characteristics as these circular arc sections closely resemble the theoretical profile shape for a flat suction side pres-

sure distribution [Rie61]. Walchner found that rounded leading edges approximately double the range of attack angles free from cavitation compared with sharp nosed profiles. This makes these profiles suitable for deeply submerged foils. Shallowly submerged foils need extra consideration for ventilation effects.

Circular arc sections have been found to have suitable ventilation characteristics close to the free surface. Investigations by Sottorf [Sot40] as well as information given by Egorov et al. [ES65] point out that circular arc profiles with flat or slightly concave pressure sides and with the maximum thickness at about 40% chord length downstream from the leading edge delay ventilation to reasonably high angles of attack ($+7^\circ$) for surface piercing and shallowly submerged hydrofoils. Such profiles also have slightly improved lift to drag ratios compared with plano-convex circular arc profiles. For the normal range of angle of attacks ($0-5^\circ$), increased camber near the leading edge and sharp leading edges have been shown to be beneficial for reducing separation of flow near the leading edge close to the free surface. Unfortunately, even small nose radii, $r_{LE}/C = 0.003$ show dramatic deterioration in the profile's ability to resist flow separation close to the free surface.

Given that hydrofoil-assisted catamaran hydrofoils are usually not surface piercing (but can sometimes be very shallowly submerged), the use of circular-arc type profiles with slightly rounded leading edges offer a good trade-off between suitable cavitation and ventilation characteristics. The Hysucat development at the University of Stellenbosch originally made use of NACA16 profiles, but the difficulty in manufacturing such profiles resulted in suitable circular arc profiles being developed with slightly concave pressure sides and rounded leading edges. These profiles were found to have better efficiencies close to the free surface over a wider range of attack angles as found by Sottorf and Egorov et al. Figure 5.11 shows an example of such foil being manufactured.

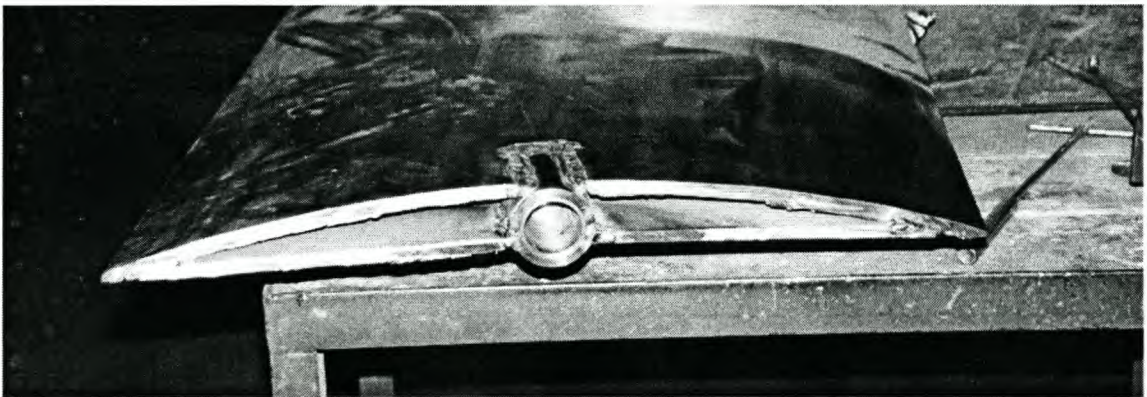


Figure 5.11: A circular arc type hydrofoil being manufactured

This study has made use solely of such circular arc type profile sections during model

tests. This stems from their good hydrodynamic characteristics as well as due to practical ease and cost effectiveness with which such simple profiles can be manufactured (at prototype-scale) using rolled plates that can be welded together. Slightly rounded nose radii have been used as towing tank observations have shown that ventilation only appears in extreme free surface effect, $h/c \leq 0.1$ making it unnecessary to sacrifice good cavitation characteristics for the sake of ventilation.

5.3.2 Planform Considerations

The planform of hydrofoils used for hydrofoil-assisted catamarans varies with respect to mainly aspect ratio, dihedral and sweep.

Aspect Ratio

The actual span of the hydrofoil system, and hence the aspect ratio is largely fixed by the demi-hull separation, which is chosen considering other factors including sea-keeping, deck area, design speed and weight considerations over and above the foil design. The Hysuwac configuration presents perhaps the largest span hydrofoil that can practically be used, without introducing high damage risk for the foils. In this configuration the foils usually have a span about equal to the craft overall beam. As hydrofoil efficiency is strongly linked to aspect ratio, this explains the high efficiency of this foil system.

Sweep

The benefits and disadvantages of introducing sweep are similar to those of all lifting wings. For hydrofoil craft in general, the sweep angle Γ , is well known to delay the onset of cavitation on hydrofoils by increasing the pressure on the suction side of the hydrofoil proportional to $COS^2(\Gamma)$ for the same wing at the same angle of attack [Cri70]. This cavitation onset delay allows more design freedom in terms of foil thickness, which is beneficial in extending cavitation free range of angles of attack. Swept foils are also known to improve stability during maneuvering, as sweep induces the craft to bank into the turn.

Concerning hydrofoil-assisted catamarans in particular, increased sweep angle has been found by Hoppe [Hop80] to be beneficial in reducing spray and water disturbance when the hydrofoil is close to or breaking the water surface. Also in the case of the hydrofoil emerging fully from the water, the re-entry of the foil was found to be smoother for swept hydrofoils with sweep angles greater than 15 degrees.

Dihedral

Dihedral has been found to aid in the roll stability of hydrofoil-assisted catamarans [Cal81], but it plays a more fundamental role in reducing interference drag between the hull and hydrofoils. As discussed in section 2.8.4 the interference drag is minimized by maintaining at least a 90 degree angle at the intersection of the hull and foils. Using increased dihedral close to the intersection is useful to achieve the required angle. This is illustrated in Figure 5.12.

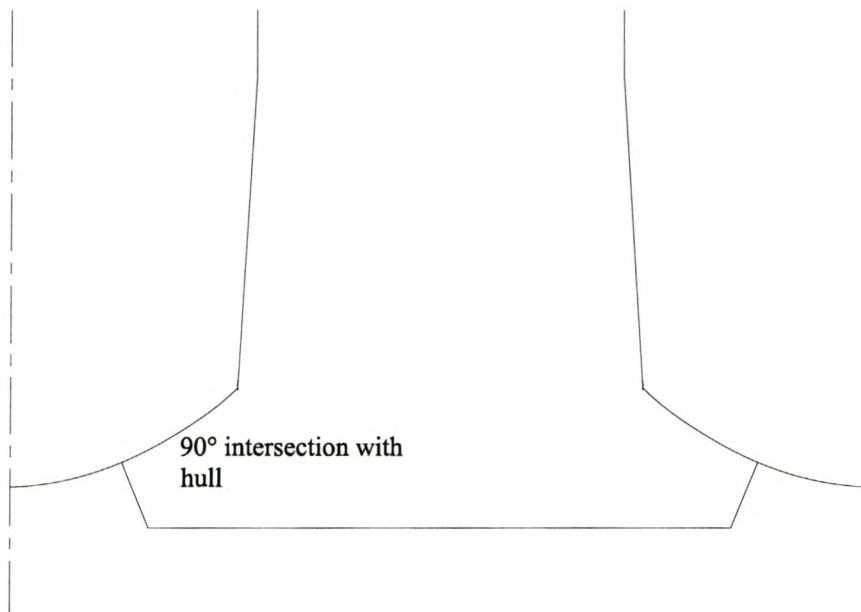


Figure 5.12: Hydrofoil hull connection showing ideal connection

Chapter 6

Hull Design for Hydrofoil Assistance

Abstract

The hydrodynamics of catamaran hullforms are investigated, with emphasis on how the influence of different hullform parameters influence design and behaviour of catamaran hulls with hydrofoil assistance. It is found that symmetrical hard chine hullforms with minimal aft buttock curvature are the most suitable for the majority of hydrofoil-assisted catamarans (vessels with their design speed in the transition phase). For such hulls, the length-displacement ratio, length to beam ratio, block coefficient, transom submergence ratio and demi-hull separation are the most important design parameters to consider.

6.1 Introduction

Chapter 1 identifies that two potential applications exist for hydrofoil assistance: hydrofoil retrofits to existing vessels and design of new hydrofoil-assisted catamarans. In the former, the hydrofoil system is designed to match an existing hull that may or may not be well suited to hydrofoil assistance. The latter allows for the design of a hydrofoil system and hull form that are adapted to compliment each other. The vessels described in Chapter 1 show examples of both types. Investigations of hullform design for hydrofoil assistance therefore need to cover conventional catamaran hullforms as well as hullforms designed specifically for hydrofoil assistance.

Three basic lines of development have been followed in existing hullforms for hydrofoil-assisted catamarans.

- Asymmetrical hullforms derived from semi-planing and planing hull forms

- Symmetrical hullforms based on semi-displacement and semi-planing designs
- Non-conventional hullforms including those based on SES design principles

This study has focused mainly on the first and the second types mentioned above, as these types represent the majority of catamarans in existence, which could be suitable for hydrofoil assistance and also lays the foundation for the development of new improved hullforms adapted to hydrofoil assistance. The asymmetrical hull is applied mainly to smaller planing catamarans, while the symmetrical hulls are characteristic of most larger semi-displacement and semi-planing craft. The literature also describes a number of non-conventional hullforms that have been proposed for hydrofoil-assisted catamarans (see for example: [LO95, SYK96]). As such designs vary substantially from the norm and are largely unproven, they have not been considered in much detail in this study. Hulls based on the slender SES type, have been thoroughly investigated and extensive literature (see for example [AMKH93, AHSM99]) is available on this type and are also not considered in detail. Rather, focus is placed on developing and understanding of design and adaptation of more conventional hullforms (asymmetrical and symmetrical) for use with hydrofoil assistance.

6.2 Asymmetrical Hullforms

By dividing a conventional mono-hull in two along its longitudinal symmetry plane forming a catamaran with two asymmetrical demi-hulls, one can reduce the wave-making interaction between the demi-hulls, thus providing undisturbed flow through the tunnel to the hydrofoils as well as increasing the lift and decreasing the wetted area of the hull compared with the same mono-hull [XT99]. The creation of a catamaran in this manner and supporting it with hydrofoils formed the basis of the early developments in hydrofoil-assisted catamarans. This hull form has been widely used in the Hysucat development and also in the developments of the Chinese channel hydrofoil boats [ZLH97]. Figure 6.1 shows a Hysucat with an asymmetrical hull.

Experimental investigations by Yermolayev et al. [YATR72, YATR76] for asymmetrical catamarans based on the MBK planing series [EBS78] of varied demi-hull spacing have shown that this hull form is best for minimizing the wave-interaction between the demi-hulls and also provides the best tunnel flow conditions for the hydrofoils at speeds representing $1.0 \leq Fn_{\nabla} \leq 3.0$, even for very narrow demi-hull spacing. In spite of its low demi-hull interference resistance, when considering the total resistance, this hull form has been found [FG72, MG99a] to have inferior resistance characteristics compared with symmetrical catamaran hullforms. This bad resistance quality is due to the larger waterline half-angle of entrance characteristic of asymmetrical designs compared with symmetrical designs of equal size and displacement, which increases the wave resistance and hence the total resistance. Consequently there has been limited application of asymmetrical designs to non-planing speeds for conventional



Figure 6.1: A Prout catamaran with a Hysucat foil system and an asymmetrical hull design

catamarans.

At planing speeds, residual resistance is mainly due to hull pressure resistance and results of Müller-Graf [MG99b] and Yermolayev [YATR76] show that for $Fn_{\nabla} \geq 3.2$ the resistance of the asymmetrical and symmetrical forms converge as seen in Figure 6.2 reproduced from [MG99a].

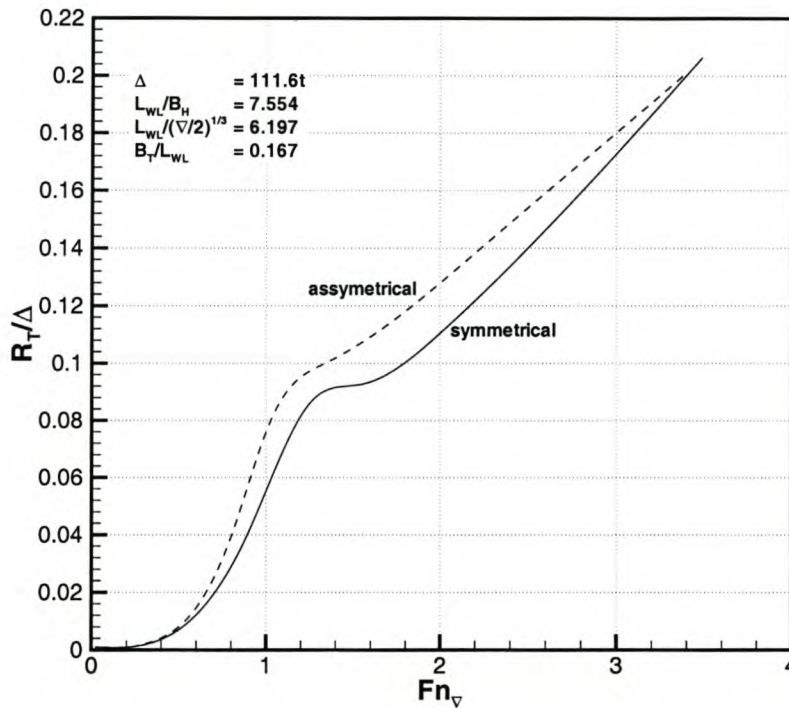


Figure 6.2: Comparison of the resistance-displacement ratio for symmetrical and asymmetrical demi-hulls

The optimum speeds of use for asymmetrical hullforms is therefore the planing phase of hydrofoil-assisted catamarans, $Fn_{\nabla} \geq 3.0$. Wave interference effects are no longer important, on the contrary, some beneficial interference can be achieved during planing (see Section 2.6.3) by utilizing reasonably small demi-hull separation distances. Asymmetrical designs further suffer from the problem of bow steering particularly in quartering seas. To solve this problem and that of increased resistance concerned with the asymmetrical bow shape, it is popular to include a symmetrical (or almost symmetrical) bow section which reduces the waterline half-angle of entrance and also the bow steering effect. This design has been widely used on Hysucat designs. Figure 6.3 shows an example of a towing tank model with a symmetrical bow.

Combining this hull form with hydrofoils is ideal as hydrofoils can easily be mounted at keel depth, safely positioned in the tunnel formed by the two demi-hulls, thus most

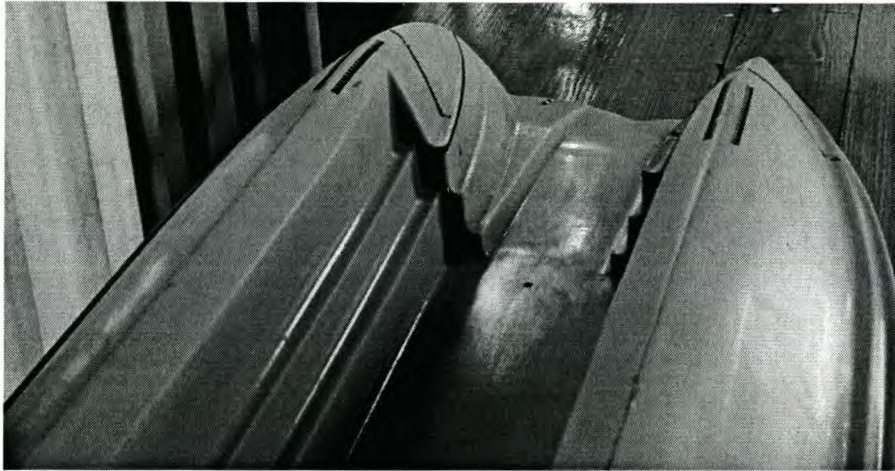


Figure 6.3: A towing tank model showing a symmetrical bow which terminates in a vertical step.

likely providing a good all-round solution for the planing speed range. At lower non-planing Froude numbers, the increased wave-making resistance (although reduced with foil assistance) makes this hullform less efficient compared with conventional symmetrical hull designs. The use of this hullform at planing speeds with hydrofoil assistance has been well documented in the literature by Hoppe [Hop80, Hop91a] and others (see for example [YATR72, YATR76, Zha94, ZLH97, DL01]) and is not considered further in this study.

6.3 Symmetrical Catamaran Hullforms

Symmetrical catamaran hullforms are representative of the majority of existing catamarans of the semi-displacement and semi-planing type. As pointed out by Migeotte et al. [MHK01], hydrofoil assistance can provide useful improvements in speed and efficiency of catamarans for $Fn_{\nabla} \geq 2.0$. This covers the design speeds of the majority of high-speed catamarans in operation today [Phi02]. To date no detailed study has been made of the use of hydrofoils with the hullforms typically used for these vessels. In this section the influence of the main hullform parameters are investigated.

The hull forms used on conventional symmetrical catamarans are round-bilge or hard chine forms that are based on semi-displacement or semi-planing hull lines. Such hulls are characterized by the following characteristics:

- symmetrical demi-hulls
- small waterline angle of entrance

- transom beam equal to midship value
- transom depth reduced compared with midship value
- tunnel width not less than the demi-hull beam

The position of the LCG of semi-displacement designs tends to be in the range 38 - 45% of L_{WL} (measured from transom); for planing hull designs in the range 30 - 38% of L_{WL} . Semi-planing designs have LCGs that are typically between these two extremes.

In the sections that follow a more detailed examination of these characteristics are given as well as the influence of the most important form coefficients characterizing the hull analyzed. The design of these hulls are analyzed with focus on the resistance and behaviour of the hull under hydrofoil assistance.

6.3.1 Round-Bilge and Hard Chine Hull Forms

The hard-chine hullforms used for high-speed catamarans tend to be deep-V types even though these catamarans are mostly semi-displacement vessels operating at $Fn_{\nabla} \leq 2.5$. Deep-V hulls are popular for small high-speed craft (operating at $Fn_{\nabla} \geq 3.0$) for good sea-keeping and resistance characteristics at high speeds in rough water. Round-bilge hulls have traditionally been used for displacement vessels and also semi-displacement vessels as hard-chine designs suffer higher resistance because of a certain amount of flow separation from submerged chines.

In the last decade deep-V hull forms have nevertheless found application for vessels operating at semi-displacement as well as semi-planing Froude numbers (see for example [GB92]) as they offer a number of other advantages over the round-bilge form. The choice of hard chine or round-bilge hull designs for conventional catamarans and hydrofoil-assisted variants is largely determined by resistance, sea-keeping, dynamic stability and propulsion considerations as well as considering the simpler manufacturing of hard chine forms. These aspects are discussed in the subsections that follow.

Resistance

For non-planing speeds, it is well established that round-bilge hull forms have superior calm water resistance to hard-chine forms. Extensive experimental investigations by Serter [Ser93] for mono-hulls as well as experimental data published by Müller-Graf [MG99b] for catamarans prove this. Added parasitic drag due to flow separation from the submerged chines accounts for about a 6% higher resistance at semi-displacement speeds. Figure 6.4 is representative of this resistance tendency for modern symmetrical catamarans of round-bilge and hard-chine types [MG99b] with equal dimensions and displacement. Modern developments in deep-V hullform design try to avoid this added

resistance by making use of high deadrise angles ($\beta = 45^\circ$) and positioning the chines at the waterline, where they are effective at separating the flow from the chines, but do not add to resistance. For such designs there is little difference between deep-V and round-bilge hull resistance [CCEP89].

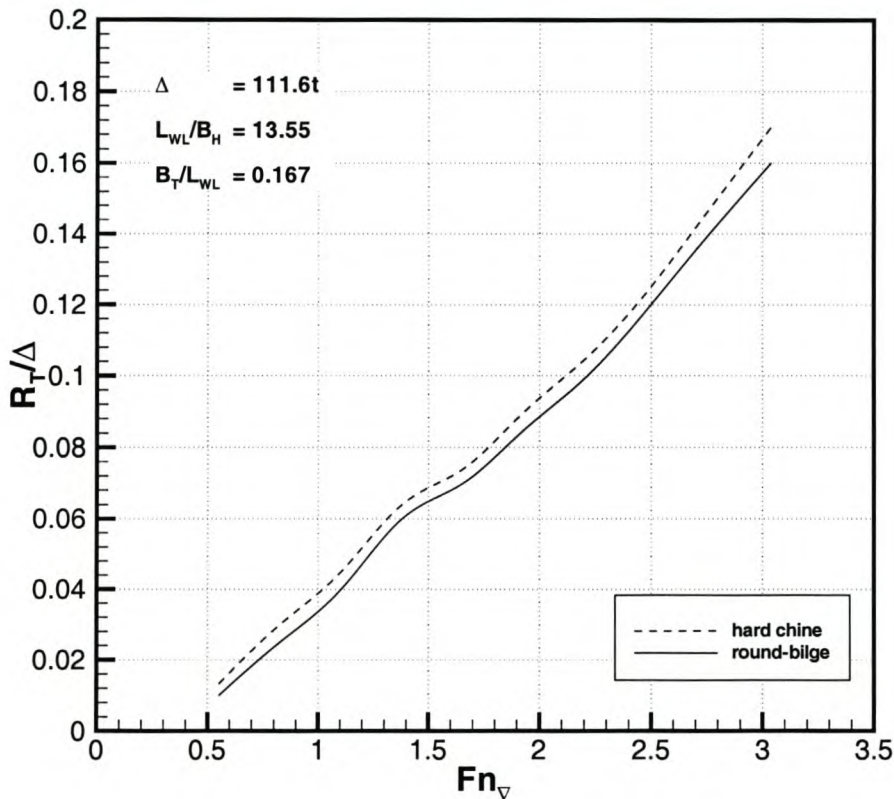


Figure 6.4: Resistance displacement ratio comparison of a round-bilge and hard chine hull form

The main difference between hard chine and round-bilge designs lies in the pressure distribution on the hull. Round-bilge hulls suffer from lower pressures (suction) on the hull associated with the curvature of the flow around the bilges. When under hydrofoil assistance, these lower pressures are detrimental to performance. This effect is stronger for larger trim angles¹ as flow around the bilges is then more pronounced. The increased suction forces around the bilges partially counters the hydrofoil lift, which in turn, reduces the rise of the hull and increases the wetted area.

The hard-chine offers the advantage that at transition and planing speeds, the hard

¹Beneficial for hydrofoil-assisted designs.

chines allow the flow to separate from the hull thus reducing the wetted area. This means that under hydrofoil assistance, chines placed at the waterline will not be optimal because the hull is lifted partially out of the water, making the chines ineffective at deflecting the flow as their position is too high. It is more effective to place chines initially submerged (with added parasitic drag at low speeds) but effectively separating the flow at transition speeds and eliminating suction effects on the hull.

The effect of suction implies that a higher foil lift fraction is needed for round-bilge hulls compared with hard chine variants to achieve equal resistance improvements. This has been found experimentally by Kim et al. [KYS⁺93], who compared calm water resistance for hydrofoil-assisted (using a single mono-foil) round-bilge and hard chine hull types and found that the hard chine hull needs 10% less power at semi-planing speeds than the round-bilge hull when under hydrofoil assistance. No explanation for the decreased resistance of the hard chine form is given, but it is most likely due to decreased wetted area and a more favorable pressure distribution (less suction) on the hull.

To investigate this phenomenon further, model tests were conducted using identical Hysuwac hydrofoil systems on two catamaran hulls - one round-bilged and the other one hard chined - of equal length, beam, tunnel width and displacement. Both hulls have straight buttock lines to eliminate the effects buttock curvature (discussed in Section 6.3.2) may have on the hull suction. The main particulars of the vessels are given in Table 6.1 and the body plans are shown in Figure 6.5.

	SD7	SD8
L	36.2	36.2
B	3.00	3.00
$L/\nabla^{\frac{1}{3}}$	6.7	6.7
L/B	12	12
B/D	2.08	2.45
i_e	8.0	8.0
C_B	0.53	0.62
C_P	0.73	0.76

Table 6.1: Main particulars of the SD7 and SD8 hulls

It is well known that the length-displacement ratio $L/\nabla^{\frac{1}{3}}$ is the most important parameter affecting resistance. This parameter being equal, means that one can expect similar resistance tendencies for both hulls. Nevertheless, an important difference between the two hulls is the difference in beam to draft ratio (B/D) and block coefficient (C_B). The beam to draft ratio is known [MWC96] to have only a slight influence on resistance within the range of values for the two hulls, so this factor does not produce a great difference in resistance. The block coefficient on the other hand has a more important influence on resistance as it is related to the fullness of the bow and

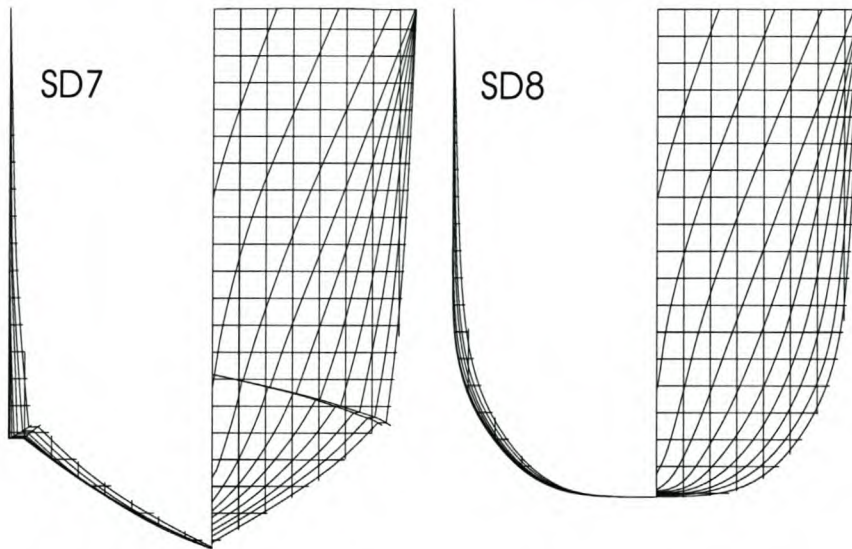


Figure 6.5: Body plans of investigated catamaran demi-hulls

stern and thus the amount of wave-making. According to the findings of Basin et al. [BLSZ95b], the SD8 hull is outside the optimum range for the block coefficient of catamarans²: $C_B = 0.4 - 0.6$ and will result in increased resistance for the hull. This is reflected in Figure 6.6 which shows the resistance comparison for the two hulls with and without hydrofoil assistance (using Hysuwac foils, shown in Figure 5.3 on page 152). The round-bilge bare-hull has a resistance approximately 12% higher than the hard chine form due to its higher block coefficient. This magnitude is in line with the findings of Semijalac and Gamulin [SG98] concerning the influence of block coefficient on resistance.

Keeping in mind this slightly higher resistance for the round-bilge hull, comparing the resistance of both hulls shows that the hard chine hull shows a much smoother transition phase indicating that suction on the hull is less than on the round-bilge design. At planing speeds the round-bilge hull also has a slightly higher resistance due to added wetted area associated with flow around the bilges.

Comparing the resistance of both hydrofoil-assisted hulls to the resistance without foils it can be seen - and should be kept in mind - that the round-bilge hull with hydrofoil assistance, while not optimal, still has resistance characteristics vastly superior to catamarans without foils. Hydrofoil assistance should therefore be considered as a viable means to improving the resistance of both hull types.

²The optimum C_B for catamarans operating at $Fn_{\nabla} \geq 1.5$ has been found to be approximately 0.4. This is related to the optimum ratio of internal volume to minimum wetted area. Smaller values for C_B also relate to increased buttock curvature in the midship section.

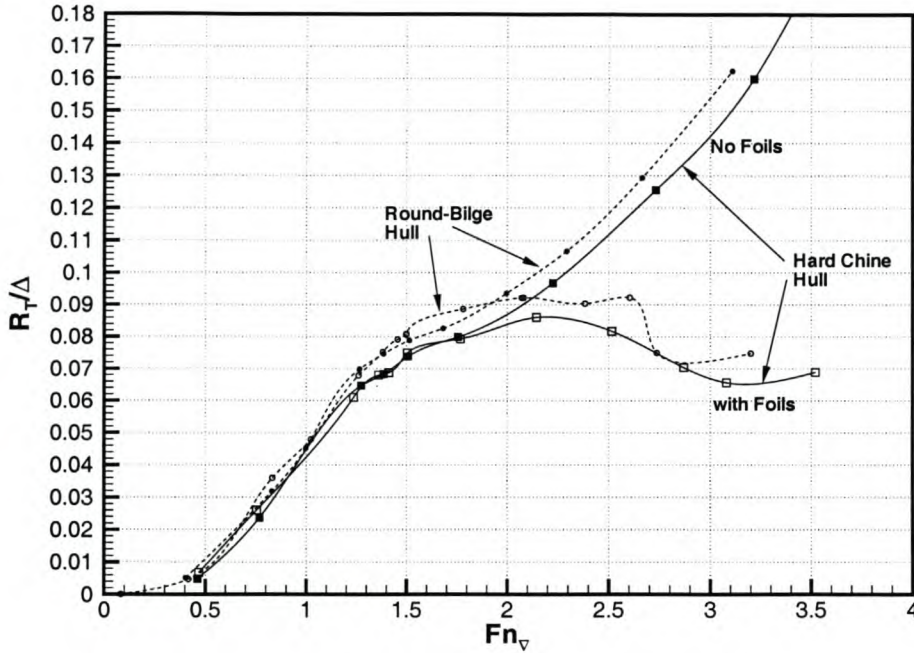


Figure 6.6: Resistance comparison for similar round-bilge and hard chine hull forms with hydrofoil assistance

Seakeeping Behaviour

Seakeeping is not dealt with in any detail in this study, but is considered in this section as the seakeeping considerations form one of the main criteria for selection of hard chine rather than round-bilge hullforms and is therefore worthy of mention.

Numerous investigations [CCEP89, Ser93] have proven the advantage of deep-V hull designs when seakeeping and speed loss in a seastate are considered. The advantages are due to more favorable pressure distributions on the hull that dampen the motions and also reduce the incidence of slamming. The use of slightly convex sections are also advantageous for lowering the impact pressures on the hull. Lower impact pressures result from the flow of water around the convex sections, which creates suction and lessens the impact force. The use of slightly convex sections on deep-V craft is therefore useful, especially at high-speeds, as impact forces increase with speed (see for example [Lev71]). The SD7 hull shown in Figure 6.5 is an example of such a design.

Similar principles concerning seakeeping apply to hydrofoil-assisted catamarans, even though this consideration may be of less importance as hydrofoils are known to improve seakeeping substantially (see for example [Wel98b]).

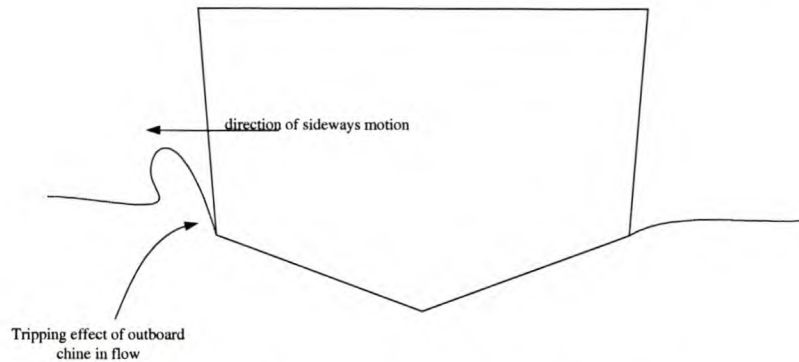


Figure 6.7: Illustration of chine tripping

Dynamic Stability

As discussed in Section 5.2.2, directional instability and risk of broaching represents the main stability problems at transition speeds and the risk of foil-induced porpoising a problem at planing speeds. Hydrofoil induced porpoising is mainly due to the foil design and cannot be influenced to any great extent by the hull design, but the hull shape is nevertheless an important consideration for directional stability. Investigations by Colombo et al. [CCEP89] have shown that deep-V mono-hulls designed for semi-displacement and semi-planing speeds have better course keeping stability as well as better manoeuvrability than round-bilge hulls. The improved directional stability is due to a deeper draft, a sharp keel that acts partially as a rudder and more favorable pressure distributions on the hull that aid stability.

Observations during towing tank experiments conducted in this study have shown similar results for hydrofoil-assisted catamarans when considering directional stability and the risk of broaching. For tests of the two hulls shown in Figure 6.5 with Hysuwac foils, the hard chined hull was observed to have better directional stability during towing tank tests. The flat bottomed round-bilge hull has its center of lateral resistance farther forward than the hard-chine hull. This results in a broaching tendency for that hull in the transition phase just before final transition to planing takes place ($Fn_{\nabla} = 2.6$) when the trim is low. In the Hysuwac planing condition (see Figure 2.2 on page 32) with the bows clear of the water, observations showed the flat aft sections tend to side slip when any disturbance is encountered, resulting in an oscillating yaw motion. This problem is not so much due to the round-bilge design but rather a result of the flat keel and also occurs on flat bottomed hard chine hulls as well. The effect is less on hard chined hulls as the chines tend to "trip" in the flow during the yawing motion as illustrated in Figure 6.7. Transom skegs or rudders were found to be beneficial and necessary for these hull types to provide directional stability for such hulls when under hydrofoil assistance.

To eliminate the problem of directional instability and side-slipping, Warren and Kecsmar [WK99] recommend using skegs whose area is 1.5-3% of the submerged lateral area of the hull: $L_{WL} \times D$. Model tests have shown that such skegs remove even severe directional instabilities.

6.3.2 The Influence of Aft Buttock Shape and the Position of the LCG

The aft buttock curvature, the cross-sectional area curve and the position of the LCG are inextricably linked as they all have important effects on the resistance (primarily wave-making), attitude and directional stability of hydrofoil-assisted catamarans.

The form of the after part of the hull, characterized by the curvature of the buttock lines, is an important consideration for optimizing the efficiency of high-speed hulls. The shape of buttock lines is employed to optimize the hull sectional area curve, as well as to achieve the desired running trim angle at speed. The curvature of buttock lines can either be convex, straight, concave or some combination of these.

Convex buttock curvature in conjunction with a reduced transom area in relation to the maximum area and a LCG position 40-43% L_{WL} from the transom, are characteristic of semi-displacement hull designs as this combination is known to reduce resistance at semi-displacement speeds and is included in the hull design of the majority of high-speed catamarans operating in this speed range.

The similarity between the pressure distribution on the underside of a hull and that on the pressure side of a foil as discovered by Wagner [Wag32], provides useful means of qualitatively examining the mechanics of the flow underneath a curved hull (see for example [MG88]). Wagner explains that a convexly curved body can produce lift or suction depending on the trim angle (angle of attack) while flat and concave sections tend to produce only lift.

Figure 6.8 [MG88] illustrates how the pressure distribution on curved surfaces change. Concave sections tend to produce the most lift for relatively small trim angles. Considering the convexly curved surfaces, it can be seen that convex surfaces³ at zero trim (2nd illustration) generate lift in the vicinity of the bow while the aft sections suffer from suction. In many cases suction forces dominate and the resultant force is downwards making the hull submerge deeper at high speed. As the trim increases (3rd illustration), a larger portion of the hull experiences positive pressure and lift is increased. A convex shape in conjunction with a concave section aft (4th illustration) is often useful for increasing the pressures near the stern but some suction remains.

The kind of hull pressure distribution obtained for a hull design with convex buttock

³Note the similarity when comparing Figure 6.8 at zero trim with actual computed pressure values shown in Figure 2.5 for a typical semi-displacement hull.

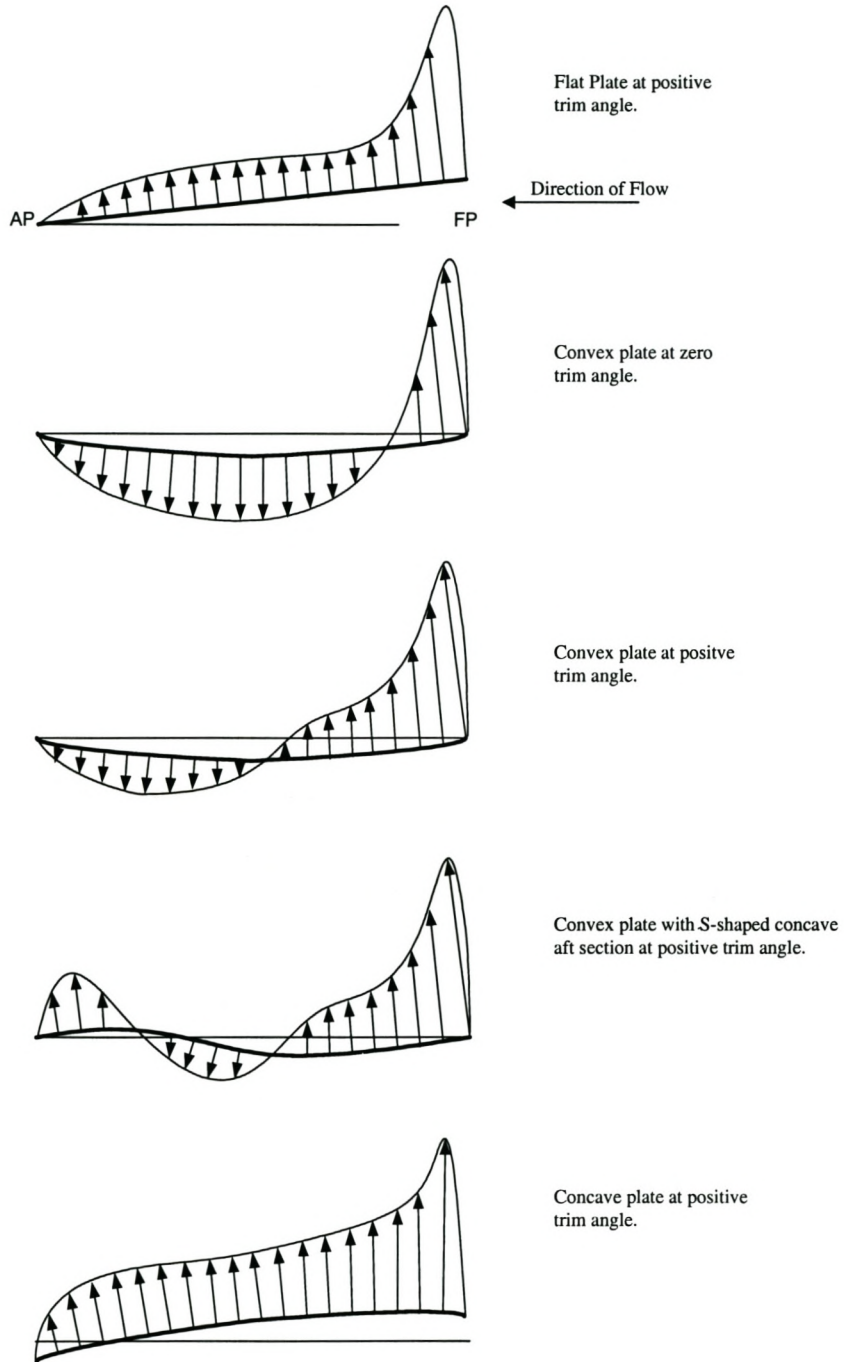


Figure 6.8: Schematic pressure distribution on curved surfaces

lines and a relatively forward LCG position, results in low operating trim and is useful for reducing the wave-making resistance at semi-displacement speeds (hence the popularity of this configuration), but for the same hull under hydrofoil assistance, the convex curvature is partially responsible for the unwanted suction effects on the hull, which are increased for low running trim. These hull shapes perform satisfactorily for conventional catamarans without hydrofoil assistance well into the transition phase⁴, but experience some increase in draft as the suction forces cause the hull to sink slightly.

When considering the same hull with hydrofoil assistance, the suction effects - as explained in Chapter 2 - are detrimental primarily in the transition phase. Suction limits the extent that hydrofoil assistance can lift the hull from the water and also for the sharply varying resistance tendencies of the transition phase illustrated in Figure 2.1. For the transition phase hull designs with less curvature and the LCG farther aft is beneficial for improving resistance. Similar to considerations for the foil design, as explained in the previous chapter, there are conflicting requirements concerning buttock curvature and the position of the LCG for the three phases. These are discussed in the subsections that follow.

The Displacement phase

At displacement speeds, the primary mechanism for reducing total resistance is by reducing the amount of wave-making. When considering buttock curvature this is best achieved by introducing convex curvature into the buttock lines, which results in a reduced transom area. Such a reduction of submerged transom area is favorable for reducing wave-making resistance (see for example [Fun91]). A low trim angle is maintained by making use of a LCG position relatively far forward (40-45% of L_{WL} from the transom) or by increasing the lift generated aft. This may be achieved by utilizing an adjustable aft hydrofoil, the use of which has been described in the previous chapter, or by introducing some concave curvature into the after part of the hull as illustrated in Figure 6.8. Concave curvature can be practically implemented on hydrofoil-assisted catamarans by making use of adjustable transom trim tabs [Hop97] or interceptors [PPNE00, THCC01] in conjunction with a main load carrying foil located further forward. Trim tabs and interceptors in effect create concave buttock curvature, in this way increasing the lift in the vicinity of the transom which further reduces trim. Figure 6.9 illustrates the concept of these two devices. Such devices are particularly useful for reducing trim of vessels with fuller transoms, which generally have the LCG further aft (semi-planing and planing vessels).

⁴A large number of such hull designs are commercial vessels operating at $Fn_{\nabla} \geq 2.5$, where strictly speaking, semi-planing designs with less buttock curvature would be more suitable.

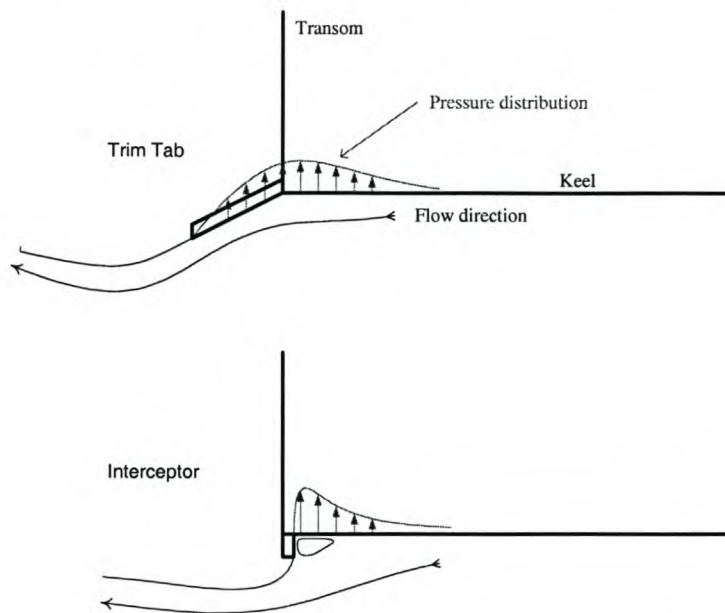


Figure 6.9: Hydrodynamic principle of a trim tab and interceptor

Transition Phase

In the transition phase, the main mechanism for reducing resistance of hydrofoil-assisted catamarans is by overcoming suction, allowing the hull to be lifted farther out of the water. Buttock curvature has a very important effect, in conjunction with the running trim angle, on hull suction. When considering hull designs with convex buttock curvature, hull suction is easiest overcome by introducing a higher running trim angle, which creates positive pressure over a greater part of the hull. Higher running trim angles can be induced by utilizing a suitably aft LCG location or by increasing lift forward (i.e by the use of a strong bow foil as explained in the previous chapter). In terms of hull design, convex buttock curvature is useful to increase the trim angle if used in conjunction with a suitably aft LCG position⁵ so that the vessel floats with a bow-up trim. This is in conflict with the requirements for the displacement phase. As the running trim angle increases, the waterline length of convex shapes decreases quickly and hence the wetted area also, which in turn reduces friction resistance. Hellström and Blount [HD95] have systematically investigated this effect for planing mono-hulls and conventional hydrofoil craft that have successfully utilized convex buttock curvature for decreasing the take-off speed [Pie76, ES65].

To initially investigate the use of convex hull shapes typically used on the majority of high-speed catamarans with hydrofoil assistance, an experimental study [Hop96] was

⁵Often conventional semi-displacement catamarans which are over-driven to higher speeds, make use of LCG positions too far forward to effectively achieve this.

	SD6	SD7
L	36.2	36.2
$L/\nabla^{\frac{1}{3}}$	6.7	6.7
L/B	12	12
B/D	2.08	2.08
i_e	8.0	8.0
C_B	0.53	0.50
C_P	0.73	0.70

Table 6.2: Main hull particulars of SD6 and SD7 hulls

carried out for a semi-displacement hull with a Hysucat hydrofoil system. The hull used is shown in Figure 6.11 (SD6). The hull was tested with varying transom wedge angles to investigate the effect of concave buttock curvature. Figure 6.10 shows the model test results and the sensitivity of the aft hull shape to performance. It can be seen that the best resistance improvements with hydrofoils for the transition phase are achieved for the highest running trim condition which corresponds to the smallest transom wedge angle. Further, the sensitivity of resistance to the wedge angle is clearly seen. At $Fn_{\nabla} = 3.4$, increasing the wedge angle by 3.5° results in a reduction in running trim angle by about 0.5° , which in turn increases the resistance by about 30%, mainly because of increased waterline length and wetted area associated with the lower trim. One can deduce from these results that use of convex buttock curvatures that include aft lifting devices (trim tabs, transom wedges, interceptors etc.), as shown in Figure 6.8 will be detrimental to the performance of hydrofoil-assisted hulls in the transition phase.

To further investigate the effect of aft buttock hull shape and LCG position, experimental investigations [MH01] were conducted on two hard chine hullforms of equal size, displacement and main dimensions, but differing in the shape of the buttock lines. Both hulls were tested with and without hydrofoil assistance (using a Hysuwac hydrofoil system). Figure 6.11 shows the lines for the two hull forms. Table 6.2 summarizes their main dimensions.

The SD7 hull has straight lines in the after part that is characteristic of semi-planing hulls. The sections forward of amidships are identical for both hulls, and both were tested with similar foil systems. During the investigations, the foils for the two hulls differed only in angles of attack. This was necessary so that the centre of lift of the foil system corresponded to the same position: about 2% of L_{WL} ahead of the even floating LCG for each hull. The foil lift fraction of both hulls is approximately equal.

Figure 6.12 shows the measured data for the two hulls. Firstly considering the resistance tendencies for the two hulls without hydrofoil assistance, well known tendencies are seen: an increased hump resistance for the SD7 hull over the SD6 hull at $Fn_{\nabla} = 1.5$

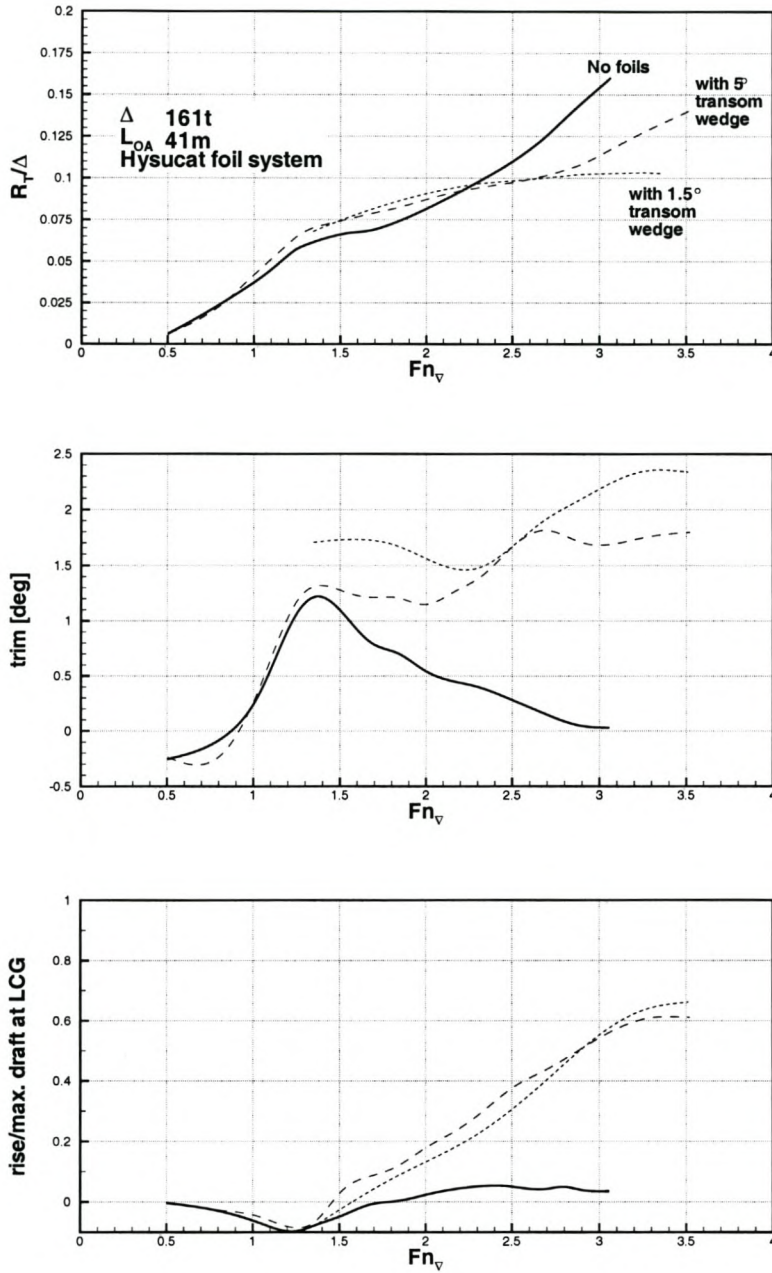


Figure 6.10: Resistance and attitude of a semi-displacement hull showing the influence of a transom wedge. The bare hull includes the wedge.

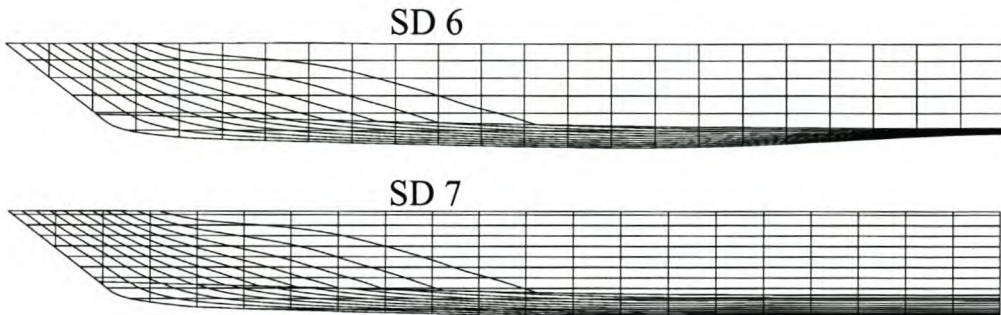


Figure 6.11: Buttock lines of SD6 and SD7 hard chine hull designs

(due to larger submerged transom area). Once semi-planing speeds $Fn_{\nabla} \geq 3.0$ are reached, the SD7 hull shows improved resistance over the SD6 hull as it suffers less from suction effects at high speed. The effects of suction can be clearly seen when comparing the midship rise for the two hulls: the SD7 hull rises farther out of the water than the SD6 at speed.

Under hydrofoil assistance, both hulls show similar tendencies, but differ in some important aspects. Considering first the even floating condition for both hulls: resistance improvements for both hulls begin at $Fn_{\nabla} \approx 1.8$ and follow similar resistance tendencies until the final transition to planing occurs ($Fn_{\nabla} = 2.8$). The SD6 hull suffers a steep transition to planing while the SD7 hull shows a more gradual transition to planing, indicating that - predictably - the SD6 hull under hydrofoil assistance suffers more from suction than the SD7 hull. Once the planing phase is reached, both hulls show similar resistance characteristics and the shape of the buttock lines no longer plays any important role.

Also shown on the figure are the resistance tendencies of both hulls for a LCG position 2% of L_{WL} aft of the even-floating position. The resulting increase in hump resistance of both hulls at $Fn_{\nabla} = 1.5$ is clearly seen (due to increased transom submergence) but more importantly, there are substantially improved transition phase resistance characteristics for both hulls. One can see that this is associated with a significantly higher running trim angle for both hulls. Note that the SD6 hull shows a much larger increase in trim angle compared with the SD7 hull across the whole speed range. This is associated with the convex buttock curvature of the SD6 hull. The sudden transition to planing associated with the SD6 hull has also disappeared, now showing a much smoother transition. Also indicated on the figure is that the minimum resistance for both hulls, which occurs at $Fn_{\nabla} = 2.75$ and $Fn_{\nabla} = 2.5$ respectively for the SD6 and SD7 hulls and is associated with the highest running trim angle of each vessel.

In the planing phase, $Fn_{\nabla} \geq 3.0$ it can be seen that both the LCG position and buttock curvature no longer play any significant role in regulating trim or in affecting resistance. At these speeds the large forces generated by the Hysuwac foil design

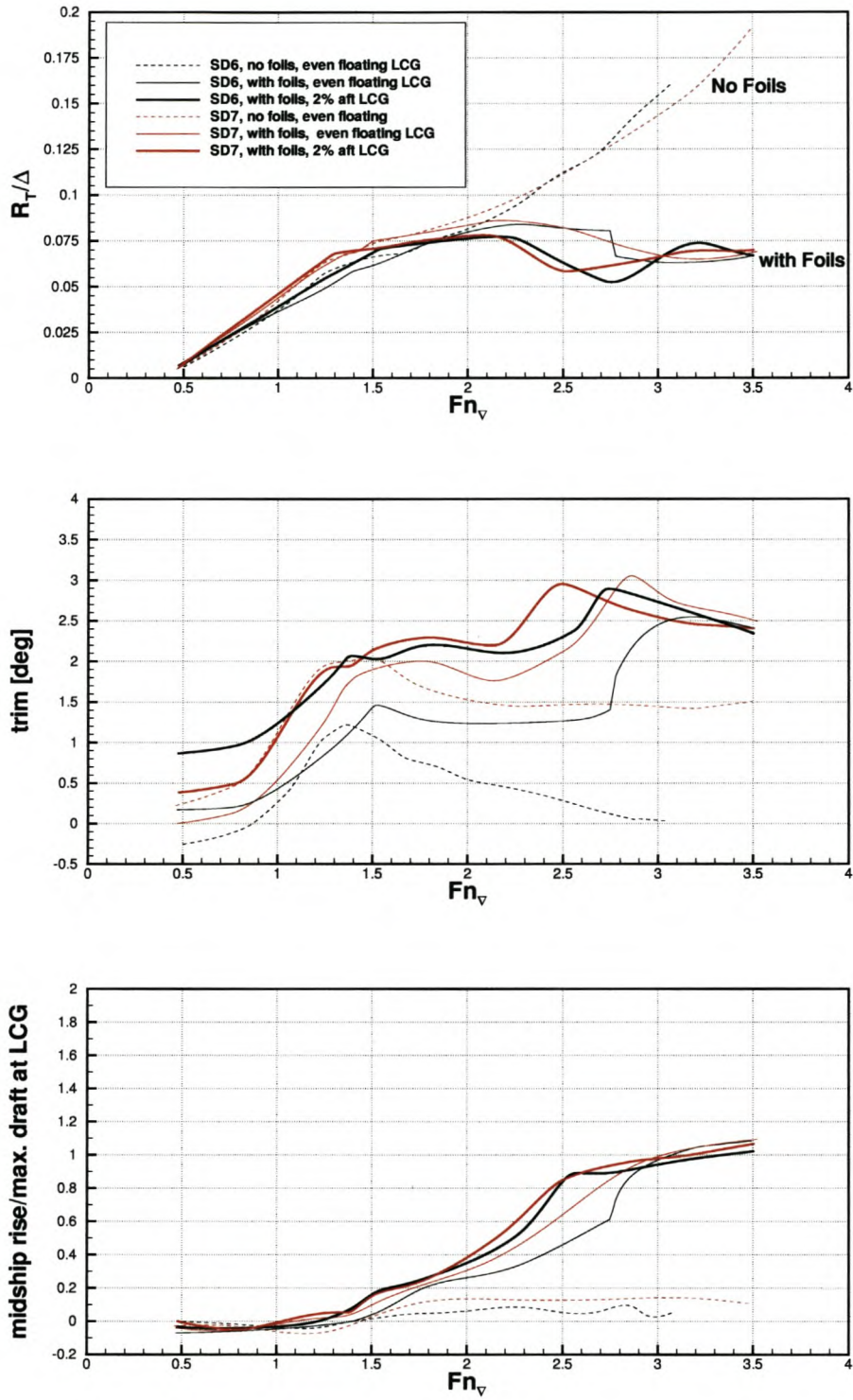


Figure 6.12: Resistance comparison for SD6 and SD7 hullforms with and without hydrofoil assistance.

dominate and as the hull bow is lifted largely clear of the water, the hull shape no longer has any important influence on resistance. From the data of Figure 6.12, it is clear that aft buttock shape and LCG position have important effects on resistance in the transition phase, both associated with the development of suction forces on the hull.

It should further be pointed out that shifting the LCG forward so that the centre of lift of the foils and the LCG positions corresponds, (i.e. the foil system does not produce any bow-up moment) the effect on transition phase resistance is large. The lower trim associated with the forward LCG effectively increases the buttock curvature of the hull and hence suction. Figure 6.13 shows the effect of shifting the LCG forward. The most important effect of this forward LCG shift is the increase in maximum resistance by about 30% in the transition phase and the much steeper transition to planing for both hulls. The increase in resistance is important as it is the maximum resistance, which usually occurs close to the design speed of the vessel, and therefore can result in the vessel not reaching the desired speed. Similarly to earlier results, note the transition phase correlation of high resistance with low trim and increased suction, experienced by both hulls.

The importance of hull design on the suction effect can be further illustrated by analysis of Shin et al.'s [SYK96] proposal for a tandem body hydrofoil catamaran illustrated in Figure 6.14. This idea of splitting the hydrofoil-assisted catamaran demi-hull longitudinally into fore and aft sections was proposed as a way of improving the pitch response of catamarans in waves. The proposed vessel that has been model tested, uses hard-chine sections forward and round-bilge sections aft.

Analysis of the model test data presented by Shin et al., reproduced in Figure 6.15, indicates that this design has some interesting resistance tendencies. Similar to performance tendencies of more conventional hydrofoil-assisted catamaran hullforms, the tandem body design has a typical sudden transition associated with a sharp drop in resistance and a sharp increase in trim, after which a fairly flat resistance tendency is found similar to that normally found during the planing phase. Unlike conventional catamaran hullforms, there is a substantial shift of the phases to lower Froude numbers. The figures show that the planing phase (low resistance; high trim) starts at $Fn_{\nabla} = 2.1$, normally only the beginning of the transition phase for standard designs. This phase shift can be attributed to the double bottom hull design, which does not suffer to any great extent from the hull suction effects during transition because the mid-section of the hull is removed. This allows the vessel to take up a high running trim angle (even without the bow foil extending below the keel) from relatively low Froude numbers compared with conventional hydrofoil-assisted catamarans and has the low resistance characteristic of the planing phase. This design therefore merits further research for hydrofoil-assisted vessels designed for operation at $2.0 \leq Fn_{\nabla} \leq 3.0$.

From the numerous results and explanations given in this section on symmetrical catamaran hullforms of the semi-displacement and semi-planing type, it has been

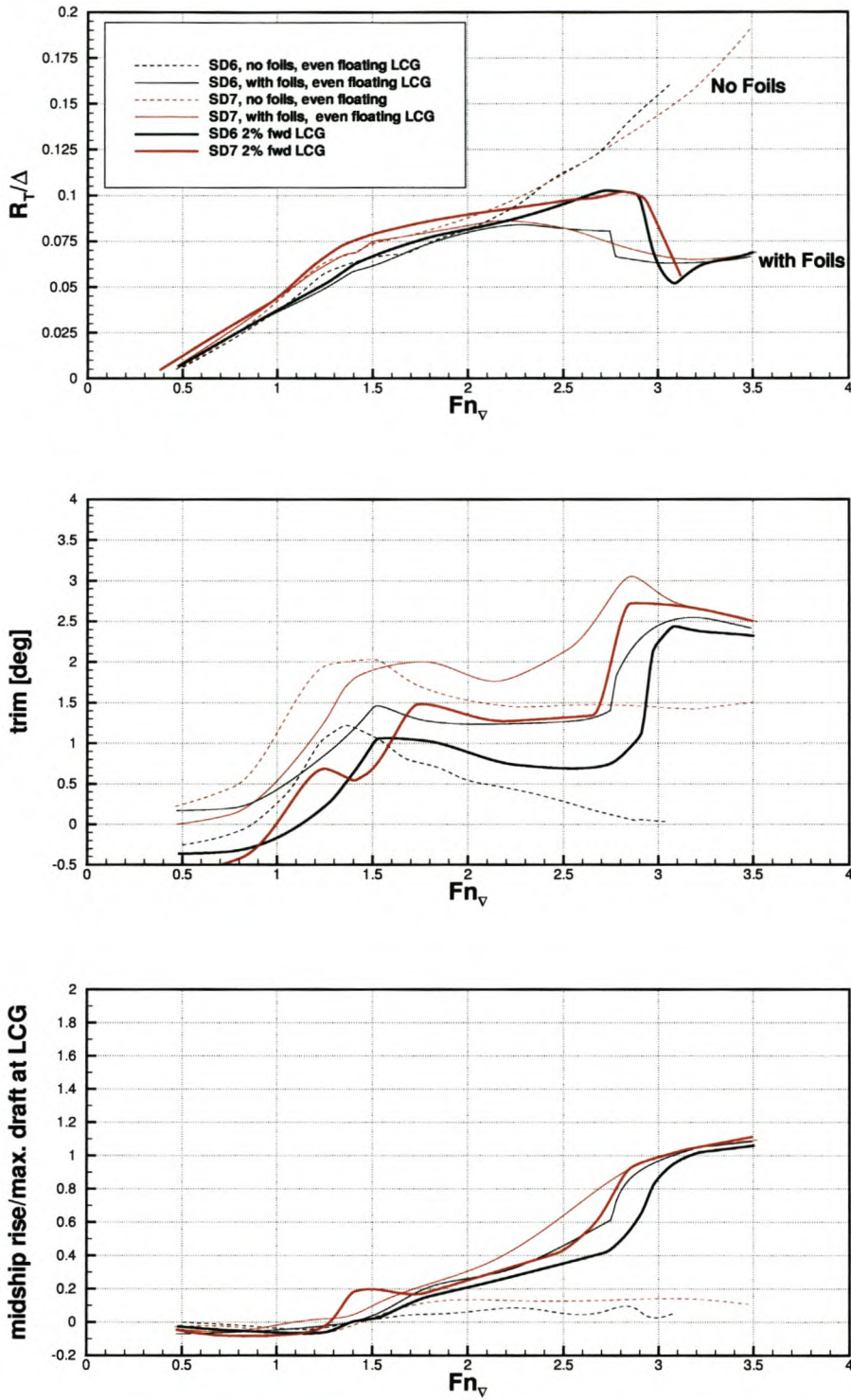


Figure 6.13: The effect of forward shifts in LCG on resistance, trim and rise

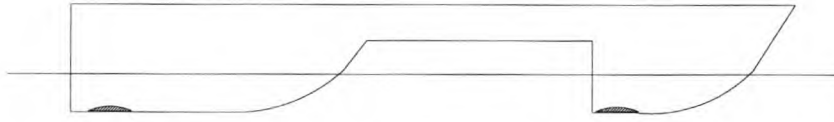


Figure 6.14: Tandem body hydrofoil-assisted catamaran proposed by Shin et al.

found that in the displacement phase, the standard semi-displacement hullform offers the lowest hump resistance even with hydrofoil assistance. In the transition phase, the hull suction effects related to convex buttock curvature in conjunction with low running trim are responsible for poor performance. This condition can be substantially improved by increasing the running trim angle by choice of a suitable LCG. The inverse was also found to be true with a substantial increase in maximum resistance for the vessel in the transition phase if the trim angle is reduced. This rule applies to round-bilge and hard chine hullforms with straight buttocks and those with convex curvature. Concave buttock curvature is undesirable because it increases suction effects.

6.4 The Influence of Hullform Parameters on Design

The pressure distribution (and hence the amount of suction) on the hull is dependent on a number of different hullform parameters, which influence the two most important parameters namely, curvature of the buttocks and the running trim angle. The following form parameters are important concerning hull design of hydrofoil-assisted catamarans.

The Length-Displacement Ratio $L/\nabla^{1/3}$

The length- displacement ratio, $L/\nabla^{1/3}$, is the predominant hull parameter affecting residual resistance. At displacement and semi-displacement speeds: $Fn_{\nabla} \leq 2.5$, resistance decreases strongly with increasing $L/\nabla^{1/3}$. Figure 6.16 shows the relation between residual resistance and volumetric Froude number for semi-displacement catamarans based on statistical analysis [Wer90].

From the figure it can be seen that as Fn_{∇} increases, there is diminished improvement in residual resistance, particularly for $L/\nabla^{1/3} \geq 6.5$, the values most common for high-speed catamarans. Keeping in mind that increased length-displacement ratio leads to a higher wetted area (and therefore higher friction resistance) for the same displacement, the usefulness of increasing $L/\nabla^{1/3}$ therefore diminishes with increasing

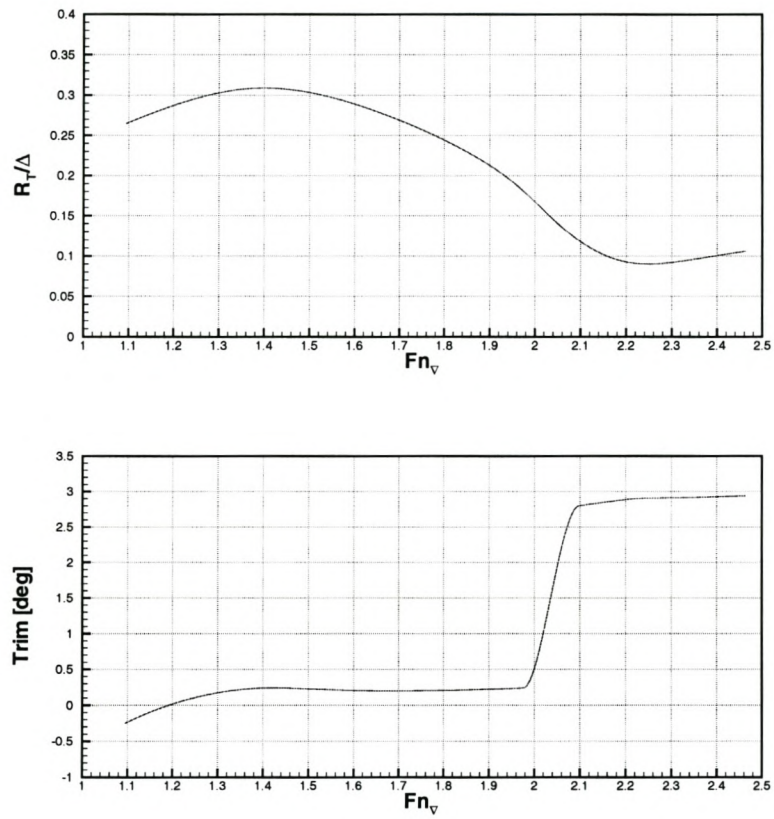


Figure 6.15: Resistance and trim tendencies of tandem body catamaran with hydrofoils tested by Shin et al. [SYK96]

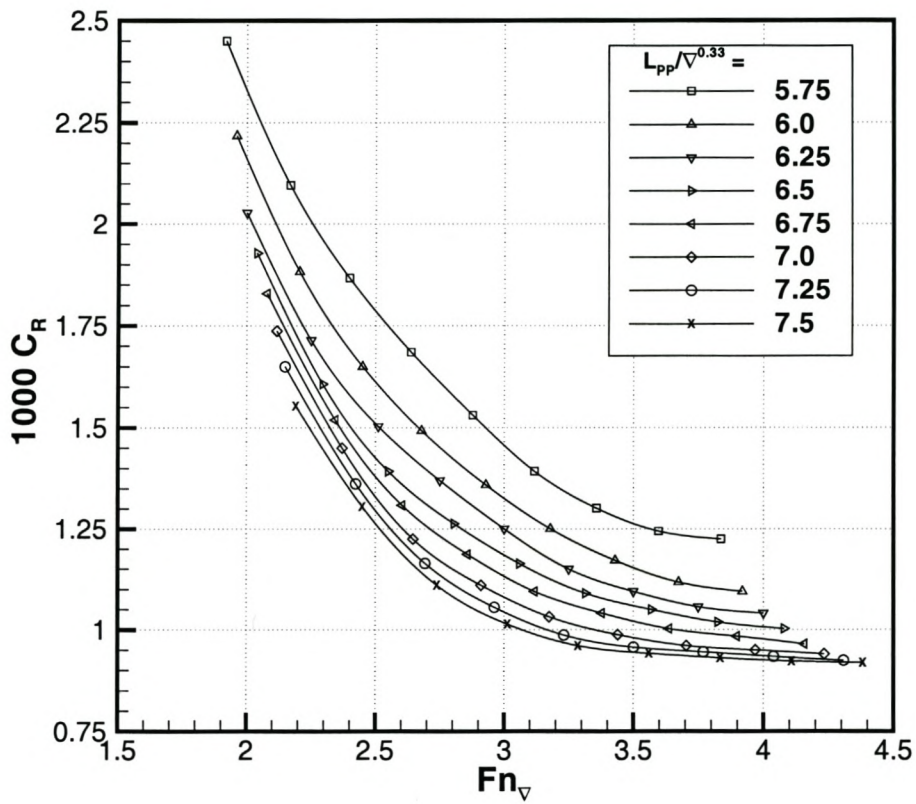


Figure 6.16: Residual resistance coefficient for semi-displacement catamarans

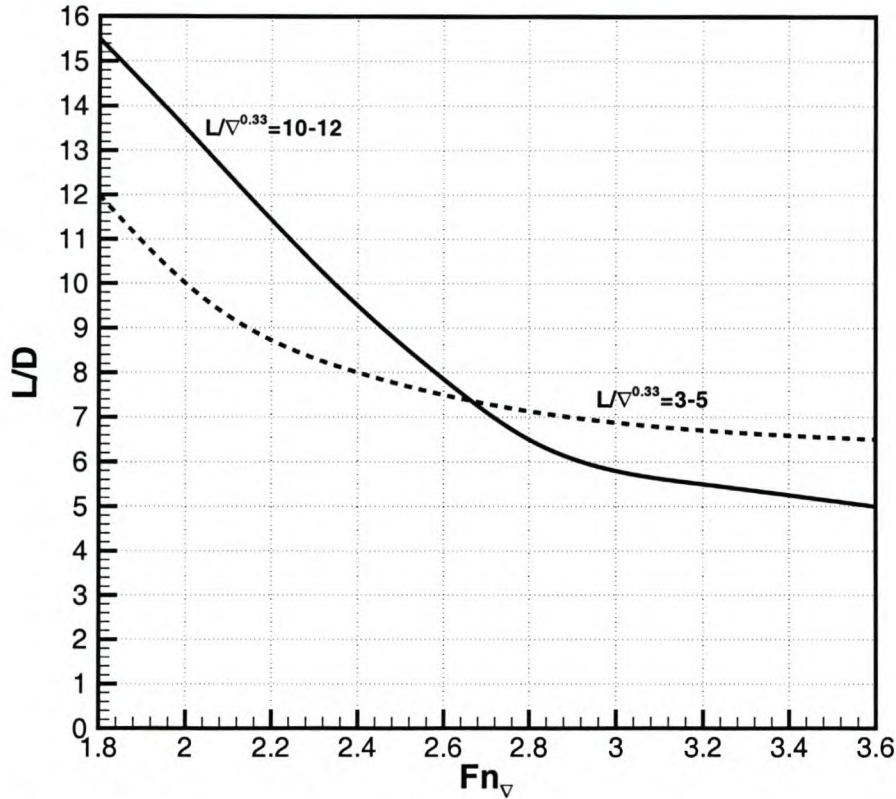


Figure 6.17: Comparison of L/D for different length-displacement ratios

speed. Investigations by Lyakhovitsky [Lya96] have established that for $Fn_{\nabla} \geq 2.7$ it is effective to reduce the length-displacement ratio for improvements in total resistance. Figure 6.17 shows the general tendency of lift to drag ratio versus Froude number for vessels with different length-displacement ratios.

In the design of hydrofoil-assisted catamarans, the relationship between resistance and $L/\nabla^{\frac{1}{3}}$ implies that for the top half of the transition phase as well as the planing phase of hydrofoil-assisted catamarans, reducing the waterline length of the hull by lifting the bows clear of the water is effective for reducing resistance. Figure 1.2 shows examples of two vessels that apply this logic in their design.

Finally it can be said that the optimum hull length-displacement ratio (in terms of resistance) for hydrofoil-assisted catamarans is larger than for conventional catamarans. The larger length-displacement ratio reduces resistance at displacement speeds and

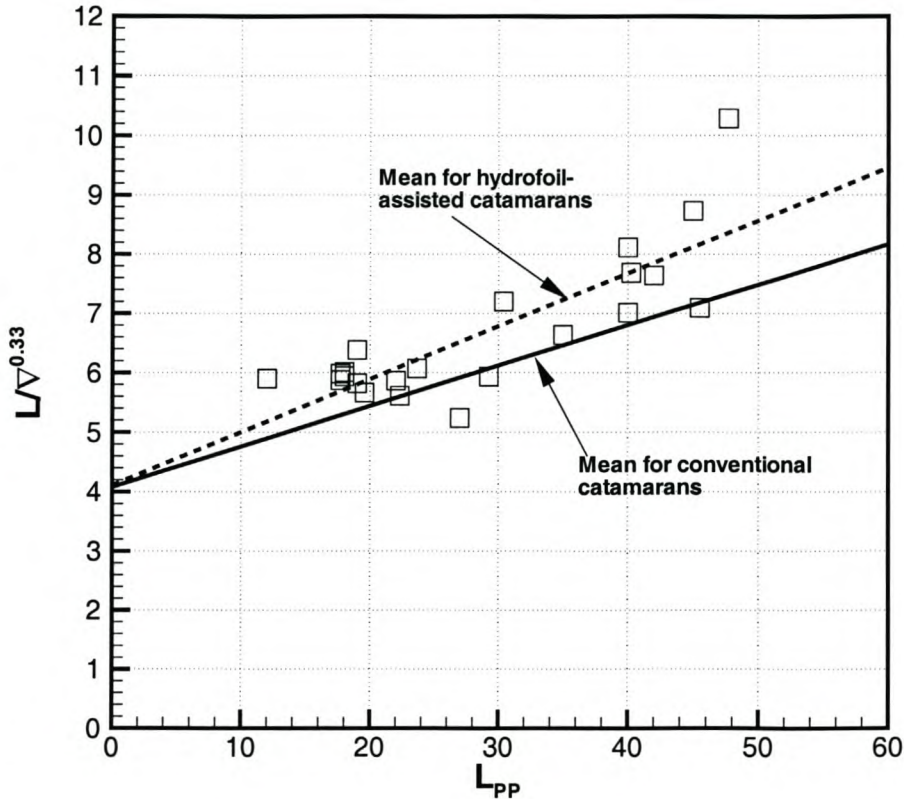


Figure 6.18: Comparison of length-displacement ratios for conventional catamarans (solid line) and hydrofoil-assisted catamarans (dashed line and squares)

reduces hull suction in the transition phase⁶, allowing the hydrofoils to lift the bows clear of the water for the planing phase. Examining the existing hydrofoil-assisted catamaran ferries listed in Appendix C and comparing their length-displacement ratios against the mean for conventional catamarans [Wer90] as shown in Figure 6.18, it can be seen that the mean for hydrofoil-assisted variants is slightly higher than for conventional catamarans.

⁶A large length-displacement ratio relates to small draft in relation to the ship length. This means that buttock curvature will be less for hulls with high length-displacement ratios and suction effects on the hull will be reduced.

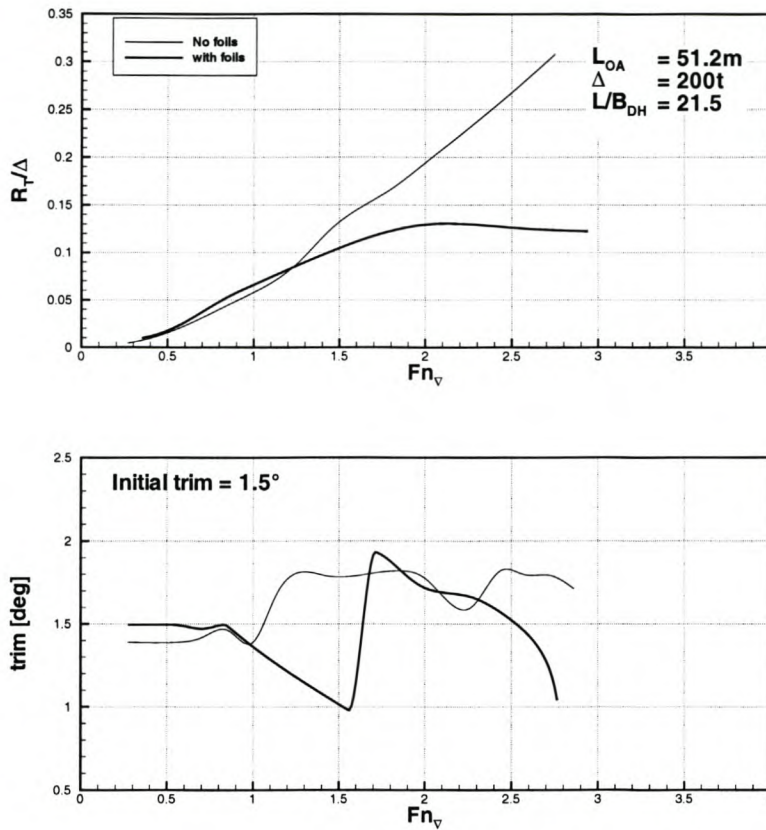


Figure 6.19: Resistance and trim comparison for the HC200A model

The Length to Beam Ratio L/B_{DH}

The length to beam ratio of a hull usually correlates very closely with the length-displacement ratio. One can therefore expect decreased resistance in the displacement phase and transition phase with increasing length to beam ratio. Making use of extremely slender hulls such as for example the Hitachi Zosen vessels described in Section 1.4.1 is beneficial for reducing suction. From the model test data of the slender Hitachi hullform (HC200A model) ($L/\nabla^{1/3} = 8.0$; $L/B_{DH} = 21.5$) shown in Figure 6.19, it can be seen that the sudden increase in trim occurring once the foils overcome suction, occurs at $F_n_\nabla = 1.6$, a vast improvement over conventional hullforms ($L/B_{DH} = 10 - 14$).

The Block Coefficient C_B

Small values for the block coefficient relate to increased buttock curvature for the hull. The optimum value of block coefficient of high-speed conventional catamarans is $C_B \approx 0.4 - 0.5$ [BLSZ95a, BLSZ95b], with decreasing values of C_B as Froude number increases up to $Fn_{\nabla} = 1.5$, as this relates to the optimum ratio of internal volume versus wetted area. For $Fn_{\nabla} > 1.5$, the optimum C_B remains at about 0.4 for craft with dynamic support but can be increased as this is useful for taking advantage of dynamic lift (i.e. flat buttock lines aft result in a higher C_B).

In the displacement phase the optimum C_B is similar to a conventional catamaran ($C_B = 0.4$). To take advantage of hydrodynamic lift and reduce suction in the transition phase, the optimum block coefficient for hydrofoil-assisted catamarans lies at the upper end of the optimum range: $C_B = 0.5$. The block coefficient has minimal influence on resistance during planing and need not be considered.

The Transom Submergence Ratio A_T/A_X

The ratio of the submerged transom area (A_T) to the maximum sectional area (A_X), is strongly related to the aft buttock curvature of the hull. A smaller transom submergence ratio is beneficial for reducing resistance of semi-displacement vessels and therefore also for reducing resistance in the displacement phase of hydrofoil-assisted catamarans. Evaluating the submergence ratios of a number of optimized semi-displacement catamarans in commercial use, show that the optimum lies at $A_T/A_X = 0.6 - 0.9$, with values increasing for volumetric Froude numbers above $Fn_{\nabla} = 1.5$. Hydrofoil-assisted catamarans have optimal values of transom submergence ratio $A_T/A_X = 0.8 - 1.0$, as this eliminates excessive buttock curvature ($A_T/A_X = 1.0$ signifying buttocks without curvature), but allows a high running trim angle to be taken up at speed with an appropriate LCG position.

Demi-Hull Separation Ratio B_T/B_{DH}

Demi-hull separation is an important parameter in the hump speed range [Mig97]. Increasing demi-hull separation reduces the hump resistance as well as shifting the resistance hump to a slightly higher speed [PAE⁺95]. The interference effects are caused by wave-making interactions between the demi-hulls [IM91] as well as by an increase in the flow velocity (about 5% at displacement speeds) around the demi-hulls [Miy79]. As forces are proportional to V^2 , catamarans with narrow demi-hull spacing will suffer higher suction forces. Perhaps more importantly, narrower demi-hull spacing limits the aspect ratio of the hydrofoils thus decreasing their efficiency. Hydrofoil-assisted catamarans that have wide demi-hull separation ratios have shown good efficiency (for example the Superjet30 described in Section 1.4.1) and those

designs with small demi-hull separation ratios less improvements (for example the Channel hydrofoil boats described in Section 1.3.4).

Other hullform parameters tend to be similar for both conventional and hydrofoil-assisted catamarans. The geometry of the SD6 and SD7 hullforms are considered by the author to be close to the optimum shapes for hydrofoil-assisted catamarans based on conventional high-speed catamaran lines. These hullforms together with a highly efficient hydrofoil system designed on the principles presented in the previous chapter allow for efficiencies that are not achievable for conventional catamarans or conventional hydrofoil craft [MHK01].

Chapter 7

Conclusions

This chapter is divided into three parts. The first part summarizes the main conclusions of this study. The detailed conclusions section follows and lists more specific conclusions that have been drawn from different parts of this study. Finally recommendations for future work are presented.

7.1 Main Conclusions

1. The design and hydrodynamic characteristics of a large number of existing semi-displacement, semi-planing and planing hydrofoil-assisted catamarans have been studied. Evaluation of the transport efficiency of these craft in comparison with conventional catamarans and hydrofoil craft shows that hydrofoil-assisted catamarans can offer superior efficiencies to both catamarans and hydrofoils in the volumetric Froude number range $Fn_{\nabla} \geq 2.0$. For lower Froude numbers hydrofoil-assisted catamarans can be designed so that their efficiencies are not worse than those for conventional catamarans.
2. The model tests conducted in this study have shown that three specific phases exist in the operating speed range of hydrofoil-assisted catamarans. These have been classified as displacement, transition and planing phases and each phase implies specific resistance and attitude characteristics for the vessel based on the extent of the hydrodynamic forces generated by the hull and the foils. It has been found that useful resistance improvements using hydrofoil-assistance is possible for catamarans operating in the transition and planing phases.
3. Extensive model tests for different hull shapes and hydrofoil-configurations conducted during this study indicate that while model testing is a necessary part of the design process, its accuracy in predicting the performance of full-scale vessels cannot be considered as accurate as that achievable for displacement craft

when using relatively small models. The primary difficulty lies in viscous scale effects due to dissimilar flow conditions (laminar as opposed to turbulent) over the hydrofoils, which results in increased profile drag and decreased lift for the hydrofoils if relatively small models are used. These effects cannot be properly accounted for in the scaling procedure. Model testing therefore requires experience in performing the tests using suitable turbulence stimulation as well as incorporation of special procedures for scaling up the model test data to full scale, for which the accuracy can be expected to be in the order of 5-15%.

4. The use of suitable theoretical methods plays an important part in the design of hydrofoil-assisted vessels. In this study a non-linear vortex lattice method has been developed and comparison with suitable model test data has shown that the method is suitable for quantitatively modeling the hydrodynamics of such craft and can be usefully applied as design and optimization tool.
5. The foil lift fraction is identified as the most important hydrofoil design parameter to consider. At least 20%, of the weight needs to be supported on foils to obtain resistance improvements over the bare hull, although it is usually more beneficial to consider higher foil lift fractions (50-90%). Use of such high foil lift fractions requires consideration for directional and pitch-heave instabilities.
6. The resistance of the majority of catamaran hullforms can be reduced with hydrofoil-assistance. The extent of the resistance improvements depends to a large extent on the geometry of the hull. In general, those hulls that suffer from high wave-making resistance are easiest to improve, while highly efficient hullforms tend to experience less improvement unless the hull is lifted largely clear of the water. Symmetrical, hard chined demi-hulls with minimal aft buttock curvature and a suitably rearward LCG (in comparison to that used on conventional catamarans) are the most suitable for hydrofoil assistance.
7. The results of this study have contributed to the recent design and construction of a number of hydrofoil-assisted craft. Some of these have been described in Chapter 1 (Figures 1.2 and 1.3). The most recent applications are described by Hoppe [Hop01] and their main particulars are given in Table C.2 on page 220. The development of these craft proves the usefulness of this study and the information contained herein for design purposes. It can be concluded that the results of this study are useful and have fulfilled the aim of this study: successful hydrodynamic design of hydrofoil-assisted catamarans.

7.2 Detailed Conclusions

1. The available literature shows that most of the new developments to date follow similar paths in that they rely on extensive testing of towing tank and sometimes

manned models to arrive at a suitably working hydrofoil-assist system for a given hull. Relatively few have considered optimizing the hull and foil system together. Such developments show that most designers often have limited understanding of the hydrodynamic principles governing performance of such vessels and the present study should be of value to designers.

2. The hydrodynamics of hydrofoil-assisted catamarans is the most complicated in the transition phase, which covers the design speeds of the majority of semi-displacement type catamarans used in the fast ferry industry. The transition phase is characterized by large variations in resistance and attitude for the craft with speed for those craft designed to carry a large fraction of the craft weight on foils. These are due to interaction between negative suction pressures acting on the hull and the positive lift forces of the hydrofoils.
3. To improve the accuracy of model tests it is necessary to consider the viscous scale effects on the hydrofoils. Accounting for viscous scale effects is best achieved by making use of a 2D panel method that incorporates boundary layer theory such as XFOIL. Such methods still underestimate the drag increase and lift loss but provide a quantitative means for estimating these effects in absence of better methods. Making use of trip wires for turbulence stimulation is recommended for improving the XFOIL predictions.
4. For certain hydrofoils in extreme free surface effect the scale effects disappear. This is due to the increase in pressure and subsequent reduction in the pressure gradients on the upper side of a hydrofoil close to the free surface. This applies in particular to foil profiles that are asymmetrical with a flat lower surfaces. Such conditions are usually found in the planing phase of operation. For other profiles which have lower side curvature, the free surface effect is less marked.
5. It is well known that theoretical methods often provide more accurate estimates of hydrofoil forces than model tests. The use of the vortex lattice method that includes models for the wake roll-up process and also for the non-viscous interactions between the hull and the foils is suitable to capture the hydrodynamics of these craft sufficiently for resistance prediction with accuracy at least as good as that achievable with model tests.
6. For the planing phase a simplified computational model can be used as hull-foil interactions are less important. The planing hull can then be modeled using the similarity between a lifting wing and a planing surface. Such a model is found to be useful for optimization at high speed.
7. The interactions between the hull and the hydrofoils as well as between multiple foils can favorably be used to optimize certain designs. In particular, optimal spacing of the hydrofoils for wave cancellation and also positioning of the foils to maximize the hull lift can provide useful benefits in performance.

7.3 Recommendations for Future Work

The resistance components and the main parameters influencing design of hydrofoil-assisted catamarans have been presented in this study. The hydrodynamic design of hydrofoil systems as well as hull-foil interactions are reasonably well understood. Further research should therefore focus on the design and development of suitable novel hullforms that are less prone to suction and do not suffer from instabilities or high low-speed resistance.

Theoretical methods also need to be further validated to establish their reliability for varying hull and hydrofoil configurations. In particular development of the non-linear methods for modeling transition speeds needs to be further developed and improved.

Stability theory for hydrofoil-assisted catamarans needs to be developed to better understand the inception of pitch-heave instabilities.

Further development of experimental techniques and methods for scaling model test data is needed. In particular methods for avoiding flow separation at low Reynolds numbers as well as methods for accurately calculating the scale effects. The use of special profiles differing from those that would be used on prototype ships may offer a solution. Such profiles could be designed to limit laminar separation and thus have more predictable lift and drag characteristics at low Reynolds numbers.

Appendix A

Convergence of Numerical Schemes

A.1 Introduction

In this section investigations concerning the convergence of the vortex lattice method described in Chapter 4 and implemented in the AUTOWING code is presented. These investigations have been done for hydrofoil and hulls typical of those hydrofoil-assisted catamarans investigated in this study.

A.2 Application of AUTOWING for Hydrofoils

The steps used in AUTOWING for solving the flow around a hydrofoil and calculating the resulting forces is outlined in the flowchart of Figure 4.5. Calculation of the vortex intensities, the roll-up process and the deformation of the free surface all depend on the sizes of the panels used to represent the continuous vortex sheets on the hydrofoils, vortex wakes and the free surface.

Kornev and Taranov [KT99] have presented the results of some convergence investigations for a hydrofoil under the free surface with the same vortex method used in this study. Their investigations showed that:

1. The free surface computational domain should start at least two chord lengths ahead of the leading edge of the foil.
2. The aft end of the computational domain has negligible influence if the aft end of the computational domain is ten chord lengths downstream of the hydrofoil.
3. Approximately 70 iterations are needed for convergence of the free surface shape.

Further, the results of Kornev and Taranov show good agreement with experiments for the free surface elevation. Other convergence investigations done in this study are presented in the sections that follow.

A.2.1 Numerical Convergence

To obtain results that are independent of panel density and iteration numbers, tests were conducted to determine the following:

- the vortex lattice density for hydrofoils
- free surface panel size to calculate foil forces

Each of these tests is described in more detail in the following sections.

Hydrofoil Vortex Lattice Density for Hydrofoils

It is well known that the lift and drag characteristics of a wing are sensitive to the vortex panel density over the foil. Foil lift and drag is sensitive to both span and chordwise panel density as well as the geometry of the hydrofoil: in general, swept and tapered hydrofoils require higher panel densities and a larger number of iterations to obtain convergence [Wal99]. To improve convergence, a number of numerical tricks can be introduced, such as cosine spacing of panels over the chord length of the foil, a tip inset of the outermost panel [Hou73, Hou76, DeJ76] and free surface panel clustering at the position of the foil [TB98].

The disadvantage of such numerical tricks is that it is more difficult to construct suitable grids for complex geometries consisting of more than one foil. For this reason AUTOWING does not include the tip inset or a cosine spacing of chordwise elements but does include free surface panel clustering. Initial convergence tests were conducted to establish panel density for Hysuwac type hydrofoils being used in this study. These were done in the presence of the free surface but using a large Froude number approximation¹ to model the free surface. This way the influence of free surface panel size is eliminated.

Figure A.1 and A.2 show the influence of span and chordwise panel density on drag and lift respectively. The results show that drag is fairly independent of spanwise number of elements but is quite sensitive to chordwise number of elements for the configuration being used here. 32 chordwise elements is the minimum number that is

¹The large Froude number approximation to model the free surface boundary condition allows one to assume that the velocity on the free surface is equal to the freestream velocity. It is therefore possible to model the free surface by a system of negative images (see for example: [BSK⁺98]) of the hydrofoil.

required for the drag coefficient to converge. The lift coefficient is sensitive to both chord and spanwise number of elements although only slightly. Figure A.2 indicates that at least 24 chordwise elements are needed while 12 spanwise elements are needed to ensure convergence. Considering both lift and drag at least 12 spanwise elements are needed while 32 chordwise elements are needed.

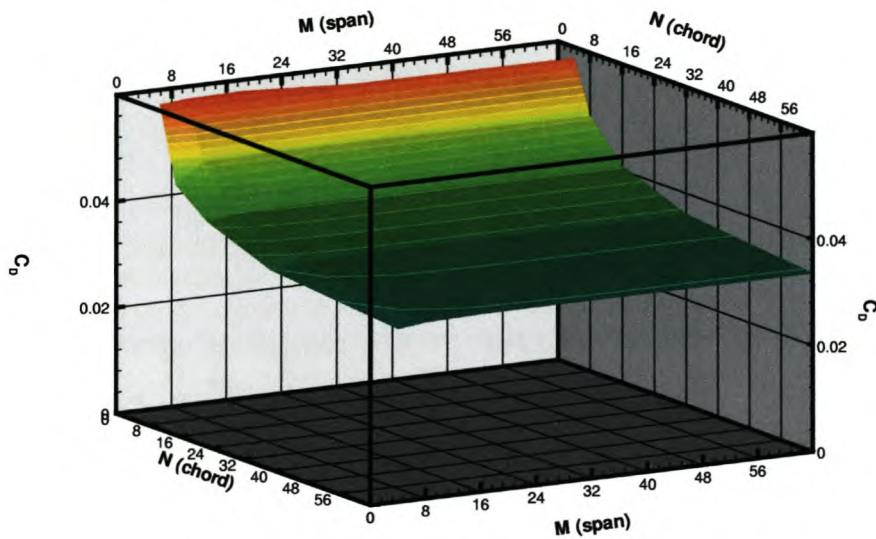


Figure A.1: Drag coefficient as a function of span and chord panel density

Further convergence investigations were done to investigate the influence of the free surface on the required panel density, a number of calculations were done varying the hydrofoil panel densities and also the submergence of the hydrofoil. These results are presented in Figures A.3 and A.4 for variations in spanwise and chordwise panel densities respectively.

The results show that the free surface has only a slight influence on the convergence characteristics. The only significant difference with the previous results is that at least 40 chordwise panels are needed to ensure convergence of the hydrofoil drag coefficient close to the free surface. As before, 12 spanwise panels are needed to

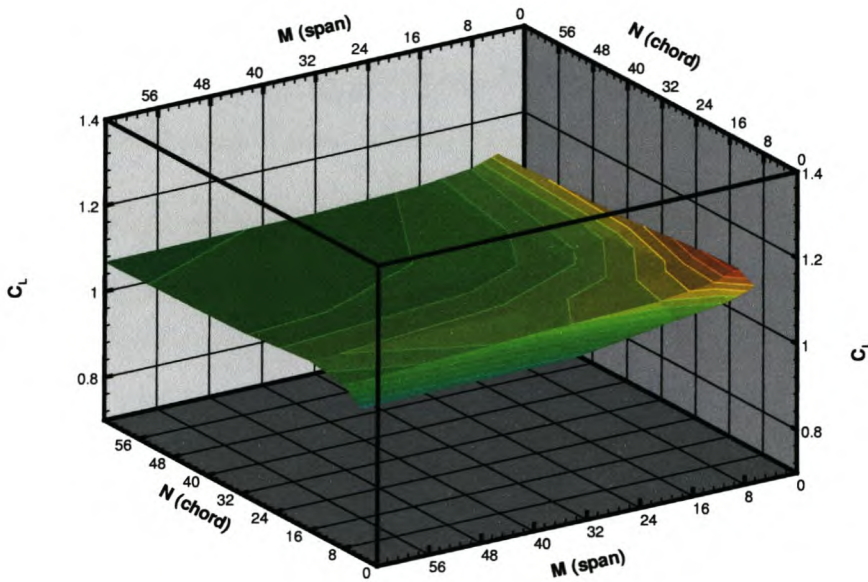


Figure A.2: Lift coefficient as a function of span and chord panel density

ensure convergence.

Free Surface Panel Density

The free surface panel density affects both the shape of the free surface as well as the foil forces. It is fair to assume that the free surface panel density required for convergence varies with submergence of the hydrofoil. For this reason, investigations of the free surface panel size Dx on hydrofoil forces were done for submergences of $h/c = 0.125, 0.5, 1.0$ and 1.44 . The results for lift and drag are presented in Figures A.5 and A.6 respectively.

The figures clearly show that a higher free surface panel density is needed for shallower submergences to obtain convergence. The lift coefficient converges relatively quickly and is not highly dependent on free surface panel size. In contrast, the drag coefficient

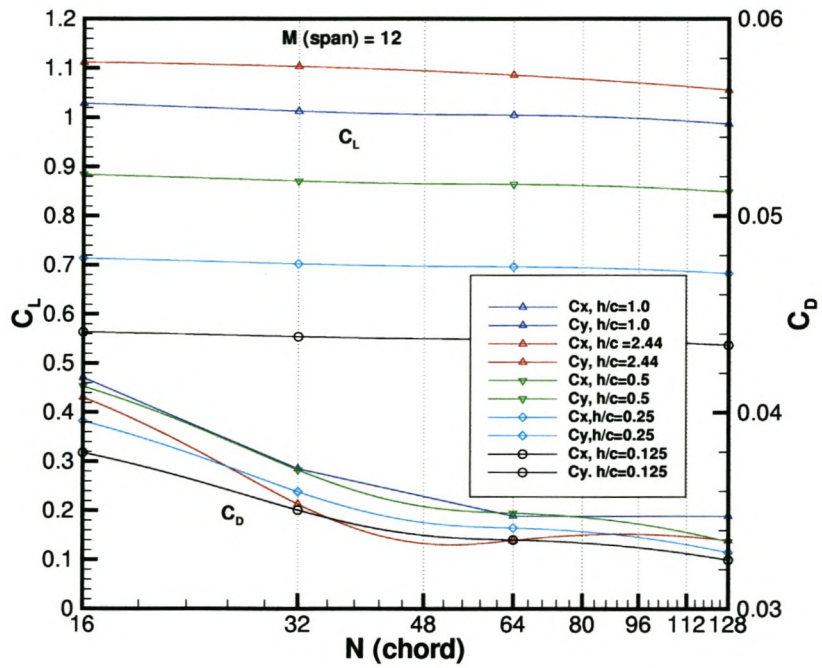


Figure A.3: Lift and drag as a function of chordwise panel density and submergence.

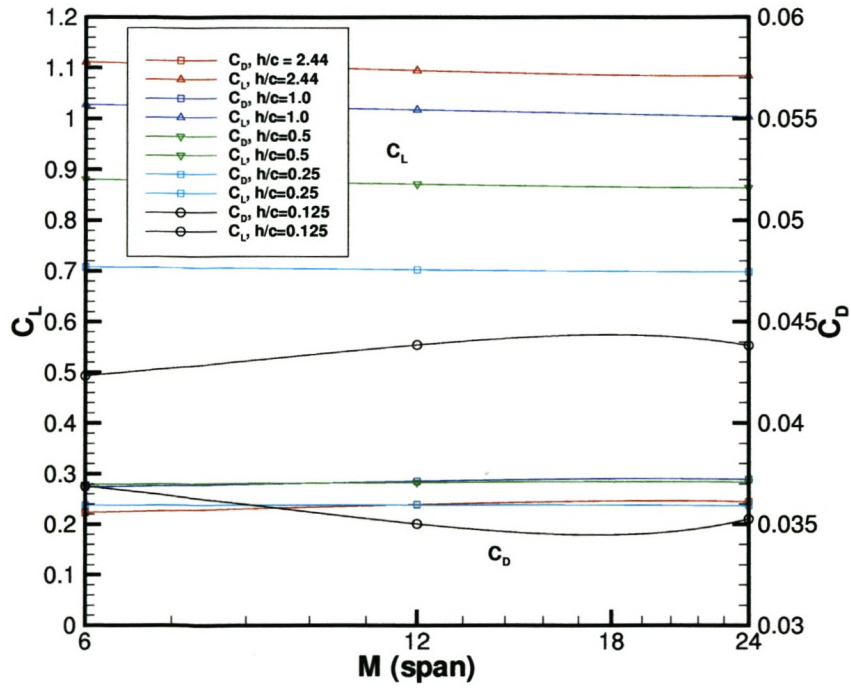


Figure A.4: Lift and drag as a function of spanwise panel density and submergence.

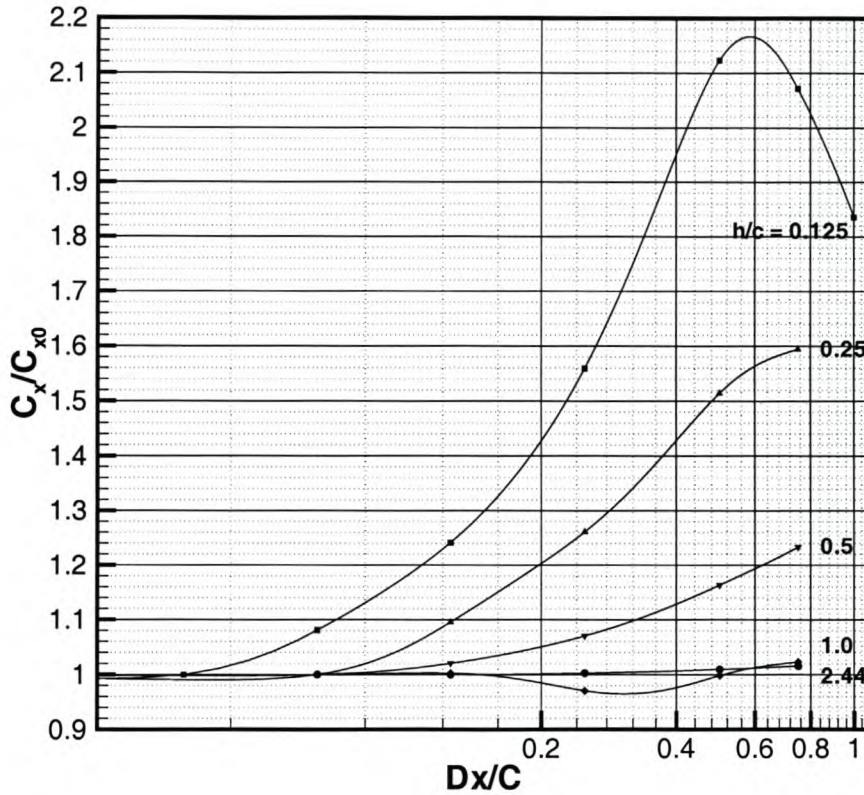


Figure A.5: Variation of drag coefficient with panel size

is very sensitive to the free surface panel density and shows that even for 20 free surface panels per chord length the drag has not fully converged for submergences, $h/c < 0.5$.

To calculate the free surface deformation takes approximately 45 hours for $Dx/C = 0.05$ with a reasonably small computational domain ($length = 20C$; $span = 10C$). The use of such small free surface panels is impractical for design purposes especially when computational domains of at least 40 chord lengths are needed for computing a hydrofoil-assisted catamaran flow field. To reduce the amount of computation time needed, tendency curves for very fine free surface panels were established. For the finest free surface mesh solution of the hydrofoil forces one requires about six weeks computation time. The tendency curves both for lift and drag allow an empirical correction to be introduced for the drag and lift coefficient when larger free surface grids are used. The tendencies of Figures A.5 and A.6 have been implemented in a spreadsheet used to analyze the numerical results (see Appendix B) and are used to correct the hydrofoil forces.

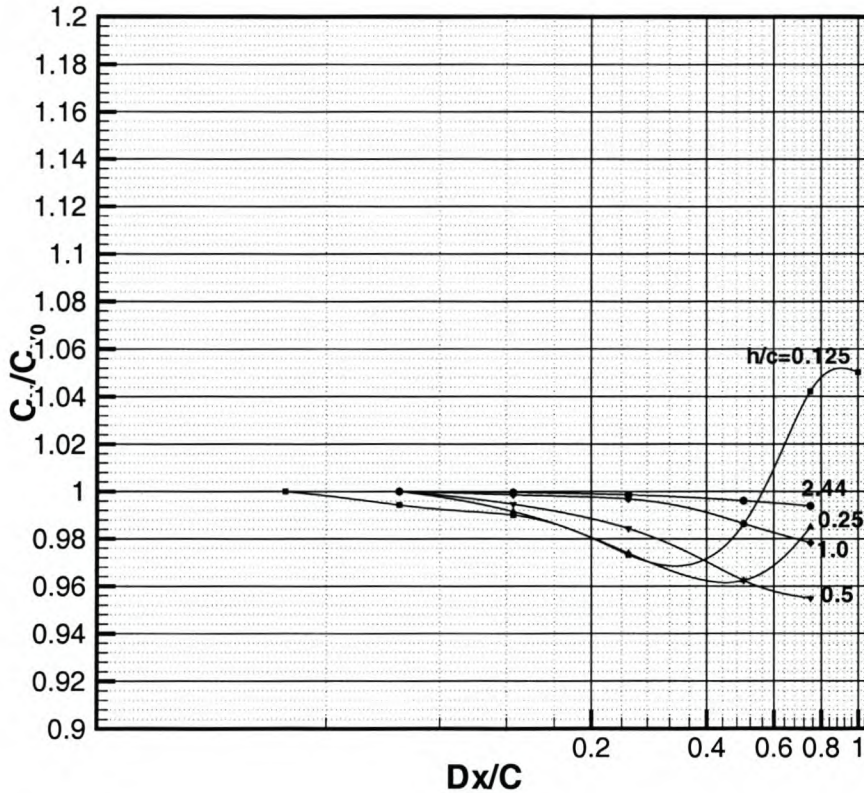


Figure A.6: Variation of lift coefficient with panel size

A.3 Validation of AUTOWING for Planing Hulls

Similar to the requirements for hydrofoils, convergence of the forces acting on a planing surface when using Wagner's wing analogy [Wag32] also need to be established. A number of calculations were performed with the SD6 demi-hull to determine the required lattice density for a typical planing catamaran.

These tests were done for a number of sinkage and trim angles that result in varying length to beam ratios for the wetted planing surface. It is well known that this parameter is important in lift to drag ratio of planing hulls and therefore might be important in terms of convergence. Figure A.7 shows the results of the chord-wise panel spacing for the SD6 hull for different pitch angles. The results are given in reference to those obtained for the highest panel density, $M = 200$.

The result show that for positive trim angles ($\tau = 1.0$ and 2.0) approximately 50

panels per chord are needed to ensure convergence. This result is very similar to that found for hydrofoils. For zero running trim angle ($\tau = 0.0$) convergence is not achieved for the lift coefficient and LCP even for $M = 200$. At this low trim angle the dynamic forces acting on the hull are negative and therefore, strictly speaking, the assumption of planing is no longer valid. It can therefore be said that the planing model is suitable only if the dynamic forces acting on the hull are positive and then at least 50 panels per chord length should be used.

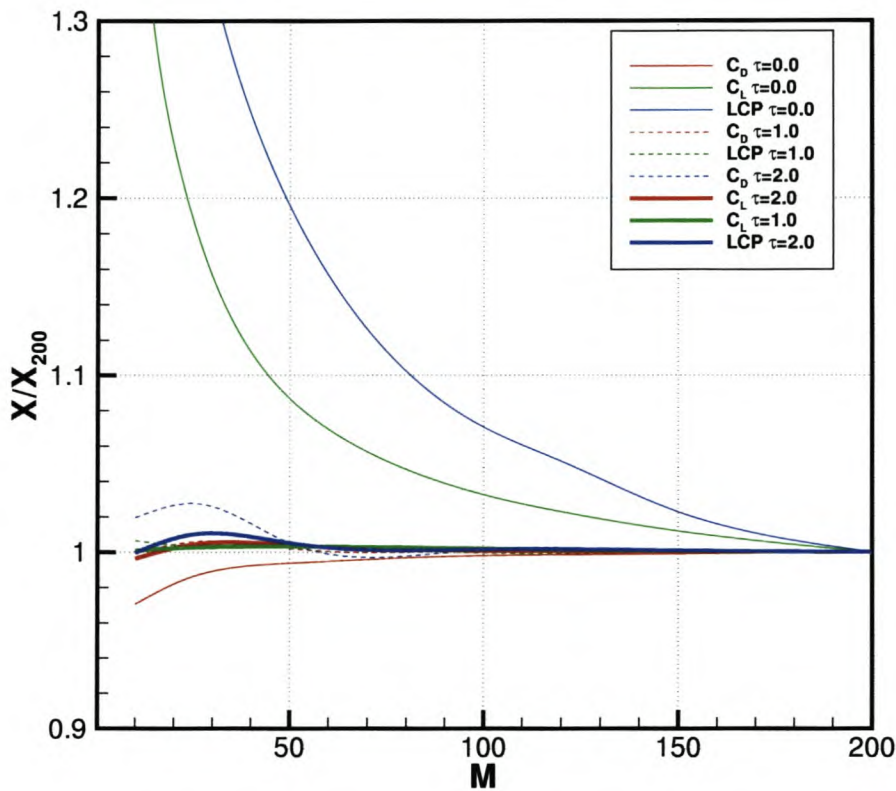


Figure A.7: C_D , C_L and LCP as a function of chord-wise panel density for planing hulls

As explained in Chapter 4, the planing surface is divided into a large number of longitudinal strips (or chords) for which the chordwise panel density is specified. The number of spanwise strips is dictated by the need to accurately determine the wetted area. If the leading edge of the wetted area has a sufficiently curvilinear leading edge, a large number of longitudinal strips are needed. The number of longitudinal strips has little influence on convergence of the numerical result as shown in Figure A.8.

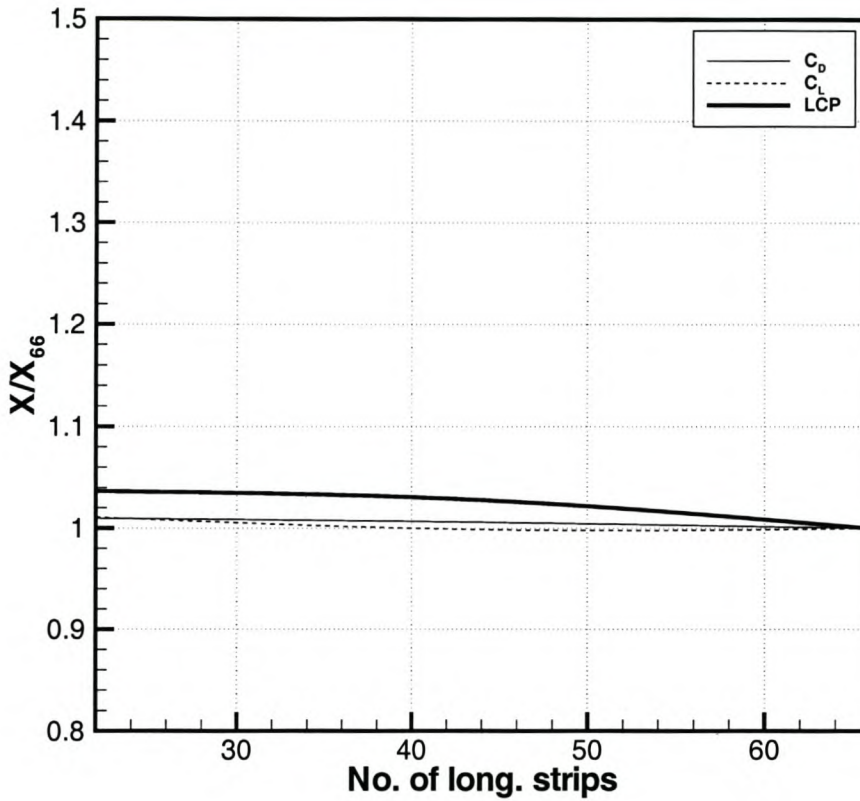


Figure A.8: Drag, lift and centre of pressure as a function of span wise number of longitudinal strips

A.4 Application of Transition Speed Model

The numerical method for modeling hydrofoil-assisted catamarans operating in the transition phase has been presented in Chapter 4. A number of different parameters define the paneling of the hull, hydrofoils and the free surface. The required panel densities for the hydrofoils has been established and described in the previous section. Still required are the panel densities for the hull and the free surface.

The computational domain is defined by specifying a number of different parameters, which are listed below.

1. X_{inlet} , X_{outlet} the longitudinal coordinates of the computational domain.
2. The width of the computational domain.

3. The number of panels along the hull.
4. The number of panels across the hull.
5. The number of panels along the X-axis in front of the ship.
6. The total number of panels along the X-axis.
7. The number of panels on the free surface to the right and left of the hull.

The longitudinal spacing of the free surface panels has been set up so that the free surface panels are equal in size to the hull panels. Only ahead of the hull and behind the transom can the panel sizes differ to those of the hull.

All the parameters defining the computational domain were systematically investigated keeping in mind that high panel densities would be required to resolve the hydrofoil forces accurately.

Investigations for the size of the computational domain showed that the computational domain needs to extend approximately half a ship length in front of the hull and a similar amount behind the hull. Extending the computational domain farther showed no change in the calculated forces. This result is different to that of KELVIN, where it was recommended that the computational domain should increase in length behind the hull as speed increases. This difference is most likely due to the fully-non linear boundary condition being solved by KELVIN and a linear boundary condition being solved by AUTOWING.

Keeping in mind that a high hull panel density would be required to capture the hull-foil interactions, it was felt that the panel size should be at least half a chord length or 80 panels on the hull. This panel density was found to fulfill convergence requirements. Lateral panel dimensions were chosen to be similar to the dimensions needed to model the foils, i.e. 12 panels over the span of the foil. Increasing or decreasing the panel size in this range was found to have negligible influence on the forces and did not need further consideration.

Appendix B

Numerical Results Spreadsheet

This appendix gives an example of the spreadsheet developed for evaluating numerical results, so that a design can be analyzed.

The results from each of the 5 calculations described in Chapter 4 on page 120 are entered into a separate table (see pages 214 and 215). From these inputs, the force coefficients and LCP values for each lifting surface is calculated (page 216). The calculated numerical forces are corrected for any discretization errors that may arise from course panel arrangements as described in Appendix A. The various interference effects between the hull and the foils are also calculated and represented. Finally the total resistance prediction and LCPs are calculated (page 217).

APPENDIX B. NUMERICAL RESULTS SPREADSHEET

N	V	pitch	subm.	Rear foil planing behind front foil								
				Total Force and Moment coeff.			Hydrost. forces on planing surface			Force on Planing Surface		
				Cx	Cy	Mz	Cx	Cy	Mz	Cx	Cy	Mz
1	19.49	1.321	-0.426	-0.05688	1.58316	23.70001	0	0	0	-0.03051	0.82279	3.20422
2	20.13	1.415	-0.48	-0.0584	1.58492	23.80562	0	0	0	-0.03151	0.82034	3.19436
3	20.23	1.782	-0.486	-0.06392	1.63815	24.62336	0	0	0	-0.03482	0.84842	3.31482
4	23.46	2.545	-0.767									
5	25.52	2.414	-0.864									
6	0	0	0									
7	0	0	0									
8	0	0	0									
9	0	0	0									
10	0	0	0									

N	V	pitch	subm.	Hull +Rear foil planing behind front foil											
				Total Force and Moment coeff.			Forces on configuration (+suc.)			Hydrost. forces on planing surface			sum rear foil lifting surface 1 to n		
				Cx	Cy	Mz	Cx	Cy	Mz	Cx	Cy	Mz	Cx	Cy	Mz
1	19.49	1.321	-0.426	-0.11325	1.87202	26.53096	n/a	n/a	n/a	-0.00376	0.18195	1.62538	-0.01446	0.42317	1.65237
2	20.13	1.415	-0.48	-0.1055	1.80367	25.76538	n/a	n/a	n/a	-0.00225	0.12163	1.02516	-0.01621	0.42001	1.6393
3	20.23	1.782	-0.486	-0.09983	1.85307	26.13535	n/a	n/a	n/a	-0.00145	0.09103	0.624276	-0.01676	0.4357	1.70586
4	23.46	2.545	-0.767												
5	25.52	2.414	-0.864												
6	0	0	0												
7	0	0	0												
8	0	0	0												
9	0	0	0												
10	0	0	0												

N	V	pitch	subm.	Hull only behind front foil								
				Total Force and Moment coeff.			Hydrost. forces on planing surface					
				Cx	Cy	Mz	Cx	Cy	Mz			
1	19.49	1.321	-0.426	-0.08449	0.94565	22.79416	-0.00373	0.18125	1.61996			
2	20.13	1.415	-0.48	-0.07531	0.89175	22.11609	-0.00223	0.1208	1.01876			
3	20.23	1.782	-0.486	-0.06545	0.92171	22.39987	-0.0014	0.08984	0.61427			
4	23.46	2.545	-0.767									
5	25.52	2.414	-0.864									
6	0	0	0									
7	0	0	0									
8	0	0	0									
9	0	0	0									
10	0	0	0									

N	V	pitch	subm.	wave resistance calculations						
				Michiel calculation			kevin calculation			
				Rv [kN]	Rw [kN]	Rwater [kN]	Rv [kN]	Rw [kN]		
1	19.49	1.321	-0.426	37.738833	0.775345	0.102445				
2	20.13	1.415	-0.48	37.233	0.564418	0.06449				
3	20.23	1.782	-0.486	36.543	0.588981	0.068324				
4	23.46	2.545	-0.767							
5	25.52	2.414	-0.864							
6	0	0	0							
7	0	0	0							
8	0	0	0							
9	0	0	0							
10	0	0	0							

APPENDIX B. NUMERICAL RESULTS SPREADSHEET

Front Foil Forces (potential flow calc.)

N	V [m/s]	pitch [deg]	subm. [m]	total			viscous			suction			hydraulic					
				drag Cx	lift Cy	LCP [m]	drag Cx	lift Cy	LCP [m]	drag Cx	lift Cy	LCP [m]	drag Cx	lift Cy	LCP [m]			
1	19.49	1.321	-0.426	-0.02637	0.76037	26.9550219	-0.01425	0.7584	26.90712022	-0.01212	0	n/a	0.02575	0	n/a	0	0.001969	26.89791772
2	20.13	1.415	-0.48	-0.02889	0.76548	26.9292983	-0.01483	0.76273	26.91363916	-0.01206	0	n/a	0.02537	-1E-05	n/a	0	0.001846	26.89493971
3	20.23	1.782	-0.486	-0.0291	0.78973	26.94205716	-0.01704	0.7879	26.9374413	-0.01206	0	n/a	0.0246	0	n/a	0	0.001828	26.89156443
4	23.46	2.545	-0.767	0	0	#DIV/0!	0	0	#DIV/0!	0	0	n/a	0	0	n/a	0	0	#DIV/0!
5	25.52	2.414	-0.864	0	0	#DIV/0!	0	0	#DIV/0!	0	0	n/a	0	0	n/a	0	0	#DIV/0!
6	0	0	0	0	0	#DIV/0!	0	0	#DIV/0!	0	0	n/a	0	0	n/a	0	0	#DIV/0!
7	0	0	0	0	0	#DIV/0!	0	0	#DIV/0!	0	0	n/a	0	0	n/a	0	0	#DIV/0!
8	0	0	0	0	0	#DIV/0!	0	0	#DIV/0!	0	0	n/a	0	0	n/a	0	0	#DIV/0!
9	0	0	0	0	0	#DIV/0!	0	0	#DIV/0!	0	0	n/a	0	0	n/a	0	0	#DIV/0!
10	0	0	0	0	0	#DIV/0!	0	0	#DIV/0!	0	0	n/a	0	0	n/a	0	0	#DIV/0!

Rear Foil Forces: rear foil only behind front foil (pot. flow calc.)

N	V [m/s]	pitch [deg]	subm. [m]	total			viscous			suction			hydraulic					
				drag Cx	lift Cy	LCP [m]	drag Cx	lift Cy	LCP [m]	drag Cx	lift Cy	LCP [m]	drag Cx	lift Cy	LCP [m]			
1	19.49	1.321	-0.426	-0.03068	0.68486	3.91080071	-0.02647	0.680983	3.786907544	-0.00861	0	n/a	0.02153	-0.000737	n/a	0	0.001908	3.979393203
2	20.13	1.415	-0.48	-0.03702	0.68127	3.907731448	-0.02745	0.677627	3.782594256	-0.00857	0	n/a	0.02151	-0.001573	n/a	0	0.001797	3.958263772
3	20.23	1.782	-0.486	-0.03983	0.71149	3.920434581	-0.03008	0.707892	3.840639533	-0.00855	0	n/a	0.02142	-0.000628	n/a	0	0.001777	3.979096045
4	23.46	2.545	-0.767	0	0	#DIV/0!	0	0	#DIV/0!	0	0	n/a	0	0	n/a	0	0	#DIV/0!
5	25.52	2.414	-0.864	0	0	#DIV/0!	0	0	#DIV/0!	0	0	n/a	0	0	n/a	0	0	#DIV/0!
6	0	0	0	0	0	#DIV/0!	0	0	#DIV/0!	0	0	n/a	0	0	n/a	0	0	#DIV/0!
7	0	0	0	0	0	#DIV/0!	0	0	#DIV/0!	0	0	n/a	0	0	n/a	0	0	#DIV/0!
8	0	0	0	0	0	#DIV/0!	0	0	#DIV/0!	0	0	n/a	0	0	n/a	0	0	#DIV/0!
9	0	0	0	0	0	#DIV/0!	0	0	#DIV/0!	0	0	n/a	0	0	n/a	0	0	#DIV/0!
10	0	0	0	0	0	#DIV/0!	0	0	#DIV/0!	0	0	n/a	0	0	n/a	0	0	#DIV/0!

Rear Foil Forces: rear foil only (planing calc. after front foil)

N	V [m/s]	pitch [deg]	subm. [m]	total			viscous			suction			hydraulic					
				drag Cx	lift Cy	LCP [m]	drag Cx	lift Cy	LCP [m]	drag Cx	lift Cy	LCP [m]	drag Cx	lift Cy	LCP [m]			
1	19.49	1.321	-0.426	-0.03051	0.82279	3.884335128	n/a	n/a	n/a	n/a	n/a	n/a	n/a	n/a	n/a	0	0	0
2	20.13	1.415	-0.48	-0.03151	0.82034	3.893846412	n/a	n/a	n/a	n/a	n/a	n/a	n/a	n/a	n/a	0	0	0
3	20.23	1.782	-0.486	-0.03482	0.84842	3.907080783	n/a	n/a	n/a	n/a	n/a	n/a	n/a	n/a	n/a	0	0	0
4	23.46	2.545	-0.767	0	0	#DIV/0!	n/a	n/a	n/a	n/a	n/a	n/a	n/a	n/a	n/a	0	0	0
5	25.52	2.414	-0.864	0	0	#DIV/0!	n/a	n/a	n/a	n/a	n/a	n/a	n/a	n/a	n/a	0	0	0
6	0	0	0	0	0	#DIV/0!	n/a	n/a	n/a	n/a	n/a	n/a	n/a	n/a	n/a	0	0	0
7	0	0	0	0	0	#DIV/0!	n/a	n/a	n/a	n/a	n/a	n/a	n/a	n/a	n/a	0	0	0
8	0	0	0	0	0	#DIV/0!	n/a	n/a	n/a	n/a	n/a	n/a	n/a	n/a	n/a	0	0	0
9	0	0	0	0	0	#DIV/0!	n/a	n/a	n/a	n/a	n/a	n/a	n/a	n/a	n/a	0	0	0
10	0	0	0	0	0	#DIV/0!	n/a	n/a	n/a	n/a	n/a	n/a	n/a	n/a	n/a	0	0	0

Rear Foil Forces: rear foil combined with hull (planing calc. after front foil)

N	V [m/s]	pitch [deg]	subm. [m]	total			viscous			suction			hydraulic					
				drag Cx	lift Cy	LCP [m]	drag Cx	lift Cy	LCP [m]	drag Cx	lift Cy	LCP [m]	drag Cx	lift Cy	LCP [m]			
1	19.49	1.321	-0.426	-0.017	0.847511	3.988300892	-0.00739	0.845603	3.908146021	-0.00861	0	n/a	0.02153	0	n/a	0	0.001908	3.979393203
2	20.13	1.415	-0.48	-0.02048	0.840244	3.910427209	-0.01091	0.838447	3.910324684	-0.00857	0	n/a	0.02151	0	n/a	0	0.001797	3.958263772
3	20.23	1.782	-0.486	-0.02165	0.872542	3.918184396	-0.0121	0.870772	3.918040543	-0.00855	0	n/a	0.02142	0	n/a	0	0.001777	3.979096045
4	23.46	2.545	-0.767	0	0	#DIV/0!	0	0	#DIV/0!	0	0	n/a	0	0	n/a	0	0	#DIV/0!
5	25.52	2.414	-0.864	0	0	#DIV/0!	0	0	#DIV/0!	0	0	n/a	0	0	n/a	0	0	#DIV/0!
6	0	0	0	0	0	#DIV/0!	0	0	#DIV/0!	0	0	n/a	0	0	n/a	0	0	#DIV/0!
7	0	0	0	0	0	#DIV/0!	0	0	#DIV/0!	0	0	n/a	0	0	n/a	0	0	#DIV/0!
8	0	0	0	0	0	#DIV/0!	0	0	#DIV/0!	0	0	n/a	0	0	n/a	0	0	#DIV/0!
9	0	0	0	0	0	#DIV/0!	0	0	#DIV/0!	0	0	n/a	0	0	n/a	0	0	#DIV/0!
10	0	0	0	0	0	#DIV/0!	0	0	#DIV/0!	0	0	n/a	0	0	n/a	0	0	#DIV/0!

Hull Planing Forces: Hull only (planing Calc. after front foil)

N	V [m/s]	pitch [deg]	subm. [m]	total			viscous			suction			hydraulic					
				drag Cx	lift Cy	LCP [m]	drag Cx	lift Cy	LCP [m]	drag Cx	lift Cy	LCP [m]	drag Cx	lift Cy	LCP [m]			
1	19.49	1.321	-0.426	-0.05812	0.18528	12.40484672	-0.05439	0.00403	168.3399504	-0.00373	0.18125	8.937710345	0	0	#DIV/0!	0	0	#DIV/0!
2	20.13	1.415	-0.48	-0.04842	0.12627	11.91735781	-0.04619	0.00547	88.86106033	-0.00223	0.1208	8.433443708	0	0	#DIV/0!	0	0	#DIV/0!
3	20.23	1.782	-0.486	-0.03635	0.13198	8.289904379	-0.03495	0.04214	11.32083531	-0.0014	0.08984	8.83737756	0	0	#DIV/0!	0	0	#DIV/0!
4	23.46	2.545	-0.767	0	0	#DIV/0!	0	0	#DIV/0!	0	0	#DIV/0!	0	0	#DIV/0!	0	0	#DIV/0!
5	25.52	2.414	-0.864	0	0	#DIV/0!	0	0	#DIV/0!	0	0	#DIV/0!	0	0	#DIV/0!	0	0	#DIV/0!
6	0	0	0	0	0	#DIV/0!	0	0	#DIV/0!	0	0	#DIV/0!	0	0	#DIV/0!	0	0	#DIV/0!
7	0	0	0	0	0	#DIV/0!	0	0	#DIV/0!	0	0	#DIV/0!	0	0	#DIV/0!	0	0	#DIV/0!
8	0	0	0	0	0	#DIV/0!	0	0	#DIV/0!	0	0	#DIV/0!	0	0	#DIV/0!	0	0	#DIV/0!
9	0	0	0	0	0	#DIV/0!	0	0	#DIV/0!	0	0	#DIV/0!	0	0	#DIV/0!	0	0	#DIV/0!
10	0	0	0	0	0	#DIV/0!	0	0	#DIV/0!	0	0	#DIV/0!	0	0	#DIV/0!	0	0	#DIV/0!

Hull Planing Forces: Hull +rear foil (planing Calc. after front foil)

N	V [m/s]	pitch [deg]	subm. [m]	total			viscous			suction			hydraulic					
				drag Cx	lift Cy	LCP [m]	drag Cx	lift Cy	LCP [m]	drag Cx	lift Cy	LCP [m]	drag Cx	lift Cy	LCP [m]			
1	19.49	1.321	-0.426	-0.06988	0.264139	10.30836794	-0.06812	0.084097	13.14006445	-0.00376	0.180042	8.98582227	0	0	#DIV/0!	0	0	#DIV/0!
2	20.13	1.415	-0.48	-0.05813	0.197946	9.439573205	-0.05588	0.078113	10.88628013	-0.00225	0.119833	8.49554791	0	0	#DIV/0!	0	0	#DIV/0!
3	20.23	1.782	-0.486	-0.04908	0.190798	7.37977814	-0.04763	0.101538	7.788355095	-0.00145	0.08926	8.91505112	0	0	#DIV/0!	0	0	#DIV/0!
4	23.46	2.545	-0.767	0	0	#DIV/0!	0	0	#DIV/0!	0	0	#DIV/0!	0	0	#DIV/0!	0	0	#DIV/0!
5	25.52	2.414	-0.864	0	0	#DIV/0!	0	0	#DIV/0!	0	0	#DIV/0!	0	0	#DIV/0!	0	0	#DIV/0!
6	0	0	0	0	0	#DIV/0!	0	0	#DIV/0!	0	0	#DIV/0!	0	0	#DIV/0!	0	0	#DIV/0!
7	0	0	0	0	0	#DIV/0!	0	0	#DIV/0!	0	0	#DIV/0!	0	0	#DIV/0!	0	0	#DIV/0!
8	0	0	0	0	0	#DIV/0!	0	0	#DIV/0!	0	0	#DIV/0!	0	0	#DIV/0!	0	0	#DIV/0!
9	0	0	0	0	0	#DIV/0!	0	0	#DIV/0!	0	0	#DIV/0!	0	0	#DIV/0!	0	0	#DIV/0!
10	0	0	0	0	0	#DIV/0!	0	0	#DIV/0!	0	0	#DIV/0!	0	0	#DIV/0!	0	0	#DIV/0!

APPENDIX B. NUMERICAL RESULTS SPREADSHEET

Hull wave resistance

N	V	pitch	subm.	hull disp.	Michiel			Kohn		
					residual	friction	total	wave	friction	total
	[m/s]	[deg]	[m]	m ³	C _{sw}	C _{df}	C _{dt}	C _{sw}	C _{df}	C _{dt}
1	19.49	1.321	-0.426	24.48517778	-0.00066064	-0.041631786				
2	20.13	1.415	-0.48	19.55806034	-0.000648841	-0.038413086				
3	20.23	1.782	-0.486	19.03959699	-0.00067145	-0.037329421				
4	23.46	2.545	-0.767	0	0	0				
5	25.52	2.414	-0.864	0	0	0				
6	0	0	0	0	#DIV/0!	#DIV/0!				
7	0	0	0	0	#DIV/0!	#DIV/0!				
8	0	0	0	0	#DIV/0!	#DIV/0!				
9	0	0	0	0	#DIV/0!	#DIV/0!				
10	0	0	0	0	#DIV/0!	#DIV/0!				

Corrections

N	V	pitch	subm.	subm.	front foil		rear foil	
					[h/c]	[h/c]	lift	drag
1	19.49	1.321	-0.426	1.163836048	0.617777417	1.028631714	1.0915295832	
2	20.13	1.415	-0.48	1.0416233	0.488928506	1.10295182	1.0875896548	
3	20.23	1.782	-0.486	0.81981919	0.420244178	1.099287465	1.0817028471	
4	23.46	2.545	-0.767	#DIV/0!	#VALUE!	#VALUE!	#VALUE!	
5	25.52	2.414	-0.864	#DIV/0!	#VALUE!	#VALUE!	#VALUE!	
6	0	0	0	#DIV/0!	#VALUE!	#VALUE!	#VALUE!	
7	0	0	0	#DIV/0!	#VALUE!	#VALUE!	#VALUE!	
8	0	0	0	#DIV/0!	#VALUE!	#VALUE!	#VALUE!	
9	0	0	0	#DIV/0!	#VALUE!	#VALUE!	#VALUE!	
10	0	0	0	#DIV/0!	#VALUE!	#VALUE!	#VALUE!	

Sw Michiel

N	V	Sw
	[m/s]	[m ²]
1	19.49	
2	20.13	196.358
3	20.23	189.703
4	23.46	
5	25.52	
6	0	
7	0	
8	0	
9	0	
10	0	

Interference Factors

N	V	pitch	subm.	Hull			rear foil		
				drag	lift	LCP	drag	lift	LCP
	[m/s]	[deg]	[m]	C _x /C _{xo}	C _y /C _{yo}	LCP/LCPo	C _x /C _{xo}	C _y /C _{yo}	LCP/LCPo
1	19.49	1.321	-0.426	1.202339986	1.425620682	0.830995189	0.587194383	1.030048334	1.003586175
2	20.13	1.415	-0.48	1.200536968	1.56764077	0.780022498	0.849992398	1.02426311	1.004232415
3	20.23	1.782	-0.486	1.390208227	1.445658433	0.89247357	0.821795096	1.028431873	1.002844451
4	23.46	2.545	-0.767	#DIV/0!	#DIV/0!	#DIV/0!	#DIV/0!	#DIV/0!	#DIV/0!
5	25.52	2.414	-0.864	#DIV/0!	#DIV/0!	#DIV/0!	#DIV/0!	#DIV/0!	#DIV/0!
6	0	0	0	#DIV/0!	#DIV/0!	#DIV/0!	#DIV/0!	#DIV/0!	#DIV/0!
7	0	0	0	#DIV/0!	#DIV/0!	#DIV/0!	#DIV/0!	#DIV/0!	#DIV/0!
8	0	0	0	#DIV/0!	#DIV/0!	#DIV/0!	#DIV/0!	#DIV/0!	#DIV/0!
9	0	0	0	#DIV/0!	#DIV/0!	#DIV/0!	#DIV/0!	#DIV/0!	#DIV/0!
10	0	0	0	#DIV/0!	#DIV/0!	#DIV/0!	#DIV/0!	#DIV/0!	#DIV/0!

Total Vessel Corrected Predictions

N	V	pitch	subm.	front foil			rear foil			hull			TOTAL		
				lift	drag	LCP	lift	drag	LCP	lift	drag	LCP	lift	drag	LCP
	[m/s]	[deg]	[m]	[tons]	[tons]	[m]	[tons]	[tons]	[m]	[tons]	[tons]	[m]	[tons]	[tons]	[m]
1	19.49	1.321	-0.426	70.42726446	-2.507498329	26.9550216	63.33622616	-1.704317778	3.915049955	24.48517778	4.961929674	10.30836796	60.1119961	10.73734978	15.018972
2	20.13	1.415	-0.48	76.63338989	-2.735297375	26.92292883	68.94622849	-2.08234607	3.824270285	19.55806034	4.907656036	9.43891259	64.117097	10.62529992	13.463071
3	20.23	1.782	-0.486	78.80695614	-2.883040213	26.98205716	73.01770478	-2.068991448	3.931586206	19.03959699	-4.95466193	7.379778614	60.8439579	9.55621293	14.947262
4	23.46	2.545	-0.767	0	#VALUE!	#DIV/0!	#DIV/0!	#VALUE!	#DIV/0!	0	0	#DIV/0!	#DIV/0!	#VALUE!	#DIV/0!
5	25.52	2.414	-0.864	0	#VALUE!	#DIV/0!	#DIV/0!	#VALUE!	#DIV/0!	0	0	#DIV/0!	#DIV/0!	#VALUE!	#DIV/0!
6	0	0	0	0	#VALUE!	#DIV/0!	#DIV/0!	#VALUE!	#DIV/0!	0	0	#DIV/0!	#DIV/0!	#VALUE!	#DIV/0!
7	0	0	0	0	#VALUE!	#DIV/0!	#DIV/0!	#VALUE!	#DIV/0!	0	0	#DIV/0!	#DIV/0!	#VALUE!	#DIV/0!
8	0	0	0	0	#VALUE!	#DIV/0!	#DIV/0!	#VALUE!	#DIV/0!	0	0	#DIV/0!	#DIV/0!	#VALUE!	#DIV/0!
9	0	0	0	0	#VALUE!	#DIV/0!	#DIV/0!	#VALUE!	#DIV/0!	0	0	#DIV/0!	#DIV/0!	#VALUE!	#DIV/0!
10	0	0	0	0	#VALUE!	#DIV/0!	#DIV/0!	#VALUE!	#DIV/0!	0	0	#DIV/0!	#DIV/0!	#VALUE!	#DIV/0!

Appendix C

Efficiency of some High-Speed Craft

The Appendix presents the transport efficiencies of some existing hydrofoils, catamarans and hydrofoil-assisted catamarans. Examination of the data shows the superior efficiency of hydrofoil-assisted catamarans over conventional catamarans and in some cases over the most efficient conventional hydrofoil craft as well.

The data presented in the tables that follow should be viewed in relation with the state of the art curves given in Figure 1.23.

APPENDIX C. EFFICIENCY OF SOME HIGH-SPEED CRAFT

219

Country	Description	L_{OA}	Δ [t]	V [kn]	Pb [kW]	$F n_{\nabla}$	ep
China	VS high-speed Craft	21	28	43.2	1380	4.09	0.226
China	CSSRC JetFoil	29.1	118	43.0	6368	3.20	0.249
USA	Navatek Westfoil	26	85	42.0	2950	3.30	0.164
USA	Boeing Jetfoil	27.4	110	42.0	5534	3.16	0.238
USA	Boeing PHM	40.5	218	48.0	19625	3.22	0.371
USA	Tuccumcari	22	58	53.0	2353	4.44	0.152
Swiss	Supramar PT150	37.9	150	36	5058	2.57	0.186
Swiss	Supramar PT75	30.38	78.5	36	2420	2.87	0.170
Swiss	Supramar PT50	27.75	63	34	1620	2.81	0.150
Swiss	Supramar PT20	20.75	20.4	33	810	3.13	0.143
Swiss	Supramar PT10	16.34	13.5	34	454.9	3.63	0.196
Russia	Aleksandr Kunakhovitch	50	465	60	40268	3.55	0.286
Russia	Sokol	50	500	60	37500	3.511	0.247
Russia	Chaika 1706	26.3	14.5	46	673	4.85	0.200
Russia	Raketa 340	27	26	33	671	3.16	0.155
Russia	Voskhod 352	27.1	27.6	34	736	3.22	0.155
Russia	Meteor 3423	34.6	54.3	35	1640	2.97	0.17
Russia	Meteor 2000	34.6	57.24	41	1872	3.44	0.158
Russia	Lastocka	29	37.3	48	1988	4.33	0.220
Russia	Kometa 342ME	35.1	59.3	34	1640	2.83	0.161
Russia	Kolkhida 10390	34.5	71.6	34	2100	2.75	0.171
Russia	Cyclon 1235	49.9	145	42	5920	3.02	0.193
Russia	Olympia 14600	43.3	138	37	4000	2.68	0.155
Russia	Belorussia	18.6	14.8	34	447	3.58	0.176
Russia	Polesie	21.3	20	35	586	3.50	0.166
Russia	Voskhod 2	27.6	28	32.4	745	3.06	0.162
Russia	Voskhod 2M	27.6	32.5	30	745	2.77	0.151
Russia	JSC Dolphin	10	3.1	35	147	4.77	0.268
Italy	Fincantieri Sparviero	22.9	60.5	44	3356	3.66	0.249
Italy	Rodriquez RHS110	25.6	54	37	2012	3.13	0.200
Italy	Rodriquez RHS140	28.7	65	32.5	2014	2.67	0.188
Italy	Rodriquez RHS150	28.7	65.5	32.5	2132	2.67	0.198
Italy	Rodriquez RHS160	30.9	95	32	2800	2.47	0.182
Italy	Rodriquez RHS200	35.8	130	35	3876	2.56	0.169
Italy	Rodriquez MEC1	25	55	38	2032	3.21	0.163
Italy	Rodriquez Foilmaster	31.4	107	38	3100	2.87	0.151

Table C.1: Transport efficiency for conventional hydrofoil craft

APPENDIX C. EFFICIENCY OF SOME HIGH-SPEED CRAFT

220

Country	Description	L_{OA}	Δ [t]	V [kn]	Pb [kW]	$F n_{\nabla}$	ep
Russia	Almaz Autojet	40	123	55	6960	4.06	0.204
Ukraine	Moyre Superfast 30	30	77	45	3152	3.59	0.18
Norway	Kvaerner Foilcat	35	150	50	8948	3.57	0.236
Norway	Westamarin Foilcat	29.3	123	45	4000	3.33	0.143
UK/RSA*	Prout Panther Hysucat	19.6	42	43	2049	3.80	0.224
UK/RSA	NGA Chief Flying Sun	45	140	38	4000	2.75	0.149
Thai/RSA	Thailand patrol boat	19	35	37	1254	3.32	0.191
Thai/RSA	Thai custom patrol boat	18	29	47	1460	4.43	0.215
Germany	Hysucat Eng. Rheinjet	18	28	37	1000	3.54	0.193
Germany	Hysucat Eng. Nordblitz	22	54	34	1452	2.88	0.157
Germany	Ultimar Ultimario	19	27	37	1000	3.52	0.198
Germany	Hysucat 27	27	140	40	4412	2.89	0.156
USA	Kvichak/Technicraft	17.7	28	30	984	2.84	0.232
Russia	Project 15220	47.7	102	22	1200	1.69	0.105
Japan	Hitachi Superjet40	40	190	40	8088	2.87	0.118
S.Korea	Daewoo F-CAT40	40.3	147	40	4000	2.89	0.133
USA/RSA*	Halter E-CAT	42	170	45	4000	3.15	0.103
RSA*	Sea Princess	22	60	34	2000	2.83	0.19
France/RSA*	KingCat	21	72	44	3520	3.52	0.21
Aus./RSA*	Cougar WildCat	14.6	22	49	1176	4.82	0.22
Aus./RSA*	Crowther Hysucat	16	22	34	626	3.35	0.165

Table C.2: Efficiencies of some designed and existing hydrofoil-assisted catamarans. Those vessels marked with a '*' are designs that were developed from findings in this study.

Country	Description	L_{OA}	Δ [t]	V [kn]	Pb [kW]	$F n_{\nabla}$	ep
Italy	Rodriquez Marconi	46.9	136.9	34	2960	2.47	0.126
Italy	Rodriquez Marconi	37.0	106	35	2960	2.65	0.158
Russia	Matka class, Vikhr	38.6	268	42	10738	2.73	0.189
Russia	Turya class, Shtorm	38.6	250	37	11185	2.43	0.240

Table C.3: Efficiencies of some existing hydrofoil-assisted mono-hulls

Country	Description	L_{OA}	Δ [t]	V [kn]	Pb [kW]	$F n_{\nabla}$	ep
Italy	Moschini	20.2	58	30	2300	2.514	0.261
UK	FBM	27.5	73	38	2520	3.06	0.18
Australia	NQEA Sun eagle	29.2	110	30	3000	2.25	0.180
Japan	Mitsui Supamaran	33.2	217	25	2556	1.68	0.0933
Italy	Rodriquez city Cat	39.5	100	39	4700	2.98	0.239
USA/UK	NGA/Derecktor	41	170	36	5000	2.52	0.161
Australia	AMD	41.3	161	36	4000	2.54	0.137
Italy	Rodriquez Seagull	43.2	150	34	4000	2.43	0.155
USA/UK	NGA/Derecktor	45.6	202	52	11950	3.53	0.225
UK	FBM	46.3	180	25	1932	1.73	0.085
Russia	Anatoly Uglovsky	47.7	90	23	1270	1.8	0.121
Australia	Stena Sea Lynx	74	790	37	22000	2.00	0.149
Australia	Incat	81	1118	38.2	22520	1.95	0.104
Australia	Incat	91	1423	42	28974	2.06	0.096
Australia	Incat Evolution B	97.2	750	38	28800	2.07	0.200

Table C.4: Efficiencies for some existing catamarans of different sizes

Bibliography

- [Ada95] J. Adams. Motion control of high speed ferries. *Fast Ferry International*, pages 128–135, June 1995.
- [AHSM99] T. Arii, K. Hatta, M. Sugano, and H. Miyata. Development and operation of hydrofoil catamaran "SuperJet". In *FAST'99 5th International Conference on Fast Sea Transportation*, pages 511–522, Seattle, 1999.
- [Alm93] J.M. Almeter. Resistance prediction of planing hulls: State of the art. *Marine Technology*, 30(4):297–307, October 1993.
- [AMKH93] T. Arii, H. Miyata, H. Kawaguchi, and K. Hatta. Development of a foil assisted catamaran 'Superjet-30'. In *FAST'93 2nd International Conference on Fast Sea Transportation*, volume 1, pages 295–304, Yokohama, 1993.
- [AMN98] J. Ando, S. Maita, and K. Nakatake. A new surface panel method to predict steady and unsteady characteristics on marine propeller. In *Twenty Second Symposium on Naval Hydrodynamics*, volume 1, pages 126–138, Washington D.C., 1998.
- [Arm99] T. Armstrong. The correlation of model testing and full scale resistance of high speed catamarans. In *International Conference Hydrodynamics of High Speed Craft*, London, 1999. RINA.
- [Av58] I.H. Abbot and A.E. von Doenhoff. *Theory of Wing Sections*. Dover Publications, New York, 1958.
- [AYTS93] T. Arii, H. Yamato, T. Takai, and R. Shigehiro. Development of a motion control system for a foil assisted catamaran 'Superjet-30'. In *Fast'93, 2nd International Conference on Fast Sea Transportation*, volume 1, pages 305–316, Yokohama, 1993.
- [BBC+98] S. Brizzolara, D. Bruzzone, P. Cassella, A. Scamardell, and I. Zotti. Wave resistance and wave patterns for high speed crafts; validation of numerical results by model test. In *Twenty Second Symposium on Naval Hydrodynamics*, pages 55–69, Washington D.C., 1998.

- [BEKM00] K. Benedict, J. Ebert, N. Kornev, and M. Meyer. Complex mathematical model of the WIG motion including the take-off regime. *Ocean Engineering*, 29(3):315–357, 2000.
- [Ber99a] V. Bertram. Computational fluid dynamics for the marine industry an introduction. In *31st WEGEMT School, CFD for Ship and Offshore Design*, volume 1, pages 1–15, Hamburg, May 1999.
- [Ber99b] V. Bertram. Panel methods for wave resistance computations. In *31st WEGEMT School: CFD for Ship and Offshore Design*, Hamburg, 1999. WEGEMT.
- [Ber00] V. Bertram. *Practical Ship Hydrodynamics*. Butterworth Heinemann, 2000.
- [BL93] S.M. Belotserkovsky and I.K. Lifanov. *Method of Discrete Vortices*. CRC Press, 2000 Corporate Blvd., N.W., Boca Raton, Florida 33431, 1993.
- [BLSZ95a] M. Basin, A.G. Lyakhovitsky, S.B. Shur, and B.M. Zelensky. Hydrodynamics of fast catamarans. In *FAST'95 Third International Conference on Fast Sea Transportation*, pages 57–66, Lübeck-Travemünde, 1995.
- [BLSZ95b] M.A. Basin, A.G. Lyakhovitsky, S.B. Shur, and B.M. Zelensky. The methods of determining of fast catamarans hydrodynamic complex characteristics. In *VII-th Congress of the IMAM*, pages 127–135, Dubrovnic, 1995.
- [Bro80] J.M. Broeck van den. Nonlinear stern waves. *Journal of Fluid Mechanics*, 96(3):603–611, 1980.
- [BSK⁺98] E. Besnard, A. Schmitz, K. Kaups, G. Tzong, H. Hefazi, O. Kural, H. Chen, and T. Cebeci. Hydrofoil design and optimization for fast ships. In *Proceedings of the ASME International Congress and Exhibition*, pages 1–11, Anaheim, November 1998.
- [Cal81] D. Calkins. Hycat: Hybrid hydrofoil catamaran. In *AIAA 6th Marine Systems Conference*, number AIAA-81-2079, Seattle, Sept. 1981.
- [Cal84] D. Calkins. Hycat: Hybrid hydrofoil catamaran concept. *Ocean Engineering*, 11(1):1–21, 1984.
- [CCEP89] A. Colombo, A. Coscia, I. Elice, and M. Parodi. Assessment of a deep-V advanced mono-hull. Technical report, Fincantieri -CNI Naval Shipbuilding, Genoa, Italy, 1989.
- [CCMF97] F. Castro, A. Crespo, F. Manuel, and D.H. Fruman. Equilibrium of ventilated cavities in tip vortices. *Journal of Fluids Engineering*, 119:759–767, December 1997.

- [Cha72] R.B. Chapman. Spray drag of surface piercing struts. In *Advanced Marine Vehicles Conference*. AIAA/SNAME, 1972.
- [CMAU97] P.R. Couser, A.F. Molland, N.A. Armstrong, and I.K.A.P. Utuma. Calm water powering predictions for high speed catamarans. In *FAST'97 Fourth International Conference on Fast Sea Transportation*, volume 2, pages 765–773, Sydney, 1997.
- [Cri70] P. Crimi. Experimental study of the effects of sweep on hydrofoil loading and cavitation. *Journal of Hydronautics*, 4(1):3–9, January 1970.
- [Cro85] B. Crook. Powering predictions and propeller disk wake survey data for the USNS HAYES T-AGOR 16. Technical Report DTNSRDC/SDP-072-14, David W. Taylor Naval Ship Research and development Center, 1985.
- [CW94] X. Cheng and J.F. Wellicome. Study of planing hydrodynamics using strips of transversely variable pressure. *Journal of Ship Research*, 38(1):30–41, 1994.
- [CW99] X. Cheng and J.F. Wellicome. Numerical prediction of forces on planing flat catamaran hulls and prismatic hulls. *International Shipbuilding Progress*, 46(448):365–385, 1999.
- [Das00] M. Daskovsky. The hydrofoil in surface proximity, theory and experiment. *Ocean Engineering*, 27:1129–1159, 2000.
- [dC72] P. du Cane. *High Speed Small Craft*. David and Charles: Newton Abbot, 1972.
- [DD97] L. Doctors and A. Day. Resistance prediction for transom stern vessels. In *FAST'97 Fourth International Conference on Fast Sea Transportation*, volume 2, pages 743–750, Sydney, 1997.
- [DeJ76] F.R. DeJarnette. Arrangement of vortex lattice methods on subsonic wings. Technical Report SP-405, NASA, Washington D.C., 1976.
- [DL01] V. Dubrovsky and A. Lyakhovitsky. *Multi-Hull Ships*. Backbone Publishing Company, PO Box 562, Fair Lawn, NJ 07410, USA, 2001.
- [Dob69] Z.N. Dobrovolskaya. On some problems of similarity flows of fluids with a free surface. *Journal of Fluid Mechanics*, 36:805–829, 1969.
- [Doc98] L.J. Doctors. Intelligent regression of resistance data for hydrodynamics in ship design. In *Twenty Second Symposium on Naval Hydrodynamics*, pages 21–36, Washington D.C., 1998.

- [Dre89] M. Drela. XFOIL: An analysis and design system for low reynolds number airfoils. *Conference on Low Reynolds number Airfoil Aerodynamics, University of Notre Dame*, 1989.
- [Dre96] M. Drela. *XFOIL 6.8 User Primer*. MIT, Aero and Astro, October 1996.
- [EB68] L.A. Epstein and B.I. Blumin. On the hydrodynamics of submerged wings. Technical Report 1103, TSAGI, 1968. in Russian.
- [EBS78] I.T. Egorov, M.M. Bunkov, and M. Sadovnikov. *Propulsive Performance and Seaworthiness of Planing Vessels*. Sudostroenie, 1978. In Russian. (English Translation: Naval Sea Systems Command Translation No. 1965, Oct. 1981).
- [ES65] I.T. Egorov and V.T. Sokolov. *Hydrodynamics of Fast Craft*. 1965. In Russian. (English Translation: NTIS AD A032120; 1976).
- [ES79] R. Eppler and Y.T. Shen. Wing sections for hydrofoils-part 1: Symmetrical profiles. *Journal of ship Research*, 23(3):209–217, September 1979.
- [ES81] R. Eppler and Y.T. Shen. Wing sections for hydrofoils-part 2: Nonsymmetrical profiles. *Journal of ship Research*, 25(3):191–200, September 1981.
- [Eve68] J.T. Everest. Some research on the hydrodynamics of catamarans and multi-hulled vessels in calm water. In *Transactions NECI*, pages 129–148, 1968.
- [Fal90] O.M. Faltinsen. *Sea Loads on Ships and Offshore Structures*. Cambridge University Press, The Edinburgh Building, Cambridge CB2 2RU, UK, 1990.
- [FC97] E. Fontaine and S. Cordier. Recent experience using high speed slender body theory. In *FAST'97 Fourth International Conference on Fast Sea Transportation, Proceedings*, volume 1, pages 405–411, Sydney, 1997.
- [Fei81] W.M. Feifel. Advanced numerical methods hydrofoil system design and experimental verification. In *3rd International Conference on Numerical Ship Hydrodynamics*, pages 365–374, Paris, 1981.
- [FFC00] E. Fontaine, O.M. Faltinsen, and R. Cointe. New insight into the generation of ship bow waves. *Journal of Fluid Mechanics*, 421:15–38, 2000.
- [FG72] E. Fry and T. Graul. Design and application of modern high speed catamarans. *Marine Technology*, pages 345–357, July 1972.

- [Fro55] W. Froude. Observations and suggestions on the subject of determining by experiment the resistance of ships. *The Papers of William Froude, INA*, 1955.
- [Fun91] S.C. Fung. Resistance prediction and powering prediction for transom stern hull forms during early stage ship design. *SNAME Transactions*, 99:29–84, 1991.
- [GB92] B. Galtier and C. Buccini. Acquastrada - a complete model testing and numerical evaluation of a new deep-V monohull design. In *Eight International High Speed Surface Craft Conference*. High Speed Surface Craft, 1992.
- [GD01] G.J. Grigoropoulos and D.P. Damala. The effect of trim on the resistance of high-speed craft. In V. Bertram, editor, *HIPER2001, 2nd International EuroConference on High Performance Marine Vehicles*, pages 187–199, Hamburg, 2001.
- [Geb68] J.C. Gebhardt. The skin friction of a hydrofoil near a free surface. Technical Report 08368-1-F, University of Michigan, Dept. of Nav. Arch. and Mar. Eng., October 1968. (available from NTIS: AD736631).
- [Gre64] E.P. Grebeshov. Investigation of hydrodynamic characteristics of wings with semi-circular and aviation profiles under the free surface. issue 264, TSAGI, 1964. In Russian.
- [Gri97] G. Grigoropoulos. Model testing of small craft. In *Twenty Fifth School: Small Craft Technology*, Athens, October 1997. WEGEMT Association.
- [Gro01] Nihon University Aero Student Group. NASG airfoil database. Internet: www/nasg.com/afgb/index-e.phtml, 2001.
- [Had32] J. Hadamard. *Le probleme de Cauchy et les equations aux derives partielles lineaires hyperboliques*. Hermann, 1932.
- [Hau80] H.J. Haussling. Two-dimensional linear and nonlinear stern waves. *Journal of Fluid Mechanics*, 97(4):759–769, 1980.
- [HB75] S. F. Hoerner and H. V. Borst. *Fluid Dynamic Lift*. Hoerner Fluid Dynamics, 1975.
- [HD95] S.A. Hellström and Blount. D.L. The influence of aft buttock shape on high speed hull performance. In *FAST'95 3rd International Conference on Fast Sea Transportation*, pages 21–32, Lübeck-Travemünde, 1995. Vol. 1.

- [HHH91] T. Hino, N. Hirata, and T. Hori. Calculation of free surface flows generated by planing crafts. In *FAST'91 First International Conference on Fast Sea Transportation, Proceedings*, volume 1, pages 317–330, Trondheim, 1991.
- [HM86] A.F. Huber II and T.J. Mueller. The effect of grit roughness on the performance of the wortmann FX63-137 airfoil at a chord Reynolds number of 100,000. In *Aerodynamics at Low Reynolds Numbers $1 \times 10^4 \leq Re \leq 1 \times 10^6$* , pages 28.1–28.16. The Royal Aeronautical Society, 1986.
- [Hoe65] S. Hoerner. *Fluid Dynamic Drag*. Published by the Author, 148 Busted Drive, Midland Park, New Jersey, 07432, 2nd edition, 1965.
- [Hop80] K.G. Hoppe. The hydrofoil supported catamaran. Progress Research Report 1980-2, University of Stellenbosch, Mechanical Engineering Dept., Univ. of Stellenbosch, Stellenbosch, South Africa, 1980.
- [Hop82] K.G. Hoppe. Boat, hydrofoil supported catamarans. S.A. Patent No. 82/3505 and foreign patents, 1982.
- [Hop90] K.G. Hoppe. Experimental data of a modified Göttingen K11 profile tested under the free surface. Unpublished, 1990.
- [Hop91a] K.G. Hoppe. The Hysucat development. *Ship Technology Research*, 38(3):134–139, 1991.
- [Hop91b] K.G. Hoppe. The Hysucat development. Technical report, University of Stellenbosch, Mechanical Engineering Department, 1991.
- [Hop91c] K.G. Hoppe. Performance evaluation of high speed surface craft with reference to the Hysucat development (part 1). *Fast Ferry International*, 30(1), 1991.
- [Hop91d] K.G. Hoppe. Performance evaluation of high speed surface craft with reference to the Hysucat development (part 2). *Fast Ferry International*, 30(3), 1991.
- [Hop95a] K.G. Hoppe. Optimization of hydrofoil assisted planing catamarans. In *Fast'95, 3rd International Conference on Fast Sea Transportation*, pages 307–317, Lübeck-Travemünde, 1995.
- [Hop95b] K.G. Hoppe. Ship fluid dynamics, lecture notes, 1995. Dept. of Mechanical Engineering, University of Stellenbosch.
- [Hop96] K.G. Hoppe. Preliminary report on model tests on a catamaran and hydrofoil assist system. ITM report, Institute for Thermodynamics and Mechanics, Department of Mechanical Engineering, University of Stellenbosch, 1996.

- [Hop97] K.G. Hoppe. Feasability study on a hydrofoil-assist-system for the K55 semi-displacement catamaran. ITM report, Institute for Thermodynamics and Mechanics, Department of Mechanical Engineering, University of Stellenbosch, 1997.
- [Hop98] K.G. Hoppe. Model tests on the K55 semi-displacement catamaran with F9-hydrofoil system. ITM report, Institute for Thermodynamics and Mechanics, Dept. of Mechanical Engineering, University of Stellenbosch, Private Bag X1, Matieland, 7602, South Africa, March 1998.
- [Hop99] K.G. Hoppe. Hydrofoil catamaran developments in South Africa. In *HIPER'99 1st International Conference on High Performance Marine Vehicles*, pages 92–101, Cape Town, 1999.
- [Hop00] K.G. Hoppe. Hydrofoil supported watercraft. United States Patent: 6,164,235, December 26 2000.
- [Hop01] K.G. Hoppe. Recent applications of hydrofoil supported catamarans. *Fast Ferry International*, pages 30–36, September 2001.
- [Hou73] G.R. Hough. Remarks on vortex lattice methods. *Journal of Aircraft*, 10(5):314–317, 1973.
- [Hou76] G.R. Hough. Lattice arrangements for rapid convergence. Technical Report SP-405, NASA, Washington D.C., 1976.
- [IM91] M. Insel and A.F. Molland. An investigation into the resistance components of high speed displacement catamarans. In *Transactions of the Royal Institute of Naval Architects*, April 1991.
- [Ish92] S. Ishikawa. Study on hydrodynamic interaction between hull and submerged foils. *Journal of the Society of Naval Architects of Japan*, 169:135–142, 1992.
- [ITT90] Report of the high-speed vehicle committee. In *19th ITTC Conference*. International Towing Tank Conference, 1990.
- [Jef98] A. Jeffs. *The World Fast Ferry Market*. Baird Publications PTY LTD Melbourne, 135 Sturt Street, Southbank, Victoria, Australia, 1998.
- [JF91] G. Jensen and M. Fritsch. Foil-Assisted Katamaran. Hamburgische Schiffsbau-Versuchsanstalt (HSVA) report, 1991. In German.
- [JM79] E.A. Jones and M. Mackay. Evaluation of the theory for the flow pattern of a hydrofoil of finite span. Technical Memorandum 79/C, Defence Research Establishment Atlantic, 1979.

- [Kar74] G. Karafiath. An investigation into the performance of NSRDC Model 5184 configured as a partial hydrofoil supported planing craft and a comparison with a powering prediction technique. Technical Report SPD-585-01, NSRDC, 1974.
- [Kar76] G. Karafiath. Powering prediction for various hybrid ship concepts. Technical Report SPD-675-01, David W. Taylor Ship Research and Development Centre, Bethesda, Md, 20064, April 1976.
- [Kat96] K. Kataoka. Hydrodynamic interaction between hull and hydrofoils. In A.T. Chwang, editor, *Hydrodynamics - Theory and Applications: 2nd International Conference on Hydrodynamics*, pages 233–238, Rotterdam, 1996. AA Balkema.
- [KK80] K.L. Kirkman and J.W. Kloetzli. Scaling problem of model appendages. In *Proceedings of the Nineteenth General Meeting of the American Towing Tank Conference (ATTC)*, pages 129–154, 1980.
- [KKT95] T Kawamura, H. Kawasima, and Y. Tsuchiya. CFD simulation of the flow around planing craft and tandem hydrofoils. In *FAST'95, Third International Conference on Fast Sea Transportation*, pages 1181–1192, Lübeck-Travemünde, 1995.
- [KLT98] C. Kennel, D.R. Lavis, and M.T. Templeman. High-speed sealift technology. *Marine Technology*, 35(3):135–150, July 1998.
- [KMH01] N.V. Kornev, G. Migeotte, and K.G. Hoppe. Development of a numerical vortex method for calculation of the 2D water impact problem. *South African Institute of Mechanical Engineers Research and Development Journal*, November 2001.
- [KMHN01] N.V. Kornev, G. Migeotte, K.G. Hoppe, and A. Nesterova. Design of high speed hydrofoil assisted catamarans using a non-linear vortex lattice method. In *HIPER'01 2nd International Conference on High Performance Marine Vehicles*, Hamburg, 2001.
- [KMY91] M. Kaji, N. Maeda, and T. Yamano. Resistance characteristics of a hydrofoil catamaran. *Journal of the Kansai Society of Naval Architects*, (215):53–60, March 1991.
- [KMYT91] H. Kawaguchi, H. Miyata, H. Yamato, and T. Takai. Full-scale experiments by the first hydrofoil catamaran WINGSTAR 12 "exceller". In *Fast'91, 1st International Conference on Fast Sea Transportation*, pages 1195–1213, Trondheim, 1991.
- [Koc49] Ye. N. Kochin. *Wave Drag and Lift of Bodies immersed in a liquid (Collected Works)*, volume 2. AN SSSR, Moscow, 1949.

- [Kor98] N. Kornev. *The Computational Method of Vortex Elements and its Application to Problems of Hydro-Aerodynamics*. 2nd doctor thesis, St. Petersburg Marine Technical University, Dept. of Hydromechanics, 1998.
- [KP91] J. Katz and A. Plotkin. *Low-Speed Aerodynamics, from Wing Theory to Panel Methods*. McGraw-Hill, Singapore, 1991.
- [Kri92] D. Kring. Free surface flows for semi-displacement craft. In *7th International Workshop Water Waves and Floating Bodies*, Val du Reil, 1992.
- [Kru95] A. Kruglov. A novel approach to improvement of fast catamarans seaworthiness. In *11th Fast Ferry International Conference*, Hong Kong, 1995.
- [KT] N. Kornev and A. Taranov. Autowing 2.4. <http://www.cl.spb.ru/u/taranov/Index.htm>.
- [KT99] N. Kornev and A. Taranov. Investigation of a vortex wave wake behind a hydrofoil. *Ship Technology Research*, 46(1):8–13, February 1999.
- [KT01] N. Kornev and A. Taranov. Behaviour and potential hazard of WIG trailing vortices. *Ocean Engineering*, 29(3):315–357, 2001.
- [KYS+93] B-S. Kim, S-Y. Yoo, Y-T. Son, M-S. Shin, C-D. Ko, and S-I. Yang. Improvements of hydrodynamic characteristics of catamaran with hydrofoil. In *FAST'93, 2nd International Conference on Fast Sea Transportation*, pages 631–642, Yokohama, 1993.
- [Lai94] C. Lai. *Three Dimensional Planing Hydrodynamics Based on a Vortex Lattice Method*. PhD thesis, University of Michigan, Ann Arbor, Michigan, 1994.
- [Laz97] L. Lazouskas. A note on the drag of hulls with transom sterns. 1997. published on internet: <http://www.maths.adelaide.edu.au/Applied/llazausk/hydro/hydro.htm>.
- [LB93] R. Lattore and D. Bourg. Validation of hydrofoil design program hyf3. In *FAST'93, 2nd International Conference on Fast Sea Transportation*, volume 1, pages 831–836, Yokohama, 1993.
- [Lee82] T-S. Lee. Interference factor for catamaran planing hulls. *AIAA Journal*, 20(10):1461–1462, 1982.
- [Lev71] R. Levi. *Dhows to Deltas*. Nautical Publishing Company, Nautical House, Lymington, Hampshire, 1971.

- [Lew88] E. Lewis, editor. *Principles of Naval Architecture*, volume 2. The Society of Naval Architects and Marine Engineers, 601 Pavonia Avenue, Jersey City, NJ, 3 edition, May 1988.
- [Lew89] E.M. Lewandowski. The effects of Reynolds number, section shape, and turbulence stimulation on the lift of a series of model control surfaces. In *22nd American Towing Tank Conference*, pages 398–407, 1989.
- [Li81] B-Q. Li. A prediction method of foilborne performance characteristics of hydrofoil craft in calm sea. In *Conference on High Speed Surface Craft*, London, 1981.
- [LLYY94] J. Li, G. Li, S. Yang, and L. Yu. High speed hydrofoil catamaran design study II. In *International Conference for New Ship Technology into 21st Century (NEWS-TEC'94)*, pages 119–127, Shanghai, 1994.
- [LO95] J.C. Lewthwaite and H. Oehlmann. Predicted performance and seakeeping of the semi-planing ship. In *FAST'95 3rd International Conference on Fast Sea Transportation*, volume 1, pages 331–340, Lübeck-Travemünde, 1995.
- [LT92] R. Lattore and S. Teerasin. Calculation of hydrofoil craft take-off speed including influence of foil size, foil angle and propellor shaft angle. *Ocean Engineering*, 19(2):183–197, 1992.
- [LT95] C. Lai and A. Troesch. Modeling issues related to the hydrodynamics of three-dimensional planing. *Journal of Ship Research*, 39(1):1–24, March 1995.
- [LT96] C. Lai and A. Troesch. A vortex lattice method for high-speed planing. *Int. Journal for Numerical Methods in Fluids*, 22:495–513, 1996.
- [LT01] U. La Roche and H. Trevisani. Replacing cavitation and supercavitation bubbles on profiles for high speed propellers and foils by two-phase boundary layers on profiles at high speed and low sigma. In *HIPER 2001, 2nd International EuroConference on High Performance Marine Vehicles*, Hamburg, May 2001.
- [Lya96] A.G. Lyakhovitsky. Influence of the ship hydrodynamics on development of the high-speed vessels of the transient-regime of motion. In *International Conference CRF'96*, pages 432–441, St. Petersburg, Russia, June 1996.
- [Mar63a] M. Martin. The stability derivatives of a hydrofoil boat - Part I. Technical report 001-10(i), Hydronautics Incorporated, 1963.

- [Mar63b] M. Martin. The stability derivatives of a hydrofoil boat - part II. Technical report 001-10(ii), Hydronautics Incorporated, 1963.
- [May91] A.N. Mayboroda. Mathematical model of the hydrodynamics for the body piercing the free surface of the ideal flow. In *Proceedings, Ukrainian Academy of Sciences*, volume 5, pages 50–53, 1991. In Russian.
- [McK97] C.B. McKesson. Hull form and propulsor technology for high speed sealift. Technical report, John J. McMullen Associates, Inc., 1997.
- [Mey92] J. Meyer. Hybrid hydrofoil technology applications. In *High Performance Marine Vehicles Conference*, pages HF25–HF36, 1992.
- [MG81] B. Müller-Graf. Status of hydrodynamic technology as related to model tests of high-speed marine vehicles. Technical Report 81/026, DTNSRDC, 1981. Section 3.4: Semisubmerged Hydrofoil Craft.
- [MG88] B. Müller-Graf. Der Rumpf als Tragflügel - Fiktion oder Realität. In *Proceedings of the Fach Seminar Jacht Entwurf*, pages 9–46, Hamburg, D., 1988. Hamburg Messe und Congress GmbH. und Deutscher Boots- und Schiffbau Verband. in German.
- [MG89] B. Müller-Graf. *Systematische Untersuchung von Spritzleisten*. PhD thesis, Technischen Universität Berlin, 1989. In German.
- [MG97a] B. Müller-Graf. Factors affecting the reliability and accuracy of the resistance prediction. In *WEGEMT 25th School: Small Craft Technology*, Athens, October 1997.
- [MG97b] B. Müller-Graf. Resistance components of high speed craft. In *WEGEMT 25th School: Small Craft Technology*, pages 1–61, Athens, 1997.
- [MG99a] B. Müller-Graf. Leistungsbedarf und Propulsionseigenschaften der schnellen Knickspant-Katamarane der VWS Serie '89. Technical report, Versuchsanstalt für Wasser und Schiffbau, VWS, Berlin, 1999. In German.
- [MG99b] B. Müller-Graf. Widerstand und Hydrodynamische Eigenschaften der schnellen Knickspant-Katamarane der VWS Serie '89. In *20. Symposium Yachtentwurf und Yachtbau*, Hamburg, November 1999. Deutscher Boots- und Schiffbauer-Verband und Hamburg Messe und Congress GmbH. In German.
- [MH98] G. Migeotte and K.G. Hoppe. F22 Hysucat model tests. Itm report, Institute for Thermodynamics and Mechanics, Dept. of Mechanical Engineering, University of Stellenbosch, April 1998.

- [MH99a] G. Migeotte and K.G. Hoppe. Development of hydrofoil assisted catamarans with semi-displacement hulls. In *HIPER'99, International Conference on High-Performance Marine Vehicles*, pages 164–173, Cape Town, 1999.
- [MH99b] G. Migeotte and K.G. Hoppe. KINGCAT 21m hysucat model tests. Itm technical report, Institute for Thermodynamics and Mechanics, Department of Mechanical Engineering, University of Stellenbosch, 28 June 1999.
- [MH00] G. Migeotte and K.G. Hoppe. Model tests on the voyager II foil assisted catamaran. Itm report, Institute for Thermodynamics and Mechanics, Dept. of Mechanical Engineering, University of Stellenbosch, Private Bag X1, Matieland, 7602, R.S.A., November 2000.
- [MH01] G. Migeotte and K.G. Hoppe. The University of Stellenbosch experimental database on hydrofoil-assisted craft. 2001.
- [MHK01] G. Migeotte, K.G. Hoppe, and N.V. Kornev. Design and efficiency of hydrofoil assisted catamarans. In *FAST 2001 6th International Conference on Fast Sea Transportation*. RINA, 2001.
- [Mic98] J.H. Michell. The wave resistance of a ship. *Phil. Mag.*, 5(45):106–123, 1898.
- [Mig97] G. Migeotte. Development of hydrofoil supported catamarans with semi-displacement hulls. Master's thesis, Department of Mechanical Engineering, University of Stellenbosch, December 1997.
- [Min91] K-S. Min. Long range high speed catamaran ship design. In *FAST'91 First International Conference on Fast Sea Transportation*, pages 591–606, Trondheim, 1991.
- [Min92] K-S. Min. Design and construction of the long range high speed catamaran ship. In *19th Symposium on Naval Hydrodynamics*, pages 116–135, Seoul, 1992.
- [Min93] K.J. Minsaas. Design of hydrofoil catamarans in Norway. In *Fast'93 2nd International Conference on Fast Sea Transportation*, volume 1, pages 83–99, Yokohama, 1993.
- [Miy79] M. Miyazawa. A study on the flow around a catamaran. *Journal of the Society of Naval Architects of Japan*, 145:46–53, 1979.
- [Miy89] H. Miyata. Development of a new type hydrofoil catamaran. *Journal of Ship Research*, 33(2), 1989.

- [MKS98] K-S. Min, S-H. Kang, and H. Streckwall. Numerical and experimental studies for the prediction of hydrodynamic characteristics of two dimensional hydrofoils operating under the free surface. In *22nd Symposium on Naval Hydrodynamics*, pages 770–778, Washington D.C., 1998.
- [MLY99] X. Mei, Y. Lui, and D.K.P. Yue. On the water impact of general two-dimensional sections. *Applied Ocean Research*, 21:1–15, 1999.
- [MM00] K.I. Matveev and I.I. Matveev. Tandem hydrofoil system. *Ocean Engineering*, 28(2):253–261, January 2000.
- [Mol75] V.F. Moltchanov. Some problems of flows with a tangential discontinuity of the velocity field. *Proceedings of the TSAGI*, 5(4):1–11, 1975.
- [Mor91] H.J.B. Morch. Aspects of hydrofoil design; with emphasis on hydrofoil interaction in calm water. In *FAST'91 First International Conference on Fast Sea Transportation*, volume 1, pages 143–161, Trondheim, 1991.
- [MT90] H. Miyata and Y. Tsuchiya. Development of a new type hydrofoil catamaran (4th report: Hydrofoil interactions and hydrodynamical properties of a 4000t type ship). *Journal of the Society of Naval Architects of Japan*, 168:1–7, December 1990.
- [MT96] L.M. Milne-Thomson. *Theoretical Hydrodynamics*. Dover Publications, Inc., 31 East 2nd Street, Mineola, New York, 5th edition, 1996.
- [MTM99] M. Miyagawa, Y. Terao, and H. Morihana. The study on resistance and propulsion of a catamaran-type high speed passenger ship with hydrofoils. *Journal of the School of Marine Science and Technology, Tokai University*, (48):1–17, 1999.
- [MWC96] A.F. Molland, J.F. Wellicome, and P.R. Couser. Resistance experiments on a systematic series of high speed displacement catamaran forms: Variation of length displacement ratio and breadth draft ratio. In *Transactions of the Royal Institute of Naval Architects*, volume 138a, pages 55–71, 1996.
- [MYS93] K-S. Min, D.J. Yum, and K.J. Song. A study on the prediction method of motion characteristics of the high speed catamaran ship. In *FAST'93 2nd International Conference on Fast Sea Transportation*, volume 1, pages 127–137, Yokohama, 1993.
- [NGF79] A.E. Noreen, P.R. Gill, and W.M. Feifel. Foilborne hydrodynamic performance of jetfoil. *Journal of Hydronautics*, 14(2):56–62, 1979.
- [Ogi77] T.F. Ogilvie. Singular perturbation problems in ship hydrodynamics. *Advanced Applied Mechanics*, 17, 1977.

- [OM97] H. Orihara and H. Miyata. CFD simulation of a semi-planing boat in unsteady motion. In *FAST'97 4th International Conference on Fast Sea Transportation*, pages 35–41, Sydney, 1997.
- [PAE⁺95] K. Patrakka, J-P. Arjava, H. Enlund, O. Kyyrö, and J. Lausmaa. Influence of the distance between demi-hulls on the characteristics of a big, high-speed catamaran. In *FAST'95 Third International Conference on Fast Sea Transportation*, Lübeck-Travemünde, 1995.
- [Pay88] P.R. Payne. *Design of High Speed Boats, Planing*, volume 1. Fishergate, Annapolis, Maryland, 1988.
- [Pay95] P.R. Payne. Contributions to planing theory. *Ocean Engineering*, 22(7):699–729, 1995.
- [Pet95] F. Peterson. Recent hydrofoil developments in East Asia. In *Proceedings of the 25th Anniversary Celebration and Conference, International Hydrofoil Society*, pages 155–168, Arlington, 1995.
- [Phi02] S.J. Phillips, editor. *High-Speed Marine Transportation*. Jane's publishing group, Sentinel House, 163 Brighton Road, Coulsdon, Surrey CR5 2YH, UK, thirty third edition, 2001/2002.
- [Pie76] C.G. Pieroth. Hydrofoil hullform selection. *Hovering Craft and Hydrofoil*, 16:18–31, December 1976.
- [PPNE00] S.D. Pavlov, S.A. Porodnikov, C. Norrstrand, and H. Eriksson. Method and mechanism for dynamic trim of a fast moving, planning or semi-planning ship hull. United States patent 6,148,756, November 21 2000.
- [Pre86] M.S. Pressnell. The performance of model aircraft using flow invigorators, gliding in the critical range of reynolds numbers. In *Aerodynamics at Low Reynolds Numbers* $10^4 < Re < 10^6$, pages 32.1–32.32. The Royal Aeronautical Society, 1986.
- [Rie61] F.W. Riegels. *Aerofoil sections*. Butterworths, London, 1961.
- [RTS91] A. Reed, J. Telste, and C. Scragg. Analysis of transom stern flows. In *Eighteenth Symposium on Naval Hydrodynamics*, pages 207–219, Ann Arbor, 1991.
- [Sar89] T. Sarpkaya. Computational methods with vortices- The 1988 Freeman Scholar Lecture. *Journal of Fluids Engineering*, 111:5–60, 1989.
- [Sav64] D. Savitsky. Hydrodynamic design of planing hulls. *Marine Technology*, pages 71–95, October 1964.

- [Sav88] D. Savitsky. Wake shapes behind planing hull forms. In *International High-Performance Vehicle Conference*, Shanghai, November 1988. Chinese Society of Naval Architecture and Marine Engineering.
- [Sch73] H. Schertel von. The design and application of hydrofoils and their future prospects. In *Proceedings, Institute of Marine Engineers*, 1973.
- [Sch79] H. Schlichting. *Boundary-Layer Theory*. Classic Textbook Reissue. McGraw-Hill, 7th edition, 1979.
- [SD54] D. Savitsky and A. Dingee. Some interference effects between two flat surfaces planing parallel to each other at high speed. *Journal of the Aeronautical Sciences*, 21:419–420, June 1954.
- [SDF89] M.S. Selig, J.F. Donovan, and D.B. Fraser. *Airfoils at Low Speeds*. Soartech Publications, H.A. Stokely, 1504 North Horseshoe Circle, Virginia Beach, Virginia, 23451, USA, 1989.
- [SDR99] P.K. Sahoo, L.J. Doctors, and M.R. Renilson. Theoretical and experimental investigation of resistance of high-speed round-bilge hull forms. In *FAST'99 5th International Conference on Fast Sea Transportation*, pages 803–814, Seattle, 1999.
- [SE95] J. Selmer and D.O. Ellingsen. The CPS speed propulsion programme. In *International Symposium: High Speed Vessels for Transport and Defence*, London, November 1995. RINA.
- [Ser93] E.H. Serter. *Hydrodynamics and Naval Architecture of Deep-Vee Hull Forms*. Hydro Research Systems, 245 Knightsbridge, London SW7 1DG, U.K., 1993.
- [SG98] G. Semijalac and A. Gamulin. The influence of block coefficient on hydrodynamic characteristics of semi-displacement ship. *Brodogradnja*, 46(2):123–128, 1998.
- [She59] M.G. Sheglova. Calculation of the wetted length of a plate of finite aspect ratio gliding with constant speed. In *Proceedings of the Central Aero-Hydrodynamic Institute, TSAGI*, 1959. in Russian.
- [She85] Y.T. Shen. Wing sections for hydrofoils-part 3: Experimental verifications. *Journal of ship Research*, 29(1):39–50, March 1985.
- [shi98] Foil assistance - riding higher now? *Ship and Boat International*, (1):39–41, January/February 1998.
- [Shi00] V. Shigunov. Development of Eulerian approaches for free-surface problems. Bericht 606, Institut für Schiffbau, Technische Universität Hamburg-Harburg, April 2000.

- [SIS01] E. Ya. Semionicheva, A.N. Ivanov, and S.B. Startsev. Designing of hydrofoils: Strategy, tactics and results. In *SP2001: Lavrentiev Lectures*, St. Petersburg, 2001.
- [SMFI93] K. Shimizu, K. Masuyama, M. Fukushima, and N. Ishii. A study on the hydrodynamics aspects of hybrid hydrofoil catamaran. In *Fast'93, 2nd International Conference on Fast Sea Transportation*, pages 951–962, Yokohama, 1993.
- [Soe99a] H. Soeding. Das Wellenwiderstands-Programmsystem KELVIN. Technical report, Institut für Schiffbau, Technische Universität Hamburg-Harburg, 1999.
- [Soe99b] H. Soeding. Stationäre Schiffsumströmung mit Wellenbildung. Institut für Schiffbau, Technische Universität Hamburg-Harburg, 1999.
- [Sot37] W. Sottorf. Gestaltung von Schwimmwerken. *Luftfahrtforschung*, 14(4/5):157–167, 1937.
- [Sot40] W. Sottorf. Experimentelle Untersuchungen zur Frage des Wassertragflügels. Forschungsbericht 1319, Deutsche Versuchsanstalt für Luftfahrt E. V., 1940.
- [SRZM99] S. Steen, H.J. Rambech, R. Zhao, and K.J. Minsaas. Resistance prediction for fast displacement catamarans. In *FAST'99 Fifth International Conference on Fast Sea Transportation*, pages 915–922, Seattle, 1999.
- [SS57] S. Schuster and H. Schwaneke. Über den Einfluss der Wasseroberfläche auf die Auftriebsverteilung von Tragflügeln. *Schiffstechnik*, 4(21):117–125, 1957.
- [SS60] S. Schuster and H. Schwaneke. On hydrofoils near a free surface. In *3rd International Symposium on Naval Hydrodynamics*, pages 147–189, 1960.
- [Stu00] S. Stumbo. Wake wash measurement trials, E CAT with foil assist. Technical report, Washington State Ferries, Colman Dock/Pier 52, 801 Alaskan Way, Seattle, WA 98104-1487, January 2000.
- [SYK96] M-S. Shin, S-I. Yang, and E-C. Kim. New concept hull forms for fast sea transportation. In *WEGEMT Workshop: Conceptual Designs for Fast Sea Transportation*, Glasgow, 1996.
- [Tao98] M. Tao. Development of the foil augmented wave piercing catamaran. In *RINA International Conference on Fast Freight Transportation by Sea*, pages 1–6, London, 1998. Royal Institute of Naval Architects.

- [Tao00] M. Tao. Resistance prediction method of foil augmented cat. In *Third International Conference on High Performance Marine Vehicles, HPMV2000*, pages 172–176, Shanghai, 2000.
- [TB98] G. Thiart and V. Bertram. Staggered-grid panel method for hydrofoils with fully nonlinear free-surface effect. *International Shipbuilding Progress*, 45(444):313–328, 1998.
- [TH86] M.P. Tulin and C.C. Hsu. Theory of high-speed displacement ships with transom sterns. *Journal of Ship Research*, 30(3):186–193, September 1986.
- [THCC01] J-F. Tsai, J-L. Hwang, S-W. Chau, and S-K. Chou. Study of hydrofoil assistance arrangement for catamaran with stern flap and interceptor. In *FAST 2001, 6th International Conference on Fast Sea Transportation*, pages 69–78, Southampton, 2001.
- [Thi97] G.D. Thiart. Vortex lattice method for a straight hydrofoil near a free surface. *International Shipbuilding Progress*, 44(5):5–26, September 1997.
- [Tik94] A.I. Tikhonov. Planing of tandem plates with deadrise angle. *Proceedings of the Central Aero- Hydrodynamic Institute*, (2574):1–10, 1994. In Russian.
- [TT68] H. Turner and A. Taplin. The resistance of large powered catamarans. In *SNAME Transactions*, pages 180–213, 1968.
- [Tul56] M.P. Tulin. The theory of slender surfaces planing at high speed. *Schiffstechnik*, 4:125–133, 1956.
- [Wag32] H. Wagner. Über Stoss- und Gleitvorgänge an der Wasseroberfläche von Flüssigkeiten. *Zeitschrift für Angewandte Mathematik und Mechanik.*, 12(4):193–215, 1932.
- [Wal32] O. Walchner. Profilmessungen bei Kavitation. In *Hydromechanische Probleme des Schiffsantriebs*, pages 257–267. Hamburgische Schiffbau - Versuchsanstalt e.V., 1932. (English summary available: Profile measurements during Cavitation, NACA Technical Memorandum No. 1060, Washington, Jan. 1944).
- [Wal99] F. Walree van. *Computational Methods for Hydrofoil Craft in Steady and Unsteady Flow*. PhD thesis, Technische Universiteit Delft, Wageningen, Netherlands, March 1999.
- [WC58] K.L. Waldin and K.W. Christopher. A method for calculation of hydrodynamic lift for submerged and planing rectangular lifting surfaces. Technical Note 4168, NACA, Langley Aeronautical Laboratory, January 1958.

- [Weh73] J.V. Wehausen. The wave resistance of ships. *Advanced Applied Mechanics*, 13:93–245, 1973.
- [Wel98a] W. Welnicki. The enhancement of seakeeping qualities of fast catamaran by means of stabilizing foils. *Polish Maritime Research*, 5(3(17)):10–13, September 1998.
- [Wel98b] W. Welnicki. The influence of fixed foils on sea keeping qualities of fast catamaran. In *Practical Design of Ships and Mobile Units: Proceedings of the 7th International Symposium on Practical Design of Ships and Mobile Units*, The Hague, The Netherlands, September 1998.
- [Wer90] P. Werenskiold. Design tool for high speed slender catamarans. In *High Speed Marine Craft Conference*, Kristiansand, 1990.
- [Whi91] F.R. White. *Viscous Fluid Flow*. MacGraw-Hill, Inc., Singapore, 1991.
- [WK99] N. Warren and J. Kecsmar. Practical design aspects in the hydrodynamics of fast craft. In *International Conference: Hydrodynamics of High Speed Craft*, London, 24-25 November 1999. RINA.
- [Woo93] Hydrofoil applications for luxury yachts. *The Wood Report*, (1):30–33, January 1993.
- [WSM95] Y. Wang, J.L. Sproston, and A. Millward. A theoretical determination of the wave resistance of a fast displacement hull with a transom stern. *Journal of Ship Research*, 39(2):103–107, June 1995.
- [WSM96] Y. Wang, J.L. Sproston, and A. Millard. Calculations of wave resistance for a high speed displacement ship. *International Shipbuilding Progress*, 43(435):189–207, 1996.
- [XT99] L. Xu and W. Troesch. A study on hydrodynamics of asymmetric planing surfaces. In *FAST'99 5th International Conference on Fast Sea Transportation*, pages 471–480, Seattle, 1999.
- [Yam93] K. Yamaguchi. Model tests with a hydrofoil: Experimental results and comparison with DAWSON and HYDSIM. Technical Report 52277-2-SO, MARIN, Maritime Research Institute Netherlands, PO Box 28, 6700 AA Wageningen, The Netherlands, January 1993.
- [YATR72] S.G. Yermolayev, E.A. Aframayev, L.A. Teder, and Ya.S. Rabinowich. New prospective types of high-speed vessels: gliding, foiled, catamarans, catamarans with hydrodynamic and aerodynamic lifting. *Transactions NTOSP.*, 186:24–32, 1972. In Russian.

- [YATR76] S.G. Yermolayev, E.A. Aframayev, L.A. Teder, and Ya.S. Rabinowich. Specifics of the hydrodynamics of high speed catamarans. *Sudostroenie*, (8):6–9, 1976. In Russian. (English Translation in *Hovercraft and Hydrofoil*, 16:45-48, 1977).
- [Yeh65] H.Y.H. Yeh. Series 64 resistance experiments on high-speed displacement forms. *Marine Technology*, pages 248–272, July 1965.
- [YHTC94] C.T. Yang, J.L. Hwang, J.F. Tsai, and Y.N. Chen. The effects of lifting surface configurations on the developments of tip-vortex structures. *Ship Technology Research*, 41:17–30, 1994.
- [ZFA96] R. Zhao, O. Faltinsen, and J. Aarsnes. Water entry of two-dimensional sections with and without flow separation. In *Proceedings 21st Symposium on Naval Hydrodynamics*, pages 408–423, Trondheim, Norway, 1996.
- [ZFH97] R. Zhao, O. Faltinsen, and H.A. Haslum. A simplified nonlinear analysis of a high speed planing craft in calm water. In *FAST'97 Third International Conference on Fast Sea Transportation*, pages 431–438, Sydney, 1997.
- [ZG90] B-Q. Zhu and W-Z. Ge. Experimental study on the spray performance of surface piercing struts. In *19th International Towing Tank Conference*, pages 369–379, Madrid, Spain, September 1990.
- [Zha94] L. Zhao. Experimental study on the performance of channel-hydrofoil type planing boats. In *International Conference for New Ship Technology into 21st Century (NEWS-TEC'94)*, Shanghai, 1994.
- [ZLH97] L. Zhao, J. Li, and Y. He. A study on performance of channel hydrofoil type planing boats. *Shipbuilding of China, Transactions*, (138):1–8, August 1997. In Chinese.